Validation Document Delft3D-FLOW

a software system for 3D flow simulations

Report

December 2007

Validation Document Delft3D-FLOW

a software system for 3D flow simulations

H. Gerritsen, E.D. de Goede, F.W. Platzek,
M. Genseberger, J.A.Th.M. van Kester and R.E. Uittenbogaard

Report

X0356, M3470

WL | delft hydraulics

Client:	
Title:	Validation Document Delft3D-FLOW; a software system for 3D flow simulations

Abstract:

This report is the validation document for the mathematical model Delft3D-FLOW. The document is organised conforming to the Guidelines for documenting the validity of computational modelling software.

Chapter 1 contains a short overview of the computational model and introduces the main issues to be addressed by the validation process. The model overview includes information about the purpose of the model, about pre- and post-processing options and other software features, and about reference versions of the software. Validation priorities and approaches are briefly described, and a list of related documents is included.

Chapter 2 summarises the available information about the validity of the computational core of the model. In this chapter, claims are made about the range of applicability of the model and about the accuracy of computational results. Each claim is followed by a brief statement regarding its substantiation. This statement indicates the extent to which the claim has in fact been substantiated and points to the available evidence.

Chapter 3 contains such evidence, in the form of brief descriptions of relevant validation studies. Each description includes information about the purpose and approach of the study and a summary of main results and implications. About thirty validation studies have been documented.

This Delft3D-FLOW validation document, the input and result files of the validation can be supplied to users of the Delft3D-FLOW system, so that the validity and performance of Delft3D-FLOW can be verified.

References:

Ver	Author		Date	Remarks	Review		Approved by	
0.3	H. Gerritsen, E.D. de Goede		16 March 2004	Incomplete, draft version				
1.0	H. Gerritsen, E.D. de Goede		30 December 2007	Final version	B. Jagers		A.E. Mynett	

Project number:	X0356, M3470
Keywords:	Validation, Delft3D-FLOW
Number of pages:	266
Classification:	None
Status:	Final version 1.0

.

Contents

List of Figures

Chapter 1: Introduction

Chapter 2: Model Validity

Chapter 3: Validation Studies

Vertical mixing layer (horizontal splitter plate)

One-dimensional dam break

Horizontal mixing layer (vertical splitter plate)

Numerical scale model of an estuary

Numerical scale model of an estuary and a tidal dock

List of Abbreviations

2D	Two dimensional
3D	Three dimensional
BSS	Brier Skill Score
IAHR	International Association of Hydraulics Engineering and Research
SWE	Shallow Water Equations
RANS	Reynolds-averaged Navier Stokes

Summary

This document is the validation document for the mathematical model Delft3D-FLOW. The document is organised conforming to the Guidelines for documenting the validity of computational modelling software (IAHR, 1994).

The subject of this document is the validation of a computational model. The term computational model refers to software which primary function is to model a certain class of physical systems, and may include pre- and post-processing components and other necessary ancillary programmes. Validation applies primarily to the theoretical foundation and to the computational techniques that form the basis for the numerical and graphical results produced by the software. In the context of this document, validation of the model is viewed as the formulation and substantiation of explicit claims about applicability and accuracy of the computational results. This preface explains the approach that has been adopted in organising and presenting the information contained in this document.

Standard validation documents

This document conforms to a standard system for validation documentation. This system, the Standard Validation Document, has been developed by the hydraulic research industry in order to address the need for useful and explicit information about the validity of computational models. Such information is summarised in a validation document, which accompanies the technical reference documentation associated with a computational model. In conforming to the Standard, this validation document meets the following requirements:

1. It has a prescribed table of contents, based on a framework that allows separate quality issues to be clearly distinguished and described.
2. It includes a comprehensive list of the assumptions and approximations that were made during the design and implementation of the model.
3. It contains claims about the performance of the model, together with statements that point to the available substantiating evidence for these claims.
4. Claims about the model made in this document are substantiable and bounded: they can be tested, justified, or supported by means of physical or computational experiments, theoretical analysis, or case studies.
5. Claims are substantiated by evidence contained within this document, or by specific reference to accessible publications.
6. Results of validation studies included or referred to in this document are reproducible. Consequently the contents of this document are consistent with the current version of the software.
7. This document will be updated as the process of validating the model progresses.

Organisation of this document

Chapter 1 contains a short overview of the computational model and introduces the main issues to be addressed by the validation process. The model overview includes information about the purpose of the model, about pre- and post-processing options and other software

features, and about reference versions of the software. Validation priorities and approaches are briefly described, and a list of related documents is included.

Chapter 2 summarises the available information about the validity of the computational core of the model. In this chapter, claims are made about the range of applicability of the model and about the accuracy of computational results. Each claim is followed by a brief statement regarding its substantiation. This statement indicates the extent to which the claim has in fact been substantiated and points to the available evidence.

Chapter 3 contains such evidence, in the form of brief descriptions of relevant validation studies. Each description includes information about the purpose and approach of the study and a summary of main results and implications.

A glossary and complete list of references are contained in this document too.

A word of caution

This document contains information about the quality of a complex modelling tool. Its purpose is to assist the user in assessing the reliability and accuracy of computational results, and to provide guidelines with respect to the applicability and proper use of the modelling tool. This document does not, however, provide mathematical proof of the correctness of results for a specific application. The reader is referred to the License Agreement for pertinent legal terms and conditions associated with the use of the software.

The contents of this validation document attest to the fact that computational modelling of complex physical systems requires great care and inherently involves a number of uncertain factors. In order to obtain useful and accurate results for a particular application, the use of high-quality modelling tools is necessary but not sufficient. Ultimately, the quality of the computational results that can be achieved will depend upon the adequacy of available data as well as a suitable choice of model and modelling parameters.

Electronic standard validation document

This document is also available in electronic form in Portable Document Format (PDF). The electronic version may be read using the ACROBAT READER™ software which is available for many computer platforms.

The present version of the Validation Document Delft3D-FLOW (Version 1.0, 30 December 2007) can be downloaded from the Delft3D website:
http://www.wldelft.nl/soft/d3d/intro/validation/valdoc_flow.pdf

Acknowledgements

The guidelines [IAHR, 1994] provide a logical set up of the document. In the preparation of the present document, we aimed to share the look and feel with other validation documents in the market place, notably that of TELEMAC-2D [EDF-DRD, 2000] and of UnTRIM [Bundesanstalt für Wasserbau, 2002].

List of Symbols

Symbol	Units	Meaning
B_k	m^2/s^3	buoyancy flux term in transport equation for turbulent kinetic energy
B_e	m^2/s^4	buoyancy flux term in transport equation for the dissipation of kinetic energy
C, C_{2D}	$m^{1/2}/s$	2D Chézy coefficient
C_{3D}	$m^{1/2}/s$	3D Chézy coefficient
C_d	-	wind drag coefficient
c	kg/m^3	mass concentration
$c^{(\ell)}$	kg/m^3	mass concentration of sediment fraction (ℓ)
c_D	-	constant relating mixing length, turbulent kinetic energy and dissipation in the $k-\varepsilon$ model
c_p	J/kg°C	specific heat of sea water
c_μ	-	calibration constant
c_μ'	-	constant in Kolmogorov-Prandtl's eddy viscosity formulation
D	kg/m^2s	deposition rate cohesive sediment
D_{back}	m^2/s	background turbulent eddy viscosity in x- and y-direction
D_h, D_v	m^2/s	eddy diffusivity in the horizontal and vertical direction
D_{mol}	m^2/s	molecular eddy diffusivity in x- and y-direction
d	m	water depth below some horizontal plane of reference (datum)
d_s	m	representative diameter of suspended sediment
d_{50}	m	median diameter of sediment
d_{90}	m	sediment diameter
E	m/s	evaporation
E	kg/m^2s	erosion rate cohesive sediment
F_x	m/s^2	radiation stress gradient in x-direction
F_y	m/s^2	radiation stress gradient in y-direction
f	1/s	Coriolis coefficient (inertial frequency)
g	m/s^2	acceleration due to gravity
H	m	total water depth ($H = d + \zeta$)
H_{rms}	m	root-mean-square wave height
I	m/s	spiral motion intensity (secondary flow)
k	m^2/s^2	turbulent kinetic energy
k_s	m	Nikuradse roughness length
L	m	mixing length
ℓ	-	index number of sediment fraction
M_x^S	kg m/s	depth-averaged mass flux due to Stokes drift in x-direction
M_y^S	kg m/s	depth-averaged mass flux due to Stokes drift in y-direction

Symbol	Units	Meaning
M_ξ M_η	m/s^2	source or sink of momentum in x- and y-direction
n	m$^{1/3}$/s	Manning's coefficient
P	kg/ms^2	hydrostatic water pressure
P	m/s	precipitation
P_k	m^2/s^3	production term in transport equation for turbulent kinetic energy
P_ξ P_η	kg/m^{2}s^2	gradient hydrostatic pressure in x- and y-direction
P_ε	m^2/s^4	production term in transport equation for the dissipation of turbulent kinetic energy
Q	m/s	global source or sink per unit area
q_{in}	1/s	local source per unit volume
q_{out}	1/s	local sink per unit volume
R	m	radius of the Earth
Ri	-	gradient Richardson's number
S	ppt	salinity
S_b''	-	magnitude of the bed-load transport vector
s		relative density of sediment fraction. $(=\rho_s/\rho_w)$
T	$^\circ$C	temperature (general reference)
$\overline{T}$	$^\circ$K	temperature (general reference)
$T_{\xi\xi}, T_{\eta\eta}, T_{\xi\eta}$	kg/ms^2	contributions secondary flow to shear stress tensor
t	s	time
U	m/s	depth-averaged velocity in x-direction
$\hat{U}$	m/s	velocity of water discharged in y-direction
u	m/s	flow velocity in the x-direction
u_*	m/s	friction velocity due to currents or due to current and waves
u_{*_b}	m/s	friction velocity at the bed
u_*^s	m/s	friction velocity at the free surface
$\lvert\vec{U}\rvert$	m/s	magnitude of depth-averaged horizontal velocity vector $(U,V)^T$
U_{10}	m/s	averaged wind speed at 10 m above free surface
$\hat{U}$	m/s	velocity of water discharged in x- or y-direction
$\hat{U}_{orb}$	m/s	amplitude of the near-bottom wave orbital velocity
u^S	m/s	Stokes drift in x- or y-direction
$\tilde{u}$	m/s	total velocity due to flow and Stokes drift in x- or y-direction
v	m/s	fluid velocity in the y- direction
v_b	m/s	velocity at bed boundary layer in y- direction
V	m/s	depth-averaged velocity in y- direction
$\hat{V}$	m/s	velocity of water discharged in y- direction
v^S	m/s	Stokes drift in y- direction
$\tilde{v}$	m/s	total velocity due to flow and Stokes drift in x- direction
w	m/s	fluid velocity in z -direction
$w_{s,0}$	m/s	particle settling velocity in clear water (non-hindered)
$w_s^{(\ell)}$	m/s	(hindered) sediment settling velocity of sediment fraction (ℓ)

Symbol	Units	Meaning
x, y, z ,	m	Cartesian co-ordinates
z_0	m	bed roughness length
β_c	-	coefficient to account for secondary flow in momentum equations
χ	deg	astronomical argument of a tidal component
Δt	s	computational time-step
$\Delta x^{(n,m)}$	m	cell width in the x - direction, held at the V point of cell (n, m)
$\Delta y^{(n,m)}$	m	cell width in the y - direction, held at the U point of cell (n, m)
Δz_b	m	thickness of the bed layer
Δz_s	m	thickness of the surface layer
$\Delta \sigma_b$	-	thickness of the bed boundary layer in relative co-ordinates
ε_ε	m^2/s^4	dissipation in transport equation for dissipation of turbulent kinetic energy
ε	m^2/s^3	dissipation in transport equation for turbulent kinetic energy
ε		emissivity coefficient of water at air-water interface
ε_f	m^2/s	fluid diffusion in the z - direction
$\varepsilon_{f,x}$, $\varepsilon_{f,y}$, $\varepsilon_{f,z}$	m^2/s	fluid diffusion coefficients in the x, y, z - directions, respectively
ε_s	m^2/s	sediment diffusion in the z - direction
$\varepsilon_{s,x}$, $\varepsilon_{s,y}$, $\varepsilon_{s,z}$	m^2/s	sediment diffusion coefficients in the x, y, z - directions, respectively
ϕ	deg.	latitude co-ordinate in spherical co-ordinates
ϕ	$J/sm^{2\circ}C$	exchange coefficient for the heat flux in excess temperature model
φ	m	equilibrium tide
φ^e	m	perturbation of the equilibrium tide due to earth tide
φ^{eo}	m	perturbation of the equilibrium tide due to tidal load
φ^o	m	perturbation of the equilibrium tide due to oceanic tidal load
λ	deg	longitude co-ordinate in spherical co-ordinates
λ_d	1/s	first-order decay coefficient
ν	m^2/s	kinematic viscosity coefficient
ν_{back}	m^2/s	background turbulent eddy viscosity
ν_H	m^2/s	horizontal eddy viscosity in horizontal direction)
ν_{mol}	m^2/s	molecular eddy viscosity in horizontal direction)
ν_V	m^2/s	vertical eddy viscosity
ν_{2D}	m^2/s	part of eddy viscosity due to horizontal turbulence
ν_{3D}	m^2/s	part of eddy viscosity due to 3D turbulence
ρ	kg/m^3	density of water
ρ_a	kg/m^3	density of air
ρ_0	kg/m^3	reference density of water
$\rho_s^{(\ell)}$	kg/m^3	specific density of sediment fraction (ℓ)
σ	$J/m^2s^\circ K^4$	Stefan-Boltsmann's constant

Symbol	Units	Meaning
σ	-	scaled vertical co-ordinate; $\sigma = \frac{z-\zeta}{d+\zeta}$; (surface $\sigma = 0$; $\sigma \quad -1$)
σ_C	-	Prandtl-Schmidt number
τ	kg/ms^2	shear stress
τ_b	N/m^2	bed shear stress due to current and waves
$\tau_{b\xi}$	kg/ms^2	bed shear stress in x-direction
$\tau_{b\eta}$	kg/ms^2	bed shear stress in y-direction
τ_c	kg/ms^2	magnitude of the bed shear stress due to current alone
τ_w	kg/ms^2	magnitude of the at bed shear stress due to waves alone
τ_m	kg/ms^2	magnitude of the wave-averaged at bed shear stress for combined waves and current
$\tau_{b,c}$	kg/ms^2	bed shear stress due to current
$\tau_{b,cr}$	kg/ms^2	critical bed shear stress
$\tau_{b,cw}$	kg/ms^2	bed shear stress due to current in the presence of waves
$\tau_{b,w}$	kg/ms^2	bed shear stress due to waves
τ_{cr}	kg/ms^2	critical bed shear stress
$\tau_{cr,d}$	kg/ms^2	user specified critical deposition shear stress
$\tau_{cr,e}$	kg/ms^2	user specified critical erosion shear stress
τ_{cw}	kg/ms^2	mean bed shear stress due to current and waves
$\tau_{\max}$	kg/ms^2	maximum bottom shear stress with wave-current interaction
τ_{mean}	kg/ms^2	mean (cycle averaged) bottom shear stress with wave-current interaction
$\tau_{s\eta}$	kg/ms^2	shear stress at surface in x-direction
$\tau_{s\eta}$	kg/ms^2	shear stress at surface in y-direction
ω	m/s	velocity in the σ-direction in the σ - co-ordinate system
ω	1/s	angular frequency waves
ω	deg./hour	angular frequency of tide and/or Fourier components
ξ, η		horizontal, curvilinear co-ordinates
ψ	J/m^{2}s	heat flux through free surface
ζ	m	water level above some horizontal plane of reference (datum)
ζ^b	m	bottom tide
ζ^e	m	earth tide
ζ^{eo}	m	tidal loading

1 Introduction

This chapter refers to the model Delft3D-FLOW as a software product, and clarifies the relation of that which is being validated to the rest of the software. It includes brief descriptions of pre- and post-processing options, as well as an explanation of the modular structure of the computational core of the model.

Delft3D-FLOW is the hydrodynamic module of Delft3D, which is Delft Hydraulics' fully-integrated program for the modelling of water flows, waves, water quality, particle tracking, ecology, sediment and chemical transports and morphology. In Figure 1.1 a system overview of Delft3D is given.

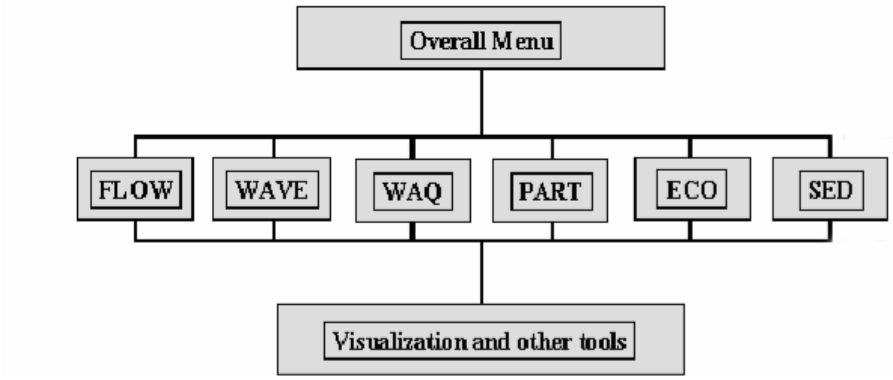

Figure 1.1: System overview of Delft3D

We note that in previous versions of Delft3D also contained a MOR(phology) module. However, the morphology functionality is now part of the FLOW module and a separate MOR module does not exist anymore.

The present Validation Document concerns the properties and validity of Delft3D-FLOW. It focuses on the computational part of Delft3D-FLOW. For example, the pre- and postprocessing, and the coupling with other modules in Delft3D, such as WAVE, WAQ, PART and ECO, are beyond the scope of this description.

1.1 Model overview

1.1.1 Purpose

The primary purpose of the computational model Delft3D-FLOW is to solve various one-, two- and three-dimensional, time-dependent, non-linear differential equations related to hydrostatic and non-hydrostatic free-surface flow problems on a structured orthogonal grid to cover problems with complicated geometry. The equations are formulated in orthogonal curvilinear co-ordinates on a plane or in spherical co-ordinates on the globe. In Delft3D-FLOW models with a rectangular or spherical grid (Cartesian frame of reference) are considered as a special form of a curvilinear grid, see [Kernkamp et al., 2005] and [Willemse et al., 1986].

The equations solved are mathematical descriptions of physical conservation laws for:

- water volume (continuity equation),
- linear momentum (Reynolds-averaged Navier-Stokes (RANS) equations), and
- tracer mass (transport equation) , e. g. for salt, heat (temperature) and suspended sediments or passive pollutants.

Furthermore, bed level changes are computed, which depend on the quantity of bottom sediments.

The following physical quantities can be obtained in dependence on three-dimensional space *(x,y,z)* and time *t*:

- water surface elevation $\zeta(x,y,t)$ with regard to a reference surface (e. g. mean sea level),
- current velocity $u(x,y,z,t)$, $v(x,y,z,t)$, $w(x,y,z,t)$,
- non-hydrostatic pressure component $q(x,y,z,t)$,
- tracer concentration $C(x,y,z,t)$, e. g. temperature, salinity, concentration of suspended sediments or passive pollutants; and
- bed level $d(x,y,t)$,representing changes in bathymetry.

Delft3D-FLOW can be used in either hydrostatic or non-hydrostatic mode. In case of hydrostatic modelling the so-called shallow water equations are solved, whereas in non-hydrostatic mode the Navier-Stokes equations are taken into account by adding non-hydrostatic terms to the shallow water equations. A fine horizontal grid is needed to resolve non-hydostatic flow phenomena.

When the computational model Delft3D-FLOW is used in one- or two-dimensional mode (with one *z*-layer in vertical direction) the results for *u*, *v* and *C* will be the respective depth averaged values for current velocity and tracer concentration.

For the vertical grid system two options are available in Delft3D-FLOW, namely so-called σ- or *z*-coordinates. For a detailed discussion of these two grid systems we refer to Section 1.1.4. In the remainder of this document "z" will be used as vertical coordinate.

1.1.2 Properties of the computational model

The computational model Delft3D-FLOW can be characterised by means of the following distinguished properties:

- Grid alignment with complicated boundaries and local grid refinements to meet the needs of resolving finer spatial resolution in various numerical modelling tasks, which results in an accurate description of geometry (orthogonal curvilinear grid, see Figure 1.2);
- application for one- and two-dimensional vertically averaged as well as hydrostatic or non-hydrostatic three-dimensional problems;
- a solution technique that allows for solution based on accuracy considerations rather than stability (alternating direction implicit finite difference method);

- conservation of fluid and tracer mass locally and globally;
- computationally efficient and robust;
- a computational core and a separate user interface.
- efficient coupling with other physical processes via the other modules of the integrated Delft3D modelling system.

1.1.3 Horizontal grid

In Delft3D-FLOW the horizontal physical model domain *(x,y)* is covered with a curvilinear orthogonal grid, designed and optimised for a given application through a grid generator. This includes simple rectangular, spherical and curvilinear grids. The computations are performed on a transformed, simple rectangular computational domain. For the horizontal direction the grid concept is illustrated in Figure 1.2.

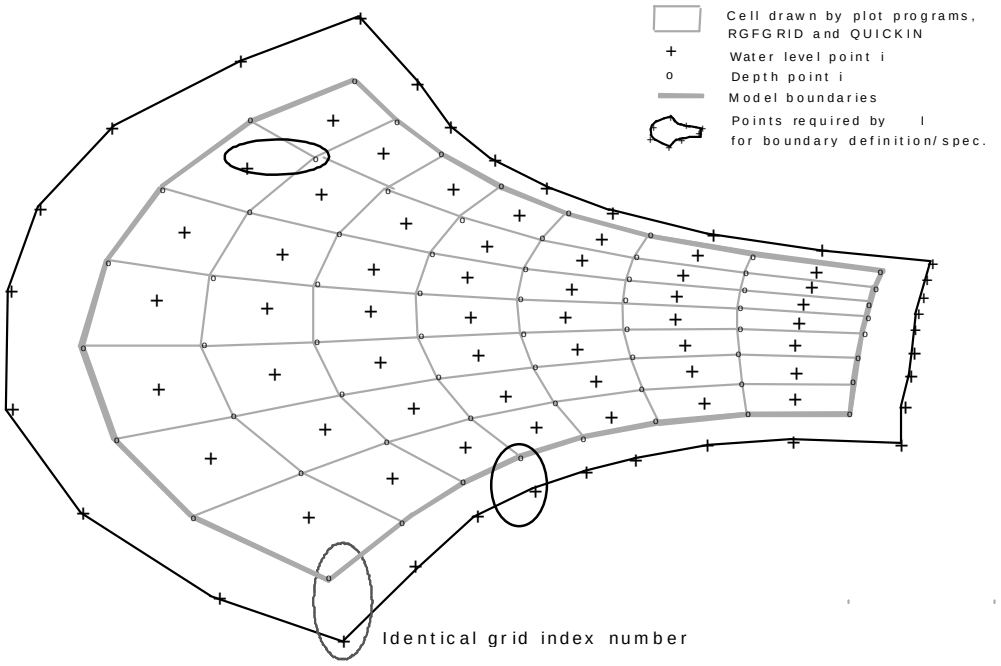

Figure 1.2 Horizontal curvilinear grid concept

1.1.4 Vertical grid

3D numerical modelling of the hydrodynamics and water quality in these areas requires accurate treatment of the vertical exchange processes. The existence of vertical stratification influences the turbulent exchange of momentum, heat, salinity and passive contaminants. The accuracy of the discretisation of the vertical exchange processes is determined by the vertical grid system. The vertical grid should:

- resolve the boundary layer near the bottom and surface to allow an accurate evaluation of the bed stress and surface stresses, respectively;
- be fine around pycnoclines;
- avoid large truncation errors in the approximation of strictly horizontal gradients.

The two commonly used vertical grid systems in 3D shallow-water models are the z-coordinate system (Z-model) and the so-called σ-coordinate system (σ-model), see Figure 1.3. Neither meets all the requirements. The Z-model has horizontal coordinate lines which are (nearly) parallel with isopycnals, but the bottom is usually not a coordinate line and is represented instead as a staircase (zig-zag boundary). This leads to inaccuracies in the approximation of the bed stress and the horizontal advection near the bed. The sigma-model has quasi-horizontal coordinate lines. The first and last grid line follow the free surface (σ = 0) and the sea bed boundary (σ = -1), respectively, with a user defined σ-distribution in between. The grid lines follow the bottom topography and the surface but generally not the isopycnals. Inaccuracies associated with these numerical artefacts have been addressed in Delft3D, which has led to acceptable solutions for practical applications.

In Delft3D-FLOW both the options of fixed horizontal layers (Z-model) and the sigma grid (σ-model) are operational. The two grid concepts are illustrated in Figure 1.3.

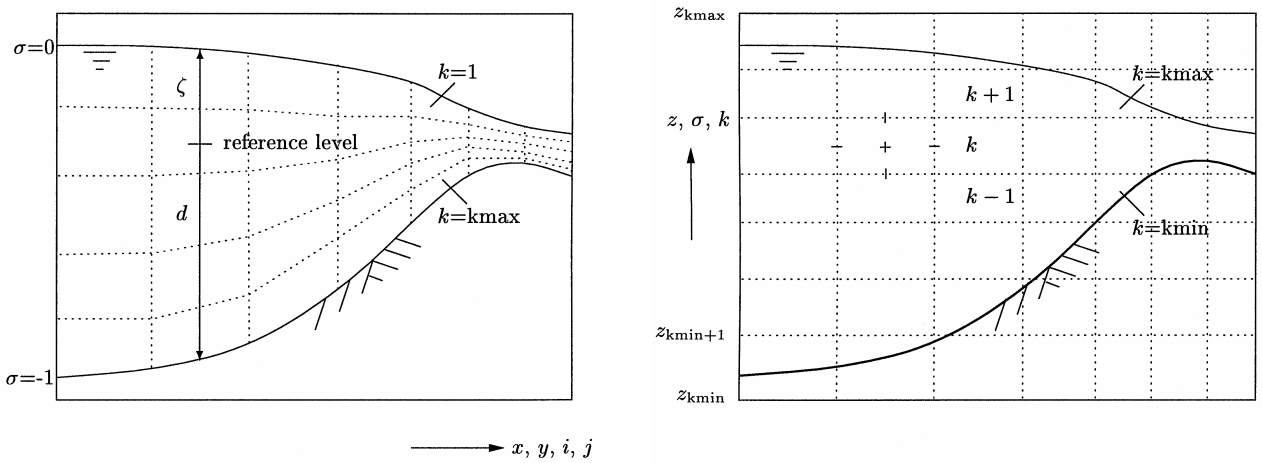

Figure 1.3. Vertical grid concepts: the σ–model (left) and z-coordinate model (right)

In practice, this means that depending on the application the user can choose the best option for the representation of the processes in the vertical. In case of stratified flow problems in coastal seas, estuaries and lakes where steep topography is a dominant feature, this is an important issue. For lakes a Z-model is preferred, because the vertical exchange process should not be dominated by truncation errors.

1.1.5 Pre- and post-processing and other software features

Delft3D-FLOW can be used as a stand-alone software package. For using Delft3D-FLOW the following auxiliary software tools are important:

• RGFGRID	for generating and optimising curvilinear grids
• QUICKIN	for preparing and manipulating grid oriented data, such as bathymetry or initial conditions for water levels, salinity or concentrations of constituents.
• Delft3D-FLOW GUI	Graphical user Interface for preparing a complete Delft3D-FLOW input file, which is called a Master Definition (MD) file.
• TRIANA	for performing off-line tidal analysis of time series generated by Delft3D-FLOW
• TIDE	for performing tidal analysis on time-series of measured water levels or velocities
• NESTHD	for generating (offline) boundary conditions from an overall model for a nested model
• GPP	for visualisation and animation of simulation results
• QUICKPLOT	for visualisation and animation of simulation results; package based on MATLAB

Table 1.1 Overview of auxiliary software tools for Delft3D-FLOW

For details on using these utility programs we refer to the respective User Manuals.

1.1.6 Version information

The content of this document is consistent with the (operational) version 3.55.04 of the Delft3D-FLOW software, which has been released in November 2007 [WL | Delft Hydraulics, 2007].

1.2 Validation priorities and approaches

In this DELFT3D-FLOW validation document at first the model functionality of Delft3D-FLOW is described by means of its applications (see Chapter 2.2.1) and its physical processes (see Chapter 2.2.2). Next, the following three phases are distinguished:

- **Conceptual model** (mathematical description of a physical system together with some fundamental assumptions and/or simplifications), see Chapter 2.3.
- **Algorithmic implementation** (conversion of the conceptual model into a set of procedures for computation; e.g., discretisations, solution procedures), see Chapter 2.4.
- **Software implementation** (conversion of algorithmic implementation into computer code; coding of algorithms, data structures, etc.), see Chapter 2.5.

These three phases are according to the IAHR guidelines for validation, as described in [IAHR, 1994], see also [Dee, 1993].

In Chapter 3 the claims and substantiations that have been formulated in Chapter 2 for the model functionality, the conceptual model, the algorithmic implementation and the software implementation of Delft3D-FLOW are validated for a large number of validation studies.

This Delft3D-FLOW validation document, the input and result files of the validation studies (of Chapter 3) can be supplied to users of the Delft3D-FLOW system, so that they are able to verify the validity and performance of Delft3D-FLOW.

1.3 Quantification of model output

This version hardly contains any quantification of model results. All validation studies have been described and lot of figures are shown. By visual inspection and by reading the conclusions for each validation study, the reader will have an impression of the quality of the computed results. However, a quantitative assessment of the accuracy of model predictions is lacking. In a next version of this validation document, a quantitative assessment will be added.

For a quantitative assessment various options are available. Preferably, a uniform performance indicator will be applied for all validation studies, possibly supported by additional quantification parameters. An appropriate candidate might be the so-called Brier Skill Score (BSS), which is an objective performance indicator. The *BSS* is defined as:

$$BSS = 1 - \frac{\langle (Y - X)^2 \rangle}{\langle (B - X)^2 \rangle} \tag{1.3.1}$$

where Y is the set of predictions, X is the set of measurements/analytical data and B is a baseline prediction. The difficulty lies in choosing a suitable baseline prediction. The *BSS* can be derived for each test case, for one or more key parameters. The *BSS* is independent of the type of model, i.e. tidal forcing, transport [Murphy et al., 1989]. For more details, we refer to [Wallingford, 200X].

1.4 Related documents

The validation studies, as described in Chapter 3 of this validation document, are also available via the Wiki/Internet side of WL | Delft Hydraulics, see “http://wiki.wldelft.nl/display/DSC/Validation+document”.

Further documents related to the current version of the computational model Delft3D-FLOW can be found in the User Manual [WL | Delft Hydraulics, 2007].

1.5 Project team

This validation document has been prepared by Herman Gerritsen and Erik de Goede. The figures and WL | Delft Hydraulics Wiki/Internet pages with model results of the validation studies have been prepared by Frank Platzek, Menno Genseberger. Rob Uittenbogaard, Firmijn Zijl, Daniel Twigt and Jan van Kester have provided valuable assistance.

1.6 Status of current version

The present version of the Validation Document Delft3D-FLOW (Version 1.0, 30 December 2007) is a complete version. The previous version (Version 0.3, dated 16 March 2004) contained results for only two validation studies, namely the tidal flume and the North Sea validation studies. This version is complete with respect to the description of the model validity, the conceptual model, the algorithmic implementation, the software implementation and the validation for all validation studies.

However, twenty-nine validation studies are reported in this validation document. It is evident that all functionality in Delft3D-FLOW can not be validated with twenty-nine studies. For example, only a few morphologic studies are reported and the reader is referred to other documents such as [WL | Delft Hydraulics, 1994]. Nevertheless, this document provides a clear view of what is possible with Delft3D-FLOW.

Moreover, a quantitative assessment of the Delft3D-FLOW model accuracy is lacking and will be incorporated in a next version.

2 Model validity

This chapter summarises all available information pertaining to the validation of the computational core of the model. This includes the assumptions and approximations that were introduced during the design and implementation of the model. It further includes claims about the applicability and/or accuracy of (aspects of) the model, together with statements about the substantiations of those claims.

The nature of a claim and its substantiation varies depending on the subject, as explained below under the headings of the various subsections in which they appear. We have aimed to make claims as explicit as possible and to provide useful information about model validity. Substantiation aims to be thorough but brief, which can be achieved by using references.

Note that a substantiation may be incomplete, due to the nature of the claim, or because the evidence is not (yet) available. In such cases we prefer to admit this rather than to invent a substantiation that appears convincing.

These claims and substantiations together comprise the essential information in this document. The remainder of the document serves either to provide context, necessary background material or substantiating evidence.

2.1 Physical system

This section describes the physical system or systems being modelled. It describes what is being modelled, rather than how it is being modelled. The hydrodynamic module Delft3D-FLOW simulates two-dimensional (2D, depth-averaged) or three-dimensional (3D) unsteady flow and transport phenomena resulting from tidal and meteorological forcing, including the effect of density differences due to a non-uniform temperature and salinity distribution (density-driven flow). The flow model can be used to predict the flow in shallow seas, coastal areas, estuaries, lagoons, rivers and lakes. It aims to model flow phenomena of which the horizontal length and time scales are significantly larger than the vertical scales, which is the so-called shallow water assumption.

If the fluid is vertically homogeneous, a depth-averaged approach is appropriate. Delft3D-FLOW is able to run in two-dimensional mode (one computational layer), which corresponds to solving the depth-averaged equations. Examples in which the two-dimensional, depth-averaged flow equations can be applied are tidal waves, storm surges, tsunamis, harbour oscillations (seiches) and transport of pollutants in vertically well-mixed flow regimes.

Three-dimensional modelling is of particular interest in transport problems where the horizontal flow field shows significant variation in the vertical direction. This variation may be generated by wind forcing, bed stress, Coriolis force, bed topography or density differences. Examples are dispersion of passive materials or cooling water in lakes and coastal areas, upwelling and downwelling of nutrients, salt intrusion in estuaries, fresh water river discharges in bays and thermal stratification in lakes and seas.

2.2 Model functionality

This section describes the functionality of the model by referring to specific instances or configurations of the physical system described in Section 2.1 above. It consists of claims about what the model is actually able to represent, and (to the extent that this is possible) how well it does so. For the purposes of this section the model can be regarded as a black box, taking input information and producing computational results.

2.2.1 Applications

This section presents an overview of the domain of applicability of the model. This is done by making claims about the types of practical and realistic situations in which the model can be employed, and showing the nature and quality of the information that the model is capable of generating in those situations.

The purpose of providing the reader with this inventory of application types is to allow the reader to quickly recognise whether the model is indeed suitable for a particular application.

The computational model Delft3D-FLOW can be used in a wide range of applications, which are listed below:

- Tide and wind-driven flow resulting from space and time varying wind and atmospheric pressure (See Section 2.2.1.1)
- Density driven flow and salinity intrusion (See Section 2.2.1.2)
- Wind driven flow (See Section 2.2.1.3)
- Horizontal transport of matter on large and small scales (See Section 2.2.1.4).
- Hydrodynamic impact of engineering works such as land reclamation, breakwaters, dikes (See Section 2.2.1.5)
- Hydrodynamic impact of hydraulic structures such as gates, weirs, barriers and floating structures (See Section 2.2.1.6)
- Spreading of waste water discharges from coastal outfalls (See Section 2.2.1.7)
- Thermal recirculation of cooling water discharges from a power plant (See Section 2.2.1.8)
- Hydrostatic and non-hydrostatic flow (See Section 2.2.1.9).
- Thermal stratification in seas, lakes and reservoirs (See Section 2.2.1.10).
- Small scale current patterns near harbour entrances (See Section 2.2.1.11).
- Flows resulting from dam breaks (See Section 2.2.1.12).

The model results have the form of distributions of the simulated quantities (water levels, currents, salinity, temperature, pollutant concentrations) in all grid points at user specified points in time, plus detailed time series of such parameters at user-selected locations. Each application is described in more detail in subsequent sections.

Tidal dynamics of estuaries or coastal seas

Claim 2.2.1.1: Delft3D-FLOW can be used for an accurate prediction of the tidal dynamics (water elevation, currents) in estuaries or coastal seas.

Substantiation: Validation Study 3.1.1 (Simple channel flow);
Validation Study 3.2.6 (Numerical scale model of an estuary).
Validation Study 3.2.7 (Numerical scale model of an estuary and a tidal lock).
Validation Study 3.4.1 (North Sea).

Example(s) of application studies:
1. 2D tidal modelling of the Indonesian waters using a spherical grid modelling approach, [Gerritsen et al., 2003]
2. 3D tidal modelling of the North Sea in the curvilinear PROMISE model, [Gerritsen et al., 2000]

Density driven flow and salinity intrusion

Claim 2.2.1.2: Delft3D-FLOW can be used for an accurate prediction of the density (salinity and/or temperature) driven flow. Moreover, sediment concentrations can be taken into account with respect to density values.

Substantiation: Validation Study 3.1.5 (Lock exchange flow);
Validation Study 3.2.6 (Numerical scale model of an estuary).
Validation Study 3.2.7 (Numerical scale model of an estuary and a tidal lock).
Validation Study 3.2.1 (Tidal flume).

Example(s) of application studies:
1. Baroclinic adjustment of an initial density front [Tartinville et al., 1998]
2. Tidal flume [Karelse, 1996]
3. Salinity and temperature stratification in the Rhine plume [De Kok et al., 2001]
4. Salinity stratification in Hong Kong waters [Postma et al., 1999]

Wind driven flow and storm surges

Claim 2.2.1.3: Delft3D-FLOW can be used for an accurate prediction of wind driven flow and storm surges.

Substantiation: Validation Study 3.1.4 (Wind driven channel flow).
Validation Study 3.4.1 (North Sea).

Example(s) of application studies:
1. 2D tidal and surge modelling in the North Sea [Gerritsen et al., 1995; Gerritsen and Bijlsma, 1988]
2. Cyclone-induced storm surges in the Bay of Bengal [Vatvani et al., 2002]
3. North Sea storm surge model [Verboom et al., 1992]

Horizontal transport of matter on large and small scales

Claim 2.2.1.4: Delft3D-FLOW can be used for an accurate prediction of horizontal transport of matter, both on large and small scales.

Substantiation: Validation Study 3.1.5 (Lock exchange flow);
Validation Study 3.2.1 (Tidal flume)

Example(s) of application studies:
1. 3D sediment transport in the North Sea on seasonal scales [Gerritsen et al., 2000]
2. Midfield spreading of matter from an outfall [Gerritsen and Verboom, 1994]

Hydrodynamic impact of engineering works

Claim 2.2.1.5: Delft3D-FLOW can be used to investigate the hydrodynamic impact of engineering works, such as land reclamation, breakwaters and dikes.

Substantiation: Not in list of validation studies yet.

Example(s) of application studies:
1. Impacts of Maasvlakte 2 on the Wadden Sea and North Sea coastal zone [De Goede et al., 2005]

Hydrodynamic impact of hydraulic structures

Claim 2.2.1.6: Delft3D-FLOW can be used to investigate the hydrodynamic impact of hydraulic structures, such as gates, weirs and barriers.

Substantiation: Validation Study 3.1.7 (Flow over a weir).

Example(s) of application studies:
1. Complex flows around groynes [Van Schijndel and Jagers, 2003]
2. Impact of coastal structures [Roelvink et al., 1999]

Spreading of waste water discharges from coastal outfalls

Claim 2.2.1.7: Delft3D-FLOW can be used for an accurate prediction of waste water dispersion from coastal outfalls.

Substantiation: Not in list of validation studies yet.

Example(s) of application studies:
1. Midfield spreading of matter from an outfall [Gerritsen and Verboom, 1994]

Thermal recirculation of cooling water discharges

Claim 2.2.1.8: Delft3D-FLOW can be used to describe and quantify the thermal recirculation between discharge and intake points, by which e.g. the design and efficiency of a power plant can be assessed.

Substantiation: Not in list of validation studies yet.

Example(s) of application studies:
1. Thermal discharges for the Maasvlakte-2 [Kleissen, 2007]
2. Pembroke Power Station, marine discharge study-phase 2, 3D hydrodynamic and water quality model [Karelse and Hulsen, 1995]

Hydrostatic and non-hydrostatic flow

Claim 2.2.1.9: Delft3D-FLOW can be used for an accurate prediction of hydrostatic and non-hydrostatic flow. Depending on the application (ratio between horizontal and vertical length scale), the user can choose the most suitable modelling approach.

Substantiation: Validation Study 3.1.5 (Lock exchange flow);
Validation Study 3.3.4 (Buoyant yet).

Example(s) of application studies:
1. 2D and 3D transport in the North Sea on seasonal scales [Gerritsen et al., 2000]
2. Near-field and far-field modelling of bouyant discharges [Van der Kaaij, 2007]

Thermal stratification in seas, lakes and reservoirs

Claim 2.2.1.10: Delft3D-FLOW can be used for an accurate prediction of thermal stratification in seas, lakes and reservoirs

Substantiation: Validation Study 3.3.3 (Schematised Lake Veere);
Validation Study 3.4.1 (North Sea);
Validation Study 3.4.2 (Zegerplas).

Example(s) of application studies:
1. Seasonal temperature stratification in the North Sea [De Kok et al. 2001]
2. Modelling framework for water quality management in Lake Victoria [Smits, 2000]

Small scale current patterns near harbour entrances

Claim 2.2.1.11: Delft3D-FLOW can be used for an accurate prediction of small scale current patterns near harbour entrances. For example, a so-called Horizontal Large Eddy Simulation (HLES) can be applied to resolve small scale turbulent behaviour.

Substantiation: Validation Study 3.2.5 (Horizontal mixing layer).

Example(s) of application studies:
1. Stroomonderzoek Sluizen IJmuiden [Van Banning, 1995]
2. Numeriek modelonderzoek naar de reductie van de neer in de monding van de voorhaven van IJmuiden [Bijlsma, 2007]

Flows resulting from dam breaks

Claim 2.2.1.12: Delft3D-FLOW can be used for an accurate prediction of flows resulting from dam breaks.

Substantiation: Validation Study 3.2.4 (Two-dimensional dam break).

Example(s) of application studies:
1. A numerical method for every Froude number in shallow water flows, including large scale inundations. [Stelling and Duinmeijer, 2003]

2.2.2 Processes

This section further characterises the domain of applicability of the model. This is done by making claims about the individual physical processes represented in Delft3D-FLOW. The idea is to break down the physics into elements that are as simple as possible, yet still meaningful.

The information contained in this section supplements that in the previous section. It is intended to allow the reader to judge whether or not the model is suitable for his purpose, by considering separately the individual processes that play a role in the application he has in mind.

Delft3D-FLOW is able to represent a large number of processes, which are listed below:
- Propagation of long waves (barotropic flow) (See Section 2.2.2.1)
- Baroclinic flow, salinity, suspended sediment and temperature driven flow, including prognostic or diagnostic modelling (See Section 2.2.2.2)
- Transport of dissolved material and pollutants (See Section 2.2.2.3)
- Transport of sediments, including erosion, sedimentation and bed load transport (See Section 2.2.2.4)
- Propagation of short waves (See Section 2.2.2.5)
- Subcritical and supercritical flow (See Section 2.2.2.6)
- Steady and unsteady (time varying) flow (See Section 2.2.2.7)
- Drying and flooding of intertidal flats (See Section 2.2.2.8)
- The effect of the Earth's rotation (Coriolis force) (See Section 2.2.2.9)

- Turbulent mixing (See Section 2.2.2.10)
- Time varying sources and sinks; e.g. river discharges (See Section 2.2.2.11)
- Impact of space and time varying wind shear stress at the water surface (See Section 2.2.2.12)
- Impact of space varying shear stress at the bottom (See Section 2.2.2.13)
- Impact of space and time varying atmospheric pressure on the water surface (See Section 2.2.2.14)
- Heat exchange through the free surface, evaporation and precipitation (See Section 2.2.2.15)
- Wave driven currents (See Section 2.2.2.16)
- Impact of secondary flow on depth-averaged momentum equations (See Section 2.2.2.17)
- Barotropic tide generation (See Section 2.2.2.18)

In subsequent sections each process will be described in more detail.

Propagation of long waves

Description: For long waves (in shallow water) the vertical acceleration can be assumed to be negligible and the pressure to be hydrostatic. Under these assumptions the celerity of the wave only depends on gravity and water depth. It is also independent of the wave length. Relevant examples of long waves are tidal waves. The free surface gradients represent so-called barotropic flow. A special surface gradients generated by of long waves are the surges along coasts generated by wind (storm surge modelling).

Claim 2.2.2.1: Delft3D-FLOW can accurately simulate the propagation of long waves.

Substantiation: Validation Study 3.1.2 (Standing wave);

Example(s) of application studies:

1. Tidal propagation for the North Sea [Gerritsen and Verboom, 1994; Gerritsen and Bijlsma, 1988; Gerritsen et al., 1995)]
2. Irish Sea Model [Hulsen, 1989]
3. South China Sea Model [Gerritsen et al., 2000;Schrama, 2002, Twigt et al., 2007]
4. Tide in the Westerschelde estuary [Wang et .al., 2002]

Baroclinic flow - salinity and temperature driven flow

Description: Baroclinic flow is the result of varying density in horizontal direction, due to salinity and or temperature differences. The salinity and temperature can either be model variables in their own (fully baroclinic flow), or can be prescribed as fixed distributions (diagnostic flow).

Claim 2.2.2.2: Delft3D-FLOW can accurately simulate density driven (or baroclinic) flows.

Substantiation: Validation Study 3.1.5 (Lock exchange flow with hydrostatic pressure or non-hydrostatic pressure).
Validation Study 3.2.1 (Salt intrusion in laboratory flume)
Validation Study 3.2.6 (Salt intrusion in 3D Numerical Scale Model with σ-coordinates of an estuary)
Validation Study 3.2.7 (3D Numerical Scale Model with υ-coordinates and HLES for the complex exchange flow between a tidal dock and the estuary)
Validation Study 3.4.1 (3D σ-model of the North Sea)
Validation Study 3.4.3 (3D Z-model of Lake Grevelingen)
Validation Study 3.4.4 (3D Z-model of Sea of Marmara)
Validation Study 3.4.5 (3D σ-model of the South China Sea)

Transport of dissolved material and pollutants

Description: In estuaries and coastal seas spreading of dissolved material and suspended sediment which moves with the flow.

Claim 2.2.2.3: Delft3D-FLOW can accurately simulate the (advective and diffusive) transport of dissolved material, suspended sediment and pollutants.

Substantiation: Validation Study 3.2.6 (Numerical scale model of an estuary).
Validation Study 3.2.7 (Numerical scale model of an estuary and a tidal dock).

Example(s) of application studies:
1. Suspended sediment modelling in a shelf sea ([Gerritsen et al., 2000]

Transport of sediments, including erosion, sedimentation and bed load transport

Description: Transport of suspended sediment contributes to a large amount to the total sediment transport in estuaries and coastal seas. In the stratified and/or gradient zone of an estuary a turbidity maximum, formed by accumulation of suspended sediments, is a common phenomenon.

Claim 2.2.2.4: Delft3D-FLOW can accurately simulate the transport of sediment, both in horizontal and vertical direction including deposits (deposition) and uptake (erosion) at the water-bottom interface.

Substantiation: Validation Study 3.1.9 (Equilibrium slope for a straight channel).
Validation Study 3.3.7 (migrating trench in a 1D channel)

Example(s) of application studies:
1. Suspended sediment modelling in a shelf sea ([Gerritsen et al., 2000]

Reference: **[**WL | Delft Hydraulics, 1994]

Propagation of short waves

Description: For short waves the vertical acceleration of the fluid can no longer be neglected and the pressure is non-hydrostatic. The celerity of the wave then depends on gravity, water depth as well as wave length.

Claim 2.2.2.5: Delft3D-FLOW can accurately simulate the propagation of short waves.

Substantiation: Validation Study 3.1.5 (Lock exchange flow);
Validation Study 3.2.2 (Water elevation in a wave flume).

Subcritical and supercritical flow

Description: In shallow water flow different flow regimes occur, such as subcritical or supercritical flows. Supercritical flow e.g. occurs near hydraulic structures such as weirs and barriers or are generated by sills on the bottom, or during flooding of an initial dry bed (dam break problem).

Claim 2.2.2.6: Delft3D-FLOW can accurately simulate subcritical and supercritical flows and the transition region when the flow changes from subcritical to supercritical or vice versa. Such conditions may e.g. occur in case of hydraulic jumps.

Substantiation: Validation Study 3.2.4 (One-dimensional dam break);
Validation Study 3.2.8 (Two-dimensional dam break).

Reference: A numerical method for every Froude number in shallow water flows, including large scale inundations. [Stelling and Duinmeijer, 2003]

Steady and unsteady flow

Description: The Delft3D-FLOW system has been developed for simulating unsteady shallow water flow. However, the system can also be used for simulating steady state systems. In particular, this is relevant for river applications, which often are modelled with steady boundary conditions as forcing. The boundary conditions determine the steady state solution, while the initial conditions determine the spinning up period of the model.

Claim 2.2.2.7: Delft3D-FLOW can accurately simulate steady and unsteady flow.

Substantiation: All validation studies are relevant to this claim.

Drying and flooding of intertidal flats

Description: In estuaries and coastal seas with significant tidal range quite often vast areas of land (tidal fiats) are subsequently covered and uncovered with water during each tidal cycle.

Claim 2.2.2.8: Delft3D-FLOW can accurately simulate drying and flooding of tidal areas.

Substantiation: Validation Study 3.2.4 (1D dam break).
Reference(s): **[**Vatvani et al., 2002], [Stelling and Duinmeijer, 2003].

The effect of the Earth's rotation (Coriolis force)

Description: Earth rotation results in inclination of flows to the right on the northern hemisphere, and to the left on the southern hemisphere. The Coriolis parameter f depends on the geographic latitude and the angular speed of rotation of the earth, Ω: $f = 2\Omega \sin\phi$. This results in an inclination of the flow direction, which varies with the depth and also depends on the latitude.

Claim 2.2.2.9: Delft3D-FLOW can take into account the impact of the Coriolis force arising from the rotation of the earth.

Substantiation: Validation Study 3.1.8 (Coriolis testcase).

Turbulent mixing including Internal Wave Model

Description: Vertical mixing processes, which determine salinity or temperature stratification, are the result of small-scale turbulence flow properties, which are determined by adding an accurate (vertical) turbulence model.

Claim 2.2.2.10: In Delft3D-FLOW turbulent exchange of momentum and mass in the vertical direction can be modelled with increasing complexity: constant viscosity/diffusivity (one equation turbulence model), the k-L model, (two equations turbulence model) and the k-ε model. Similarly, in horizontal direction a constant viscosity, or space varying (and time constant) viscosity or a space and time varying viscosity can be applied or a turbulent closure coefficient that is flow and grid size dependent (Horizontal Large Eddy Simulation (HLES) model).

Furthermore, in Delft3D-FLOW there is a formulation for the vertical exchange of momentum due to breaking of internal waves. The formulation for the internal-wave-induced mixing of momentum is determined using an additional transport equation for Internal Wave Energy (IWE-model). The IWE model describes the energy transfer from internal waves to turbulence as well as the excitation of internal waves by turbulence.

Substantiation Validation Study 3.2.3 (Vertical mixing layer);

Example(s) of application studies:
1. Complex flow around groynes [Van Schijndel and Jagers, 2003] ([Gerritsen et al., 2000]
2. Complex flow due to Maasvlakte 2 [Bijlsma et al., 2003]

Time varying sources and sinks; e.g. river discharges

Description: Time varying forces and discharges or withdrawals can have a significant effect on the flow, for example, on the stratification in a water system. Examples are time varying river discharges or discharges from outfalls.

Claim 2.2.2.11: Delft3D-FLOW can take into account time varying sources and sinks for e.g. river flows and discharges from outfalls.

Substantiation: Validation Study 3.4.1 (3D North Sea)

Example(s) of application studies:
1. Spreading of the Rhine plume along the Dutch Coast [De Kok et al., 2001]

Impact of space and time varying wind shear stress at the water surface

Description: Wind causes a wind stress at the free surface, which can yield a considerable set-up in the water elevation. Storm surge modelling is also an example of space and time varying wind stresses.

Claim 2.2.2.12: Delft3D-FLOW can accurately simulate the effects of space and time varying wind stresses at the free water surface.

Substantiation: Validation Study 3.1.4 (Wind driven flow);
Validation Study 3.4.3 (Sea of Marmara).

Example(s) of application studies:
1. Generation and dissipation of storm surges in the North Sea [Bijlsma, 1988]
2. Typhoon driven storm surges in the South China Sea [Kernkamp e.a., 2004]

Impact of space varying shear stress at the bottom

Description: Especially in shallow area the bottom roughness plays an important role when computing the water elevation or currents. The bed stress may be the combined effect of flow and waves. For 2D depth-averaged flow the shear-stress at the bed induced by a turbulent flow is assumed to be given by a quadratic friction law based on the depth-averaged current. The bed shear stress in 3D is related to the current just above the bed.

Claim 2.2.2.13: Delft3D-FLOW can take into account the impact of the space varying shear stress at the bottom. Several formulations are possible (Chezy, Manning, White-Colebrook or roughness height Z0). The input coefficients for bottom friction can vary in space.

Substantiation: Validation Study 3.1.6 (Wave force and a mass flux in a closed basin).

Impact of space and time varying atmospheric pressure on the water surface

Description: In particular for storm surge modelling, space and time varying atmospheric pressure fields are used, which should be consistent with the wind fields. If the wind and pressure distributions in the wind and pressure fields are not sufficiently accurately due to smoothing (too coarse grid for meteorological data) one may use an analytically prescribed distribution of the cyclone wind and pressure fields to force the flow with a spatially detailed ("enhanced") wind field for the cyclone [Vatvani et al.., 2002, Gerritsen, 1988].

Claim 2.2.2.14: Based on an accurate space and time varying wind and pressure fields as input, Delft3D-FLOW can compute accurate storm surges.

Substantiation: Validation Study 3.4.3 (Sea of Marmara)

Example(s) of application studies:

1. Generation and dissipation of storm surges in the North Sea [Gerritsen en Bijlsma, 1988, Bijlsma 1988]
2. Cyclone flood forecasting model for India [Vatvani, 2002]

Heat exchange through the free surface, evaporation and precipitation

Description: The heat radiation emitted by the sun reaches the earth in the form of electromagnetic waves with wavelengths in the range of 0.15 to 4 μm. In the atmosphere the radiation undergoes scattering, reflection and absorption by air, cloud, dust and particles. On average neither the atmosphere nor the earth accumulates heat, which implies that the absorbed heat is emitted back again. The wavelengths of these emitted radiations are longer (between 4 and 50 μm) due to the lower prevailing temperature in the atmosphere and on Earth.

Claim 2.2.2.15: In Delft3D-FLOW the heat exchange at the free surface is accurately modelled by taking into account the separate effects of solar (short wave) and atmospheric (long wave) radiation, and heat loss due to back radiation, evaporation and convection.

Substantiation: Validation Study 3.4.1 (North Sea Model, 3D σ-model);
Validation Study 3.4.3 (Zegerplas, 3D Z-model and 3D σ-model);
Validation Study 3.4.3 (Sea of Marmara, 3D Z-model);
Validation Study 3.4.4 (Lake Grevelingen, 3D Z-model);
Validation Study 3.4.5 (South China Sea, 3D σ-model)

Reference(s): **[**De Goede et al., 2000]

Wave driven currents

Description: In relatively shallow areas (coastal seas), wave action can become important. For example, vertical mixing processes are enhanced due to turbulence generated near the surface by whitecapping and wave breaking, and near the bottom due to energy dissipation in the bottom layer. Moreover, in the surf zone long-shore currents and a cross-shore set-up is generated due to variations in the wave-induced momentum flux (radiation stress). In case of an irregular surf zone, bathymetry strong circulations may be generated (rip currents).

Claim 2.2.2.16: Delft3D-FLOW can take into account wave and wave-induced effects by coupling with wave models. In Delft3D-FLOW coupling with two wave models are operational: HISWA, a second generation wave model (Holthuijsen, 1998) and SWAN, a third generation wave model (Ris, 1997).

Substantiation: Validation Study 3.1.6 (Wave force and a mass flux in a closed basin).

Reference: **[**Walstra et al., 2000]

Impact of secondary flow on depth-averaged momentum equations

Description: The flow in a river bend is basically three-dimensional. The velocity has a component in the plane perpendicular to the river axis. This component is directed to the inner bend near the riverbed and directed to the outer bend near the water surface. This so-called "secondary flow" (or spiral motion) is of importance for the computation of changes of the riverbed in morphological models and of the dispersion of matter. In a 3D model the secondary flow is resolved on the vertical grid, but in 2D depth-averaged simulations the secondary flow has to be parameterized in some way.

Claim 2.2.2.17: Delft3D-FLOW can take into account the impact of secondary flow in a depth-averaged model. This is done by adding a term in the momentum equations.

Substantiation: Not in list of validation studies yet.

Barotropic tide generation

Description: Numerical models of tidal motion in coastal seas generally do not account for the direct local influence of the tide generating forces. The amount of water mass in these models is relatively small and the effect of these forces on the flow can be neglected. For coastal areas, the prescription of tidal forcing along open boundaries is sufficient in generating the appropriate and accurate tidal motion. However, the need to model larger seashore areas with sections of the deep ocean has increased. In the numerical models of such very large areas the contribution of the gravitational forces on the water motion increases considerably and can no longer be neglected. The tide generating forces originate from the Newtonian gravitational forces of the terrestrial system (Sun, Moon and Earth) on the water mass.

Claim 2.2.2.18: Delft3D-FLOW can take into account tide generating forces when simulating very large scale water systems.

Substantiation: Not in list of validation studies yet.

Example(s) of application studies:

1. Tidal model validation of the seas of South-East Asia [Gerritsen et al., 2003]

2.3 Conceptual model

This section describes technical aspects of the conceptual model that are relevant to the validation process. In particular, it addresses the simplifications and assumptions of the conceptual model compared to the actual physical world.

2.3.1 Governing equations

The shallow water equations for hydrostatic flow

The governing three-dimensional equations describing free-surface flows can be derived from the Navier-Stokes equations after averaging over turbulence time-scales (Reynolds-averaged Navier-Stokes equations). Such equations express the physical principle of conservation of volume, mass and momentum.

In this section we describe the shallow water equations, for which the depth is assumed to be much smaller than the horizontal length scales of flow and bathymetry. Under the further assumption that the vertical accelerations are small compared to the horizontal ones the shallow water assumption is valid. This means that the vertical momentum equation is reduced to the *hydrostatic pressure* relation. The equations in case of a *non-hydrostatic pressure* are described in a separate section. In the latter case non-hydrostatic pressure terms are added to the shallow water equations, which make the equations practically equivalent to the incompressible Navier-Stokes equations. This means that in Delft3D-FLOW the user has the possibility to either apply a hydrostatic or a non-hydrostatic pressure model.

The three-dimensional hydrostatic shallow water equations, which for convenience of presentation are given in Cartesian rectangular coordinates in the horizontal and σ-coordinates in the vertical, are described by:

$$\frac{\partial u}{\partial t}+u\frac{\partial u}{\partial x}+v\frac{\partial u}{\partial y}+\frac{\omega}{d+\zeta}\frac{\partial u}{\partial \sigma}-fv=-\frac{1}{\rho}P_u+F_u+\frac{1}{(d+\zeta)^2}\frac{\partial}{\partial \sigma}\left(\nu_V\frac{\partial u}{\partial \sigma}\right) \qquad (2.3.1.1)$$

$$\frac{\partial v}{\partial t}+u\frac{\partial v}{\partial x}+v\frac{\partial v}{\partial y}+\frac{\omega}{d+\zeta}\frac{\partial v}{\partial \sigma}+fu=-\frac{1}{\rho}P_v+F_v+\frac{1}{(d+\zeta)^2}\frac{\partial}{\partial \sigma}\left(\nu_V\frac{\partial v}{\partial \sigma}\right) \qquad (2.3.1.2)$$

$$\frac{\partial \omega}{\partial \sigma}=-\frac{\partial \zeta}{\partial t}-\frac{\partial[(d+\zeta)u]}{\partial x}-\frac{\partial[(d+\zeta)v]}{\partial y}+H(q_{in}-q_{out})+P-E \qquad (2.3.1.3)$$

The vertical velocities ω in the σ-coordinate system are computed from the continuity equation

$$\frac{\partial \zeta}{\partial t}+\frac{\partial[(d+\zeta)U]}{\partial x}+\frac{\partial[(d+\zeta)V]}{\partial y}=Q \qquad (2.3.1.4)$$

by integrating in the vertical from the bottom to a level σ ($-1\le\sigma\le 0$). The (comparatively small) vertical velocity w in the x-y-z Cartesian coordinate system can be expressed in the horizontal velocities, water depths, water levels and vertical σ-velocities according to:

$$w = \omega + u\left(\sigma\frac{\partial H}{\partial x} + \frac{\partial \zeta}{\partial x}\right) + v\left(\sigma\frac{\partial H}{\partial y} + \frac{\partial \zeta}{\partial y}\right) + \left(\sigma\frac{\partial H}{\partial t} + \frac{\partial \zeta}{\partial t}\right)$$

In Eq. (2.3.1.4), Q represents the contributions per unit area due to the discharge or withdrawal of water, precipitation and evaporation:

$$Q = H\int_{-1}^{0}\left(q_{in} - q_{out}\right)d\sigma + P - E\ ,$$

In Eqs. (2.3.1.1-4) *u(x,y, σ,t,), v(x,y, σ,t)* and *ω(x,y, σ,t)* are the velocity components in the horizontal *x, y* and vertical σ-directions, respectively; *ζ(x,y)* is the water level above a reference plane; *d(x,y)* is the depth below this plane; *H(x,y)=d(x,y)+ζ(x,y)* is the total water depth, *t* is the time; *f* is the Coriolis parameter; *g* is the gravitational acceleration and ν_v is the vertical eddy viscosity coefficient. Furthermore q_{in} and q_{out} are the local sources and sinks of water per unit of volume (1/s), respectively, P represents the non-local source term of precipitation and E non-local sink term due to evaporation. We remark that the intake of, for example, a power plant is a withdrawal of water and should be modelled as a sink. At the free surface there may be a source due to precipitation or a sink due to evaporation.

From now, it is assumed that ν_v can be prescribed as a non-negative function of space and time (often a constant) and that no specific closure model is required. In later paragraphs the turbulence closure models in Delft3D-FLOW are described, which determine ν_v. The horizontal pressure terms P_u and P_v are described in (2.3.1.8), the horizontal viscosity terms F_u and F_v in (2.3.1.9). Equations (2.3.1.1) and (2.3.1.2) are the momentum equations, whereas the (depth-integrated) continuity equation is described in (2.3.1.4). The depth averaged velocities read

$$U = \int_{-1}^{0} u\,d\sigma' \qquad , \qquad V = \int_{-1}^{0} v\,d\sigma'$$

In the vertical direction a scaled coordinate,

$$\sigma = \frac{z - \zeta}{\zeta + d} \tag{2.3.1.5}$$

the so-called σ-coordinate is used, introduced in (Phillips, 1957). At the bed σ=-1 and at the free surface σ=0. The σ-coordinate system is boundary fitted in the vertical plane.

By integration of the equations (2.3.1.1)-(2.3.1.2) from the bottom to the free surface we arrive at the 2D (depth averaged) momentum equations, which are described in Eq. 2.3.1.25. We remark that the continuity equation (2.3.1.4) already uses depth-averaged velocities.

Barotropic and baroclinic effects

The hydrostatic pressure is given by:

$$P = P_{atm} + gH\int_{\sigma}^{O} \rho(x,y,\sigma',t)d\sigma' \tag{2.3.1.6}$$

For water of constant density ρ, the pressure gradients in the horizontal momentum equations can be written as:

$$\frac{1}{\rho} P_u = g \frac{\partial \zeta}{\partial x} \ , \qquad \frac{1}{\rho} P_v = g \frac{\partial \zeta}{\partial y} \tag{2.3.1.7}$$

In case of a non-uniform density, Leibnitz' rule is used to obtain the following expressions for the horizontal pressure gradients:

$$\frac{1}{\rho} P_u = g \frac{\partial \zeta}{\partial x} + g \frac{d+\zeta}{\rho_0} \int_\sigma^0 \left(\frac{\partial \rho}{\partial x} + \frac{\partial \sigma}{\partial x} \frac{\partial \rho}{\partial \sigma} \right) d\sigma' \tag{2.3.1.8}$$

$$\frac{1}{\rho} P_v = g \frac{\partial \zeta}{\partial y} + g \frac{d+\zeta}{\rho_0} \int_\sigma^0 \left(\frac{\partial \rho}{\partial y} + \frac{\partial \sigma}{\partial y} \frac{\partial \rho}{\partial \sigma} \right) d\sigma'$$

with ρ_0 the ambient density of water. In (2.3.1.8) the first term in the right-hand side represents the barotropic effect, whereas the second term describes the baroclinic influence. In (2.3.1.8) the density variations are neglected except in the buoyancy term. This is known as the Boussinesq approximation.

Horizontal viscosity

The forces F_u and F_v in the momentum equations (2.3.1.1-2) represent the horizontal Reynolds stresses. In Delft3D-FLOW, however, for F_u and F_v a simplified version of the above-described formulations is applied, see [Mellor and Blumberg, 1985]. The formulation reads

$$F_u = \nu_H \left(\frac{\partial^2 u}{\partial x^2} + \frac{\partial^2 u}{\partial y^2} \right) \tag{2.3.1.9}$$

$$F_v = \nu_H \left(\frac{\partial^2 v}{\partial x^2} + \frac{\partial^2 v}{\partial y^2} \right)$$

in which the gradients are taken along σ-planes (planes of constant σ-value).

The equations for non-hydrostatic flow

The application of three-dimensional hydrostatic shallow water models for understanding and assessing free surface flows has become widely used in the past decades. In most of these cases the flows are of boundary layer type, which means that the vertical acceleration component is relatively small. Under these circumstances, the pressure distribution in the vertical is assumed to be hydrostatic, and hence the hydrodynamic part of the pressure may be neglected. This yields the shallow water equations, which have been described in the previous section.

For many small scale flows such as over abruptly changing bottom topography, orbital movements in short wave motions, or intensive vertical circulations the vertical acceleration can not be neglected and the non-hydrostatic pressure component is important. The requirements for shallow-water flow are no longer met, and the hydrodynamic component

of the pressure has to be resolved in order to get physically realistic flow patterns. Delft3D-FLOW incorporates such a non-hydrostatic model. Note that the non-hydrostatic functionality is only available for the z-coordinate model and not for the σ grid system (see Section 1.1.4 for a description of the vertical grid systems).

Non-hydrostatic equations
In case of a non-hydrostatic model, the momentum equations of the Reynolds-averaged Navier-Stokes equations may be written as:

$$\frac{\partial u}{\partial t}+u\frac{\partial u}{\partial x}+v\frac{\partial u}{\partial y}+w\frac{\partial u}{\partial z}-fv=-\frac{1}{\rho}P_u+F_u-\frac{\partial q}{\partial x}+\frac{1}{(d+\zeta)^2}\frac{\partial}{\partial z}\left(\nu_V\frac{\partial u}{\partial z}\right) \qquad (2.3.1.10)$$

$$\frac{\partial v}{\partial t}+u\frac{\partial v}{\partial x}+v\frac{\partial v}{\partial y}+w\frac{\partial v}{\partial z}+fu=-\frac{1}{\rho}P_v+F_v-\frac{\partial q}{\partial y}+\frac{1}{(d+\zeta)^2}\frac{\partial}{\partial z}\left(\nu_V\frac{\partial u}{\partial z}\right) \qquad (2.3.1.11)$$

$$\frac{\partial w}{\partial t}+u\frac{\partial w}{\partial x}+v\frac{\partial w}{\partial y}+w\frac{\partial w}{\partial z}=-\frac{1}{\rho}P_w+F_w-\frac{\partial q}{\partial z}+\frac{1}{(d+\zeta)^2}\frac{\partial}{\partial z}\left(\nu_V\frac{\partial w}{\partial z}\right) \qquad (2.3.1.12)$$

with

$$F_w=\nu_H\left(\frac{\partial^2 w}{\partial x^2}+\frac{\partial^2 w}{\partial y^2}\right) \qquad (2.3.1.13)$$

The pressure terms have been split into a hydrostatic part (see Eq. (2.3.1.6)) and a non-hydrostatic part *q*. The non-hydrostatic is computed via a so-called pressure correction step. This requires the solution of a Poisson-type equation. The continuity equation is given by Eq. (2.3.1.4), which is valid for the σ-model as well.

The transport equations

The flows in rivers, estuaries and coastal seas often transport dissolved substances, salinity and/or heat. In Delft3D-FLOW the transport of matter and heat is modelled by an advection-diffusion equation in three co-ordinate directions. Source and sink terms are included to simulate discharges and withdrawals. First-order decay processes may be taken into account as well. A first-order decay process corresponds to a situation in which the concentration is exponentially decreasing. Note that for more complex processes e.g. eutrophication, biological and/or chemical processes, the water quality module Delft3D-WAQ should be used.

The transport equation formulated in a conservative form in Cartesian co-ordinates in the horizontal and in σ coordinates in the vertical, reads:

$$\frac{\partial[(d+\zeta)C]}{\partial t}+\frac{\partial[(d+\zeta)\mathrm{u}C]}{\partial x}+\frac{\partial[(d+\zeta)\mathrm{v}C]}{\partial y}+\frac{\partial(\omega C)}{\partial\sigma}= \qquad (2.3.1.14)$$

$$\left[\frac{\partial}{\partial x}\left(D_h(d+\zeta)\frac{\partial C}{\partial x}\right)+\frac{\partial}{\partial y}\left(D_h(d+\zeta)\frac{\partial C}{\partial y}\right)\right]+\frac{1}{d+\zeta}\frac{\partial}{\partial\sigma}\left[D_v\frac{\partial C}{\partial\sigma}\right]+-\lambda_d(d+\zeta)C+S$$

with λ_d representing the first-order decay process. S represents the source and sink terms

per unit area due to the discharge q_{in} or withdrawal q_{out} of water and the exchange of heat through the free surface Q_{tot}.:

$$S = \left(d + \zeta\right)\left(q_{in}C_{in} - q_{out}C\right) + Q_{tot}\,. \tag{2.3.1.15}$$

The turbulence closure models

Delft3D-FLOW solves the Navier-Stokes equations for an incompressible fluid. Usually the grid (horizontal and/or vertical) is too coarse and the time step too large to resolve all turbulence scales. The length scales of the turbulent processes are therefore of "sub-grid" scale. The primitive variables are space- and time-averaged (turbulence-averaged) quantities. This averaging or filtering of the equations leads to the need of appropriate closure assumptions for the non-linear terms.

The horizontal (ν_H) and vertical (ν_V) viscosity have to be prescribed. For 3D shallow water flow the stress and diffusion tensors are an-isotropic. The horizontal eddy viscosity coefficient ν_H and eddy diffusivity coefficient D_H are much larger than the vertical coefficients. In Delft3D-FLOW the horizontal viscosity is assumed to be a superposition of three parts: a part due to "sub-grid scale turbulence", a part due to "3D-turbulence" see [Uittenbogaard et al., 1992] and for depth-averaged simulations a part due to dispersion. In simulations with the depth-averaged momentum and transport equations, the redistribution of momentum and matter due to the vertical variation of the horizontal velocity is denoted as dispersion. In 2D simulation this dispersion is not simulated as the vertical profile of the horizontal velocity is not resolved. Then this dispersive effect may be modelled as the product of a viscosity coefficient and a velocity gradient.

The horizontal eddy-viscosity is mostly associated with the contribution of horizontal turbulent motions and forcing that are not resolved ("sub-grid scale turbulence") either by the horizontal grid or a priori removed by solving the Reynolds-averaged shallow-water equations. For the latter we introduce the horizontal eddy-viscosity υ_H^{back} and for the former the sub-grid scale (SGS) horizontal eddy-viscosity υ_{SGS}. For the latter, Delft3D-FLOW simulates the larger scale horizontal turbulent motions through a methodology called Horizontal Large Eddy Simulation (HLES). The associated horizontal viscosity coefficient υ_{SGS} will then be computed by a dedicated SGS-turbulence model. For details of this approach, see Section "Turbulence modelling in horizontal direction".

The 3D part υ_{3D} is referred to as the three-dimensional turbulence and in 3D simulations it is computed following a 3D-turbulence closure model. The background horizontal viscosity, user-defined through the input file, is represented by υ_H^{back}. Consequently, in Delft3D-FLOW the horizontal eddy-viscosity coefficient υ_H is defined by

$$\upsilon_H = \upsilon_{SGS} + \upsilon_{3D} + \upsilon_H^{back}\,, \tag{2.3.1.17}$$

For turbulence closure models responding to shear production only, it may be convenient to specify a background or "ambient" vertical mixing coefficient in order to account for all other forms of unresolved mixing. Therefore, in addition to all turbulence closure models in Delft3D-FLOW a constant (space and time) background mixing coefficient υ_H^{back} may be specified by you, which is a background value for the vertical eddy viscosity in the momentum equations (2.3.1.1) and (2.3.1.2). Consequently, the vertical eddy viscosity coefficient υ_V is defined by:

$$\upsilon_V = \upsilon_{mol} + \max(\upsilon_V^{back}, \upsilon_{3D}), \tag{2.3.1.18}$$

with υ_{mol} the kinematic viscosity of water. Summarizing, since in Delft3D-FLOW several combinations of horizontal and vertical eddy viscosity are optional, Table 2.1 below presents an overview.

model description	υ_{SGS}	υ_H^{back}	υ_{3D}	υ_V^{back}
2D, no HLES	-	2D-turbulence + dispersion coefficient	-	-
2D, with HLES	computed by HLES	3D-turbulence + dispersion coefficient	-	-
3D, no HLES	-	2D-turbulence	computed by vertical turbulence model.	background vertical viscosity
3D, with HLES	computed by HLES	-	computed by vertical turbulence model.	background vertical viscosity

Table 2.1 Overview of eddy viscosity options in Delft3D-FLOW

Remarks:

1. We note that the "background horizontal eddy viscosity" represents a series of complicated hydrodynamic phenomena. Table 2.1 shows that this background horizontal eddy viscosity υ_H^{back} either contains zero, one or two contributions.
2. The background horizontal eddy viscosity υ_H^{back} has to be specified by the user in the GUI in addition to the Elder formulation for 3D-turbulence and dispersion for 2D simulations.
3. It is important to emphasize that the under limit of vertical eddy viscosity υ_V^{back} is only used in the momentum equations (see Eqs. 2.3.1.1 and 2.3.1.2) and is not used in the vertical turbulence models (see for example Eqs. (2.3.20a-b).

Modelling 3D turbulence in vertical direction

Four turbulence closure models have been implemented in Delft3D-FLOW to determine the 3D-turbulence eddy viscosity coefficient ν_{3D} and the vertical eddy diffusivity coefficient D_{3D}:

1. Constant coefficient;
2. Algebraic eddy viscosity closure model;
3. $k-L$ turbulence closure model (1-equation model);
4. $k-\varepsilon$ turbulence closure model (2-equation model).

The turbulence closure models differ in their prescription of the turbulent kinetic energy *k*, the dissipation rate of turbulent kinetic energy ε, and/or the mixing length *L*.

The first turbulence closure model is the simplest closure based on a constant value which has to be specified by the user. We remark that a constant eddy viscosity will lead to parabolic vertical velocity profiles (as in laminar flow). The other three turbulence closure models are based on the so-called eddy viscosity concept of Kolmogorov and Prandtl [Kolmogorov, 1942; Prandtl, 1945]. The eddy viscosity is related to a characteristic length scale and velocity scale. The eddy viscosity has the following form:

$$\nu_V = c_\mu' L\sqrt{k}\,, \tag{2.3.1.19}$$

in which c_μ' is a constant determined by calibration, derived from the empirical constant c_μ in the $k-\varepsilon$ model; $c_\mu' = c_\mu^{1/4}$, $c_\mu = 0.09$ [Rodi, 1984].

k-ε turbulence model

In the k-ε model, which is a second-order turbulence closure model, the turbulent energy k and dissipation ε are calculated by the following transport equations:

$$\frac{\partial k}{\partial t} + u\frac{\partial k}{\partial x} + v\frac{\partial k}{\partial y} + \frac{\omega}{d+\zeta}\frac{\partial k}{\partial \sigma} = \frac{1}{(d+\zeta)^2}\frac{\partial}{\partial \sigma}\left(D_v\frac{\partial k}{\partial \sigma}\right) + P_k + B_k - \varepsilon \tag{2.3.1.20a}$$

$$\frac{\partial \varepsilon}{\partial t} + u\frac{\partial \varepsilon}{\partial x} + v\frac{\partial \varepsilon}{\partial y} + \frac{\omega}{d+\zeta}\frac{\partial \varepsilon}{\partial \sigma} = \frac{1}{(d+\zeta)^2}\frac{\partial}{\partial \sigma}\left(D_v\frac{\partial \varepsilon}{\partial \sigma}\right) + P_\varepsilon + B_\varepsilon - c_{2\varepsilon}\frac{\varepsilon^2}{k} \tag{2.3.1.20b}$$

For a detailed description of the turbulence models in Delft3D-FLOW, we refer to (WL | Delft Hydraulics, 2007).

Turbulence modelling in horizontal direction

Two types of turbulence closure models have been implemented to determine the horizontal viscosity coefficient ν_{2D} and the eddy diffusivity coefficient D_{2D}:

1. A constant or space-varying coefficient, which has to be specified by the user via the Delft3D-FLOW Graphical User Interface.
2. A subgrid-scale closure or Horizontal Large Eddy Simulation (HLES) model, which computes the horizontal viscosity coefficient and the eddy diffusivity coefficient.

The horizontal viscosity coefficient ν_H and (constant) eddy diffusivity coefficient D_H are generally also needed to damp small-scale noise introduced by the advection terms. They must be chosen dependent on the grid size. Usually, the horizontal coefficients are an order of magnitude larger than the vertical coefficients determined by the turbulence closure model in vertical direction.

Below we summarise the essential aspects of the sub-grid scale model for Horizontal Large Eddy Simulation (HLES) of shallow water flows subjected to bed friction. The result of this HLES model is a formulation of the horizontal component of the sub-grid eddy viscosity and the sub-grid eddy diffusivity.

Horizontal Large Eddy Simulation (HLES) model

The HLES model is based on theoretical considerations presented by [Uittenbogaard, 1998] and summarised in [Uittenbogaard and Van Vossen, 2003]. This model for the sub-grid eddy viscosity ν_{xx} includes the damping of sub-grid eddies by bed friction reads:

$$\upsilon_{xx} = \frac{1}{k_s^2}\left(\sqrt{\left(\gamma\sigma_T S^*\right)^2 + B^2} - B\right) \tag{2.3.1.21}$$

with:

$$B = \frac{3g\left|\underline{U}\right|}{4HC^2} \tag{2.3.1.22}$$

where C is the Chézy coefficient and H is the total water depth. Correspondingly, the sub-grid eddy diffusivity Γ_{xx} for horizontal mixing of heat, salt, mud and dissolved constituents reads:

$$\Gamma_{xx} = \frac{\upsilon_{xx}}{\sigma_T}.$$

In Eq. (2.3.1.21) the sum of strain rates squared (i.e. double contraction of horizontal component of the strain rate tensor) reads:

$$\left(S^*\right)^2 = 2\left(\frac{\partial u^*}{\partial x}\right)^2 + 2\left(\frac{\partial v^*}{\partial y}\right)^2 + \left(\frac{\partial u^*}{\partial y}\right)^2 + \left(\frac{\partial v^*}{\partial x}\right)^2 + 2\frac{\partial u^*}{\partial y}\frac{\partial v^*}{\partial x}. \tag{2.3.1.23}$$

In Eq. (2.3.1.23) the superscript $(..)^*$ denotes fluctuating flow variables and these are defined through the following recursive high-pass filter operator [Bendat and Piersol, 1971]:

$$\psi^* = \psi_{n+1} - \overline{\psi}^t_{n+1}, \tag{2.3.1.24}$$

with:

$$\overline{\psi}^t_{n+1} = \left(1-a\right)\psi_{n+1} + a\overline{\psi}^t_n, \quad \overline{\psi}^t_0 = 0 \text{ and } a = \exp\left(-\Delta t/\tau\right),$$

in which Δt is the time step and τ is the relaxation time. In Eq. (2.3.1.24) ψ represents any of the velocity components *(u,v)*. For a more detailed description of the HLES model we refer to the User Manual of Delft3D-FLOW [WL | Delft Hydraulics, 2007].

The equations for depth-integrated flow

In case of a two-dimensional depth-averaged model, the momentum equations (2.3.1.1)-(2.3.1.2) reduce to

$$\frac{\partial U}{\partial t} + U\frac{\partial U}{\partial x} + V\frac{\partial U}{\partial y} + fV = -\frac{1}{\rho}P_u + \frac{\tau_{sx} - \tau_{bx}}{\rho(d+\zeta)} + F_u$$

$$\frac{\partial V}{\partial t} + U\frac{\partial V}{\partial x} + V\frac{\partial V}{\partial y} - fU = -\frac{1}{\rho}P_v + \frac{\tau_{sy} - \tau_{by}}{\rho(d+\zeta)} + F_v \qquad (2.3.1.25)$$

with the bed stresses

$$\frac{\tau_{bx}}{\rho} = \frac{gU\sqrt{U^2+V^2}}{C_{2D}^2} = c_f U\sqrt{U^2+V^2}\,, \quad \frac{\tau_{by}}{\rho} = \frac{gV\sqrt{U^2+V^2}}{C_{2D}^2} = c_f V\sqrt{U^2+V^2}$$

and the horizontal viscosity terms analoguous to Eq. (2.3.1.9). The depth-averaged continuity equation has already been described by (2.3.1.4) and does not depend on the dimensionality in the vertical direction, since it only contains the depth-averaged velocities *U* and *V*.

Online sediment and morphology

In Delft3D-FLOW three-dimensional transport of suspended sediment of different fractions is calculated by solving the three-dimensional advection-diffusion (mass-balance) equation for the suspended sediment fraction *l*:

$$\begin{aligned}&\frac{\partial c^{(\ell)}}{\partial t} + \frac{\partial uc^{(\ell)}}{\partial x} + \frac{\partial vc^{(\ell)}}{\partial y} + \frac{\partial\left(w - w_s^{(\ell)}\right)c^{(\ell)}}{\partial z} + \\ &\quad - \frac{\partial}{\partial x}\left(\varepsilon_{s,x}^{(\ell)}\frac{\partial c^{(\ell)}}{\partial x}\right) - \frac{\partial}{\partial y}\left(\varepsilon_{s,y}^{(\ell)}\frac{\partial c^{(\ell)}}{\partial y}\right) - \frac{\partial}{\partial z}\left(\varepsilon_{s,z}^{(\ell)}\frac{\partial c^{(\ell)}}{\partial z}\right) = 0,\end{aligned} \qquad (2.3.1.26)$$

The local flow velocities and eddy diffusivities are based on the results of the hydrodynamic computations. The three-dimensional transport of sediment is computed in exactly the same way as the transport of any other conservative constituent, such as salinity, heat, and constituents. Important additional processes of sediment over other constituents are, for example, the exchange of sediment between the bed and the flow, and the settling velocities $w_s^{(\ell)}$ of sediment under the action of gravity. The sediment transport formulation allows the combined use of cohesive and non-cohesive sediment. Other processes such as the effect that sediment has on the local mixture density, and hence on turbulence damping, can also be taken into account. In addition, if a net flux of sediment from the bed to the flow, or vice versa, occurs then the resulting change in the bathymetry should influence subsequent hydrodynamic calculations. The formulation of several of these processes is sediment-type specific. In particular, this applies for sand and mud. In this section we discuss some of the differences, in general terms only.

The full 3D sediment transport is computed without resorting to the use of equilibrium sediment concentration profiles. The variation of sediment transport in regions of accelerating and decelerating flow is accurately accounted for. The effects of density currents, stratification, and spiral flow are automatically taken into account without requiring any special parametric formulations. Typical time scales of the intended applications may range from those used in hydrodynamic simulations to some orders of magnitude longer, i.e. from hours to many years. Long morphological simulations are achieved by using a morphological time scale factor. Typical length scales can range from those of near field morphology such as local scour near the head of breakwaters to those of tidal inlets and estuaries and coastal areas.

For the sediment fractions one can select any mixture of “sand” and “mud”. Different formulas are used to calculate the fall velocity, erosion and sedimentation of each type of sediment. One can specify up to five sediment fractions in a single simulation. This means one can execute a simulation with, for example, more than one “sand” fraction, or a number of “sand” and “mud” sediment fractions present at any location. The simultaneous presence of multiple sediment fractions has implications to the computation of the local hindered fall velocity of any one sediment fraction as well as for the resulting mixture density.

In its standard form Delft3D-FLOW uses an empirical relation (Eckart, 1958) to adjust the density of water in order to take into account varying temperature and salinity. For sediment transport this relation is extended to include the density effect of sediment fractions in the fluid mixture. This is achieved by adding (per unit volume) the mass of all sediment fractions, and subtracting the mass of the displaced water. As a mathematical statement this translates as:

$$\rho_{mix}\left(S,c^{(\ell)}\right)=\rho_w\left(S\right)+\sum_{\ell=1}^{lsed}c^{(\ell)}\left(1-\frac{\rho_w\left(S\right)}{\rho_s^{(\ell)}}\right) \tag{2.3.1.27}$$

Horizontal density gradients (now also due to differences in sediment concentrations) can create density currents. Vertical density gradients can also have a significant effect on the amount of vertical turbulent mixing present.

The settling velocities $w_s^{(\ell)}$ for sand and mud are strongly different. In high concentration mixtures, the settling velocity of a single particle is reduced due to the presence of other particles. In order to account for this hindered settling effect we follow Richardson and Zaki (1954) and determine the settling velocity in a fluid-sediment mixture as a function of the sediment concentration and the non-hindered settling velocity:

$$w_s^{(\ell)}=\left(1-\frac{c_s^{tot}}{CSOIL}\right)^5 w_{s,0}^{(\ell)}\ , \tag{2.3.1.28}$$

in which $CSOIL$ is the reference density (input parameter), $w_{s,0}$ is the 'basic' sediment fraction specific settling velocity. The total mass concentration c_m^{tot} is the sum of the mass concentrations of the sediment fractions and is equal to

$$c_s^{tot} = \sum_{\ell=1}^{lsed} c^{(\ell)} . \qquad (2.3.1.29)$$

2.3.2 Assumptions and approximations

The following assumptions and approximations that have been introduced into the formulation of the conceptual model equations (2.3.1.1)-(2.3.1.29):

1. The **continuous medium** assumption.
2. The fluid (water) is assumed to be **incompressible**.
3. **Reynolds averaging –** use of equations which have been averaged over the time and length scales of turbulent fluctuations.
4. The **shallow water assumption**, which means that the depth is small compared to horizontal length scales and that vertical accelerations are assumed to be negligibly small compared to the gravitational acceleration. The vertical momentum equation is then reduced to the hydrostatic pressure relation.
5. The effect of variable density is only taken into account in the horizontal pressure gradient term (**Boussinesq approximation**).
6. The **Eddy viscosity concept**, in which the Reynolds-stresses are parameterised by the product of a so called eddy-viscosity with the spatial gradient of the mean quantities.
7. In a Cartesian frame of reference (model domains smaller than ~ 500 by 500 km^2) and applications at moderate latitude ($|\Phi| > 40^\circ$) the **Coriolis** parameter may be assumed to be uniform and the effect of the Earth's curvature is not taken into account.
8. The horizontal turbulent stresses at the surface and sea bed (**wind and bottom friction**) are parameterised as quadratic friction terms, representing momentum transfer (drag) from the atmosphere and momentum removal, respectively.
9. The **gravitational acceleration** is taken as uniform.
10. The immediate effect of **buoyancy on vertical acceleration** is not considered in the hydrostatic version. In Delft3D-FLOW density differences are taken into account in the horizontal pressure gradients and in the vertical exchange coefficients. In order to take into account such effects, the non-hydrostatic option of Delft3D-FLOW should be switched on. However, real-world applications with Delft3D-FLOW lead to a computational effort that are not feasible yet, which is due the small horizontal mesh sizes (namely in the order of the vertical mesh size) that are required in such applications..
11. The part of the **horizontal eddy viscosity** due to 2D turbulence is flow independent and must be specified by the user, unless the HLES approach is used.
12. The **curvature of the grid** in both the horizontal and the vertical plane is neglected for the horizontal turbulent stresses.

2.3.3 Claims and substantiations

This section serves to account for the choices that were made in formulating the conceptual model, that is, the assumptions and approximations listed in Section 2.3.2, and to explain the implications of those choices for applicability and/or accuracy.

Continuous medium assumption

According to [Malvern, 1969] the adjective continuous refers to the simplifying concept underlying the analysis: we disregard the molecular structure of matter and picture it without gaps or empty spaces. We suppose that all functions are continuous functions, except at a finite number of surfaces separating regions of continuity (e. g. free surface between water and air; interface between sea water and sea bed). This implies that the derivatives of the functions are continuous too.

Claim 2.3.3.1: This continuous medium assumption is valid as long as we are dealing with phenomena much larger in size than the free length of particles between successive collisions.

Substantiation: See [Malvern, 1969]. All validation studies of Chapter 3 are relevant to this claim.

Incompressibility

If a fluid is treated as incompressible the density of the fluid will depend on temperature and the concentration of dissolved substances but not on pressure. Under the assumption that a fluid element (volume) does neither exchange heat nor dissolved substances with its surroundings (isentropic deformation) the fluid can be regarded as incompressible [Batchelor, 1967] if the:

1. fluid particle velocity is much smaller than the speed of sound, and the
2. phase speed of the disturbances (e. g. speed of the free surface waves) is also small compared to the speed of sound, and the
3. vertical scale of motion (water depth) must be small compared to a mean value of $\rho/(d\rho/dz)$.

Claim 2.3.3.2: The above described incompressibility assumptions are normally valid for typical oceans and estuaries and therefore the incompressibility condition can be applied together with a simplified equation of state. Precisely spoken this means that volume rather than mass is conserved. Therefore, effects like thermal expansion cannot be simulated with Delft3D-FLOW.

Substantiation: See [Batchelor, 1967]. All validation studies of Chapter 3 are relevant to this claim.

Reynolds averaging

For almost all practical applications it is impossible to solve for the detailed (turbulent) velocities in rivers, estuaries, coastal seas and other similar water bodies. Around 1880 Reynolds suggested the first time, to split the variables u, v, w and p into a mean and a fluctuating component. After insertion into the Navier-Stokes equations and subsequent time- averaging we obtain the Reynolds-Averaged Navier-Stokes equations (RANS). They contain new terms, the so-called Reynolds-stresses, which describe the mean momentum transfer due to turbulence. The solutions to these equations can be obtained by making

special assumptions about the nature of these Reynolds stress terms (turbulence closure), see also Claim 2.3.3.4 below.

Claim 2.3.3.3: For practical applications it is impossible to solve for the detailed turbulent velocities in rivers, estuaries, coastal seas and other similar water bodies. Moreover, in the far majority of hydrodynamic studies it is sufficient to take into account the mean behaviour of the turbulent quantities and therefore Reynolds-averaging is justified.

Substantiation: All validation studies of Chapter 3 are relevant to this claim.

Shallow water assumption

For many civil engineering flow and transport applications in rivers, estuaries, coastal seas, the horizontal dimensions and scales are several orders of magnitude larger than the vertical ones, and vertical accelerations negligible with respect to gravitation. Neglecting the vertical accelerations leads to the so-called hydrostatic shallow water equations.

Claim 2.3.3.4a: For hydrodynamic processes in which the length scales are much larger than the water depth, the shallow water equations accurately describe the physics of free surface flows.

Substantiation: In most rivers, estuaries, coastal waters and seas the horizontal dimensions and scales are much larger than the depth. Then, the shallow water assumption is valid, see [Pedlosky, 1979] and [Vreugdenhil, 1994].

Claim 2.3.3.4b: In situations such as flows over abruptly changing bottom topography, orbital movements in short wave motions, or intensive vertical circulations such as buoyant jet plumes, the shallow water assumption is no longer met. In such cases non-hydrostatic (Navier Stokes) equations should be applied to accurately describe free surface flows.

Substantiation: All validation studies of Chapter 3 are relevant to this claim.

Boussinesq approximation

In natural waters variations of density (ρ - ρ_0) are normally small compared with the reference density ρ_0.

Claim 2.3.3.5: If the density variations are fairly small, we can to a first approximation neglect their effect on the mass (i.e. inertia) of the fluid but we must retain their effect on the weight. That is, we include the buoyancy effects but neglect the variations in momentum changes due to mass variations with density.

Substantiation: The variations in momentum changes due to mass variations are at most 3 - 4 % when dealing with natural water bodies. Therefore, it is a valid approach to apply the Boussinesq approximation.

Eddy-viscosity concept

In the Boussinesq eddy-viscosity concept the Reynolds-stresses are parameterised by the product of a so called eddy-viscosity with the spatial gradient of the mean quantities. For simplicity the resulting eddy-viscosity tensor is assumed to be diagonal. The eddy-viscosity tensor depends on the state of the turbulent motion and has therefore to be determined by a separate turbulence model. Note that in Section 2.3.1 the turbulence models (both in horizontal and vertical direction) of Delft3D-FLOW have been described.

Claim 2.3.3.6a: The conceptual description of the turbulence models in Delft3D-FLOW (e.g., the eddy-viscosity concept, k-ε model, HLES model, etc.) is valid for tidal flows in rivers, estuaries and coastal seas.

Substantiation: Validation Study 3.2.3 (Vertical mixing layer); See also [Abbott, 1997] for a description of the ranges of common turbulence models.

Claim 2.3.3.6b: Delft3D-FLOW can also compute sub-grid scale or averaged 2D-turbulence. The computation is performed by the so-called Horizontal Large Eddy Simulation (HLES) approach.

Substantiation: Validation Study 3.2.5 (Horizontal plus vertical mixing layer).

Coriolis

The Coriolis term in the equation represents the influence on the flow exerted by the earth's rotation. The Coriolis parameter f depends on the geographic latitude and the angular speed of rotation of the earth, Ω: $f = 2\Omega \sin\phi$.

Claim 2.3.3.7: A space varying Coriolis parameter is a standard option for all Delft3D-FLOW applications. At moderate latitudes ($|\Phi| > 40^\circ$) and for relative small model dimensions (< ~500 by ~500 km) the Coriolis variation can be assumed constant. For larger model areas, or model areas close to the equator, full variation in *f* can be accounted for in Delft3D-FLOW.

Substantiation: Validation Study 3.1.8 (Coriolis testcase)

Wind and bottom friction

At the free surface the boundary conditions for the momentum equations are:

$$\left.\frac{\nu_H}{H}\frac{\partial u}{\partial \sigma}\right|_{\sigma=0} = \frac{1}{\rho_0}\left|\vec{\tau}_s\right|\cos(\theta), \tag{2.3.3.4}$$

$$\left.\frac{\nu_H}{H}\frac{\partial v}{\partial \sigma}\right|_{\sigma=0} = \frac{1}{\rho_0}\left|\vec{\tau}_s\right|\sin(\theta), \tag{2.3.3.5}$$

where θ is the angle between the wind stress vector and the local coordinate direction. Without wind the free surface stress is zero. The magnitude of the wind shear-stress is defined as:

$$\left|\vec{\tau}_s\right| = \rho_0 \vec{u}_{*s}\left|\vec{u}_{*s}\right|. \tag{2.3.3.6}$$

The magnitude is often determined by the following widely used quadratic expression:

$$\left|\vec{\tau}_s\right| = \rho_a C_d U_{10}^2 \tag{2.3.3.7}$$

in which U_{10} is the wind at 10 metre height. Delft3D-FLOW offers the possibility to prescribe either uniform or space varying wind. The latter is generally applied in combination with space and time varying atmospheric pressure.

At the sea bed, the boundary conditions for the momentum equations are:

$$\left.\frac{\nu_V}{H}\frac{\partial u}{\partial \sigma}\right|_{\sigma=-1} = \frac{\tau_{bx}}{\rho}; \qquad \left.\frac{\nu_V}{H}\frac{\partial v}{\partial \sigma}\right|_{\sigma=-1} = \frac{\tau_{by}}{\rho} \tag{2.3.3.8}$$

with τ_{bx} and τ_{by} the bed stresses in x- and y-direction, respectively. The bed stress may be the combined effect of flow and waves. In this section we restrict ourselves to the resistance due to flow only.

Claim 2.3.3.8: The parameterisations as described above are valid for free surface flows.

Substantiation: Validation Study 3.1.1 (Simple Channel flow).

Gravity

The gravitational acceleration g is not a constant but varies from place to place, which depends on the geographic latitude Φ. In Delft3D-FLOW the gravitational acceleration g can be specified by the user (via the input file). The default value is 9.81.

Claim 2.3.3.9: The gravitational acceleration g is assumed to be constant.

Substantiation: This assumption is valid for relatively small model domains (and e.g. not necessarily true for ocean models). Furthermore, the user can specify the gravitational acceleration g via the GUI of Delft3D-FLOW. This means that values in the order of 9.78 near the equator to 9.83 near the poles can be applied.

2.4 Algorithmic implementation

This section describes the technical aspects of the algorithmic implementation (or discretised version) of the conceptual model that are relevant to the validation process. This section contains claims about the validity of the algorithmic implementation, and statements about the substantiation of those claims. Several items with respect to the algorithmic implementation are discussed.

The Alternating Direction Implicit solution technique used in Delft3D-FLOW has as consequence that the Algorithmic Implementation (the discretisation of the model equations) and the Software Implementation (the time stepping solution technique) are strongly linked. We have chosen to treat these issues together in this section, and discuss the claims and substantiations accordingly, instead of describing all claims and substantiations in separate sections.

2.4.1 General

Following [Stelling, 1984], a robust space and time discretisation scheme for the shallow water equations has to satisfy the following demands:

- Robustness (unconditionally stable).
- Accuracy (at least second-order).
- Suitable for both time-dependent and steady state problems.
- Computationally efficient.

Claim 2.4.1: Delft3D-FLOW uses an accurate, robust and computationally efficient algorithmic implementation for the shallow water equations (hydrostatic model) and for the incompressible Navier-Stokes equations (non-hydrostatic model). This is the case for both time-dependent and steady state problems.

Substantiation: All validation studies are relevant to this claim.

2.4.2 Computational grid

Delft3D-FLOW is a numerical model based on a finite difference discretisation of the 3D shallow water equations. The equations apply in the grid points of a well-structured orthogonal 3D grid that covers the 3D model domain, see Figures 1.2 and 1.3.

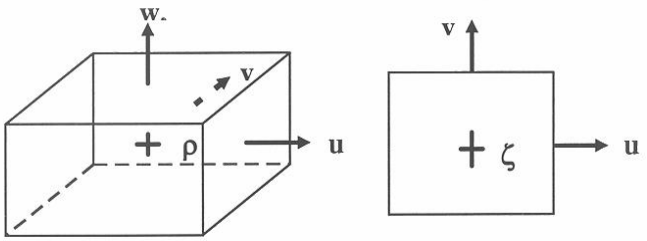

Figure 2.1 Grid staggering, 3D view (left) and horizontal view (right)

Legend:
+ water elevation (ζ) / density (ρ) = concentration (C) point
$\rightarrow$ velocity point(u, v, or w)

The arrangement of the flow variables presented in Figure 2.1 is called a staggered grid. This particular arrangement of the variables is called the Arakawa C-grid. The water level points (pressure points) are defined in the centre of a (continuity) cell. The velocity components are perpendicular to the grid cell faces where they are situated.

In the horizontal plane Delft3D-FLOW offers the opportunity to use

- orthogonal curvilinear co-ordinates (ξ,η), with Cartesian rectangular co-ordinates (x,y) as a special case;
- orthogonal (rectangular) latitude-longitude co-ordinates (λ,ϕ) on the sphere.
- orthogonal curvilinear latitude-longitude co-ordinates (λ,ϕ) on the sphere, see [Kernkamp et al., 2005].

Curvilinear co-ordinates allow smooth alignment of the grid with land boundaries and allow local grid refinement in areas with large horizontal gradients.

Claim 2.4.2: In Delft3D-FLOW the user can choose a type of grid that is suitable for the application involved. Furthermore, using a domain decomposition technique (not described in this document, but in Appendix B.13 of the user manual) additional high horizontal and vertical grid resolution can be realised in regions where it is specifically needed.

Substantiation: In particular, all validation studies of Section 3.4 (real-world applications) are relevant to this claim.

2.4.3 Discretisation and time integration of the 3D shallow water equations

The discretised equations describe the relations between the flow values in the points of the grid and between one time step and the next. A time stepping scheme is applied to determine the evolution of the grid values in time. In Delft3D-FLOW a stable combination of second-order central and third order upwind spatial discretisation is used, plus a so-called ADI-type time stepping scheme to solve the discretised equations in time. This offers a combination of accuracy, stability and acceptable computation times. The two-step Alternating Direction Implicit solution concept reads, still formulated using differential operators for spatial discretisations:

$$\frac{\vec{U}^{\ell+\frac{1}{2}}-\vec{U}^{\ell}}{\frac{1}{2}\Delta t}+\frac{1}{2}A_x\vec{U}^{\ell+\frac{1}{2}}+\frac{1}{2}A_y\vec{U}^{\ell}+B\vec{U}^{\ell+\frac{1}{2}}=\vec{d}\,, \tag{2.4.1}$$

$$\frac{\vec{U}^{\ell+1}-\vec{U}^{\ell+\frac{1}{2}}}{\frac{1}{2}\Delta t}+\frac{1}{2}A_x\vec{U}^{\ell+\frac{1}{2}}+\frac{1}{2}A_y\vec{U}^{\ell+1}+B\vec{U}^{\ell+1}=\vec{d}\,,$$

with $\vec{U}=\left(u,v,\zeta\right)^T$ and

$$A_x=\begin{bmatrix} 0 & -f & g\frac{\partial}{\partial x} \\ 0 & u\frac{\partial}{\partial x}+v\frac{\partial}{\partial y} & 0 \\ H\frac{\partial}{\partial x} & 0 & u\frac{\partial}{\partial x} \end{bmatrix},\quad A_y=\begin{bmatrix} u\frac{\partial}{\partial x}+v\frac{\partial}{\partial y} & 0 & 0 \\ f & 0 & g\frac{\partial}{\partial y} \\ 0 & H\frac{\partial}{\partial y} & v\frac{\partial}{\partial y} \end{bmatrix},$$

$$B=\begin{bmatrix} \lambda & 0 & 0 \\ 0 & \lambda & 0 \\ 0 & 0 & 0 \end{bmatrix},$$

with λ the linearised bottom friction coefficient. The essence of implicit techniques is that the equations contain more than one variable at the unknown new time step, and can therefore not be solved separately or explicitly. The linking of the variables at the new time step increases accuracy and stability, but results in a large matrix equation, which has to be solved. To improve stability the bottom friction is integrated implicitly for each stage. $\vec{d}$ is the right-hand side containing external forcings like wind and atmospheric pressure.

In the first stage the time level proceeds from ℓ to $\ell+\frac{1}{2}$ and the simulation time from $t=\ell\Delta t$ to $t=\left(\ell+\frac{1}{2}\right)\Delta t$. In this stage first the *V*-momentum equation is solved explicitly, followed by the *U*-momentum equation, which is implicitly coupled with the continuity equation by the free surface gradient. In the second stage the time level proceeds from $\ell+\frac{1}{2}$ to $\ell+1$. In this stage first the *U*-momentum equation is solved explicitly, followed by the *V*-

momentum equation which is implicitly coupled with the continuity equation by the free surface gradient. In the (x- or y-)direction in which the barotropic pressure term (i.e. water level gradient) is integrated implicitly, the horizontal advection terms and viscosity terms are integrated explicitly. Similarly in the direction in which the barotropic pressure term is integrated explicitly, the advection terms and viscosity terms are integrated in an implicit way.

The second stage in the ADI-method is almost similar to the first stage. The grid coefficients, direction dependent roughness coefficients and the *u*-velocity and *v*-velocity are interchanged. The only principal difference between the *u*- and *v*-momentum equations is the sign of the Coriolis term.

The above-described ADI solution technique of the shallow water equations avoids the strong *numerical stability* restrictions of an explicit time integration. The latter would be subject to a time step condition based on the Courant number for wave propagation (on a rectangular grid):

$$CFL_{wave} = 2\Delta t\sqrt{gH}\sqrt{\frac{1}{\Delta x^2}+\frac{1}{\Delta y^2}} < 1, \tag{2.4.2}$$

For many practical applications this would require a time step of only a few seconds to simulate tidal propagation. Exceeding the time step would generate an *instability* and from the view of robustness this is not acceptable.

Time step limitations

In this section we give an overview of the time step limitations due to *stability* and *accuracy* for the time integration of the shallow water equations in Delft3D-FLOW. We remark that in theory the ADI method is an unconditionally stable integration method. However, in real-world applications with irregular coastlines, this is not, see e.g. [Stelling et al., 1986]. In Table 2.2 the time step limitations are given for Delft3D-FLOW.

Accuracy: points per wave period T	$\Delta t \le \frac{T}{40}$
Accuracy of the barotropic mode due to ADI effects for very complex channel geometries	$C_f = 2\Delta t\sqrt{gH\left(\frac{1}{\Delta x^2}+\frac{1}{\Delta y^2}\right)} < 4\sqrt{2}$
Stability for the baroclinic mode	$2\Delta t\sqrt{\frac{\Delta\rho}{\rho}gH\left(\frac{1}{\Delta x^2}+\frac{1}{\Delta y^2}\right)} < 1$
Stability of the explicit algorithm for flooding	$\frac{\Delta t\lvert u\rvert}{\Delta x} < 2$
Stability of the horizontal viscosity term	$\Delta t\,\nu_H\left(\frac{1}{\Delta x^2}+\frac{1}{\Delta y^2}\right) < 1$

Table 2.2 Time step limitations for Delft3D-FLOW

From Table 2.2 it can be seen that time step limitations occur in Delft3D-FLOW, namely for the free surface wave propagation, baroclinic flow, the advection scheme(s), drying and flooding and the horizontal viscosity. Which of the limitations is most restrictive is dependent on the kind of application: length scale, velocity scale, with or without density-coupling, etc. Note that for the vertical terms there is no (additional) stability criterion. This means that the Delft3D-FLOW when applied in 3D mode is similarly robust compared to the application in 2D. We remark, however, that the horizontal velocities in 3D are (slightly) larger than in 2D, which might result in a (slightly) smaller time step for 3D applications.

In general, one would not expect a time step limitation for the barotropic mode. However, the ADI-method may lead to inaccurately predicted flow patterns when a relatively large time step is applied, see e.g. [Stelling, 1984]. This inaccuracy is called the ADI-effect and is introduced by the splitting of the spatial operator in two directions. The upper bound for the barotropic mode of $4\sqrt{2}$ occurs in the most critical ADI situation, namely in case of a narrow channel (width of few grid sizes) that makes an angle of 45 degrees with the computational grid [Stelling et al, 1986], which is illustrated in Figure 2.2.

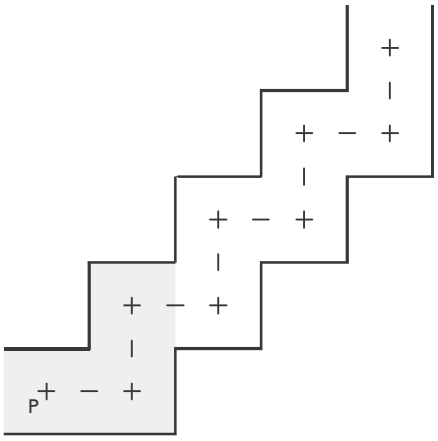

Figure 2.2 Numerical region of influence for one time step. “Zig-zag channel”

In more general practical situations a time step equivalent to a Courant number up to 10 generally still gives accurate solutions. We remark that with the bathymetry generation tool QUICKIN it is possible to check the Courant numbers. Depending on the specific application, grid and depth, the user is advised to carry out sensitivity tests in order to determine the largest time step for which the ADI-method still yields accurate results.

Claim 2.4.3a: Delft3D-FLOW is based on a robust ADI solver for the basic barotropic mode, which means that stability considerations allow a large time step well beyond the CFL condition (up to a factor 10). In case of special features such as drying and flooding, baroclinic modes and large horizontal viscosity, additional but generally weaker stability criteria apply, see quantification in Table 2.2.

Substantiation: All validation studies of Chapter 3 are relevant to this claim.

Time integration of the transport equation

A robust and accurate solver for scalar transport has to satisfy the following demands:

- Mass conservation.
- Accuracy (at least second-order).
- Suitable for both time-dependent and steady state problems.
- Computationally efficient.

Optionally, Monotonicity (i.e. a positive solution) might be required for some applications.

An explicit time integration of the scalar advection-diffusion equation on a rectangular grid has a time step limitation based on the Courant number for advection:

$$C_{adv} = \max\left(\frac{u\Delta t}{\Delta x}, \frac{v\Delta t}{\Delta y}\right) \leq 1, \tag{2.4.3}$$

with Δx and Δy the grid spaces in the physical space. Explicit integration of the horizontal diffusion term yields an upper limit of:

$$\Delta t \leq \frac{1}{D_H}\left(\frac{1}{\Delta x^2} + \frac{1}{\Delta y^2}\right)^{-1}. \tag{2.4.4}$$

For the 3D transport equation the scalar concentrations are coupled in the vertical direction by the vertical advection and diffusion term. An explicit time integration of the vertical exchange terms on the σ-co-ordinate grid would lead to very severe time step limitations:

$$\Delta t \leq \frac{\left(\Delta\sigma H\right)^2}{2D_V}, \tag{2.4.5}$$

$$\Delta t \leq \frac{\Delta\sigma H}{\omega}. \tag{2.4.6}$$

Therefore, in the vertical direction a fully implicit time integration method is applied in Delft3D-FLOW, which is first-order in time and leads to tridiagonal systems of equations. The vertical coupling of the discretized transport equations is solved by a double sweep algorithm.

To ensure that the total mass is conserved the transport equation in Delft3D-FLOW is discretized with a mass conserving Finite Volume approach (flux form).

The transport equation is coupled with the momentum equations via the baroclinic pressure term, see Eqs. (2.3.1.8). The temporal variations in salinity are slow compared to the variations in the flow and therefore the baroclinic term in the momentum equations is treated explicitly, introducing a stability condition for internal gravity waves (baroclinic

mode). The coupling with the flow is weak and in Delft3D-FLOW the transport equation is solved independently of the flow for each half time step.

For the time integration of the horizontal diffusion term along σ-planes, the Crank-Nicholson method is applied. If the spatial discretisation of the horizontal diffusion term is based on a Cartesian grid using the Finite Volume approach of [Stelling and Van Kester, 1994] the integration is explicit. Source terms are integrated explicitly. In order to avoid negative concentrations and instabilities, sink terms are integrated fully implicit.

If we substitute into the discretised transport equation a constant concentration field (e.g. C=1), then we arrive at the discretised continuity equation.

To keep the numerical diffusion as small as possible the horizontal advection terms in the scalar transport equation are approximated by the sum of a third-order upwind scheme and a second-order central scheme. A second-order central scheme is applied for the approximation of the vertical advection term. This so-called *Cyclic* method is the default option for the advection terms. In Section 2.4.4 this method and the other advective schemes in Delft3D-FLOW are described.

For the *Cyclic* method the time integration follows the ADI-method for the continuity equation. In the first stage all space derivatives in x-direction are integrated implicitly in time and all derivatives in the x-direction are taken explicitly. In the second stage the directions for explicit and implicit integration are interchanged. If the upwind discretisation is used in the stage in which both the horizontal advection and vertical viscosity term are integrated implicitly, the resulting linear system of equations has thirteen diagonals but the matrix is diagonally dominant. Thus, the system can be solved effectively by a Red Black Jacobi iterative scheme in the horizontal direction and a double sweep in the vertical direction.

Claim 2.4.3b: Delft3D-FLOW uses accurate numerical methods for the transport equation, which is based on a mass conserving discretisation.

Substantiation: In particular, all validation studies of Section 3.4 (real-world applications) are relevant to this claim.

Time integration for turbulence modelling

In this section we describe the time integration for the (second-order) k-ε turbulence closure model. In this model the transport equations (2.3.1.20a/b) for the turbulent kinetic energy and the energy dissipation are solved. For the k-L model the computation of the turbulent kinetic energy is identical to the one for the k-ε model. The algebraic turbulence model does not require the numerical integration of one or two transport equations.

The turbulent kinetic energy k and energy dissipation ε are defined in the centre cells in the horizontal, and at the vertical layer interfaces. This allows a more accurate discretisation of the production and buoyancy term than in the case of vertical discretisation of k and ε at the centre of the layers.

The time integration consists of two stages. At both stages the same time integration method is applied for the *k-ε* turbulence model. We will therefore only give a description of the first stage. An operator splitting method is applied. A stage consists of two steps. In the first step the following equation is approximated:

$$\frac{\partial k}{\partial t} + u\frac{\partial k}{\partial x} + v\frac{\partial k}{\partial y} = 0 \qquad (2.4.7)$$
$$\frac{\partial \varepsilon}{\partial t} + u\frac{\partial \varepsilon}{\partial x} + v\frac{\partial \varepsilon}{\partial y} = 0$$

In the first step a first-order upwind discretisation is used for the horizontal advection terms. The discretisation of the horizontal advection terms leads to a system of equations which is decoupled in the vertical direction, because the vertical terms are not present in this step.

In the second step we have the remaining terms

$$\frac{\partial k}{\partial t} + \frac{\omega}{H}\frac{\partial k}{\partial \sigma} = \frac{1}{H}\frac{\partial}{\partial \sigma}\left[\frac{D_V}{H}\frac{\partial k}{\partial \sigma}\right] + P_k + B_k - \varepsilon \qquad (2.4.8)$$
$$\frac{\partial \varepsilon}{\partial t} + \frac{\omega}{H}\frac{\partial \varepsilon}{\partial \sigma} = \frac{1}{H}\frac{\partial}{\partial \sigma}\left[\frac{D_V}{H}\frac{\partial \varepsilon}{\partial \sigma}\right] + P_\varepsilon + B_\varepsilon - c_{2\varepsilon}\frac{\varepsilon^2}{k}$$

For the time integration a fully implicit method (Backward Euler) is applied. This yields, in combination with the first-order upwind discretisation for the advection terms, a positive scheme. For turbulence modelling a first-order discretisation for the advection terms is assumed to be accurately enough, because it is assumed that production, buoyancy and dissipation are the dominant terms [Van Kester, 1994].

Claim 2.4.3c: Delft3D-FLOW uses an accurate and robust algorithmic implementation for turbulence modelling.

Substantiation: In particular, all validation studies of Section 3.4 (real-world applications) are relevant to this claim, because stratification plays a role in these studies.

2.4.4 Accuracy of advection discretisation schemes

Advection schemes in Delft3D-FLOW occur in the momentum equations, the transport equation and in the turbulence equations. The choice of the spatial discretisation of the advection terms has a large influence on the accuracy, monotony and efficiency of the computational method. Derivative discretisation using central differences is often second-order accurate, but may give rise to non-physical spurious oscillations, the so-called "wiggles" in the solution [Gresho and Lee, 1979]. These wiggles arise in the vicinity of steep gradients of the quantity to be resolved. In shallow water flow these wiggles may also be introduced near closed boundaries and thin dams. On the other hand, first-order upwind derivative discretisation is unconditionally wiggle-free or monotone, thus promoting the stability of the solution process. It introduces a truncation error, which has the form of a second-order artificial viscosity term [Vreugdenhil, 1994]. In advection-dominated flows,

this artificial viscosity dominates the physical viscosity and the computed solution is much smoother than the correct one. Higher order upwind discretisation is not free from numerical oscillations and introduces fourth-order artificial viscosity. This higher order viscosity suppresses the wiggles without smoothing the solution too much.

Advective schemes for the hydrodynamic equations

Delft3D-FLOW has four options for the discretisation of the horizontal advection terms in the momentum equations, namely:

- the *cyclic* method (i.e. a (third order) reduced phase error scheme);
- the *WAQUA* scheme, which is applied for (depth-veraged) river applications in The Netherlands;
- the *Flooding* scheme, which is a combination of a momentum conserving method and an energy head conserving method, for rapidly varying flows; and
- a *Multi directional upwind* method (Z-model only).

Depending on the application the user can choose the most suitable discretisation method (via the Delft3D-FLOW input file).

The cyclic method is a combination of a third order upwind finite difference scheme for the first derivative into two second-order consistent discretisations: a central discretisation:

$$u\left.\frac{\partial u}{\partial x}\right|_{m,n,k} = u_{m,n,k}\left(\frac{u_{m+1,n,k}-u_{m-1,n,k}}{2\Delta x}\right), \tag{2.4.9}$$

and an upwind discretisation

$$u\left.\frac{\partial u}{\partial x}\right|_{m,n,k} = \begin{cases} u_{m,n,k}\left(\dfrac{3u_{m,n,k}-4u_{m-1,n,k}+u_{m-2,n,k}}{2\Delta x}\right), & u_{m,n,k}\geq 0 \\ u_{m,n,k}\left(\dfrac{-3u_{m,n,k}+4u_{m+1,n,k}-u_{m+2,n,k}}{2\Delta x}\right), & u_{m,n,k}<0 \end{cases} \tag{2.4.10}$$

which are successively used in both stages of the ADI-scheme. This combination is applied for both the normal advection term $u\,\partial u/\partial x$ and the cross advection term $v\,\partial u/\partial y$. The scheme is denoted as the Cyclic Method [Stelling and Leendertse, 1991]. Near the boundaries the higher order discretisation stencils for the advection terms contain grid points on or across the boundary. To avoid an artificial boundary layer or instabilities, the discretisations are reduced to lower order discretisations with smaller stencils, see [Stelling, 1984].

For sufficiently smooth solutions the above described cyclic method works well, because its accuracy is of third order and the numerical viscosity is minimal. However, near local discontinuities in the solution, e.g. due to sharp bottom gradients or hydraulic jumps, the order of accuracy is a meaningless concept. Then, conservation properties are more important, such as conservation of mass, conservation of momentum or conservation of energy head.

In the *WAQUA* scheme [Stelling, 1984] the normal advection term $u\,\partial u/\partial x$ is discretised with central differences and the cross advection term $v\,\partial u/\partial y$, based on the dissipative reduced phase error scheme. For the cross advection term the spatial discretisation is given by (at the first and second stage, respectively):

$$\left.\nu\frac{\partial u}{\partial y}\right|_{m,n,k} = \overline{\nu}^{xy}_{m,n,k}\left(\frac{u_{m,n+1,k}-u_{m,n-1,k}}{2\Delta y}\right), \tag{2.4.11}$$

$$\left.\nu\frac{\partial u}{\partial y}\right|_{m,n,k} = \begin{cases} \overline{\nu}^{xy}_{m,n,k}\left(\dfrac{3u_{m,n,k}-4u_{m,n-1,k}+u_{m,n-2,k}}{2\Delta y}\right), & \overline{\nu}^{xy}_{m,n,k}\geq 0 \\ \overline{\nu}^{xy}_{m,n,k}\left(\dfrac{-3u_{m,n,k}+4u_{m,n+1,k}-u_{m,n+2,k}}{2\Delta y}\right), & \overline{\nu}^{xy}_{m,n,k}<0 \end{cases} \tag{2.4.12}$$

Thus, the difference between the Cyclic and the WAQUA scheme is the discretisation of the normal advection term $u\,\partial u/\partial x$.

For the third method (i.e. the flooding scheme), Delft3D-FLOW determines for each grid which of the two methods (either momentum conserving or energy head conserving) is most appropriate, depending on whether the local flow is contracting or expanding. This method, which is based on [Stelling and Duinmeijer, 2003], can be applied to rapidly varying depth-averaged flows for instance the inundation of dry land or flow transitions due to large gradients of the bathymetry (obstacles). The scheme is also accurate for obstacles, represented by only one point on coarse grids. For the *Flooding* scheme the bottom is assumed to be represented as a staircase (*DPUOPT=MIN*) of tiles, centred around water level points. In combination with the local invalidity of the hydrostatic pressure assumption, conservation properties become crucial. In flow expansions a numerical approximation is applied that is consistent with conservation of momentum and in flow contractions a numerical approximation is applied that is consistent with the Bernouilli equation. For sufficiently smooth conditions, and a fine grid size, both approximations converge to the same solution. The local order of consistency depends on the solution. The approximations are second-order, but the accuracy reduces to first-order near extreme values by the use of the so-called Minmod slope limiter [Stelling and Duinmeijer, 2003]. The limiter prevents the generation of wiggles. We remark that the conservation of momentum has been derived only for a Cartesian rectangular grid and depth averaged velocities.

We describe the discretisations for positive flow direction. For negative flow direction the discretisations are defined accordingly. The momentum conservative approximation for the normal advection term $u\,\partial u/\partial x$ derived for a control volume around a velocity point is given by:

$$
\begin{aligned}
u\left.\frac{\partial u}{\partial x}\right|_{m,n} &= \frac{2}{\left(H^{x}_{m,n}+H^{x}_{m+1,n}\right)_{m,n}}\left\{\tilde{u}^{x}_{m+1,n}\left(\frac{\overline{q}^{x}_{m+1,n}-\overline{q}^{x}_{m,n}}{\Delta x}\right)-u_{m,n}\left(\frac{\overline{q}^{x}_{m+1,n}-\overline{q}^{x}_{m,n}}{\Delta x}\right)\right\}\\
\overline{q}^{x}_{m,n} &= \frac{q^{x}_{m,n}+q^{x}_{m-1,n}}{2}\\
\tilde{u}^{\xi}_{m,n} &= u_{m-1,n}+\frac{1}{2}\psi\left(r_u\right)\left(u_{m\text{-}1,n}-u_{m\text{-}2,n}\right) \qquad \overline{q}^{x}_{m,n}>0\\
r_u &= \frac{u_{m,n}-u_{m\text{-}1,n}}{u_{m\text{-}1,n}-u_{m\text{-}2,n}};\psi\left(r_u\right)=\max(0,\min(r_u,0))
\end{aligned}
\tag{2.4.13}
$$

The momentum conservative approximation for the cross advection term $v\,\partial u/\partial y$ is given by:

$$
\begin{aligned}
v\left.\frac{\partial u}{\partial y}\right|_{m,n} &= \frac{2}{H^{\zeta}_{m,n}+H^{\zeta}_{m+1,n}}\left\{\left(\frac{\overline{q}^{y}_{m,n}\tilde{u}^{y}_{m,n}-\overline{q}^{y}_{m,n\text{-}1}\tilde{u}^{y}_{m,n-1}}{\Delta y}\right)-u_{m,n}\left(\frac{\overline{q}^{y}_{m,n}-\overline{q}^{y}_{m,n\text{-}1}}{\Delta y}\right)\right\}\\
\overline{q}^{y}_{m,n-1} &= \frac{q^{y}_{m,n-1}+q^{y}_{m+1,n-1}}{2}\\
\tilde{u}^{y}_{m,n-1} &= u_{m,n\text{-}1}+\frac{1}{2}\psi\left(r_u\right)\left(u_{m,n\text{-}1}-u_{m,n\text{-}2}\right) \qquad \overline{q}^{y}_{m,n\text{-}1}>0\\
r_u &= \frac{u_{m,n}-u_{m,n\text{-}1}}{u_{m,n\text{-}1}-u_{m,n\text{-}2}};\psi\left(r_u\right)=\max(0,\min(r_u,0))
\end{aligned}
\tag{2.4.14}
$$

From the momentum conservative formulation a so-called energy head conservative discretisation for the same Control Volume can be derived under steady state conditions (constant discharge q) in 1D (along a streamline in 2D), see Eq.(2.4.15).

$$
\begin{aligned}
&\frac{q^2}{2}\left[\frac{1}{\left(H^{\zeta}_{m+1,n}\right)^2}-\frac{1}{\left(H^{x}_{m,n}\right)^2}\right]_{Energy\_Head\_Conserv} \qquad \lambda\frac{2q^2}{\left(H^{x}_{m,n}+H^{x}_{m+1,n}\right)}\left[\frac{1}{\left(H^{x}_{m+1,n}\right)}-\frac{1}{\left(H^{x}_{m,n}\right)}\right]_{Momentum\_Conserv}\\
&\lambda=\begin{cases}1 & q>0\wedge H^{x}_{m,n}<H^{x}_{m+1,n}\\ \dfrac{\left(H^{x}_{m,n}+H^{x}_{m+1,n}\right)^2}{4H^{x}_{m,n}H^{x}_{m+1,n}} & q>0\wedge H^{x}_{m,n}>H^{x}_{m+1,n}\end{cases}
\end{aligned}
\tag{2.4.15}
$$

The energy conservative discretisation is applied for contractions in both directions. For 2D flow the direction of the grid lines do not always coincide with streamlines and this will generate small head losses.

Near the boundaries the higher order discretisation stencils for the advection terms contain grid points on or across the boundary. To avoid an artificial boundary layer or instabilities, the discretisations are reduced to lower order discretisations with smaller stencils. Stelling [1984] developed the numerical boundary treatment that is implemented in Delft3D-FLOW.

The fourth scheme, which is the only advection scheme in the Z-model and is not available for a σ-model, is a so-called *multidirectional upwind scheme*. It is an extension to two dimensions of the first-order upwind method. It is a positive and monotone scheme. For positive *u*- and *v*-velocity, this method can be written as:

$$u\frac{\partial u}{\partial x}+v\frac{\partial u}{\partial y}\bigg|_{m,n,k}=\begin{cases}u_{m,n,k}\dfrac{u_{m,n,k}-u_{m-1,n,k}}{\Delta x}+\bar{v}^{xy}_{m,n,k}\dfrac{u_{m,n,k}-u_{m,n-1,k}}{\Delta y}, & \dfrac{u_{m,n,k}}{\Delta x}\geq\dfrac{v_{m,n,k}}{\Delta y}\\ u_{m,n,k}\dfrac{u_{m+1,n-1,k}-u_{m,n-1,k}}{\Delta x}+\bar{v}^{xy}_{m,n,k}\dfrac{u_{m,n+1,k}-u_{m,n,k}}{\Delta y}, & \dfrac{u_{m,n,k}}{\Delta x}<\dfrac{v_{m,n,k}}{\Delta y}\end{cases} \tag{2.4.16}$$

We remark that this method has a Courant number stability constraint.

Claim 2.4.4a: The advection terms in the hydrodynamic equations are solved using either an accurate third order reduced phase order advection method (i.e the *Cyclic* method) or an advection scheme optimising conservation of momentum and conservation of energy head (i.e. the *Flooding* scheme). Conservation of volume is guaranteed for all three advection schemes. The user can choose the most suitable method for his problem. E.g., in transitional flows, inundation of dry land or dam break problems the user can specify a combination of the momentum and energy head conserving scheme.

Substantiation: All validation studies in Chapter 3 are relevant to this claim.

Advective schemes for the transport equation

To ensure that the total mass is conserved the transport equation is discretised with a mass conserving Finite Volume approach (flux form). For the spatial discretisation of the horizontal advection terms, two options are available:

- the cyclic method, which is almost similar to the cyclic method for the momentum equations; and
- the so-called Van Leer-2 method (Van Leer, 1974).

Depending on the application the user can choose the most suitable discretisation method. In case of a σ-model both above-described options are available. For the Z-model, however, there is only one option, namely the Van Leer-2 method.

The first (and default) option is a finite difference scheme that conserves large gradients without generating spurious oscillations and is based on the ADI - method. This scheme is denoted as the *Cyclic* method, see [Stelling and Leendertse, 1991]. The *Cyclic* method of Stelling and Leendertse is based on an implicit time integration of both advection and diffusion and does not impose a time step restriction. The cyclic method is second-order accurate in time and third-order accurate in space.

The second option is an explicit scheme that belongs to the class of monotonic schemes: the so-called *Van Leer-2* scheme [Van Leer, 1974]. The *Van Leer-2* scheme is slightly less

accurate than the scheme of Stelling and Leendertse. It combines two numerical schemes, namely a first-order upwind scheme and the second-order upwind scheme developed by Fromm. In case of a local minimum or maximum the first-order upwind scheme is applied, whereas the upwind scheme of Fromm is used in case of a smooth numerical solution. The time integration of the *Van Leer-2* scheme is explicit and therefore a CFL condition for advection and diffusion must be fulfilled. Owing to the explicit time integration the *Van Leer-2* scheme requires per time step less computation time than the *Cyclic* method of Stelling and Leendertse. However, the *Van Leer-2* scheme produces a more diffusive numerical solution, because of the fact that a first-order upwind discretisation is applied in case of a local maximum or minimum. The transport scheme for the Z-model is described in [Bijvelds, 2003].

In 3D, for both transport schemes, the central differences in the vertical may give rise to non-physical spurious oscillations, so-called "wiggles" [Gresho and Lee, 1979] in the solution. These wiggles arise in the vicinity of steep gradients of the quantity to be resolved. In case of negative concentrations an iterative filter procedure based on local diffusion along σ-lines followed by a vertical filter can be switched on in order to remove the negative values. The filtering technique in this procedure is the so-called Forester filter [Forester, 1979], a non-linear approach which removes the computational noise without inflicting significant amplitude losses in sharply peaked solutions.

Cyclic method

For the *Cyclic* method the upwind discretisation of the horizontal advective fluxes in x-direction is described by:

$$\left.\frac{\partial(huc)}{\partial x}\right|_{m,n,k} = \frac{F_{m,n,k} - F_{m-1,n,k}}{\Delta x}. \tag{2.4.17}$$

For the scalar flux $F_{m,n,k}$ at the *U*-velocity point the interpolation is given by:

$$F_{m,n,k} = u_{m,n,k} \times h_{m,n,k} \times \begin{cases} \dfrac{10c_{m,n,k} - 5c_{m-1,n,k} + c_{m-2,n,k}}{6\Delta\xi}, & u_{m,n,k} \geq 0 \\ \dfrac{10c_{m+1,n,k} - 5c_{m+2,n,k} - c_{m+3,n,k}}{6\Delta\xi}, & u_{m,n,k} < 0 \end{cases} \tag{2.4.18}$$

In the first stage in *y*-direction a central scheme is applied:

$$\left.\frac{\partial(hvc)}{\partial y}\right|_{m,n,k} = \frac{G_{m,n,k} - G_{m,n-1,k}}{\Delta y}, \tag{2.4.19}$$

with the scalar flux $G_{m,n,k}$ at the *V*-velocity point determined by:

$$G_{m,n,k} = v_{m,n,k} \times h_{m,n,k} \times \frac{c_{m,n,k} + c_{m,n+1,k}}{2}. \tag{2.4.20}$$

Near open and closed boundaries the approximations for the fluxes are reduced to lower order.

Van Leer-2 method

For the second option in Delft3D-FLOW, namely the *Van Leer-2* scheme, the interpolation formula for the horizontal fluxes is given by:

$$F_{m,n,k} = u_{m,n,k} h_{m,n,k} \begin{cases} c_{m,n,k} + \alpha\left(1 - CFL_{adv-u}\right)\left(c_{m,n,k} - c_{m-1,n,k}\right)\dfrac{c_{m+1,n,k} - c_{m,n,k}}{c_{m+1,n,k} - c_{m-1,n,k}}, \\ \qquad when\ u_{m,n,k} \geq 0, \\ c_{m+1,n,k} + \alpha\left(1 + CFL_{adv-u}\right)\left(c_{m,n,k} - c_{m-1,n,k}\right)\dfrac{c_{m+1,n,k} - c_{m+2,n,k}}{c_{m,n,k} - c_{m+2,n,k}}, \\ \qquad when\ u_{m,n,k} < 0, \end{cases} \tag{2.4.21}$$

with:

$$CFL_{adv-u} = \frac{\Delta t |u|}{\Delta x}$$

and:

$$\alpha = \begin{cases} 0, & \left|\dfrac{c_{m+1,n,k} - 2c_{m,n,k} + c_{m-1,n,k}}{c_{m+1,n,k} - c_{m-1,n,k}}\right| > 1,\ (local\ \max.\ or\ \min.), \\ 1, & \left|\dfrac{c_{m+1,n,k} - 2c_{m,n,k} + c_{m-1,n,k}}{c_{m+1,n,k} - c_{m-1,n,k}}\right| \leq 1,\ (monotone). \end{cases} \tag{2.4.22}$$

In *y*-direction a similar discretisation is applied. Eqs. (2.4.21) to (2.4.22) consist of a diffusive first-order upwind term and a higher order anti-diffusive term. The time integration of the *Van Leer-2* scheme is explicit. The Courant number for advection should be smaller than one.

Claim 2.4.4b: The advection terms in the hydrodynamic equations are solved using either the (third order accurate) Cyclic method or the Van Leer-2 scheme, which is a monotonic and positive scheme. The optional Forester filter will remove spurious solutions without significantly affecting the amplitudes. Conservation of mass is guaranteed for both advection schemes.

Substantiation: In particular, all validation studies of Section 3.4 (real-world applications) are relevant to this claim.

Advective schemes for the turbulence models

Claim 2.4.4c: First-order accuracy in the turbulence modelling is adequate since production buoyancy (sources) and dissipation (sinks), are dominant. The advection terms in the turbulence models are solved using a first-order upwind scheme to guarantee positivity of the turbulence quantities. Negative turbulence concentrations are so avoided.

Substantiation: Not in list of validation studies yet.

2.4.5 Suppression of artificial vertical mixing due to σ co-ordinates

In the boundary-fitted σ-grid the sea bed and free surface are represented by $\sigma = -1$ and $\sigma = 0$, respectively. The water column is divided into the same number of σ-layers independent of the water depth. Vertical resolution increases automatically in shallow areas. For steep bottom slopes combined with vertical stratification, the use of σ-transformed grids may lead to artificial vertical mixing and artificial flow ("creep") due to truncation errors in the approximation of horizontal gradients both in the baroclinic pressure term and in the horizontal diffusion term [Leendertse, 1990] and [Stelling and Van Kester, 1994].

Claim 2.4.5: In 3D applications using σ-transformed grids artificial vertical diffusion and artificial flow due to truncation errors are effectively suppressed by the so-called "anti-creep" option.

Substantiation: Not in list of validation studies yet. However, the Delft3D-FLOW testbank (see Section 2.5.2) contains a test model for this purpose.

2.4.6 Moving boundaries – representation of drying and flooding

In a numerical model the process of drying and flooding is represented by blocking flow through a face of a grid cell when the water level locally falls below a certain threshold and so removing grid points from the flow domain that become "dry" and by again allowing flow and so adding grid points that become "wet" when the local water level rises above a second threshold. Drying and flooding gives a discontinuous movement of the closed boundaries and may locally generate small oscillations in water levels and velocities. The oscillations introduced by the drying and flooding algorithm are small if the grid sizes are small and the bottom has smooth gradients.

The crucial items in a wetting and drying algorithm are:

- The way in which the bottom depth is defined at a water level point from the four neighbouring grid values.
- The way in which the water level is defined at velocity points from the two neighbouring grid values.
- The user-defined threshold criteria for setting velocity points and water level points wet or dry.

The time step limitation for drying/flooding specified in Table 2.2 is mainly related to flooding. It limits the propagation of area flooding to one grid cell per time step, ensuring

that the decision based on local flow values leads to a local adjustment only. Mathematically, this corresponds to satisfying the criterion set by the advective characteristic direction.

Claim 2.4.6: The algorithmic implementation of the drying and flooding concept is robust, accurate and computationally efficient for coastal regions, estuaries and rivers.

Substantiation: Validation Study 3.3.2 (Drying and Flooding).
Reference(s): **[**Balzano, 1998] for an intercomparison of wetting and drying algorithms (a.o. the Delft3D-FLOW algorithm) in shallow water models.

2.4.7 Hydraulic structures

In a Delft3D-FLOW model, so-called hydraulic structures can be defined to model the effect of obstructions in the flow. The implementation is based on the assumption that the scales of the structures are smaller than the local grid size - the algorithmic approach is based on sub-grid scale representations. Examples of such physical structures are: 3D gates, porous plates, local weirs, floating structures and 2D weirs.

A hydraulic structure generates a loss of energy apart from the loss by bottom friction. At hydraulic structure points, an additional force term is added to the momentum equation, to parameterise the extra loss of energy. The term has the form of a friction term with a contraction or discharge coefficient.

The hydraulic structures that are available in Delft3D-FLOW, are divided into four basic types:

- closed (e.g., a gate)
- quadratic friction
- linear friction
- floating structure

The special points are defined in a moving σ-co-ordinate, so the varying vertical position in time is accounted for when needed. The flow condition at hydraulic structures may be supercritical. For supercritical flow, the downstream water level has no influence on the flow rate. The energy loss formulations presently available in Delft3D-FLOW assume subcritical flow. Only for the hydraulic structure of the type “2D weir” also the supercritical flow rate is computed accurately.

Claim 2.4.7: The algorithmic implementation of the hydraulic structure options such as 3D gates, porous plates, local weirs, floating structures and 2D weirs is robust, accurate and computationally efficient.

Substantiation: Validation Study 3.1.7 (Flow over a weir)

2.4.8 Online coupling of morphology and hydrodynamics

In Delft3D-FLOW the elevation of the bed is dynamically updated at each computational time step. This is one of the distinct advantages over an offline morphological computation as it means that the hydrodynamic flow calculations are always carried out using an up-to-date bathymetry.

At each time step, the change in the mass of bed material that has occurred as a result of the sediment sink and source terms and transport gradients is computed. This change in mass is then translated into a bed level change based on the dry bed densities of the various sediment fractions. Both the bed levels at the cell centres and cell interfaces are updated.

A number of additional features have been included in the morphological updating in order to increase the flexibility. These are discussed below.

Morphological "switch"
The user can specify whether or not to update the calculated depths to the bed. It may be useful to turn bottom updating off if only the initial patterns of erosion and deposition are required, or an investigation of sediment transport patterns with a constant bathymetry is required.

Morphological delay
Frequently, a hydrodynamic simulation will take some time to stabilise after transitioning from the initial conditions to the (dynamic) boundary conditions. It is likely that during this stabilisation period the patterns of erosion and accretion that take place do not accurately reflect the true morphological development and should be ignored. The user can specify a time interval (in minutes after the start time) after which the morphological bottom updating will begin. During this time interval all other calculations will proceed as normal (sediment will be available for suspension for example) however the effect of the sediment fluxes on the available bottom sediments will not be taken into account.

Morphological time scale factor
One of the complications inherent in carrying out morphological projections on the basis of hydrodynamic flows is that morphological developments take place on a time scale several times longer than typical flow changes. For example, tidal flows change significantly in a period of hours, whereas the morphology of a coastline will usually take weeks, months, or years to change significantly. One technique for approaching this problem is to use a "morphological time scale factor" whereby the speed of the changes in the morphology is scaled up to a rate that it begins to have a significant impact on the hydrodynamic flows.

While the maximum morphological time scale factor that can be included in a morphodynamic model without affecting the accuracy of the model will depend on the

particular situation being modelled, and will remain a matter of judgement, tests have shown that the computations remain stable in moderately morphologically active situations.

The interpretation of the morphological factor differs for coastal and river applications. For coastal applications with tidal motion, the morphological variations during a tidal cycle are often small and the hydrodynamics is not significantly affected by the bed level changes. By increasing the morphological factor to for instance 10, the morphological changes during one simulated tidal cycle are increased by this factor. From a hydrodynamic point of view this increase in morphological development rate is allowed if the hydrodynamics is not significantly influenced. In that case the morphological development after one tidal cycle can be assumed to represent the morphological development that would in real life only have occurred after 10 tidal cycles. In this example the number of hydrodynamic time steps required to simulate a certain period is reduced by a factor of 10 compared to a full 1:1 simulation. This leads to a significant reduction in simulation time.

Bathymetry updating including bed-load transport

The change in the quantity of bottom sediments caused by the bed-load transport is computed by:

$$\Delta_{SED}^{(n,m)} = \frac{\Delta t\, f_{MORFAC}}{A^{(n,m)}} \left(\begin{array}{l} S_{b,uu}^{(n,m-1)}\, \Delta y^{(n,m-1)} - S_{b,uu}^{(n,m)}\, \Delta y^{(n,m)} + \\ S_{b,vv}^{(n-1,m)}\, \Delta x^{(n-1,m)} - S_{b,vv}^{(n,m)}\, \Delta x^{(n,m)} \end{array} \right), \tag{2.4.23}$$

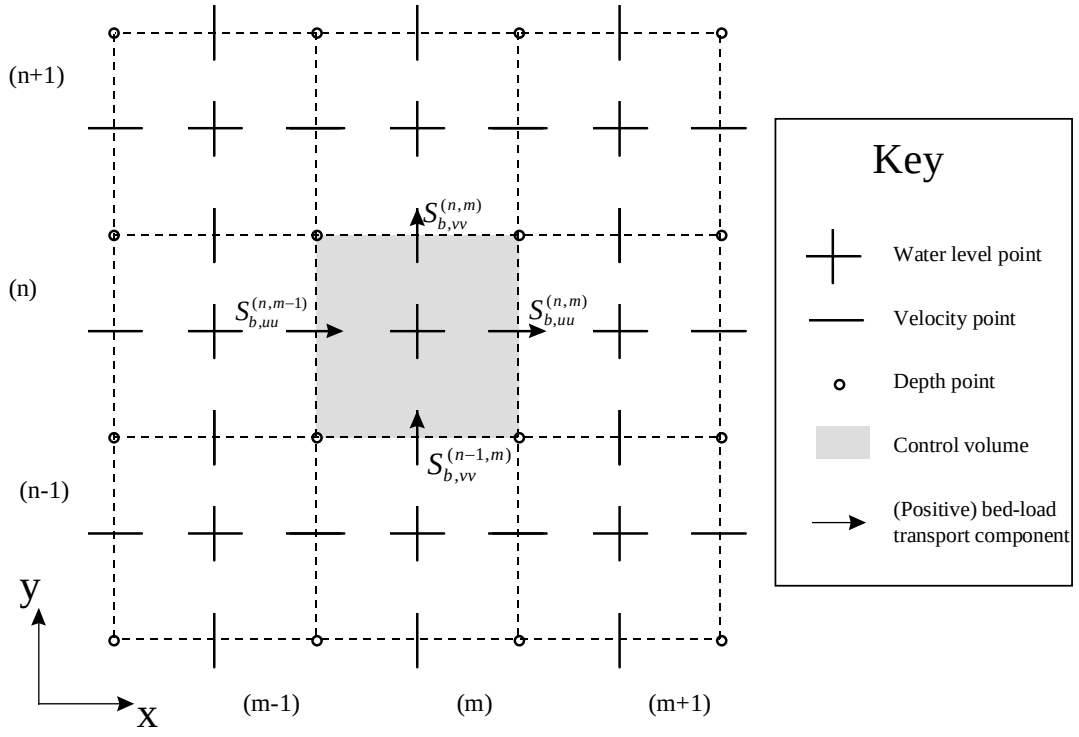

Figure 2.3 Morphological control volume and bed-load transport components

where:

$\Delta_{SED}^{(n,m)}$ change in quantity of bottom sediment at location (n,m) [kg/m^2]

Δt	computational time-step [s]
f_{MORFAC}	user-defined morphological acceleration factor, MORFAC
$A^{(n,m)}$	area of computational cell at location (n,m) [m^2]
$S_{b,uu}^{(n,m)}$	computed bed-load sediment transport vector in *u* direction, held at the *u* point of the computational cell at location (n,m) [kg/m s]
$\Delta x^{(n,m)}$	cell width in the *x* direction, held at the V point of cell (n,m) [m]
$\Delta y^{(n,m)}$	cell width in the *x* direction, held at the U point of cell (n,m) [m]

This computation is repeated for all 'sand' and 'bed load' sediment fractions, if more than one is present, and the resulting change in the bottom sediment mass is added to the change due to the suspended sediment sources and sinks and included in the bed composition and bed level updating scheme.

For further details about the interaction of hydrodynamic and morphodynamic flow we refer to Chapter 11 of the User Manual Delft3D-FLOW (WL | Delft Hydraulics, 2007).

Claim 2.4.8: The algorithmic implementation of the coupling of hydrodynamic and morphology processes is robust and accurate.

Substantiation: Validation Study 3.1.9 (Equilibrium slope for a straight flume).
Validation Study 3.3.7 (Migrating trench in a 1D channel).
Reference(s): **[**Lesser et al., 2000, Lesser et al., 2004, Ruessink and Roelvink, 2000].

2.5 Software implementation

This section describes technical aspects of the software implementation that are relevant to the validation process that have not been addressed in the previous section. In particular, it addresses the implications of software implementation choices and techniques for the technical quality of the computational model as a whole.

2.5.1 Implementation techniques

For Delft3D-FLOW the following choices have been made to convert the algorithmic implementation into software:

- Transition to the FORTRAN90 programming language;
- Application of guide lines for programming in FORTRAN90, see [WL | Delft Hydraulics, 2001];
- Dynamic memory management (via a coupling with the C programming language). (Delft3D-FLOW was originally coded in FORTRAN77, in which dynamic memory management was not possible. That problem was circumvented by using C subroutines for memory management. In near future it is foreseen that memory management will be implemented in FORTRAN90);
- Application of efficient iterative solvers for the momentum equations (a Red-Black Jacobi solver), for the continuity equation (a (direct) tridiagonal solver), for the

transport equations (a Red-Black Jacobi solver) and or domain decomposition (a Block Jacobi approach), see [Van Kester et al., 1992];
- Realisation of an essentially platform independent code for PC (Windows and Linux);
- The code is structured in a modular way.

Claim 2.5.1: Delft3D-FLOW runs on a PC (both under Windows and Linux). A parallel implementation on Linux is available as well. Noted that in 2003 it has been decided to no longer support UNIX platforms, which means that Delft3D-FLOW no longer supports the HP, SGI and SUN platforms.

Substantiation: See http://delftsoftware.wldelft.nl/ for the hardware platforms that are supported.

Claim 2.5.2: It is relatively easy to port Delft3D-FLOW to other platforms. Only a very small portion of the code (e.g. the timing subroutines) is platform dependent.

Substantiation: Delft3D-FLOW has been ported to a larger number of computers, although most of the platforms are no longer supported (HP, SUN, SGI, CRAY, NEC SX2) for reasons of market developments.

2.5.2 Software integrity and user guidance

A key aspect of complex modelling software that is used by a large community is the integrity of the whole system. The following practices and procedures have been implemented to ensure system integrity:

- Extensive testing of all new implementations for backward compatibility using a standard and continually updated testbank of analytical, laboratory and real life applications; For each update a testbank is run, which consists of more than 100 testcases;
- Full internal documentation of all modules before release;
- Rigorous version control;
- Adherence to formal module exchange and acceptance procedures;
- Explicit release schemes for version updates and upgrades;
- Extensive technical and user documentation;
- Documentation also exists for ancillary modules such as preprocessing, simulation, postprocessing.

Delft3D-FLOW uses ASCII input files (only in case of a restart a binary file might be used). The output files are (mainly) in NEFIS format, which is a Neutral File System that has been developed by WL | Delft Hydraulics. This format is platform independent.

Claim 2.5.3: Delft3D-FLOW is a thoroughly tested software product.

Substantiation: Delft3D-FLOW release notes, see http://delftsoftware.wldelft.nl.

Claim 2.5.3: Delft3D-FLOW is a well documented system.

Substantiation: The present Validation document and the Delft3D-FLOW User Manual [WL | Delft Hydraulics, 2007].

2.5.3 Computational efficiency

Delft3D-FLOW is a computationally efficient program. For example, for a 3D (10 layer) model with salinity and the k-ε turbulence model the required computation time per time step for each grid point on a 3GHz computer is roughly 2×10^{-6} sec. If we assume model dimensions of 100 by 100 (in the horizontal) and 10 layers in the vertical, then the computation time per time step is approximately 0.2 sec. Note that the 10.000 grid points in the horizontal contain both active and inactive (land) points. In general, the percentage of active grid points is roughly 50% or more. For a homogeneous 2D model the computation time per time step for each grid point on a 3GHz computer is roughly 10^{-7} sec.

Claim 2.5.1: Delft3D-FLOW is a computationally efficient program.

Substantiation: See validation studies of Chapter 3.4 (real-world applications), for which computation times are given.

3 Validation Studies

This chapter summarises validation studies and contributes to the substantiating evidence for the claims made in the previous chapter. Each section of this chapter corresponds to a validation study which' purpose can be clearly identified in the context of the material presented in the previous chapter. Such a study may involve case studies, theoretical analysis, comparison with measurements, comparisons with other models, etc., as long as it is relevant to the purpose of the study.

Delft3D-FLOW validation cases

This page last changed on 03-07-2008 by jagers.

Available validation cases

The available validation cases for Delft3D-FLOW have been subdivided in 4 categories:

1. Analytical test cases
2. Laboratory test cases
3. Schematic test cases
4. Real-world applications

Handy suggestion

If you want to see a complete overview of the stated claims and the linked validation cases, you can use the page Overview.

3.1 Analytical test cases

This page last changed on 02-07-2008 by platzek.

The following analytical test cases are available at present:

3.1.1 Simple channel flow

This page last changed on 14-08-2008 by platzek.

Purpose

The purpose of this validation study is to show that for a schematised homogeneous channel, Delft3D-FLOW computes accurate water elevations, logarithmic velocity profiles in the vertical direction, and parabolic vertical viscosity profiles. This validation study is performed for the σ-model. In addition, both 2D and 3D models are investigated, with both the algebraic and the $k-\epsilon$ turbulence model. For the 3D models, different vertical layer distributions are investigated. A tracer is also added to check conservation of mass.

Linked claims

Claim 2.2.2.7: Accurate simulation of steady and unsteady flow.
Claim 2.4.1: Accurate, robust and computationally efficient algorithmic implementation.

Approach

Flow in a simple channel with sloping bathymetry is investigated. A steady solution is reached, in which the vertical viscosity term balances the barotropic pressure gradient. For this steady situation an analytical solution is available from the 2D shallow water equations. Results from Delft3D-FLOW simulations are compared to the analytical solution. Both 2D and 3D simulations are performed. For 2D simulations water depth and depth-averaged velocity are compared to the analytical solution and for 3D simulations also vertical profiles for velocity and eddy viscosity are investigated. In the latter case, solutions are obtained with both the algebraic and the $k-\epsilon$ turbulence model. It is validated whether both models produce logarithmic velocity profiles and parabolic eddy viscosity profiles. Also, a comparison has been made between the σ-layer and with the Z-layer model results.

Model description

The properties of the model used in this validation case, are summarised in Table 3.1.1.1.

Length L (m)	10000
Constant slope i_b (-)	0.0001
Discharge q (m^2 /s)	5
Chézy coefficient C_{2D} ($m^{1/2}$/s)	65
Grid size dx=dy (m)	500
Time step dt (s)	60

Table 3.1.1.1: Properties for the simple channel flow validation case.

Using these parameters the equilibrium depth can be determined to be:

$$h_e = \left(\frac{q}{C_{2D}\sqrt{i_b}}\right)^{2/3} = 3.89677\,m \quad .$$

The discharge specified in table 3.1.1.1 is used as the upstream (inflow) boundary condition. For a cell width of 500 m, the specified discharge becomes Q = 2500 m^3/s. At the downstream (outflow) boundary a water level is prescribed:

$$\zeta|_{boundary} = 3.89677 - 1.0 - 0.025 = 2.87177\,m \quad .$$

The correction of 0.025 m is due to the staggered grid numbering. The water level point is located half a grid cell (250 m) further than the depth point at which the domain boundary is located. Therefore, the water level at the boundary is prescribed 1e-4*250 = 0.025 m lower than the water level at the domain boundary. Using the conditions and parameters specified above, a Delft3D-FLOW simulation can be performed. Both 2D and 3D models have been investigated, using many different settings concerning boundary conditions and turbulence modelling.

Results

The results obtained for the different test cases within this validation study are summarised in Table 3.1.1.2. The validity is checked by considering the (relative) difference in equilibrium depth between the simulated solution and the analytical solution.

Dimensionality	**No. of layers**	**Turbulence model**	**Depth at inflow**	**Difference with analytical solution**	**Relative difference**
			[m]	**[m]**	**[%]**
2D	1	N.A.	3.89688	2.900E-06	7.44E-05
3D	10	Algebraic	3.90756	0.0108	0.277
(equidistant)	"	$k-\epsilon$	3.91653	0.0198	0.507
	20	Algebraic	3.91159	0.0148	0.380
	"	$k-\epsilon$	3.93502	0.0386	0.982
3D	10(*1)	Algebraic	3.90322	0.00645	0.166
(non-equidistant)	"	$k-\epsilon$	3.93293	0.0362	0.928
	10(*2)	Algebraic	3.89296	-0.00381	-0.0977
	"	$k-\epsilon$	3.94340	0.0466	1.20
	10(*3)	Algebraic	3.88902	-0.00775	-0.199
	"	$k-\epsilon$	3.93620	0.0394	1.01

Layering	***Layer thickness (bottom to top) [%]***
*(*1)*	*5; 6; 7; 8; 9; 10; 12; 13; 15; 15*
*(*2)*	*2.5; 3.5; 5; 6; 8; 10; 12; 15; 18; 20*
*(*3)*	*4; 5.9; 8.7; 12.7; 18.7; 18.7; 12.7; 8.7; 5.9; 4*

Table 3.1.1.2: Water depths at inflow boundary and comparison to analytical equilibrium depth for the different test cases of the simple channel flow validation study.

In figure 3.1.1.1 the water depth at the simulation end time is given for several situations. It can be seen that on average, simulations with the $k-\epsilon$ turbulence model produce somewhat higher equilibrium depths than with the algebraic model. For the $k-\epsilon$ turbulence model the relative difference is in the order of 1%, whereas for the algebraic turbulence model the relative difference is less than 0.5%. This shows that the water levels are computed in an accurately.

Figure 3.1.1.2 shows four plots, two for the vertical velocity profiles and two for the vertical eddy viscosity profiles for different layer distributions and turbulence models. Results are shown at the end time of the simulation at location x = 9500 m. The top figures show results for equidistant vertical layers and the bottom figures for a non-equidistant layering. The velocities are on average somewhat over predicted compared to the analytical logarithmic profile. Small differences in profile shape can be noticed between results for the algebraic and the $k-\epsilon$ turbulence model. The algebraic turbulence model require less layers to achieve an accurate logarithmic velocity profile compared to the $k-\epsilon$ model. For the algebraic turbulence model, the difference with the analytical solution is more or less constant across the velocity profile (approx. 1%). The $k-\epsilon$ model shows larger variation from surface level to bottom. In the bottom layers, the largest differences with the analytical solution can be observed (approx. 4%).

Using more layers and/or different layering profiles has no significant effect on the results. Results with the algebraic model show a slightly larger velocity in the bottom layers and a smaller velocity in the top layers. The same holds for the $k-\epsilon$ model, except for the bottom layers, where the difference with the analytical solution increases rapidly. For the algebraic turbulence model, results improve when increasing the number of layers. For the $k-\epsilon$ model, using more layers has a small negative effect on the accuracy

of the velocity profile. Using a logarithmic layering in vertical direction has a positive effect on the velocity profile results with the algebraic model and a negative effect for the $k-\epsilon$ model. Summarizing, a 10-layer equidistant distribution already computes accurate vertical velocity and viscosity profiles and accurate water levels.

Although results are shown for the σ-model, we remark that also with the Z-model accurate model results are computed in Delft3D-FLOW. Despite the fact that we have a staircase bottom in a Z-model, accurate water levels and vertical velocity and viscosity profiles are computed.

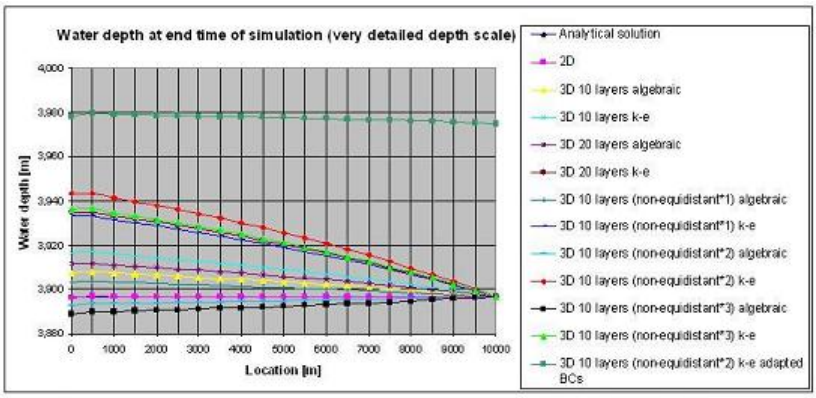

Figure 1: Water depths at end time of the simulation for the different test case of the simple channel flow validation study.

Figure 3.1.1.1: Water depths at end time of the simulation for the different test cases of the simple channel flow validation study.

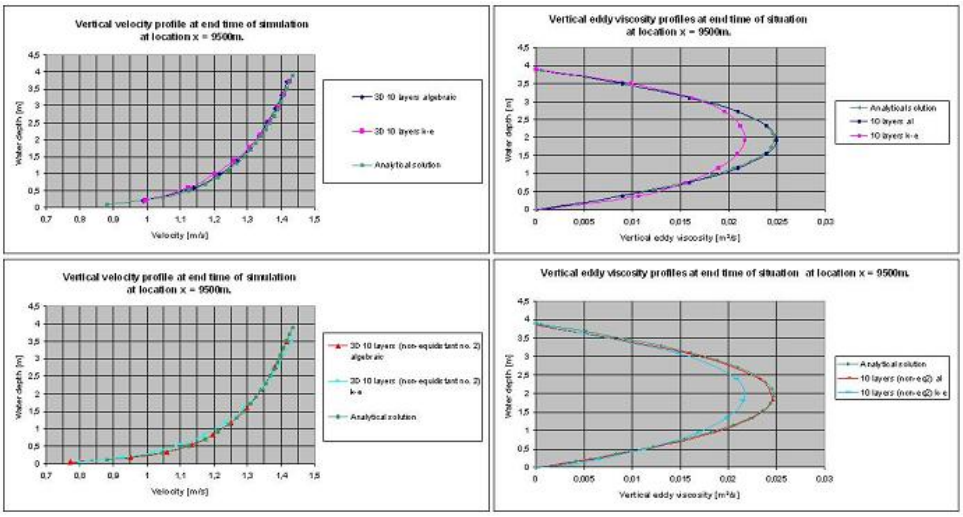

Figure 3.1.1.2: Vertical velocity (left) and eddy viscosity profiles (right) for a selection of the performed test cases of the simple channel flow. Results shown are at the end time of the simulation at location x = 9500 m.

Many more cases have been investigated, where also domain length, slope, discharge, grid size and time step have been varied. Results obtained with these variations show the same order of accuracy and stability as the results presented in this validation study.

Note:

All simulations are conducted with the same boundary and initial conditions. For the outflow boundary condition the 2D equilibrium water depth was specified, i.e. 3.89677 m. From the water depth profiles (figure 3.1.1.1) it is apparent that the equilibrium depths in 3D are not equal to the analytical equilibrium depth in 2D. The result of the small difference in equilibrium depth is that the water level does not have the exact same slope as the bottom. This also gives rise to small acceleration terms in channel direction, i.e. the flow velocity is not completely homogeneous along the channel length. This discrepancy (although small) can be reduced by taking other boundary conditions. A possible remedy is to specify two water level boundary conditions, resulting in a perfect water level slope, but with a slightly different discharge than specified (5 m^2/s). Another option is to specify only a different outflow water level, which should

be more in line with the specific 3D equilibrium depth. This results in a better water level profile, with a slightly different equilibrium depth than the analytical 2D depth, but with the discharge as specified above.

Results for a different outflow boundary condition is shown in Figure 3.1.1.1 as '3*D 10 layers (non-equidistant no. 2) k-e adapted BCs*'. An equilibrium depth is found of h_e = 3.9773 m, which is 2% higher than the 2D equilibrium depth. In this case, the analytical velocity profile has been calculated using this equilibrium depth. Differences in velocity profile and water depth compared to the solution with the normal boundary conditions occur, but are marginal for simulations with these adaptations in boundary conditions.

A similar analysis has been done for the eddy viscosity profile. The analytical solution is a parabolic profile. The results show maximum relative differences with the analytical solution (of all considered cases) of 10-12% (for the $k-\epsilon$ models). For the eddy viscosity profile, a logarithmic layering has a small positive effect for both the algebraic and the $k-\epsilon$ turbulence model.

Conclusions

From the simple channel flow validation study, it can be concluded that Delft3D-FLOW accurately reproduces steady flow (which is partly Claim 2.2.2.1) along a sloping bathymetry and the propagating waves that proceed the steady state solution (Claim 2.2.2.7). Results show differences with a maximum of 2% with respect to the analytical 2D solution for water depths, with a maximum of 4% for the vertical velocity profiles and 10-12% for the vertical eddy viscosity profiles. The computational algorithm shows robust and accurate results for different grid sizes, time steps and model properties (Claim 2.4.1). The use of more layers or local refinement in the vertical direction has a positive effect on results with an algebraic turbulence model and a negative effect on results with the $k-\epsilon$ model. Application of different types of (consistent) boundary conditions has a marginal effect on the results.

3.1.2 Standing wave

This page last changed on 02-07-2008 by platzek.

Purpose

The purpose of this validation study is to investigate the ability of Delft3D-FLOW to accurately compute the propagation of long waves, in which the treatment of boundary conditions plays a role as well. This is achieved by considering a standing wave in a closed basin. Delft3D-FLOW uses an Alternating Direction Implicit (ADI) time integration in the solution of the flow equations. This method switches between an explicit and implicit time integration method for the x- and y-directions. We examine the behaviour of a standing wave at a 45° angle with respect to the grid lines. In this way, we check whether the accuracy of the ADI solver depends on the orientation of the grid. In the absence of bottom friction, all waves should reflect on the closed boundaries without energy loss and the standing wave should not damp or spread. Therefore, the effect of numerical damping is investigated in this validation study.

Linked claims

Claim 2.2.2.1: Propagation of long waves.
Claim 2.4.1: General (robustness, accuracy, efficiency).
Claim 2.4.3a: Delft3D-FLOW uses a robust ADI solver.

Approach

The propagation of long waves is investigated for propagation in x-direction, in y-direction and under an angle of 45° with respect to the coordinate axes. The effect of the Alternating Direction Implicit (ADI) time integration solver and the added numerical damping then becomes important. In addition, the influence of the ratio of wave amplitude over water depth on the results is investigated.

Model description

A closed square basin of dimensions 20 x 20 m is used as domain. Waves with different direction, length and amplitude have been used as initial water elevation. Here, the results are presented for 3 cases:

1. a wave in x-direction
2. a wave in y-direction
3. a wave with a 45° angle with respect to both axes.

For the first two cases a wave length of 20 m is taken and for the third case a wave length of $\sqrt{2}$ x 20 = 28.28 m. For all three cases an amplitude of 0.01 m is used. This small amplitude is chosen to ensure purely linear wave behaviour. The model uses the following parameters:

- 3D model, with 20 layers.
- 40x40, rectangular grid.
- Simulation time 30 s.
- Δt = 0.03 s.
- Initial depth 10 m.
- $k-\epsilon$ turbulence model.
- Chézy coefficient C = 1000 $m^{1/2}/s$ (frictionless bed).

Results

The effect of the angle of the wave with respect to the grid is investigated. In figures 3.1.2.1-3.1.2.4 the wave celerity c and period T are plotted as a function of the non-dimensional time step dt/T. The results for the wave in x- and y-direction are exactly equal, which illustrates that in Delft3D-FLOW results for models in either x- or y-direction are identical. For non-dimensional time steps larger than approximately 0.05-0.03 the celerity and period start to differ significantly from the analytical solution. For the 45°-angle wave the effect is slightly larger. This is most likely an ADI-effect. However, the absolute (and relative) errors for the 45°-angle wave are in the same order of magnitude, which shows that the accuracy in wave propagation for Delft3D-FLOW is more or less independent of the directions of the waves.

More importantly, for values of dt/T that are sufficiently small (say < 0.025) the figures show that the absolute and relative errors are small. The value of 0.025 corresponds to 40 points per wave period, which time step limitations was given in Table 2.2. In practice, the values for dt/T are even much smaller. For example, in a North Sea model, in which the semi-diurnal tide is dominant, and a time step of 5 minutes, dt/T reads 0.007.

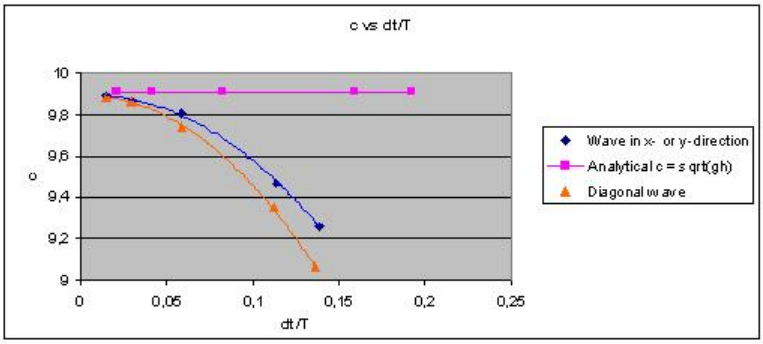

Figure 3.1.2.1: Wave celerity c versus scaled time step dt/T, for the different wave directions.

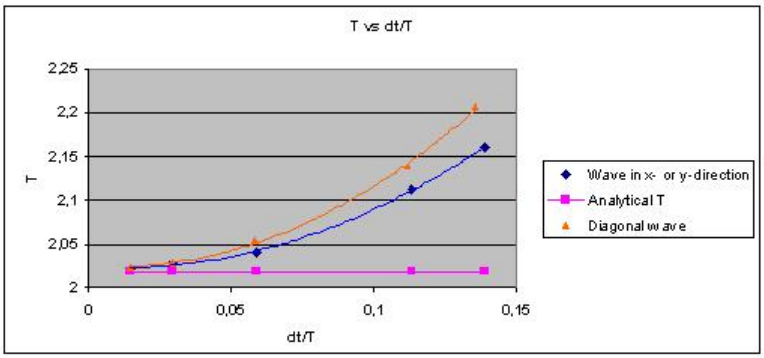

Figure 3.1.2.2: Wave period T versus scaled time step dt/T, for the different wave directions.

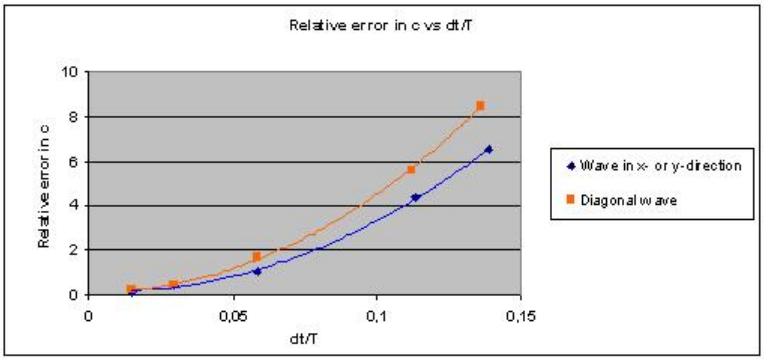

Figure 3.1.2.3: Relative error (in %) in wave celerity c with respect to the analytical solution, versus scaled time step dt/T, for the different wave directions.

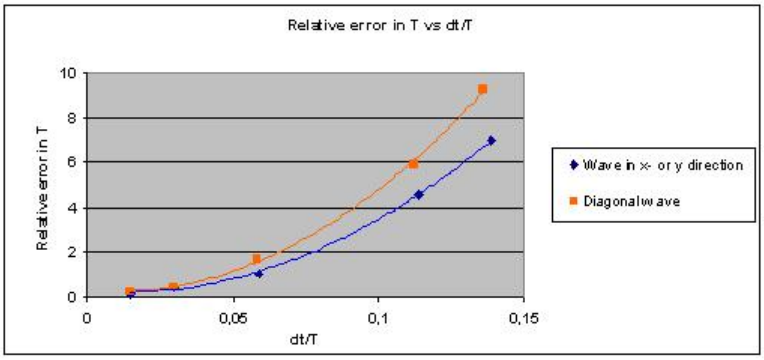

Figure 3.1.2.4: Relative error (in %) in wave period T with respect to the analytical solution, versus scaled time step dt/T, for the different wave directions.

Conclusions

The propagation, reflection against boundaries and interaction of long waves (small amplitude-water depth ratio) is simulated correctly with Delft3D-FLOW. A standing wave in a closed basin is simulated to show nice symmetric behaviour and little numerical damping. This is not only the case for wave propagation that is aligned to the computational grid, but also for waves that make an angle of 45° with the grid.

3.1.3 Grid distortion

This page last changed on 02-07-2008 by platzek.

Purpose

The purpose of this validation study is to investigate the effect of a misaligned grid, i.e. a grid that makes an angle with the flow direction, on the accuracy of the model results.

Linked claims

Claim 2.4.2: Computational grid.
Claim 2.4.3a: Robust ADI solver.
Claim 2.4.4a: Hydrodynamic advection.

Approach

A uniform flow in a simple straight channel with a sloping bottom is prescribed (see also validation study 3.1.1 *Simple channel flow*). Then, the slope of the water level should be equal to the slope of the bottom. Also the barotropic pressure force balances the vertical viscosity force and the flow is in equilibrium. In theory, the orientation of the grid should not have any effect on the accuracy of the model results. In this validation study it is investigated to which extent this is valid for a sinusoidal grid, see Figure 3.1.3.1.

Model description

A straight channel with a sinusoidal grid is used. A bathymetry with a linear slope is applied in x-direction. The grid and bathymetry are shown in Figure 3.1.3.1. The main model dimensions and parameters are:

- 2DH model
- domain length L = 500 m, width 240 m.
- bottom slope 0.001: Bottom height range: -4 to -4.5 m.
- Chézy coefficient 65 $m^{1/2}/s$.
- constant inflow velocity 2.93 m/s.
- equilibrium depth 2.037 m (outflow boundary: water level ζ = 2.037 - 4.5 = -2.463 m).
- simulation time 5 hours.

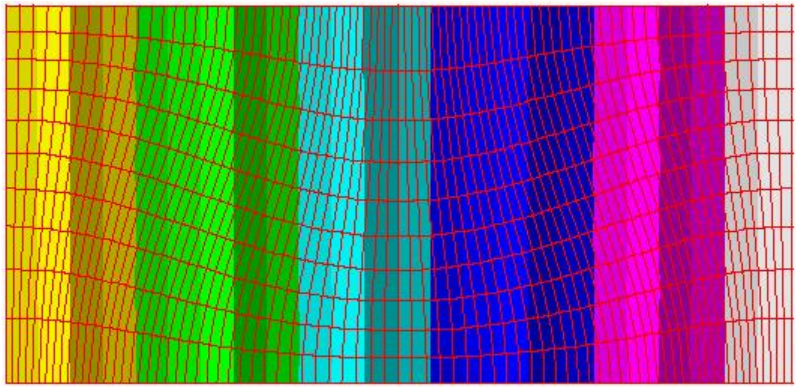

Figure 3.1.3.1 The computational grid and accompanying depth profile. Bottom height ranging from -4 m (left) to -4.5 m (right).

Results

Figure 3.1.3.2 shows the water depth at the end of the simulation time. One can see that small deviations from the analytical equilibrium depth are present, but that a large part of the interior domain has a depth approximately equal to the analytical equilibrium depth of 2.037 m. As one may expect, deviations are most prominent in the areas where the grid misalignment is largest (also largest grid size and aspect ratio). The maximum relative error is (2.052 - 2.037)/2.037 x 100 % = 0.74 %.

In addition, errors occur at inflow and outflow. This is due to the fact that the boundary conditions are constant along the width of the channel, while the grid orientation is not. Along the boundaries the flow is assumed to be perpendicular to the open boundary in Delft3D-FLOW, because so-called tangential velocity can not be specified. This is a local (open boundary) effect. This can partly be circumvented by adding one or a few columns of rectangular cells at both boundaries, as shown in Figure 3.1.3.3. The maximum relative error then reduces to (2.047 - 2.037)/2.037 x 100 % = 0.49 %. Grid refinement, for which no results are shown, even further reduces the overall error. After a mesh refinement with a factor of two the maximum relative error to approximately 0.4 % for both the original mesh and the extended mesh. This shows that the error made at the boundary dominates the error made by the grid distortion in this case.

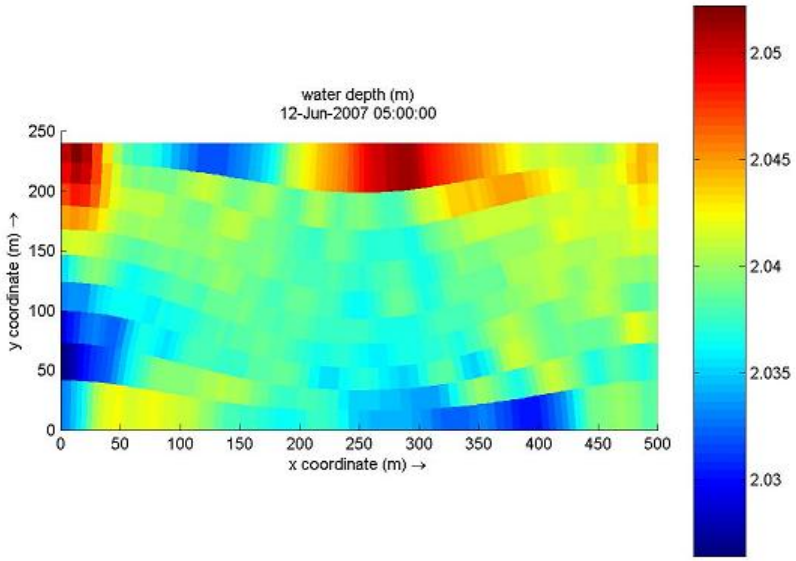

Figure 3.1.3.2 Water depth at the end of the simulation time (steady state solution).

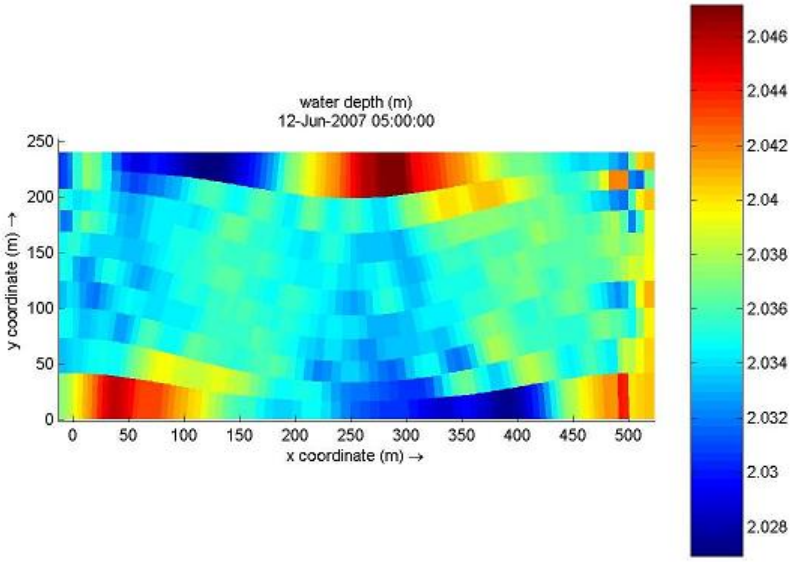

Figure 3.1.3.3 Water depth at the end of the simulation time (steady state solution) with the extended grid.

Conclusions

A misaligned mesh has a marginal distortion effect on the accuracy of the model results. Maximum errors are in the order of 1 % or less. Delft3D-FLOW can therefore deal with flows that are not aligned with the grid. As expected, grid refinement results into even smaller errors.

3.1.4 Wind driven channel flow

This page last changed on 18-08-2008 by platzek.

Purpose

The purpose of this validation study is to show that Delft3D-FLOW can accurately simulate the flow induced by a constant wind forcing in a straight channel.

Linked claims

Claim 2.2.1.3: Wind driven flow and storm surges.
Claim 2.2.3.8: Wind and bottom friction.

Approach

For the wind induced flow in a straight channel analytical solutions are available [Kocyigit and Falconer, 2004]. A comparison is made between the analytical solutions in these publications and results obtained with Delft3D-FLOW. This is done for the water levels and vertical velocity profiles.

The analytical solution presented by Kocyigit and Falconer reads:

$$\frac{d\zeta}{dx} = \frac{3}{2}\frac{\tau_w}{\rho_w g h}\frac{(2\nu_v + k_1 h)}{(3\nu_v + k_1 h)} \quad ,$$

$$u = \frac{g}{6\nu_v}\frac{d\zeta}{dx}(3z^2 - h^2) + \frac{\tau_w}{2\rho_w \nu_v}(h + 2z) \quad ,$$

in which ζ is the water level, τ_w is the wind shear stress, ρ_w is the water density, g is acceleration due to gravity, h is the water depth, ν_v is the vertical eddy viscosity, k_1 is a linearised bottom friction coefficient and u is the horizontal velocity.

Kocyigit and Falconer specified the following conditions and parameters:

- Wind speeds of 5 and 10 m/s (2 tests).
- τ_w = 0.1 and 0.325 N/m^2, for test 1 and 2 respectively.
- ρ_w = 1026 kg/m^3.
- ν_v = 0.03 m^2.
- k_1 = 5e-3 m/s.

In Delft3D-FLOW one can not specify the wind shear stress, but only the friction coefficient. The latter is determined using

$$\tau_w = \rho_a c_{d_w} u_w^2 \quad ,$$

where ρ_w is the air density, c_{d_w} is the friction coefficient and u_w is wind velocity. Wind speeds of 5 and 10 m/s and τ_w values of 0.1 and 0.235 N/m^2 respectively were specified by Kocyigit and Falconer. Using the above-described, friction coefficients c_{d_w} should be 0.004 and 0.00325, respectively, in order to arrive at the wind stresses of Kocyigit and Falconer. In this way, the simulations of Kocyigit and Falconer are reproduced with Delft3D-FLOW.

A same approach is followed for the linear bottom friction coefficient k_1. In Delft3D-FLOW the bottom roughness is prescribed in a different way. The standard approach is the (2D) Chézy coefficient. In Delft3D-FLOW this value is converted in a 3D friction coefficient in case of 3D modelling. A 2D Chézy roughness of 30 m$^{1/2}$/s is applied in case of a wind speed of 5 m/s, which corresponds to a k_1 value of 0.005 m/s. In case of a wind velocity of 10 m/s, a Chézy value of 35 m$^{1/2}$/s is used. We remark that the two simulations (wind speed of 5 or 10 m/s) yields different bottom currents. In order to meet the linear bottom friction coefficient k_1, different Chézy values have to be applied.

Model description

For this test case, the closed straight channel of [Kocyigit and Falconer, 2004] is used. The model parameters are:

- Length of the channel *L* = 12000 m.
- Width of the channel *W* = 1000 m.
- Depth of the channel *h* = 40 m.
- Grid size Δx = Δy = 1000 m.
- Simulation time T = 1 day (14400 minutes), with a time step Δt = 1 minute.
- a double-logarithmic vertical σ-layering is used with 14 layers.
- All boundaries are closed.
- Initial condition: flow at rest with uniform depth 40 m.
- A constant external wind forcing was applied, in the direction of the length of the channel (x-direction, 270 °):
  - Test 1: wind forcing of 5 m/s.
  - Test 2: wind forcing of 10 m/s.
- Two different Chézy values were used for the two tests, derived in accordance with roughness values specified by Kocyigit and Falconer:
  - Test 1: Chézy = 30 $m^{1/2}$/s.
  - Test 2: Chézy = 35 $m^{1/2}$/s.

The difference in Chézy values for the two test cases can be subscribed to the conversion from a 2D to a 3D Chézy value in Delft3D-FLOW. The resulting bottom friction stresses were compared to make sure identical bottom boundary conditions were applied. To this end the second test case requires a Chézy value of 35 $m^{1/2}$/s.

Results

Results from Delft3D-FLOW simulations are compared to the analytical solution described above. This is done for water levels and horizontal velocity profiles. Figure 3.1.4.1 and 3.1.4.2 show the water level and velocity profiles for the 5 m/s wind velocity case (test 1). Both the analytical and numerical results are shown. The same is done for test 2 with 10 m/s wind velocity in figures 3.1.4.3 and 3.1.4.4.

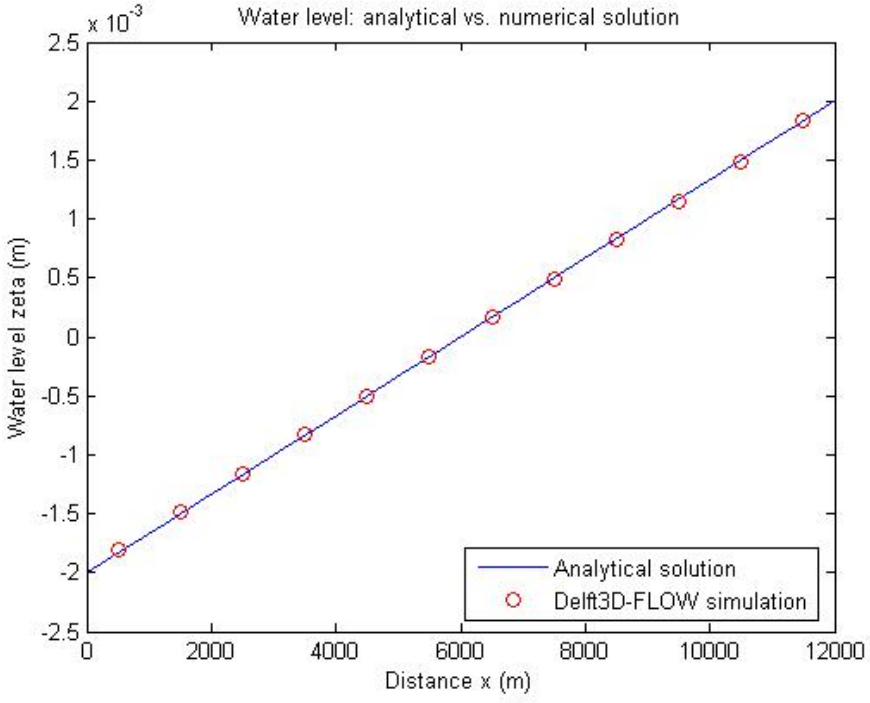

Figure 3.1.4.1 Water level for 5 m/s wind velocity. Both analytical and numerical solutions are shown.

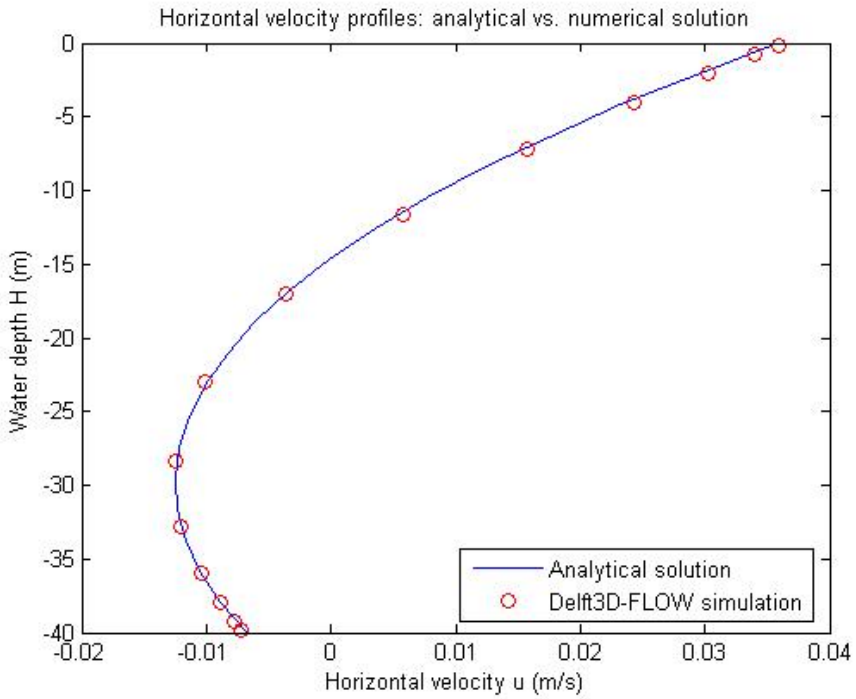

Figure 3.1.4.2 Horizontal velocity profile for 5 m/s wind velocity. Both analytical and numerical solutions are shown.

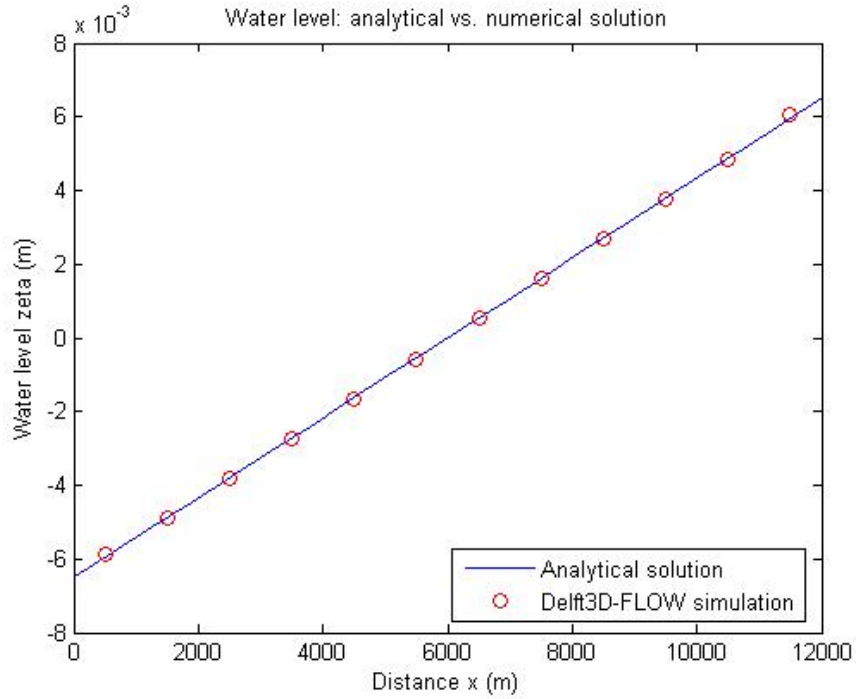

Figure 3.1.4.3 Water level for 10 m/s wind velocity. Both analytical and numerical solutions are shown.

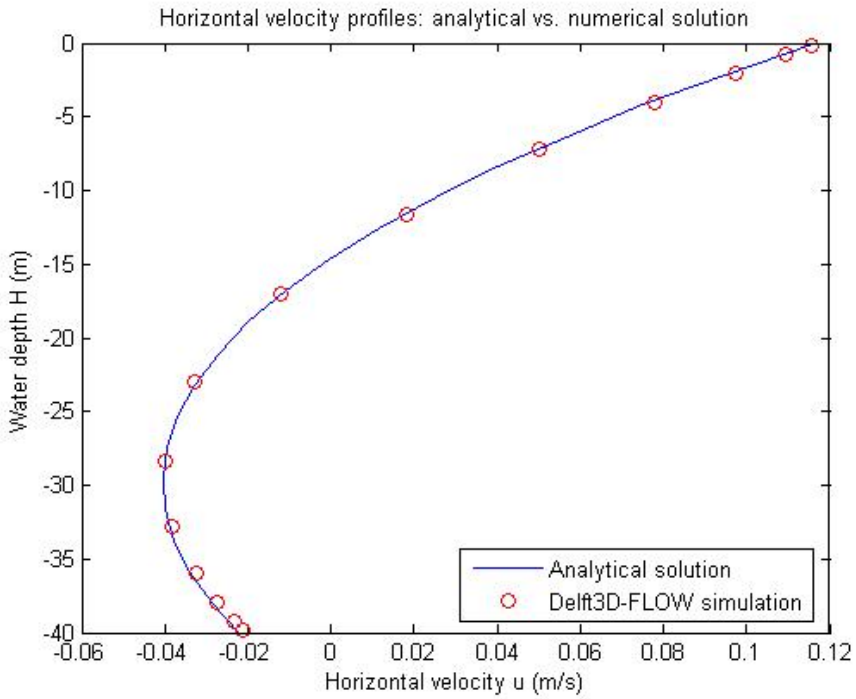

Figure 3.1.4.4 Horizontal velocity profile for 10 m/s wind velocity. Both analytical and numerical solutions are shown.

A different number of layers and also different sorts of layering were used. For less than 10 layers the results become inaccurate. For more than 20 layers, no improvement is seen in the results.

Conclusions

It can be concluded that Delft3D-FLOW can accurately reproduce the water level and horizontal velocity profiles induced by wind. Numerical results agree very well with the analytical solution provided by Kocyigit and Falconer.

3.1.5 Lock exchange flow

This page last changed on 18-08-2008 by platzek.

Purpose

The purpose of this validation study is to investigate the propagation of baroclinic flow and transport of matter due for density driven flow. Both the hydrostatic and the non-hydrostatic mode of Delft3D-FLOW are tested.

Linked claims

Claim 2.2.1.2: Density driven flow and salinity intrusion.
Claim 2.2.1.4: Horizontal transport of matter on large and small scales.
Claim 2.2.1.9: Hydrostatic and non-hydrostatic flow.
Claim 2.2.2.2: Baroclinic flow - salinity and temperature driven flow.

Approach

In this so-called lock exchange test case, a closed basin with two water masses with a different density is initially separated by a vertical wall. Next, this vertical wall is removed. Due to the existence of an internal gravity gradient, the fluid layers adjust and form a stably stratified, two-layer system with the heavier water at the bottom and the lighter water at the surface. Sharp density fronts divide the two layers both horizontally and vertically. Density fronts of this type are often observed in estuaries.

The length *L* of the basin is 112.5 m and the depth *H* is 10 m. The initial salinity concentrations of the two water bodies are:

$$c = \begin{cases} 5 & \text{ppt} \quad \text{if} \quad 0 \leq x < \frac{1}{2}L \\ 10 & \text{ppt} \quad \text{if} \quad \frac{1}{2}L \leq x < L \end{cases} .$$

This salinity distribution gives rise to a density difference of $\Delta\rho = \rho_2 - \rho_1 = 3.8 kg/m^3$. The inherent baroclinic pressure gradient induces gravity currents at the bottom and the free surface; the heavier water tends to intrude underneath the less dense fluid resulting in two fronts moving in opposite directions. The front speed u_f can be deduced by considering the energy budget of the system (assuming no viscosity), which yields:

$$u_f = \frac{1}{2}\sqrt{\frac{gH\Delta\rho}{\rho_0}} .$$

According to the above-described equation the celerity of the front is equal to 0.30 m/s for the present case. The shear that is introduced due to the gravity current gives rise to instabilities that are allowed to grow if the Richardson number falls typically below 0.25. Then so-called Kelvin-Helmholtz instabilities may be observed. According to theoretical analysis, the slope of the fronts at the stagnation point (water surface and bottom) is 60° to the horizontal [Turner, 1973].

Model description

A 2DV model is applied with 150 grid cells in the horizontal (Δx = 0.75 m) and 20 layers in the vertical (Δz = 0.5 m). In the vertical, the Z-model schematisation is used. The time step used is 0.3 sec. In this way, the stability criterion for the propagation of internal waves is satisfied. For turbulence closure, the $k-\epsilon$ model is used, without background values for viscosity and diffusivity.

The model is initialised at t = 0 s with on the left side of the basin a salinity of 5 ppt and at the right side of the basin a salinity of 10 ppt (cf. Figure 3.1.5.1). A run has been made in both the non-hydrostatic and the hydrostatic mode.

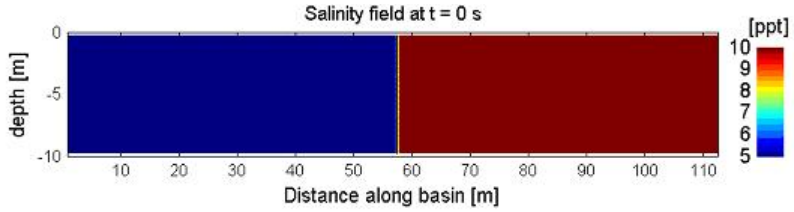

Figure 3.1.5.1 Initial distribution of salinity.

Results

After the removal (at t = 0 s) of the vertical wall separating the two fluids, two discontinuities are moving in opposite direction. Figures 3.1.5.2 and 3.1.5.3 show the salinity distribution after 120 s for the hydrostatic and the non-hydrostatic mode, respectively. In the hydrostatic mode, the shape of the front is not smooth. In the non-hydrostatic mode, the front is more smoothly curved. For both computations, the bottom and surface front speeds have been derived. In the hydrostatic mode, the computed front speeds are 0.22 m/s, whereas in the non-hydrostatic mode, the computed front speeds are 0.27 m/s.

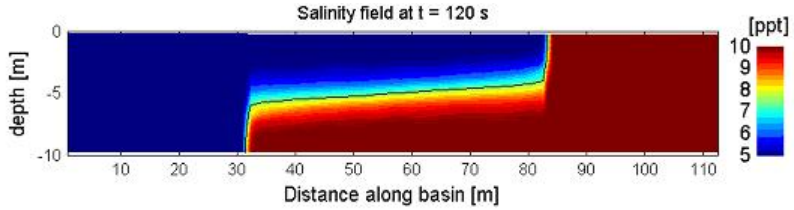

Figure 3.1.5.2 Distribution of salinity at t = 120 s; hydrostatic mode.

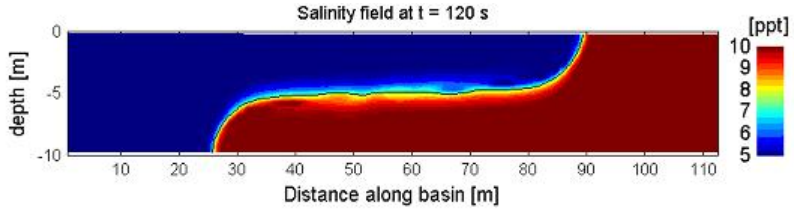

Figure 3.1.5.3 Distribution of salinity at t = 120 s; non-hydrostatic mode.

Conclusions

The computational results are consistent with theory, as the heavier water intrudes underneath the less dense fluid resulting in two fronts moving in opposite directions. The computed front speed of 0.27 m/s in the non-hydrostatic mode is close to the analytical front speed of 0.3 m/s. In the hydrostatic mode the computed front speed is considerably less.
This test case shows that Delft3D-FLOW is capable of correctly reproducing density driven flow (Claim 2.2.1.2 and Claim 2.2.2.2) as well as predicting the horizontal transport of matter (in this case salinity) in an accurate way (Claim 2.2.1.3). Delft3D-FLOW offers the possibility of either a hydrostatic or a non-hydrostatic mode (Claim 2.2.1.9). This experiment shows that significant differences can occur between the hydrostatic and non-hydrostatic results. Depending on the application, the user can choose the most suitable approach. For example, the front speeds and shapes in general differ considerably between both modes, whereas final steady state results (a stable, stratified, two density layer system) will be more or less similar.

3.1.6 Wave forces and a mass flux in a closed basin

This page last changed on 02-07-2008 by platzek.

Purpose

To investigate the combined effect of wave force and mass flux in a closed basin and comparison with a semi analytical solution.

Linked claims

2.2.2.16: Accurate flow for wave induced forces and mass fluxes.

Approach

In order to get an impression of the effect of the combination of a wave force and a mass flux on the behaviour of a water system, an analytical solution was determined for a simple case. By comparing with the analytical solution the accuracy of the Delft3D-FLOW model results is quantified.

In a stationary situation, the forces generated by the pressure gradient, by waves and those generated by the bottom shear stress are in equilibrium. Figure 3.1.6.1 shows a sketch of all horizontal forces that act on a control volume.

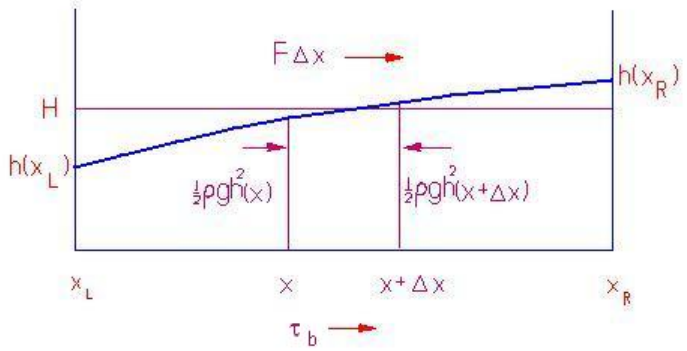

Figure 3.1.6.1: Wave force and mass flux effect.

The mass flux *M*, which is chosen to be a positive constant, is in the stationary case related to the local depth and the velocity by

$$M = -hu \quad ,$$

with *h* the local water depth. The corresponding Chézy expression for the bottom stress reads

$$\tau_b = \frac{\rho g}{C^2} u^2 \quad .$$

If we assume the wave force to be a positive constant, the sum of all forces on the control volume can in the stationary situation be written as:

$$\frac{\rho g}{C^2} \int_x^{x+\Delta x} u^2(\xi)\, d\xi + F\Delta x - \frac{1}{2}\rho g \left[h^2(x+\Delta x) - h^2(x)\right] = 0 \quad .$$

From this equation we can derive the differential equation:

$$\frac{\rho g}{C^2} u^2 + F - \frac{1}{2}\rho g \frac{dh^2}{dx} = 0 \quad .$$

Multiplying by h^2 and substituting the expression found for *M* yields a differential equation for the water depth:

$$\frac{M^2}{C^2} + \frac{F}{\rho g}h^2 - h^3\frac{dh}{dx} = 0 \quad \text{or}$$

$$\frac{dh}{dx} = \frac{A}{h} + \frac{B}{h^3} \quad \text{with } A = \frac{F}{\rho g} \quad \text{and } B = \frac{M^2}{C^2} \quad .$$

Next, we arrive at

$$x - x_0 = \int_{h_0}^{h} \frac{\xi^3\, d\xi}{A\xi^2 + B} = \frac{1}{2A}\left[h^2 - h_0^2 - \frac{B}{A} ln\left(\frac{h^2 + B/A}{h_0^2 + B/A}\right)\right] \quad ,$$

with given values for A, B and the depth h_0 at a fixed position x_0, the value h can be solved numerically from the last equation at any given value x.

The initial water level H, to be used in the FLOW computation, can be determined by first solving $h(x_L)$ and $h(x_R)$ at the left and right boundaries of the basin x_L and x_R respectively. Secondly, the following expression is determined numerically:

$$H = h(x_R) - x_0\frac{h(x_R) - h(x_L)}{x_R - x_L} - \frac{1}{x_R - x_L}\int_{h(x_L)}^{h(x_R)} \frac{1}{2A}\left[h^2 - h_0^2 - \frac{B}{A} ln\left(\frac{h^2 + B/A}{h_0^2 + B/A}\right)\right] dh \quad .$$

If we choose:

ρ = 1000.0 kg/m^3, g = 10.0 m/s^2, F = 10.0 N/m^2, C = 45.0 m$^{1/2}$/s^2 and M = 0.4 m^2/s, we find A = 1000.0 m and B = (0.4/45.0)^2 m^3. The left boundary of the model is chosen at x_L = 0.0 m, the right boundary at x_R = 500.0 m.

By choosing x_0 equal to x_L, we can iterate the last two equations above to find a value for $h_0 = h(x_L)$ such that H equals 1 m. We find $h(x_L)$ = 0.688453379 m. By inverting the equation for x - x_0, the solution for the free surface can be found.

Requirement: The results of a computation should not deviate more than 10^{-2} m from the analytical solution for the water level.

Model description

The values for x_L and x_R were chosen as 0 and 500 m, respectively. A 2D homogeneous model (closed basin) is applied with a uniform depth of 1 m. The grid size in x-direction is 10 m. In y-direction the length of the computational domain is 60 m with grid sizes of 10 m.

Results

The above described procedure is verified for the left boundary only. Delft3D-FLOW computes at the left boundary a total water depth of 0.6968 m. The difference with the analytical solution $h(x_L)$ = 0.688453379 m is 0.008 m, which is within the acceptance criterion. In Figure 3.1.6.2 computed water levels are shown (in red) along the basin. The analytical solution is represented by the black line. From this figure it can be seen that for the whole basin the computed and analytical solution are in good agreement with each other. The two lines are almost on top of each other. On the vertical axis the water elevation is shown. We remark that the water elevation above the reference level (of 0 m) is shown. In order to determine the total water depth H, these values should be increased by 1 m.

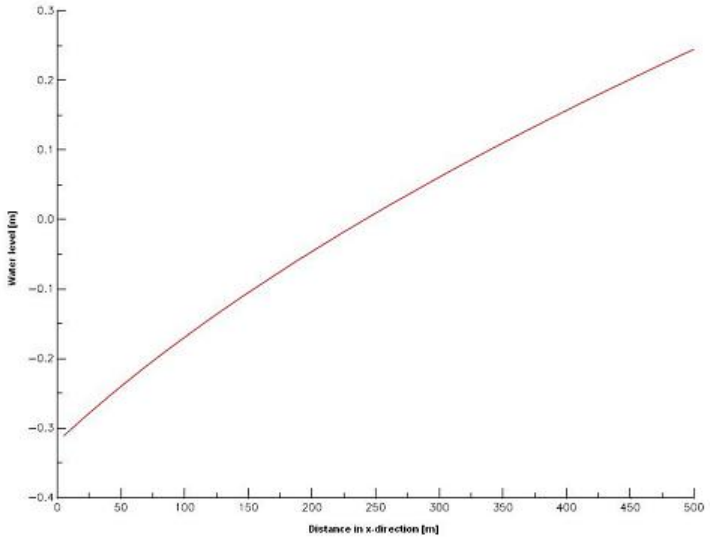

Figure 3.1.6.2: Water level (in m) along the basin; computed (in red) and according to the analytical solution (in black); on x-axis the x-coordinate (in m) of the basin.

Conclusions

Delft3D-FLOW is capable of accurately computing a stationary free surface that is driven by a constant wave force and a constant mass flux.

3.1.7 Flow over a weir

This page last changed on 18-08-2008 by platzek.

Purpose

Verification of (super)critical flow over a weir. Moreover, the advection schemes in Delft3D-FLOW are tested.

Linked claims

Claim 2.2.1.6: Delft3D-FLOW can be used to investigate the impact of hydraulic structures, such as gates, weir and barriers.
Claim 2.2.2.6: Subcritical and supercritical flow.
Claim 2.2.3.4b: Abruptly changing bathymetry, orbital movements in short wave motions, or intensive vertical circulations such as buoyant jet plumes: non-hydrostatic (Navier-Stokes) equations.
Claim 2.4.4a: Algorithm for hydrodynamic advection.
Claim 2.4.7: Algorithm for hydraulic structures is robust, accurate and efficient.

Approach

The flow condition over a weir may be sub- or supercritical. For supercritical flow the discharge at the weir is completely determined by the energy head upstream. In such a case, the discharge is limited by:

$$Q_{critical} = B\frac{2}{3}E_1\sqrt{\frac{2}{3}gE_1} \quad ,$$

which is described in detail in Section 10.9.2.4 of the Delft3D-FLOW manual. The purpose of this validation study is to verify whether Delft3D-FLOW is able to accurately compute this theoretical maximum. In Delft3D-FLOW multiple advection schemes have been implemented. One of these schemes, namely the so-called *Flooding scheme* is suited for flow over obstacles like weirs. By comparing with another advection scheme of Delft3D-FLOW (i.e. the cyclic scheme, which is the default option in Delft3D-FLOW), we will show that the flooding scheme yields accurate results for such applications, while the cyclic scheme will appear to be less accurate.

Model description

The upstream water level boundary is 2.0 m and the downstream boundary equals 1.7 m. The sill height is 1.0 m above the bottom of the channel. The discharge is critical over the top of the sill. The energy height upstream E_1 is about 1.0 m. The width B of the channel is 90 m. The Chézy coefficient is 100 $m^{1/2}/s$ (no water level gradient due to bottom friction). We simulate a channel with a grid size of 10 m and 30 m, respectively. On the coarse grid the sill is represented by one grid cell and on the fine grid by three grid cells. For our test case $Q_{critical}$ yields a maximum discharge of 153 m^3/s.

Results

We simulate the flow with two advection schemes: *cyclic*, which is the default option in Delft3D-FLOW and *flooding*. In table 3.1.7.1 below the discharge over the weir is presented, of which the theoretical value is 153 m^3/s. For this table it is evident that the discharge computed by the flooding scheme is close to the theoretical value, which is much less the case for the cyclic scheme.

	Cyclic	**Flooding**
Δx = 10 m	170 m^3/s	161 m^3/s
Δx = 30 m	207 m^3/s	157 m^3/s

Table 3.1.7.1: Discharge over the weir as simulated with two different grid sizes, using both the Cyclic and the Flooding scheme.

Below four figures are presented that show the discharge per cross section of one grid cell, for these four simulations. For the 30 m test model we have three grid cells in cross sectional direction, which means

that we have to multiply the results plotted in Figures 3.1.7.1 and 3.1.7.2 with a factor of three to arrive at the numbers in the table above. For the 30 m test model we have to multiply with a factor of nine. The figures are in the following order:

Figure 3.1.7.1: Cyclic scheme - 30 m grid size
Figure 3.1.7.2: Flooding scheme - 30 m grid size
Figure 3.1.7.3: Cyclic scheme - 10 m grid size
Figure 3.1.7.4: Flooding scheme - 10 m grid size

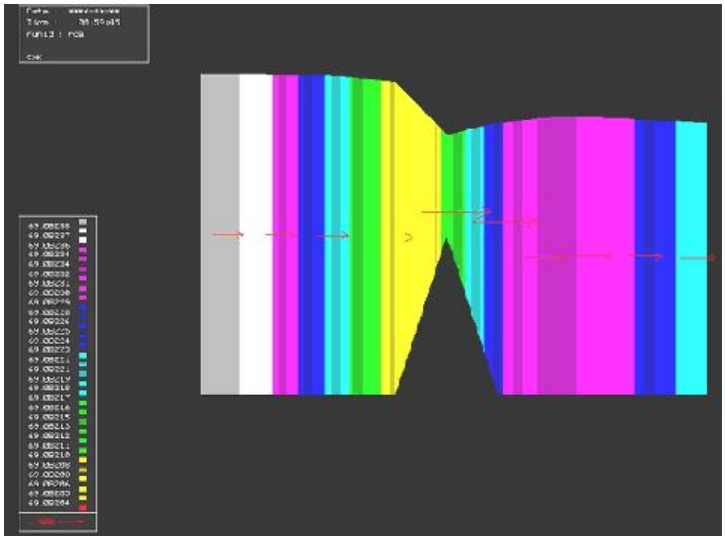

Figure 3.1.7.1: Cross sectional discharges for Cyclic scheme and a 30 m grid size.

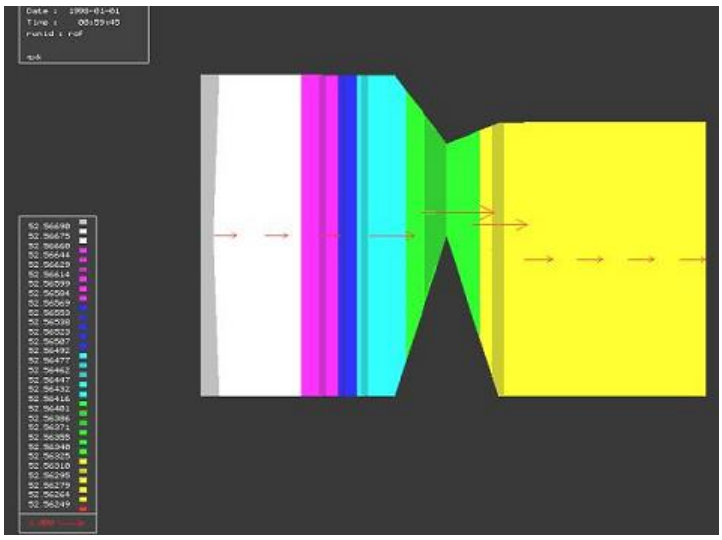

Figure 3.1.7.2: Cross sectional discharges for Flooding scheme and a 30 m grid size.

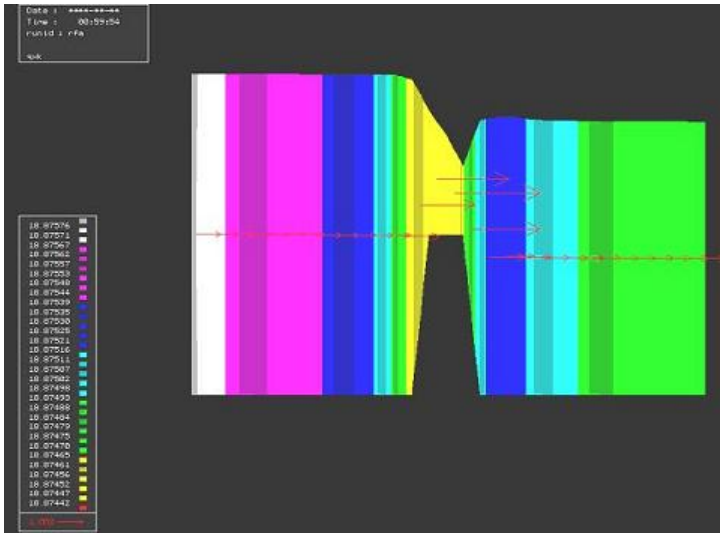

Figure 3.1.7.3: Cross sectional discharges for Cyclic scheme and a 10 m grid size.

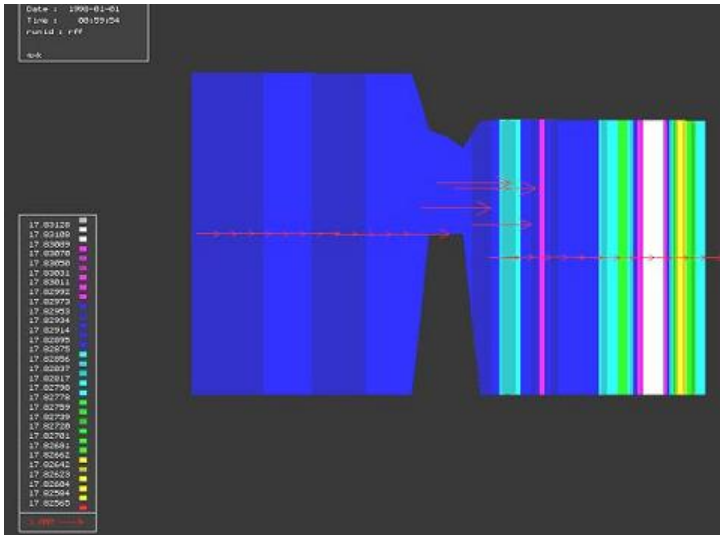

Figure 3.1.7.4: Cross sectional discharges for Flooding scheme and a 10 m grid size.

For the Flooding scheme the relative error in discharges is a few percent (2-5% for the 10 m and 30 m models, respectively). This shows that the Flooding scheme is able to accurately compute flows over a weir when the flow becomes supercritical. For other (i.e. subcritical) flow conditions Delft3D-FLOW has been tested as well. However, that is not part of this test case. For subcritical flows the discharges over a weir and the corresponding energy loss is based on experimental data ("Tabellenboek van Rijkswaterstaat", Vermaas 1987) and/or the formula of Carnot. For more details we refer to the Delft3D-FLOW manual.

Conclusions

This validation study that Delft3D-FLOW is able to accurately compute the flow over a weir. One should use the *Flooding* advection scheme for this application. The Delft3D-FLOW default *Cyclic* advection scheme is less suited for such situations. For the Flooding scheme, the relative difference with the analytical discharge for a supercritical flow over a weir is 2-5%.

3.1.8 Coriolis test case

This page last changed on 18-08-2008 by platzek.

Purpose

This validation study investigates the influence of the Earth's rotation, i.e. Coriolis forcing. For models that are of large geometrical scale, the Coriolis forcing plays an important role.

Linked claims

Claim 2.2.2.9: The effect of the Earth's rotation (Coriolis force).
Claim 2.3.3.7: Coriolis force.

Approach

A prismatic channel is considered, under the influence of wind, Coriolis forcing and bed friction. Under such conditions, the equations can strongly be simplified, so that an analytic solution can be derived. Results obtained with Delft3D-FLOW are compared to this analytical solution. Applying the β-plane approximation following Wyrtki (1961) results into a solution for the water level variation. The solution represents an equilibrium between wind forcing, bed friction and the Coriolis force.

Model description

For this large scale model spherical coordinates are used. A prismatic grid is then specified from 115 to 118.2 ^{o} West-East by -6 to 5 ^{o} South-North (i.e. around the equator), representing Makassar Strait. A grid resolution of 0.066667 x 0.22917 ^{o} is used, resulting into a 50x50 spherical-curvilinear grid, see Figure 3.1.8.1. This model is a schematic representation of Makassar Strait [Hulsen et al. (1998)]. The most important model parameters are:

- Simulation time T = 86400 s (60 days).
- Time step Δt = 300 s (5 minutes).
- (Reference) initial water depth D = 197.2 m.
- Wind velocity V_w = 5 m/s.
- Wind direction = South-North, i.e. 180 ^{o}.
- Wind friction coefficient C_{Dw} = 0.001.
- Chézy coefficient C = 60 m$^{1/2}$/s.
- Water density ρ_w = 1035 kg/m^3.
- Air density ρ_a = 1.2 kg/m^3.

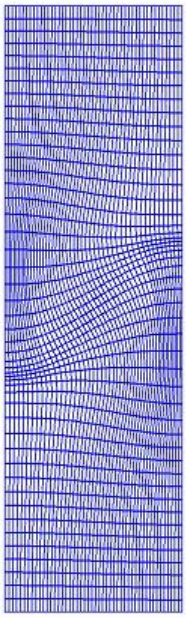

Figure 3.1.8.1: The spherical-curvilinear 50x50 grid.

Initial and boundary conditions are obtained from the β-plane solution. The velocity in u-direction (South-North) is equal to zero. The v-velocity (East-West) varies linearly from 0.3 m/s at the East boundary to 0 m/s at the West boundary.

Results

Starting from the initial β-plane solution the flow situation should not change when propagating in time. Due to small errors in determining the β-plane solution and in the formation of the spherical-curvilinear grid and due to discretisation errors, disturbances occur and the flow slightly deviates from the β-plane solution. Results computed by Delft3D-FLOW are compared to the analytical (initial) solution for the water level (Figure 3.1.8.2), v-velocity (Figure 3.1.8.3) and u-velocity (Figure 3.1.8.4).

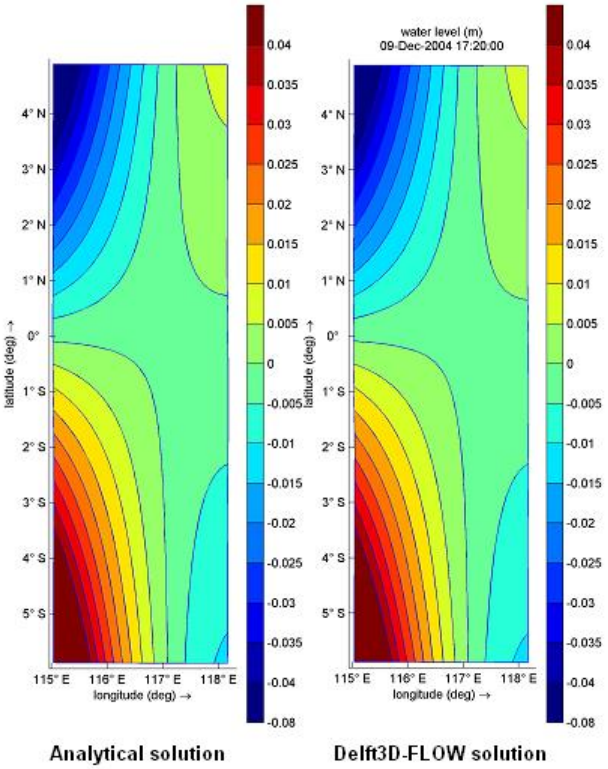

Figure 3.1.8.2: Water level for the β-plane solution. The analytical (initial) solution is depicted on the left and the numerical solution on the right.

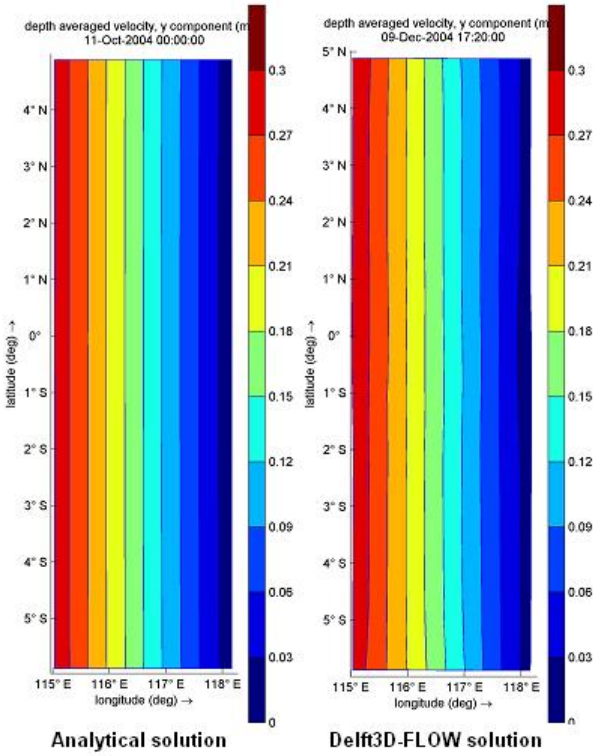

Figure 3.1.8.3: V-velocity for the β-plane solution. The analytical (initial) solution is depicted on the left and the numerical solution on the right.

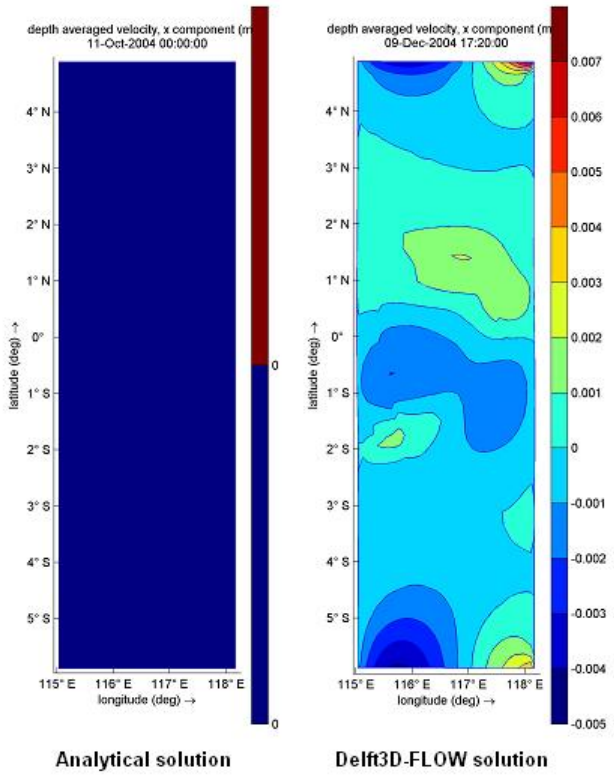

Figure 3.1.8.4: U-velocity for the β-plane solution. The analytical (initial) solution is depicted on the left and the numerical solution on the right.

Figures 3.1.8.2 and 3.1.8.3 show that for the water levels and v-velocities no differences can be observed. The u-velocity figure 3.1.8.4 might suggest that significant differences occur compared to the analytic solution. This is due to the fact that analytic solution is a zero-velocity field. However, the absolute differences in u-velocity are also very small (i.e. smaller than 0.01 m/s).

Conclusions

From this validation study it can be concluded that Delft3D-FLOW can accurately simulate flows for large geometric areas, in which the Coriolis force is important. Delft3D-FLOW can accurately reproduce the β-plane solution from Wyrtki (1961).

3.1.9 Equilibrium slope for a straight flume

This page last changed on 18-08-2008 by platzek.

Purpose

Test coupling of hydrodynamic and morphology processes.

Linked claims

Claim 2.4.8: Robust and accurate implementation of the coupling of hydrodynamic and morphology processes.

Approach

In this validation study case a relatively short straight flume with a movable bed is simulated. Initially the bathymetry is horizontal. Due to the flow through the flume and to the sediment transport, erosion of the bed starts to occur. This process continues till an equilibrium is reached (the boundary conditions are steady state). Then, the bed should match the slope of the water surface. Moreover, a two-domain model (i.e. domain decomposition) is used. In this way, it is verified whether the use of multiple domains leads to non-physical disturbances near the coupling interface of the domains.

the upstream boundary a constant discharge boundary condition is applied and the flow enters the flume carrying the local equilibrium suspended sediment concentration profile. At the downstream end of the flume a constant water level is specified. As the bed of the flume is initially horizontal, an accelerating flow is created. This in turn causes an increasing sediment transport rate along the length of the flume and erosion of the bed. This process continues until the bed of the flume matches the slope of the water surface and the process becomes stationary; equilibrium conditions have been achieved. In Delft3D-FLOW at each time step the hydrodynamic quantities and the morphodynamic quantities are updated. Substitution of this discharge gives the following expression for the bottom slope i:

$$i = \sqrt{-\frac{\partial \zeta}{\partial x}} = \frac{Q}{C_{2D} H^{3/2}} \quad .$$

Model description

The main characteristics are:

- 2DV model, with a length of 30 m and a width of 0.1 m.
- $\#x$ = 0.3 m and $\#y$ = 0.1 m.
- 2 subdomains; no grid refinement; each subdomain has 50 computational cells in x-direction.
- At inflow a discharge of Q = 0.0198 m3/s; at outflow a water level of 0 m.
- White Colebrook bottom friction with a Nikuradse roughness of 0.025 m.
- Modelling of sediment.

Results

Figure 3.1.9.1 shows the profile of the bed of the flume at steady state for the 2-domain model. A stable solution is reached after approximately 30 hours and that, after a small adaptation near the upstream boundary, the equilibrium bottom profile forms a straight line at a constant slope. By using the equation for i given above, it can be verified that the slope of the bed is very close to the theoretical slope of the water surface, given the specified discharge and bed roughness. Since H = 0.4072 m, Q = 0.198 m^2/s and C = 40 $m^{1/2}/s$, we obtain a theoretical slope of 0.0193. For the model results we have a bottom slope of 0.0183 (roughly 0.04 m over a distance of 12 m), which is close to the theoretical value.

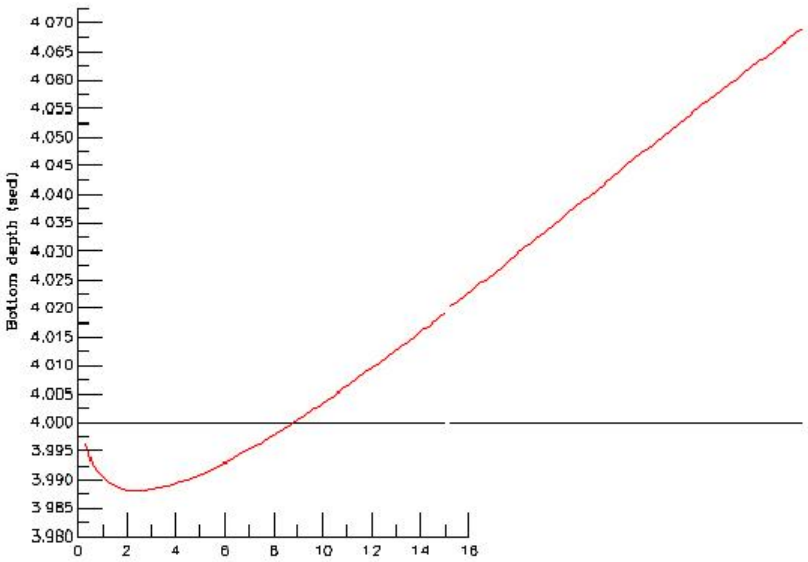

Figure 3.1.9.1 Equilibrium bed slope.

Conclusions

The equilibrium solution in a straight flume has been computed with Delft3D-FLOW and compared to the analytical solution. The results show a close resemblance. Therefore, it can be concluded that Delft3D-FLOW can correctly simulate coupled hydrodynamic and morphology processes for this validation study.

3.2 Laboratory test cases

This page last changed on 02-07-2008 by platzek.

The following laboratory test cases are available at present:

3.2.1 Tidal flume

This page last changed on 18-08-2008 by platzek.

Purpose

This validation study simulates the intrusion of salinity in a tidal flume. The goal is to validate the numerical code of Delft3D-FLOW with respect to salinity stratification by comparison with laboratory measurements in a scale model of a tidal flume at WL | Delft Hydraulics (Van Kester et al., 1993). Another goal is to examine the accuracy of the turbulent transport computed by Delft3D-FLOW.

Linked claims

Claim 2.2.1.2 Density driven flow and salinity intrusion.
Claim 2.2.1.4 Horizontal transport of matter on large and small scales.
Claim 2.2.2.10 Turbulent mixing including Internal Wave Model.

Approach

The scale model of the tidal flume has a basin with a surface area of 120 m^2, representing a sea, and a flume with a width of 1 m and a length of 130 m, representing a river. In the numerical simulation, we use a schematisation of the river (130 x 1 grid cells of 1 x 1 m^2 each). At the sea side a water level boundary is applied. The model is used to simulate salt intrusion in a river for both the σ- and the Z-model of Delft3D-FLOW.

Model description

Some characteristics of this model are:

- σ-model and Z-model.
- 2DV model (20 uniformly distributed layers for both the σ- and Z-model).
- Inflow of 12.5 ppt at the sea boundary and a fresh water inflow at the downstream river boundary.
- $k-\epsilon$ turbulence model.

The set up of the experiment with the tidal flume was chosen such that a partly stratified tidal flow occurs for a smooth bottom with:

- a minimal salt intrusion of order 20 m,
- a maximal salt intrusion less than 75 m and
- a vertical stratification characterised by a gradual transition from salt water to fresh water.

For that purpose numerical values were chosen for the quantities of interest, of which the most important ones are:

- for a smooth bottom: a 2-dimensional Chézy coefficient between 65 and 70 $m^{1/2}/s$,
- a water depth in the river of 0.2 m,
- a density difference of 10 kg/m^3 and
- for horizontal tidal forcing at the end of the river: a tidal period of 600 seconds such that there is a reasonable displacement due to the tide.

In this validation study the salt intrusion is roughly 45 m.

Results

Results are shown in Table 3.2.1.1 and Figure 3.2.1.1 (σ-model) and Table 3.2.1.2 and Figure 3.2.1.2 (Z-model).

Cross section at (from river)	Mean of difference	Standard deviation of difference	RMS of difference	Maximum of difference	Minimum of difference	Range of observation	Range of simulation

3 m	-0.05313	2.158168	2.131682	3.753557	-9.01805	13.79644	13.13299
12 m	0.56552	2.26669	2.308516	7.594468	-3.97777	11.91159	13.09592
24 m	0.106474	0.701648	0.700956	1.695141	-1.3517	12.3959	13.01761
36 m	1.27404	2.29299	2.597987	7.669337	-2.39202	12.11799	12.44464
48 m	1.205782	2.278201	2.552324	8.640538	0.163501	8.47773	0.472296

Table 3.2.1.1: Comparison of observed (measurement laboratory experiment) with simulated salinity in case of a σ-model.

Cross section at (from river)	Mean of difference	Standard deviation of difference	RMS of difference	Maximum of difference	Minimum of difference	Range of observation	Range of simulation
3 m	-0.4863	2.173942	2.200991	4.817328	-6.47257	13.79644	12.51534
12 m	-1.15774	1.70966	2.047007	1.163412	-6.01981	11.91159	12.52684
24 m	-0.56057	1.445507	1.533457	1.730078	-5.41341	12.3959	12.5
36 m	-0.28123	1.096491	1.118628	1.646807	-3.63715	12.11799	12.43679
48 m	-0.07713	0.890576	0.882749	0.901117	-3.58255	8.47773	9.198372

Table 3.2.1.2: Comparison of observed (measurement laboratory experiment) with simulated salinity in case of a Z-model.

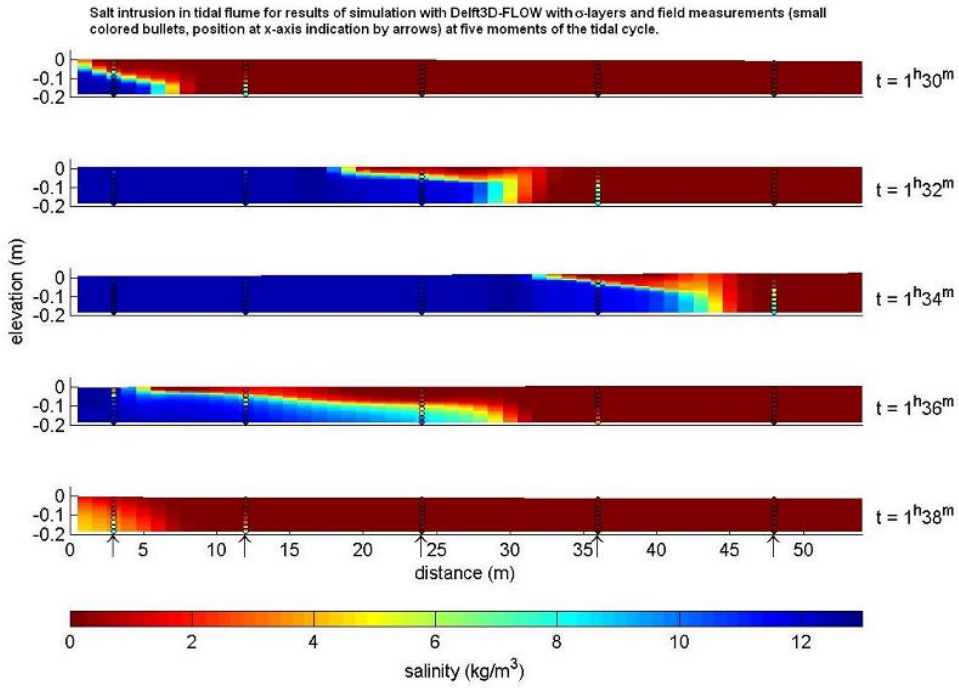

Figure 3.2.1.1: Comparison of observed (measurement laboratory experiment) with simulated salinity in case of σ-model.

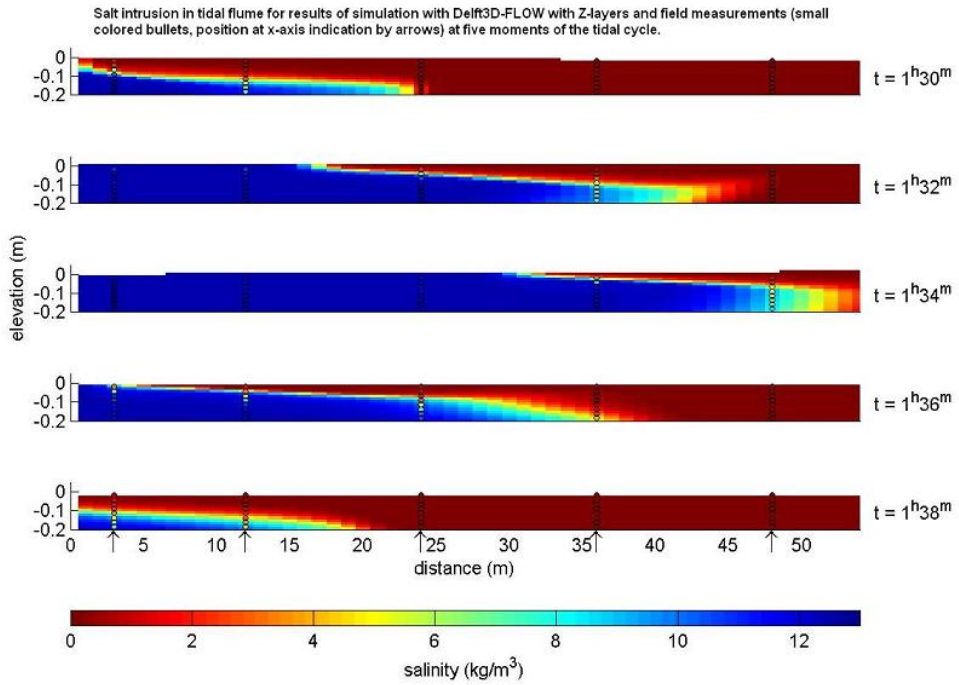

Figure 3.2.1.2: Comparison of observed (measurement laboratory experiment) with simulated salinity in case of Z-layers.

The two figures show the evolution of the salt intrusion for one tidal cycle (of 10 minutes) for a σ-model and a Z-model. The measurements are shown in open circles. For both models the computed results are in good agreement with the measurements. During inflow and outflow the salinity profiles are accurately computed. A salt wedge is entering this schematised river and the heavier salt water remains in the lower (vertical) part of the water column, with fresh water on top of it. However, from Figure 3.2.1.1 one can observe that the salt intrusion simulated with the σ-model does not reach that far the sea side (right side) as measured in the laboratory experiment (compare for instance the bullets at the 48 meter cross-section for t = 1 hour and 34 minutes). With respect to this, Figure 3.2.1.2 shows that the simulation with Z-layers performs better. This is also indicated by the last row of both tables: for the Z-model the mean, standard deviation and RMS (root mean square) of the difference between measured and simulated salinity at the 48 meter cross-section is much smaller than the corresponding values in case of σ-layers.

Conclusions

This validation study shows that Delft3D-FLOW is able to accurately model the time evolution of a salt plume that enters and leaves a river. Both the Z-model and the σ-model yield accurate results. The Z-model performs slightly better than the σ-model when considering the maximum distance of intrusion.

3.2.2 Water elevation in a wave flume

This page last changed on 18-08-2008 by platzek.

Purpose

The goal of this validation study is to investigate the propagation and dispersion of waves over a submerged bar. For this purpose a non-hydrostatic model is used. A comparison is conducted with measurements from the so-called *Beji & Battjes* experiment (Beji and Battjes, 1994).

Linked claims

Claim 2.2.1.9: Hydrostatic and non-hydrostatic flow.
Claim 2.2.2.5: Propagation of short waves.
Claim 2.2.3.4b: Abruptly changing bathymetry, orbital movements in short wave motions, or intensive vertical circulations such as buoyant jet plumes: non-hydrostatic (Navier-Stokes) equations.

Approach

Beji and Battjes performed several experiments concerning the propagation of waves over a submerged bar. Due to dispersion effects, high and low frequency waves are generated. Due to the abrupt changes in bathymetry over the bar, vertical accelerations are non-negligible and the flow is no longer hydrostatic. Using the non-hydrostatic module of Delft3D-FLOW, this experiment is simulated and the results are compared with the measurements of Beji and Battjes.

Model description

The laboratory experiment performed by Beji and Battjes comprises the geometry shown in Figure 3.2.2.1. At the left boundary of the domain a wave generator introduces sinusoidal waves that propagate into the domain and over the submerged bar. At the right boundary a sloping beach is present, absorbing the waves. At a number of measuring stations (see also Figure 3.2.2.1) the computed Delft3D-FLOW results are compared with measurements.

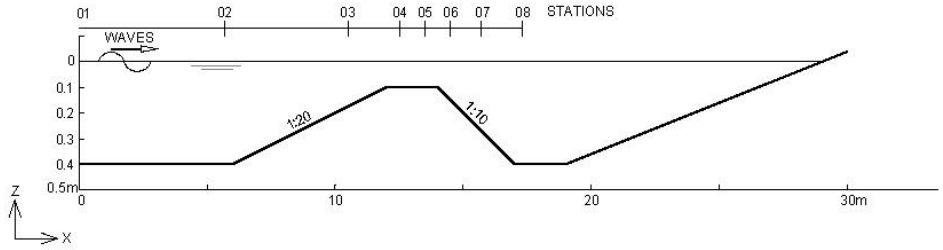

Figure 3.2.2.1: Bathymetry of laboratory experiment of Beji and Battjes.

For the Delft3D-FLOW model, the following model parameters were used:

- 2DV model, with 32 equidistant layers of 1.25 cm.
- Z-model (for using the non-hydrostatic module).
- Simulation time 1 minute.
- Δx = 2.5 cm.
- Δt = 5x10^{-5} minutes = 3x10^{-3} s.
- Chézy coefficient C = 55 m$^{1/2}$/s.
- A $k-\epsilon$ turbulence closure model.
- No additional viscosity.

Results

Using the non-hydrostatic module of Delft3D-FLOW the Beji and Battjes experiment has been conducted. Figures 3.2.2.2-3.2.2.4 show time series of water levels at three locations on top and behind the bar: at 13.5 m, 15.7 m and 19 m from the inflow boundary. From the figures it can be seen that the amplitudes and frequencies of the longest waves agree to a large extent with the measurements. In particular, this is

the case near the bar (Figure 3.2.2.2). The shorter waves are represented less accurately. Further away from the bar, the differences between the computed and measured results become apparent.

A sensitivity analysis has shown that a relatively small time step has to be applied in Delft3D-FLOW. This is due to the fact that the time integration of the Z-model in Delft3D-FLOW is first-order accurate in case of non-hydrostatic modelling. We remark that in case of hydrostatic modelling Delft3D-FLOW is second-order accurate in time. A research version of Delft3D-FLOW is available with a higher accuracy with respect to the time integration, allowing a larger time step. However, all validation studies in this document are done with the operational version of Delft3D-FLOW.

This validation study focuses on computing water levels in a non-hydrostatic model. In most of the practical applications of non-hydrostatic modelling, however, plume dispersion in horizontal and vertical direction is the main issue, for which a first-order time integration method of the non-hydrostatic part is more than sufficient.

Performing simulations with the hydrostatic model of Delft3D-FLOW yield very inaccurate water levels compared to the measurements, due to the large dispersion effects that occur when the waves pass the bar. This shows that modelling the physical phenomenon of flow over a submerged bar can not be modelled in detail with hydrostatic models.

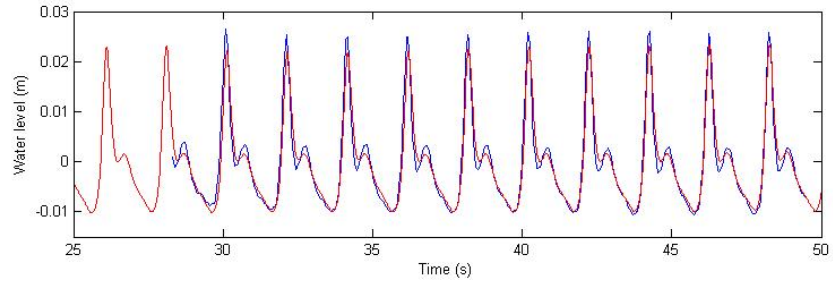

Figure 3.2.2.2: Water level history at a station located at 13.5 m from the inflow boundary. Measurements in blue, Delft3D-FLOW simulations in red.

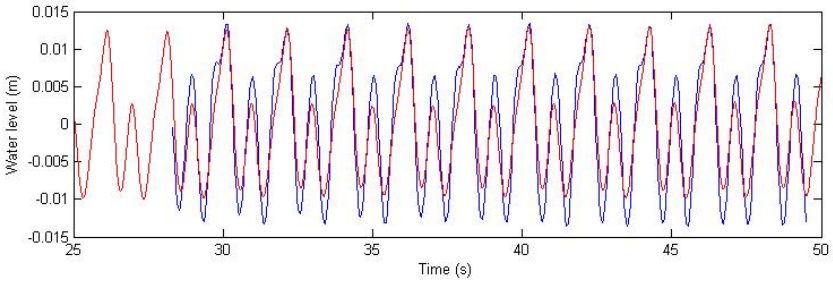

Figure 3.2.2.3: Water level history at a station located at 15.7 m from the inflow boundary. Measurements in blue, Delft3D-FLOW simulations in red.

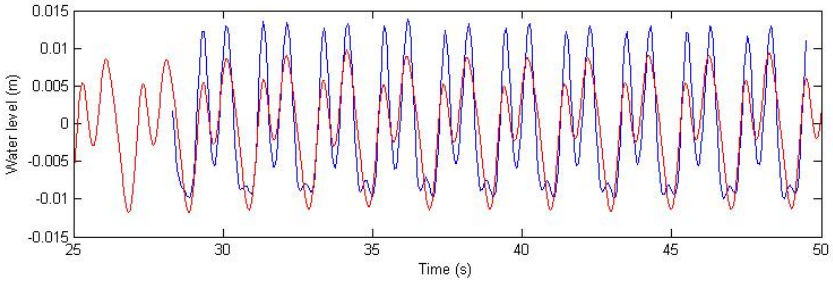

Figure 3.2.2.4: Water level history at a station located at 19.0 m from the inflow boundary. Measurements in blue, Delft3D-FLOW simulations in red.

Conclusions

From this validation study it can be concluded that accurate propagation and dispersion of short waves over a bar can only be simulated using the non-hydrostatic module of Delft3D-FLOW. The results are in reasonable agreement with the measurements. Improvements are possible (and have been realised in a

research version of Delft3D-FLOW). However, accurately computing the propagation of such small waves is not our main area of interest for non-hydrostatic modelling. The main goal is simulating dispersion of buoyant plumes (see e.g. Validation Study 3.3.4).

3.2.3 Vertical mixing layer (horizontal splitter plate)

This page last changed on 18-08-2008 by platzek.

Purpose

Test of vertical mixing and vertical exchange of momentum in stably stratified (salinity) flow. We remark that this validation study has been reported earlier, see [Van Kester, 1994], [Uittenbogaard, 1989, 1992].

Linked claims

Claim 2.2.1.2: Density driven flow and salinity intrusion.
Claim 2.2.1.11: Small scale current patterns near harbour entrances.
Claim 2.2.2.10: Turbulent mixing including Internal Wave Model.
Claim 2.4.3c: Delft3D-FLOW uses an accurate and robust algorithmic implementation for turbulence modelling.

Approach

For this validation study experimental data from a tidal flume is compared with numerical results obtained with Delft3D-FLOW.

Model description

The main characteristics are:

- Length of the test basin L = 40 m.
- Width of the test basin W = 1 m.
- 2DV Flow, with different currents and salinity above and below the (horizontal) splitter plate. We assume that there is no influence from the side walls.
- Space varying horizontal grid size Δx in the first meter from the left boundary. From the splitter plate to 1 meter inside the domain, Δx increases from 5 cm to 20 cm. In the remaining part there is a constant grid size of 20 cm.
- Uniform vertical grid size Δz with 40 layers.
- Time step Δt = 0.36 s.
- Simulation time: 6.0 minutes.
- Initial conditions:
  - Upper layer (thickness 0.324 m): salinity 22.6 ppt (water density approximately 1016 kg/m^3).
  - Lower layer (thickness 0.250 m): salinity 43.3 ppt (water density approximately 1031 kg/m^3).
- Boundary conditions:
  - Inflow (left): measured vertical velocity, turbulent kinetic energy and energy dissipation profiles are prescribed.
  - Outflow (right): water level is 0.570 m. Boundary is weakly reflective: α = 10.0 s.
- Bottom friction: A Chézy coefficient of 65 m$^{1/2}$/s.
- A constant horizontal background eddy viscosity and diffusivity of 1.0e-6 m^2/s.

Results

At four locations along the centreline of the flume the Delft3D-FLOW results are compared with measurements. This is done at 2 m, 5 m, 10 m and 40 m behind the splitter plate. The comparison is conducted for the horizontal velocity profiles (Figure 3.2.3.1), the relative density (Figure 3.2.3.2) and the turbulent kinetic energy (Figure 3.2.3.3).

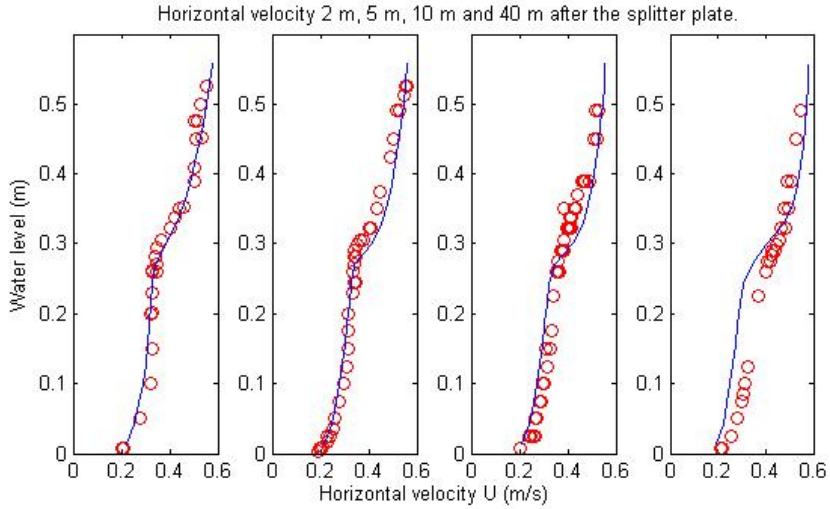

Figure 3.2.3.1: Horizontal velocity profiles at 2 m, 5 m, 10 m and 40 m behind the splitter plate. Red circles represent the measurements and the solid lines represent the profiles as simulated by Delft3D-FLOW.

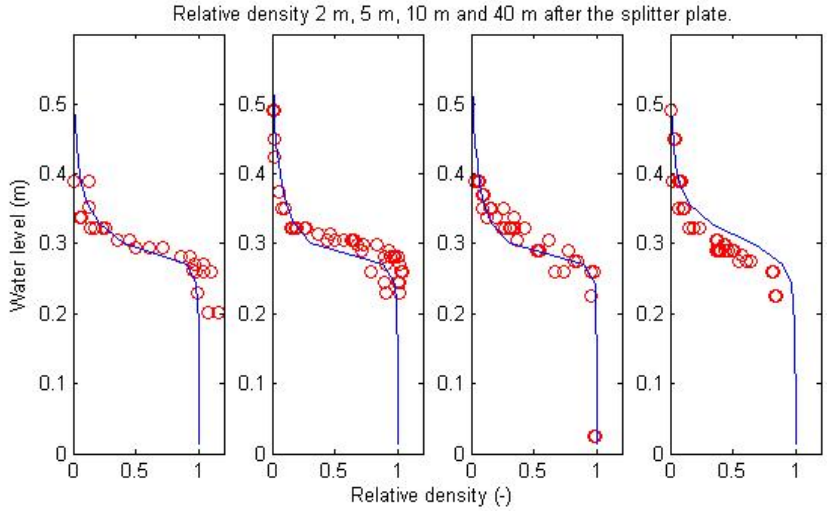

Figure 3.2.3.2: Density profiles at 2 m, 5 m, 10 m and 40 m behind the splitter plate. Red circles represent the measurements and the solid lines represent the profiles as simulated by Delft3D-FLOW.

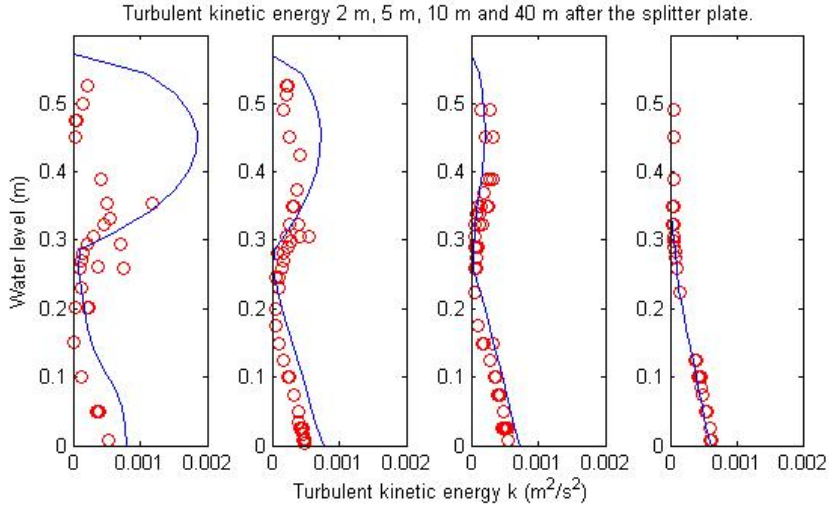

Figure 3.2.3.3: Turbulent kinetic energy profiles at 2 m, 5 m, 10 m and 40 m behind the splitter plate. Red circles represent the measurements and the solid lines represent profiles as simulated by Delft3D-FLOW.

Conclusions

From the results we concluded that Delft3D-FLOW can accurately simulate the flow around a horizontal splitter plate, resulting in a vertical mixing layer. Flow velocities, density profiles and turbulent kinetic energy profiles computed with Delft3D-FLOW agree very well with the measured quantities.

3.2.4 One-dimensional dam break

This page last changed on 18-08-2008 by platzek.

Purpose

The purpose of this validation study is to test the Delft3D-FLOW modelling accuracy for flooding over both a dry bed and a wet bed situation, resulting from a dam break. The Delft3D-FLOW model results are compared with the analytical solution, see (Stoker, 1957).

Linked claims

Claim 2.2.1.12: Flows resulting from dam breaks.
Claim 2.2.2.6: Subcritical and supercritical flow.
Claim 2.2.2.8: Accurate flow over dry or almost dry areas.
Claim 2.4.1: General (robustness, accuracy, efficiency).
Claim 2.4.6: Moving boundaries - representation of drying and flooding.

Approach and analytical solution

For rapidly varying depth-averaged flows, for instance the inundation of dry land or flow transitions due to large gradients of the bathymetry (obstacles), conservation properties become crucial. For this application a special advection scheme is available in Delft3D-FLOW, which is called the *Flooding* scheme. This scheme is accurate for simulating flows around obstacles that are represented by only one grid cell.

The flooding scheme uses a numerical approximation that is consistent with conservation of momentum in flow expansions, while in flow contractions a numerical approximation is applied that is consistent with the Bernoulli equation. For sufficiently smooth conditions and a fine grid size, both approximations converge to the same solution. The local order of consistency depends on the solution. The approximations are second-order accurate, but the accuracy reduces to first order near strong gradients in the numerical solution by the use of the so-called Minmod slope limiter [Stelling and Duinmeijer, 2003].

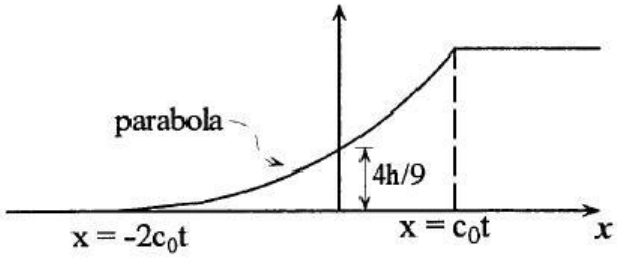

Figure 3.2.4.1: Water surface slope for a dam break scenario with initially dry bed.

In this validation study the flooding scheme is examined for a dam break situation. In Figure 3.2.4.1 the surface profile after a dam break is shown. In (Stoker, 1957) it is shown by using the theory of characteristics that the velocity *u* and wave celerity *c* can be computed according to:

$$c = \frac{1}{3}\left(2c_0 - \frac{x}{t}\right)$$
$$u = \frac{2}{3}\left(c_0 + \frac{x}{t}\right) \qquad \forall x \in [-c_0 t, 2c_0 t] \quad .$$

For our test case this solution has been determined numerically. This analytical solution will be compared with the solution computed by Delft3D-FLOW.

Model description

The dam break is simulated by a discontinuity in the water elevation at *t* = 0 (initial condition). The water level before the dam is 2.0 m and behind the dam 0 m (dry bed) or 0.1 m (wet bed).

Some model characteristics:

- Homogeneous 2D model with 602 by 3 grid points in horizontal direction.
- $\Delta x = \Delta y = 100$ m.
- Bed level at 0 m.
- Time step of 6 seconds.
- Simulation period of 3600 seconds.
- Closed boundary at both ends of the model.
- Horizontal viscosity coefficient of 5e-4 m^2/s.
- Drying flooding procedure MAX; drying-flooding criterion of 1e-5 m.
- Bed friction coefficient of 5000 $m^{1/2}/s$.

Results

Figure 3.2.4.1 contains the results for a dam break over a dry bed. The Delft3D-FLOW results for the Cyclic scheme (black line) and the Flooding scheme (blue line) are presented, as well as the analytical solution (in red). In this figure the front velocity is plotted. At about $x = 15000$ m the dam break occurs, which starts with a front velocity of 2 m/s. At about $x = 60000$ the front velocity is zero. In Figure 3.2.4.2 it can be seen that the Flooding scheme accurately predicts the front velocity, which means the flooding of the dry area occurs with a correct speed. The Cyclic scheme is clearly less accurate.

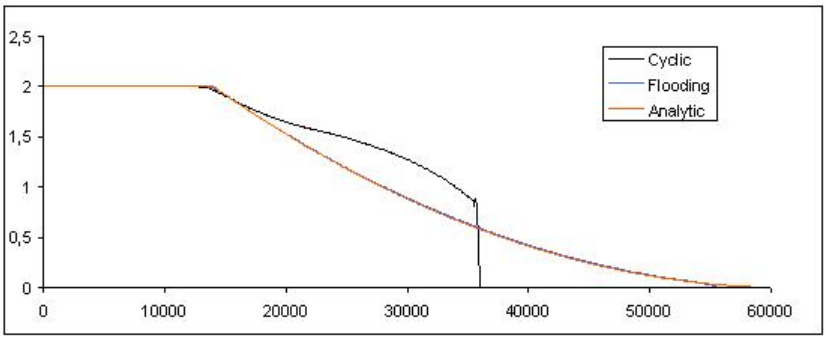

Figure 3.2.4.2: Water level for flooding of a dry bed, computed (in blue and black) and analytical (in red).

For the dam break in case of a wet bed (in our example 10 cm) the same conclusions can be drawn, see Figure 3.2.4.3. The Flooding scheme accurately predicts the flooding velocity of this initially wet (shallow) area, while the Cyclic scheme does not. This also illustrates that it is important to select for each application the most suitable advection scheme. Delft3D-FLOW offers several advection schemes, see Section 10.5.1. of the Delft3D-FLOW manual for further details.

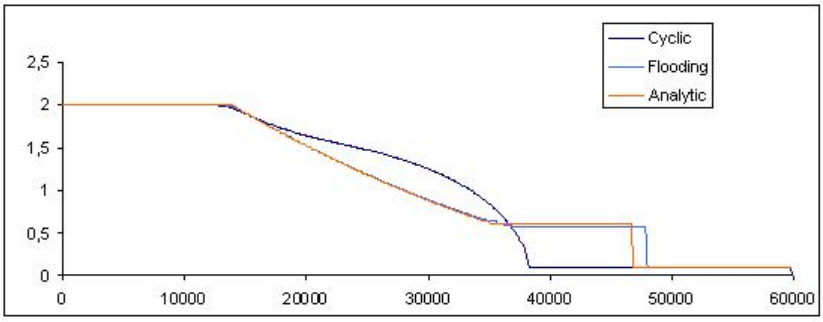

Figure 3.2.4.3: Water level for flooding of a wet bed, computed (in blue and black) and analytical (in red).

Conclusions

This validation shows proofs that Delft3D-FLOW is able to accurately predict the flow resulting from dam breaks. This is valid for dam breaks over either initially dry or initially wet beds. The *Flooding* advection scheme is more suitable for this application than the *Cyclic* scheme. Simulations with the Flooding scheme yield accurate flooding velocities and wave heights, which is illustrated by comparison with the analytical solution.

3.2.5 Horizontal mixing layer (vertical splitter plate)

This page last changed on 18-08-2008 by platzek.

Purpose

The purpose of this validation study is to show that Delft3D-FLOW can accurately compute properties of quasi-2D turbulence as observed in the free-surface mixing-layer experiments of Uijttewaal & Booij (2000). This means that the Delft3D-FLOW in combination with the HLES turbulence modelling technique is tested on its capability to reproduce the mean streamwise velocity U, its RMS |u'| and the lateral momentum flux $\overline{u'v'}$, as measured in the experiment.

Linked claims

Claim 2.2.1.11: Delft3D-FLOW can be used for an accurate prediction of small scale current patterns near harbour entrances. For example, a so-called Horizontal Large Eddy Simulation (HLES) can be applied to resolve small scale turbulent behaviour.
Claim 2.2.2.10: In Delft3D-FLOW turbulence quantities in the horizontal direction can be modelled with increasing complexity: a constant viscosity, or space varying (and time constant) viscosity or a space and time varying viscosity can be applied (Horizontal Large Eddy Simulation (HLES) model).
Claim 2.2.3.6b: HLES model.
Claim 2.4.1: Delft3D-FLOW uses an accurate, robust and computationally efficient algorithmic implementation for the shallow water equations (hydrostatic model) and for the incompressible Navier-Stokes equations (non-hydrostatic model). This is the case for both time-dependent and steady state problems.
Claim 2.4.3c: Delft3D-FLOW uses an accurate and robust algorithmic implementation for turbulence modelling.

Approach

A Delft3D-FLOW model has been set-up to simulate mixing layer characteristics in the laboratory experiment by Uijttewaal & Booij (2000). Figure 3.2.5.1 shows the laboratory experiment.

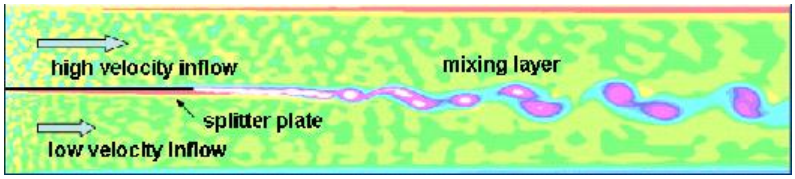

Figure 3.2.5.1: Top view of laboratory experiment.

In this experiment a mixing layer is studied with a water depth of the flume of 67 mm. The inlet section of the flume consists of two separate parts divided by a splitter plate with a length of 3 m and a width of 8 mm. The velocities at both sides of the splitter plate are 0.14 m/s (below the plate) and 0.32 m/s (above the plate). These velocities correspond to Reynolds numbers, defined by Uh/ν, of 9400 and 21400, respectively. Due to the initial velocity difference, a mixing layer starts to develop beyond the end of the splitter plate. It is known that a system of two parallel streams with different flow velocity is subject to the so-called Kelvin-Helmholtz instability, which means that wave-like disturbances grow in the downstream direction and roll-up to become vortices that form a mixing layer.

The computational model applied in this validation study is based on previous Delft3D-FLOW simulations and analysis described in Kernkamp and Uittenbogaard (2001). With this model simulations have been carried out with Delft3D-FLOW's HLES turbulence closure model. Typical flow characteristics such as the time-averaged shape of the mixing layer, magnitudes of flow fluctuations and turbulent lateral momentum flux are computed and compared with experimental data.

Model description

The grid is such that its closed boundaries follow the flume walls and the splitter plate, see Figure 3.2.5.2. The dimensions of the numerical model are 20 m x 3 m. The mesh size of the grid varies from 4 mm x 16 mm near the tip of the splitter plate to 40 mm x 40 mm at the boundaries. To avoid influences of spin-up effects in the analysis of flow characteristics, a relatively long simulation period of 50 minutes

with a time step of 0.006 s is used. For computational reasons the simulations are split in a spin-up simulations and a subsequent production simulation. The model runs in depth-averaged (2DH) mode to keep computation times reasonable.

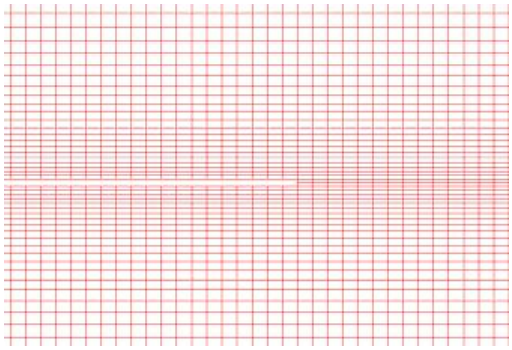

Figure 3.2.5.2: Computational grid at the tip of the splitter plate.

At the open inflow boundaries a boundary condition is imposed which consists of a mean flow component and fluctuating (kinematic turbulent) component. The mean current speed at the high-velocity side is 0.33 m/s, and at the low-velocity side 0.147 m/s. The fluctuations are imposed to have a realistic turbulence level of the inflow, and to trigger instabilities downstream of the splitter plate tip as in the experiment. The closed boundaries are modelled as hydraulically smooth: a law of the wall condition for smooth walls. Bottom friction is modelled by means of a Chézy formulation, using a Chézy coefficient of 65 $m^{1/2}/s$.

In the HLES simulation, effects of turbulent momentum exchange at scales that cannot be resolved on the computational grid (close to and below the grid resolution) are taken into account by the HLES method. HLES decomposes the flow field in a slow-varying or steady part and a fluctuating part by means of a temporal filter technique. Based the fluctuating flow field HLES computes the effect of the unknown small-scale turbulence on the flow by means of a space - and time-varying eddy viscosity. In this simulation the filter time parameter is set to 1 min, which means that roughly all flow variations with periods smaller than 1 minute are considered as fluctuation, and the remaining part as mean flow behaviour. Furthermore, default HLES settings are used, see Table 3.2.5.1. Effects of three-dimensional turbulence are accounted for by applying the Elder formulation, which is a 3D turbulence closure for depth-averaged models. No background eddy viscosity is applied.

HLES Parameter name	**Meaning**	**Value**
Htural	Slope in log-log spectrum	3
Hturnd	Dimensional number (=2 for quasi-2D turbulence)	2
Hturst	Prandtl-Schmidt number	0.7
Hturlp	Numerical low-pass coefficient	0.3
Hturrt	Filter relaxation time	1 min
Hturdm	Molecular diffusivity	0 m^2/s
Hturel	Application of so-called Elder's term to account for 3D turbulence contributions to 2D eddy viscosity	Yes

Table 3.2.5.1: Applied HLES settings.

Results

The computed flow fields are stored every three seconds over a period of 25 minutes, hence yielding 501 stored flow fields. From these data the time-averaged flow field is computed. By subtracting the time-averaged flow field from the instantaneous flow fields a series of fluctuating flow fields is obtained. The fluctuating flow fields are also determined "online" by the HLES method. Characteristics of the online computed fluctuating flow fields are compared with the "offline" computed fluctuations, and with the experimental data.
Below, the results of the simulation with both processing methods are presented in Figures 3.2.5.3 and 3.2.5.4, and compared with measurement data from Uijttewaal en Booij (2000). The definitions of the parameters that are visualised in the figures, are given in Table 3.2.5.2.

Name	Symbol	Definition
Mixing layer	δ	$\delta = \frac{u_1 - u_2}{(\partial u / \partial y)_{max}}$, where u_1 = velocity of undisturbed flow above plate u_2 = velocity of undisturbed flow below plate
Mean flow velocity	u	
Streamwise turbulence intensity	$\lvert u' \rvert$	RMS value of u
Reynolds stress	$\overline{u'v'}$	Lateral momentum flux

Table 3.2.5.2: Parameter definitions.

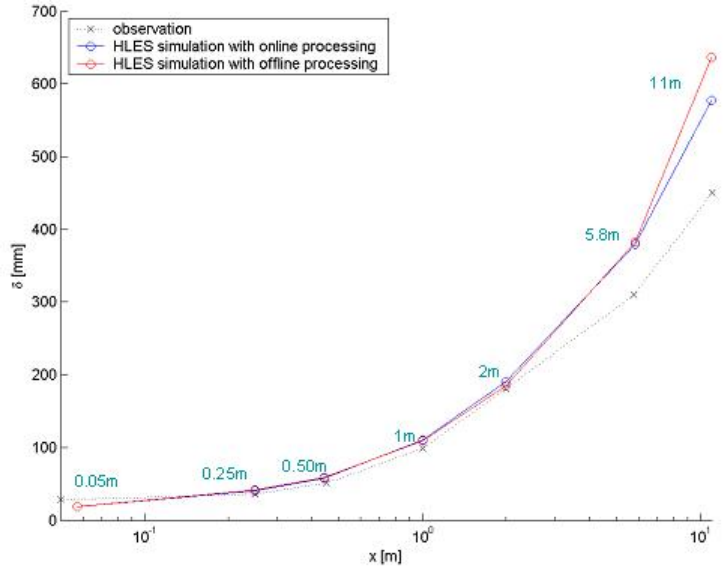

Figure 3.2.5.3: Mixing layer thickness as a function of distance from the tip of the splitter plate (which lies at x = 0).

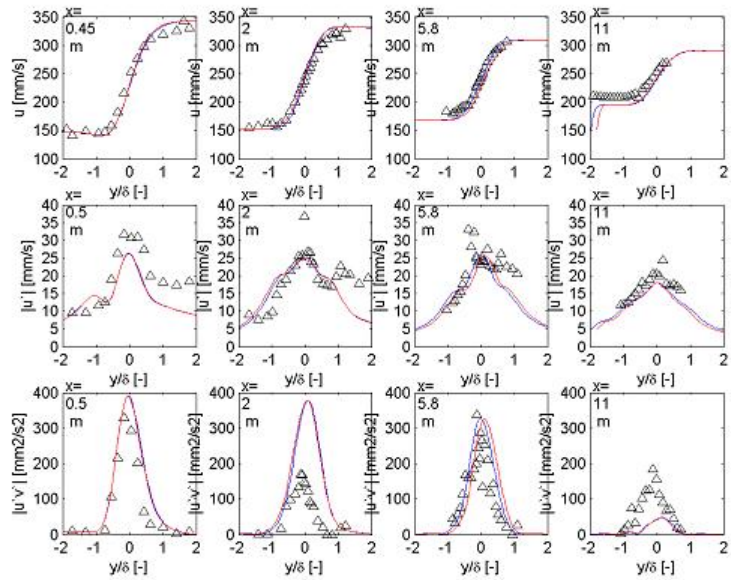

Figure 3.2.5.4: Observed (triangles) and simulated (lines) properties of mean flow and turbulence at a series of downstream cross sections; blue: offline computed flow characteristics, red: online computed flow characteristics.

Figure 3.2.5.3 shows that the growth of the width of the mixing layer is very accurately computed in the first 2 m downstream of the splitter plate tip. Further downstream, between 2 m and 11 m, the computed mixing layer width becomes increasingly larger than the measured width. The development of the mean mixing layer width is slightly better represented by the results obtained by offline processing. Figure 3.2.5.4 shows that the computed mean and turbulent characteristics at a series of downstream locations in general have comparable characteristics compared to the measurements. The computed profiles of the mean flow agree well with the measurements. This indicates that the momentum exchange across the mixing layer is accurately simulated. The computed RMS values $|u'|$ have comparable cross-section profiles and magnitudes. The computed lateral momentum exchange $\overline{u'v'}$ agrees well with the measurements at 0.5 m and 5.8 m downstream of the splitter plate tip, but deviates significantly at 2 m and 11 m . At 2 m the deviation is expected to be due to incorrect measurements, because no explanation is known for this dip in the lateral momentum flux. At 11 m the computed magnitudes are significantly lower than observed. The cause of this deviation is unclear. Furthermore, Figure 3.2.5.4 shows that the online computed turbulent fluctuations have similar characteristics as the fluctuations that were computed by postprocessing. This means that large scale turbulent characteristics are accurately computed with the online time-filter method.

Conclusions

From this validation study we conclude that:

- In general, the turbulent characteristics of the mixing layer computed with the HLES turbulence modelling technique are in reasonable agreement with the observations.
- The computed steady (mean) and unsteady (fluctuating) flow behaviour agrees well with the measurements.
- Turbulent fluctuations determined with the time-filtering method by Delft3D-FLOW have similar characteristics as turbulent fluctuations, which can be determined by Reynolds decomposition of the resolved flow fields.

3.2.6 Numerical scale model of an estuary

This page last changed on 18-08-2008 by platzek.

Purpose

Validation of a 3D Numerical Scale Model application of Delft3D-FLOW with σ-coordinates and HLES for vertical and horizontal mixing in the Physical Scale Model of a section of the Scheldt estuary without dock.

Linked claims

Claim 2.2.1.1: Tidal dynamics of estuaries or coastal areas.
Claim 2.2.1.2: Density driven flow and salinity intrusion.
Claim 2.2.2.1: Propagation of long waves.
Claim 2.2.2.2: Baroclinic flow - salinity and temperature driven flow.
Claim 2.2.2.3 Transport of dissolved material and pollutants.
Claim 2.2.2.7 Steady and unsteady flow.

Approach

The Physical Scale Model was constructed in Delft Hydraulics' Tidal Flume. The central part of the 130 m long flume was replaced by a scaled (and mirrored) section of the Scheldt estuary near the Deurganckdock. The model was slightly distorted. For more information on the numerical scale model, see [Winterwerp et al, XXXX].

Model description

The numerical flow model is characterized by:

- 3D Model.
- Curvilinear grid in the horizontal plane and sigma coordinates in the vertical.
- Tidal discharge with net fresh water inflow at the up-estuary boundary.
- Water levels and salt water at the down-estuary boundary.
- k-ϵ Turbulence model for vertical mixing.
- HLES sub-grid scale model for horizontal mixing.

The physical scale model aims at a (scaled) reproduction of prototype conditions in a bend of the Scheldt estuary:

- Tidal levels and currents extremes and time evolution (including distortion), range, current in prototype.
- Salt intrusion little stratification during flood, larger during ebb.

Some characteristic numerical parameters:

- River bend with scaled 3D bathymetry, typical depth 10 - 15 cm.
- Density difference of kg/m^3 (equivalent to prototype).
- Tidal period of 1840 s.

Results

Figure 3.2.6.1 contains an overview of the model domain (small top plot) and zooms in on the Deurganckdock section (see detailed plot with model grid). For the Deurganckdock section the bathymetry is plotted in Figure 3.2.6.2. Water levels at six different location are presented in Figure 3.2.6.3, while Table 3.2.6.1 contains absolute error values for water levels. This shows that the water levels are in good agreement with measurements, because on average the RMS errors are (much) smaller than 1 mm for a tidal range of about 40 mm.

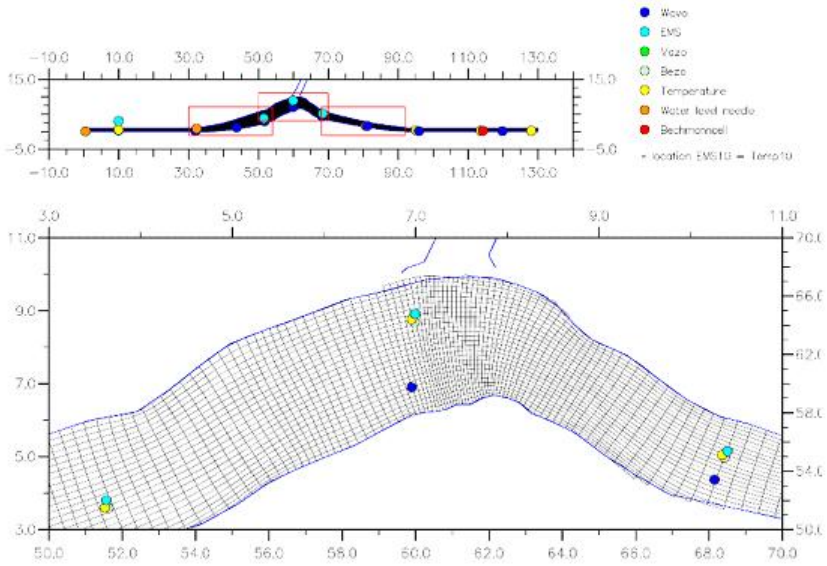

Figure 3.2.6.1: Detailed numerical scale model grid, Deurganckdock section, situation without dock (Bijlsma & Van Vossen, 2004).

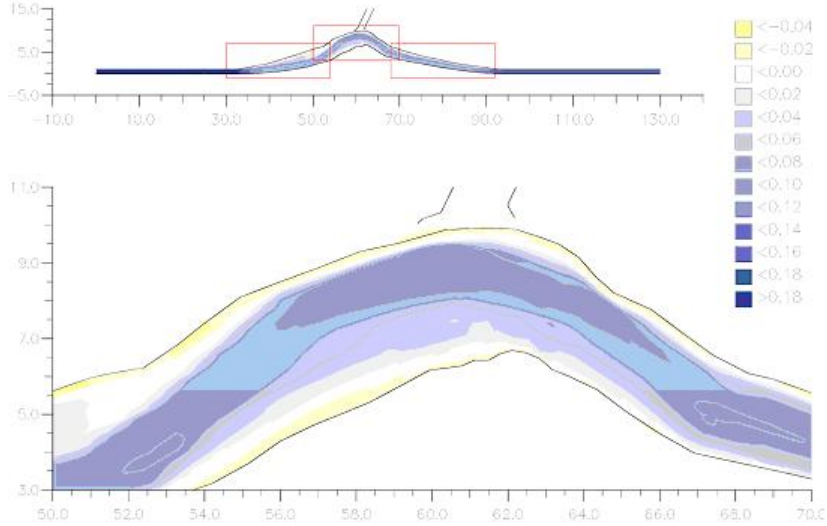

Figure 3.2.6.2: Depth of detailed numerical scale model, Deurganckdock section, situation without dock (Bijlsma & Van Vossen, 2004).

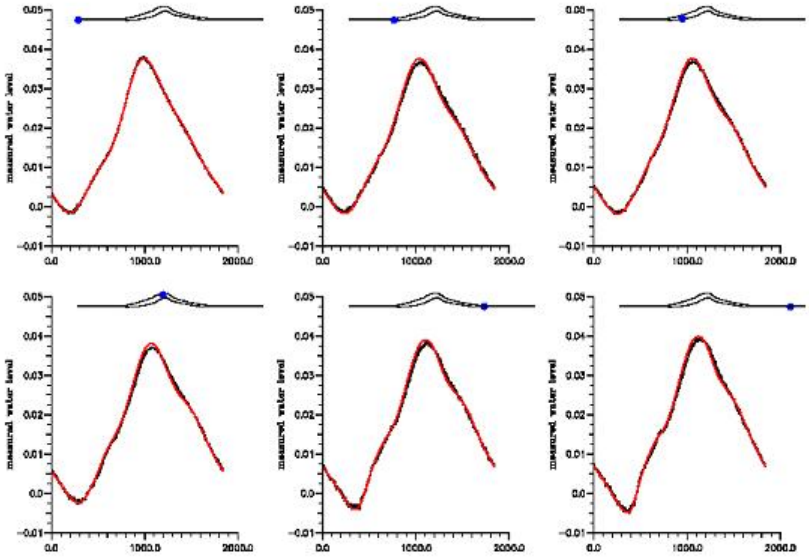

Figure 3.2.6.3: Computed (red) and measured (black) water levels at six stations along the flume, run s12 and test of 15 April 2003, cycle 23 (Bijlsma & Van Vossen, 2004).

Obs.	Simulation	Mean	Stand. dev.	RMS	Max	Min	Obs. range	Simulation range
H-regel-C	Peilnaald 0.5	-0.02	0.15	0.15	0.35	-0.41	39.30	39.15
Wavo 31m	Wavo 32	0.01	0.68	0.68	1.11	-1.47	37.99	39.32
Wavo 44m	Wavo 44-1	-0.02	0.61	0.61	1.17	-1.38	38.22	39.55
Wavo 52m	WV51/ BEZO/ T/EP98-2	-0.23	0.64	0.68	1.09	-1.60	38.52	39.88
Wavo 60m	Wavo 60	-0.16	0.70	0.72	1.15	-1.68	39.06	40.43
Wavo 68m	Wavo 68	-0.06	0.72	0.73	1.35	-1.72	39.77	40.89
Wavo 81m	Peilnaald/ Wavo-80-1	-0.17	0.68	0.70	1.29	-1.75	40.50	41.70
Wavo 96m	Wavo 96m	-0.18	0.71	0.73	1.27	-1.86	41.66	43.04
Wavo 120m	Wavo 120m	-0.10	0.76	0.76	1.64	-1.83	43.63	44.78

Table 3.2.6.1: Absolute error of water levels in mm (observed - simulated, run s12).

Time series of salinity are shown in Figure 3.2.6.4 and Table 3.2.6.2 contains RMS errors in salinity. From these results it can be concluded that salinity is reproduced in an accurate way as well, because the absolute errors are roughly 0.25 ppt, while the variation in salinity is approximately 5 ppt.

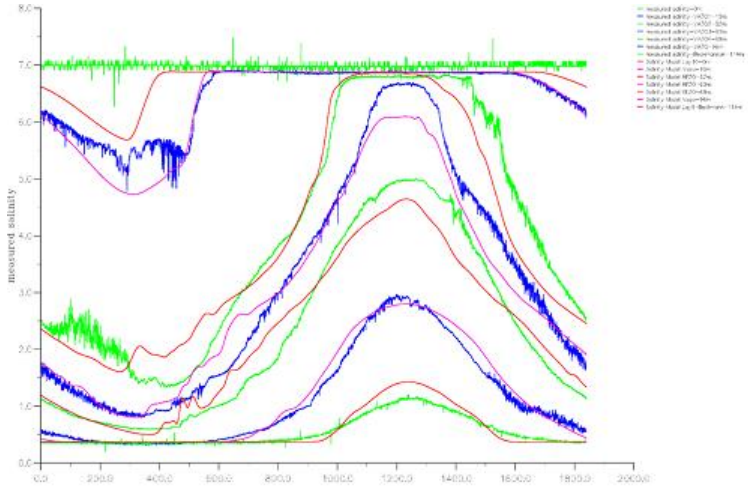

Figure 3.2.6.4: Computed (red & magenta) and measured (blue & green) salinity at 7.2 cm - TAW in six stations along the flume, run s12 and test of 15 April 2003, cycle 23 (Bijlsma & Van Vossen, 2004).

Obs.	Simulation	Mean	Stand. dev.	RMS	Max	Min	Obs. range	Simulation range
VAZO1 10m	Vazo/ Temp-10	0.13	0.28	0.31	1.01	-0.22	1.68	2.50
VAZO2 52m	WV51/ BEZO/ T/EP98-1	0.12	0.48	0.49	1.36	-0.83	5.45	5.91
VAZO3 60m	BEZO/ Temp/ EMS-60-1	0.09	0.35	0.36	0.74	-0.76	5.83	5.62
VAZO4 68m	BEZO 68	0.02	0.34	0.34	0.82	-0.64	4.38	4.34
VAZO 96m	Vazo/ Temp-95	-0.03	0.11	0.12	0.17	-0.28	2.58	2.45
Beckmann cel 114m	Temp/ Bechu?-114	-0.02	0.09	0.10	0.15	-0.31	0.79	1.06

Table 3.2.6.2: Absolute errors of salinity in ppt (observed - simulated).

Time series of current magnitude are shown in Figure 3.2.6.5 for four different locations. The computed (in red) and measured (in black) current magnitudes agree well at all locations.

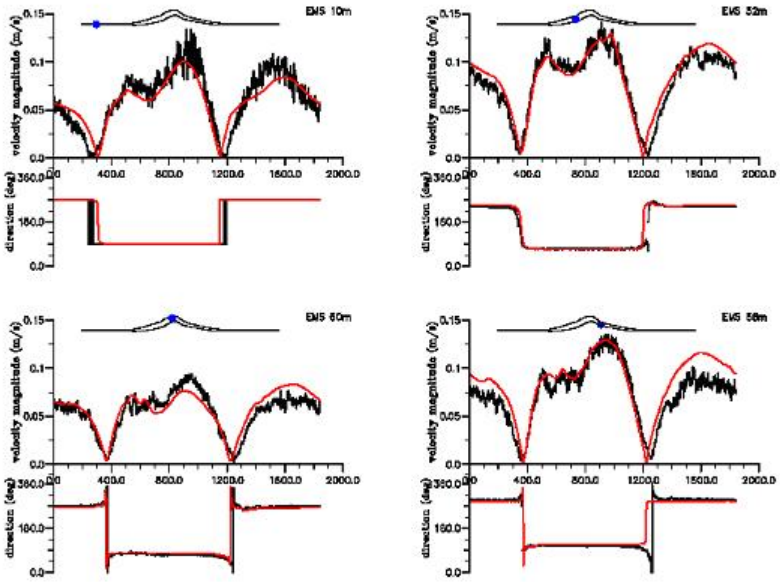

Figure 3.2.6.5: Computed (red) and measured (black) current magnitude and direction in four stations along the flume, run s12 and test of 15 April 2003, cycle 23 (Bijlsma & Van Vossen, 2004).

Conclusions

This validation study shows that the numerical scale model that was set-up with Delft3D-FLOW is able to reproduce the complex flow that is measured in the physical scale model for the Scheldt estuary.

3.2.7 Numerical scale model of an estuary and a tidal dock

This page last changed on 18-08-2008 by platzek.

Purpose

Validation of a 3D Numerical Scale Model application of Delft3D-FLOW with σ-coordinates and HLES for the complex exchange flow between a tidal dock and the estuary. We remark that the previous validation study the hydrodynamics in the Scheldt river itself was investigated, while now the focus is on flow in the dock as well.

Linked claims

Claim 2.2.1.1: Tidal dynamics of estuaries and coastal seas.
Claim 2.2.1.2: Density driven flow and salinity intrusion.
Claim 2.2.1.11: Small scale current patterns near harbour entrances.
Claim 2.2.2.1: Propagation of long waves.
Claim 2.2.2.2: Baroclinic flow - salinity and temperature driven flow.
Claim 2.2.2.3: Transport of dissolved materials and pollutants.
Claim 2.2.2.7: Steady and unsteady flow.

Approach

The Physical Scale Model was constructed in Delft Hydraulic's Tidal Flume. The central part of the 130 m long flume was replaced by a scaled (and mirrored) section of the Scheldt estuary near the Deurganckdock. The model was slightly distorted. For more information on the numerical scale model, see [Winterwerp et al., XXXX].

Model description

The numerical flow model is characterized by:

- 3D Model.
- Curvilinear grid in the horizontal plane and sigma coordinates in the vertical.
- Tidal discharge with net fresh water inflow at the up-estuary boundary.
- Water levels and salt water at the down-estuary boundary.
- k-# Turbulence model for vertical mixing.
- HLES sub-grid scale model for horizontal mixing.
- Domain decomposition (see Figure 3.2.7.1).

We remark that the horizontal resolution bear the Deurganckdock is higher compared to the previous validation study.

The set-up of this physical scale model aims at a (scaled) reproduction of prototype conditions in a bend and in a dock of the Scheldt estuary:

- Tidal levels and currents extremes and time evolution (including distortion), range, current in prototype.
- Salt intrusion little stratification during flood, larger during ebb.

Characteristic numerical parameters:

- River bend with scaled 3D bathymetry, typical depth 10 - 15 cm.
- Density difference of kg/m^3 (equivalent to prototype).
- Tidal period of 1840 s.

Results

Similarly to the previous validation study, Figure 3.2.7.1 contains the model grid and Figure 3.2.7.2 the bathymetry. In Figure 3.2.7.3 time series of computed and measured water levels are shown, which are in good agreement with each other. This also follows from Table 3.2.7.1 with RMS errors in water levels. The RMS errors are about twice as large compared to the situation without a dock, but are still small (roughly 1.5 mm) compared to its tidal range of 40 mm.

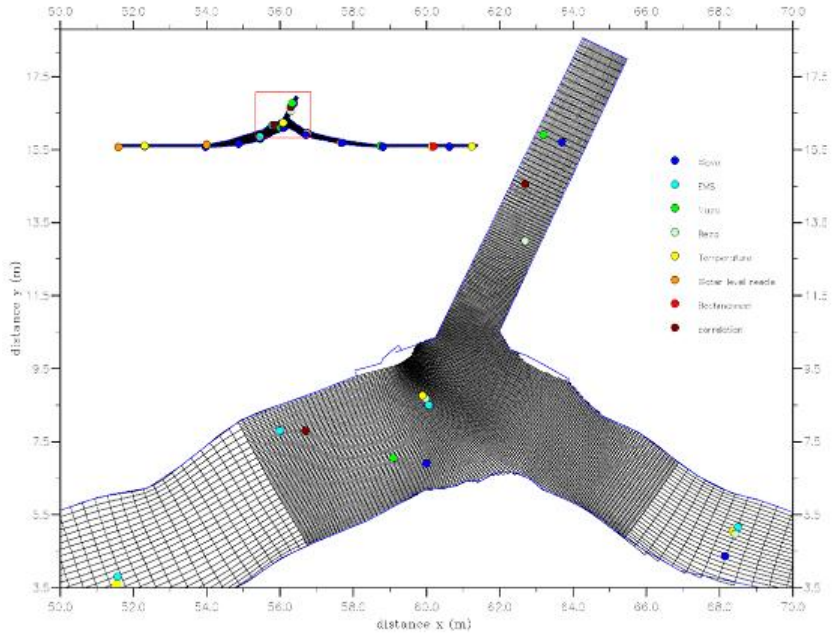

Figure 3.2.7.1: Numerical scale model grid for domain decomposition, situation with Deurganckdock and positions of instruments.

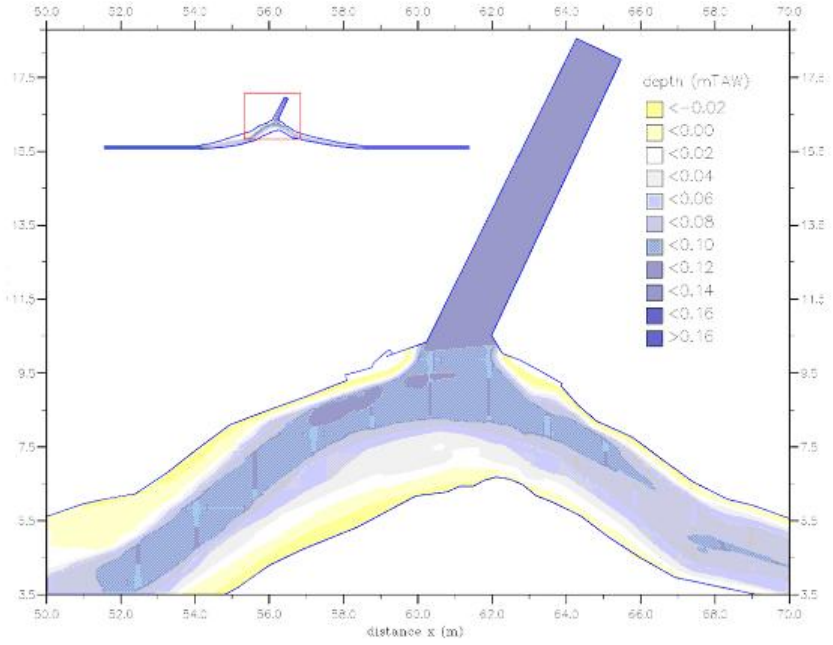

Figure 3.2.7.2: Depth of numerical scale model with domain decomposition, situation with Deurganckdock.

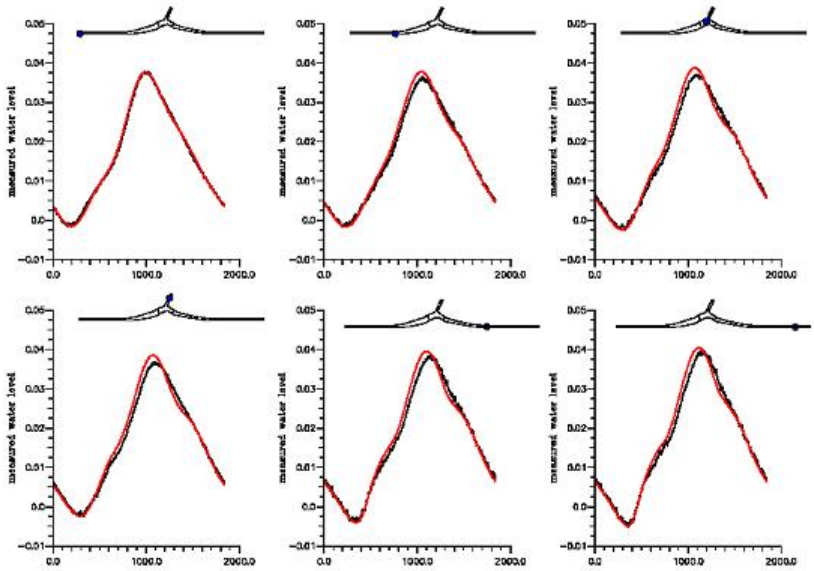

Figure 3.2.7.3: Computed (red) and measured (black) water levels at six stations along the flume, run dd14 and test of 26 May 2003, cycle 20 (Bijlsma & Van Vossen, 2004).

Obs.	Simulation	Mean	Stand. dev.	RMS	Max	Min	Obs. range	Simulation range
H-regel-C	PEILNAALD 0.5	-0.07	0.40	0.40	0.87	-0.95	38.79	39.13
Wavo 31m	WAVO 32	-0.39	1.13	1.19	1.29	-2.61	37.21	39.41
Wavo 44m	WAVO 44	-0.44	1.23	1.31	1.57	-2.90	37.38	39.87
Wavo 51m	WAVO 51	-0.49	1.35	1.43	1.71	-3.20	37.87	40.34
Wavo 60m	WAVO 60	-0.45	1.42	1.49	1.91	-3.28	38.40	40.89
Wavo Harbour	WAVO HARB	-0.37	1.38	1.43	1.99	-3.17	38.85	41.23
Wavo 68m	WAVO 68	-0.21	1.44	1.45	2.29	-3.21	39.15	41.35
Wavo 81m	WAVO 81	-0.34	1.43	1.47	2.33	-3.33	40.46	42.23
Wavo 96m	WAVO 96	-0.33	1.54	1.57	2.55	-3.50	41.54	43.51
Wavo 120m	Wavo 120	-0.34	1.57	1.61	2.81	-3.79	43.69	45.25

Table 3.2.7.1: Absolute errors of water levels in mm (observed - simulated, run dd14).

In Figures 3.2.7.4-5 computed and measured salinities are shown, while Table 3.2.7.2 contains RMS errors in salinity. The RMS errors in salinity are in the order of 10-35% of its tidal range, which is reasonable.

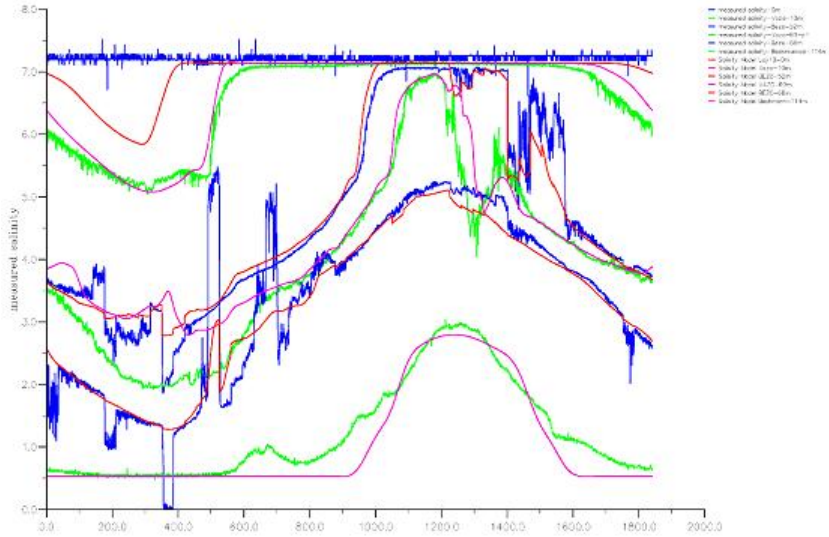

Figure 3.2.7.4: Computed (red & magenta) and measured (blue & green) salinity at six stations along the flume, run dd14 and test of 26 May 2003, cycle 20 (Bijlsma & Van Vossen, 2004).

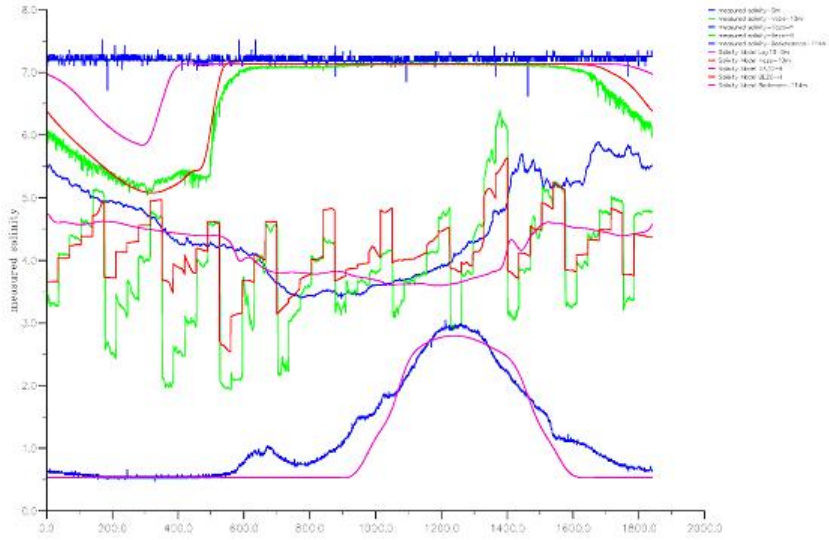

Figure 3.2.7.5: Computed (red & magenta) and measured (blue & green) salinity at two stations in the Deurganckdock, run dd14 and test of 26 May 2003, cycle 20 (Bijlsma & Van Vossen, 2004).

Obs.	Simulation	Mean	Stand. dev.	RMS	Max	Min	Obs. range	Simulation range
Vazo 10m	VAZO/ TEMP-10	-0.09	0.14	0.16	0.17	-0.52	2.03	2.20
Bezo 52m	BEZO/ TEMP-52	-0.01	0.29	0.29	1.25	-0.78	5.06	4.36
Vazo 60-p1	VAZO 60-p1	-0.42	0.80	0.91	1.23	-1.86	4.98	3.88
Vazo H	VAZO HARB	0.35	0.51	0.62	1.47	-0.38	2.45	3.76
Bezo H	BEZO HARB-p1b	-0.28	0.46	0.54	1.04	-1.64	4.31	4.16
Vazo 68m	BEZO 68	0.06	0.46	0.47	2.60	*) -1.27	*) 5.32	3.82
Beckmann cel-114m	TEMP-113/ BE-CEL	0.16	0.22	0.28	0.81	-0.29	2.42	2.27

*Table 3.2.7.2: Absolute errors of salinity in ppt (observed - simulated, run dd14). *) due to observed S = 0 at LW.*

Figure 3.2.7.6 shows that computed and measured current magnitude are in good agreement with each other.

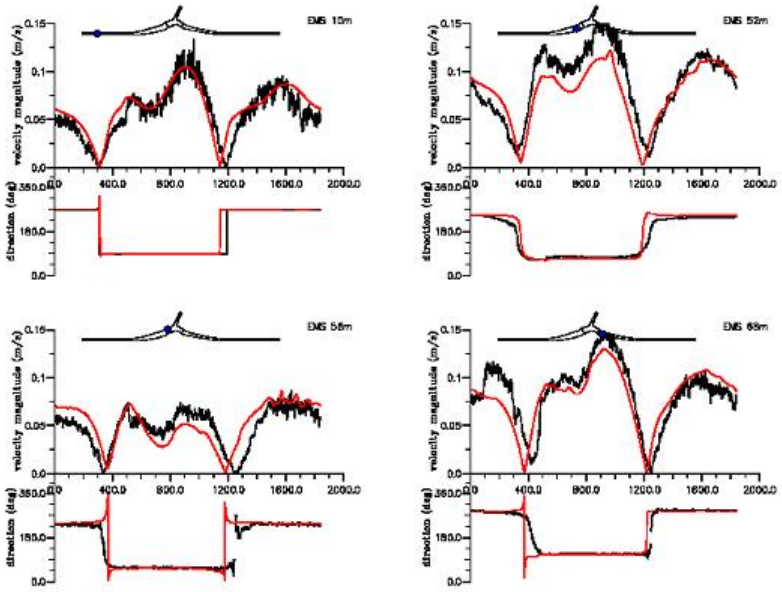

Figure 3.2.7.6: Computed (red) and measured (black) current magnitude and direction in four stations along the flume, run dd14 and test of 26 May 2003, cycle 20 (Bijlsma & Van Vossen, 2004).

Conclusions

This validation study shows that the Numerical Scale Model is able to reproduce the complex exchange flow between the tidal dock and the estuary to an acceptable level, despite limitations e.g. due to the local laminar conditions in the physical scale model.

3.2.8 Two-dimensional dam break

This page last changed on 18-08-2008 by platzek.

Purpose

This validation study investigates the flow resulting from a dam break including the interaction of reflecting bores in a 2D model. We remark that in validation study 3.2.4 a one-dimensional dam break was examined.

Linked claims

Claim 2.2.1.12: Flows resulting from dam breaks
Claim 2.2.2.6: Subcritical and supercritical flow
Claim 2.2.2.8: Accurate flow over dry or almost dry areas
Claim 2.4.6: Moving boundaries - representation of drying and flooding

Approach

For this validation study a model is applied that is described in Stelling & Duinmeijer (2003). It consists of two experiments:

- a dam break with an initially wet region; and
- a dam break with an initially dry region.

The experiments are performed in a closed domain. So, reflecting bores interact with each other, resulting into a more "challenging" validation case compared to the one-dimensional dam break (see Section 3.2.4). Results of both experiments are compared to numerical results obtained using Delft3D-FLOW.

Model description

The experimental set-up consists of two reservoirs, A and B, separated by a wall with a gate of width 0.4m that can be lifted (Figure 3.2.8.1). Reservoir B is initially filled with water of height 0.6 m. Two experiments are performed. In the first experiment, reservoir A is initially dry and in the second experiment it contains a thin layer of water with a depth of 0.05 m. The gate is then lifted with a speed of 0.16 m/s and the subsequent flooding in reservoir A is studied. The simulation period is 21 s for the wet-bed experiment and 24 s for the dry-bed experiment.

Some model parameters are:

- Domain length L = 31 m.
- Domain width D = 8.3 m.
- Grid size $\Delta x = \Delta y$ = 0.1 m.
- Time step Δt = 0.006 s (0.0001 minutes).
- Manning bottom roughness = 0.012 $m^{-1/3}$ s.
- The *Flooding* scheme was used.

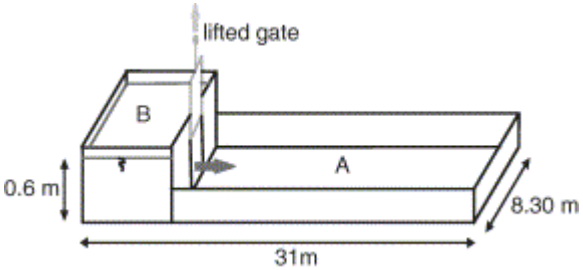

Figure 3.2.8.1 Experimental setup.

Results

The results obtained using Delft3D-FLOW are compared to the experimental results obtained with Delft3D-FLS and in the measurement done by Stelling and Duinmeijer at the Delft Technical University.

Delft3D-FLS is a software system that is no longer operational. However, the numerical discretisation of the advective terms in Delft3D-FLS is similar to the Flooding scheme of Delft3D-FLOW. In the left panel of the figures, the Delft3D-FLOW results are shown, while in the right panel contains the Delft3D-FLS and the Stelling and Duinmeijer measurements. Figures 3.2.8.2-3.2.8.7 show time histories at different locations along the centre line of the domain, for both the initially wet bed case and the initially dry bed case. Figures 3.2.8.8 and 3.2.8.9 show the 3D surface plots of the two experiments at the end time of the simulation, respectively. From all these figures it can be concluded that both codes yield accurate results for the simulation of a two-dimensional dam break when compared to the measurements. Although differences can be observed, the peak in water levels and the time evolution of the peaks are in general in agreement with each other.

Additional simulations have been performed using the Cyclic scheme of Delft3D-FLOW. These simulations, for which no results are presented in this section, show that the Cyclic scheme leads to less accurate results when modelling a bore and produces spurious oscillations around the bore. The Flooding scheme does not suffer from this discrepancy. This clearly illustrates that for simulation of bore phenomena the advective terms are important and that a well-suited advection discretisation method is required.

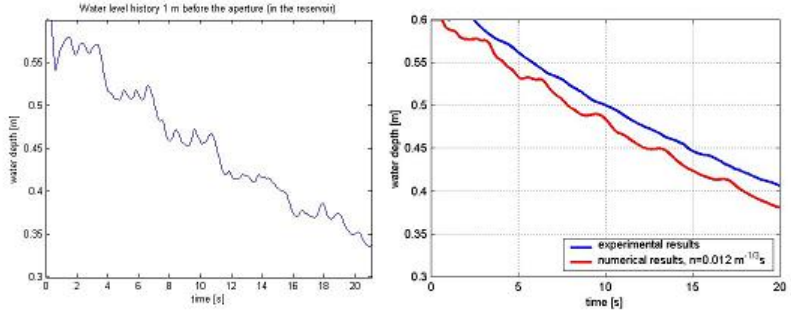

Figure 3.2.8.2 Time history of the water level in the reservoir, for the initially wet bed simulation. Delft3D-FLOW simulation results are shown in the left plot and the Stelling and Duinmeijer measurements and Delft-FLS results are shown in the right plot.

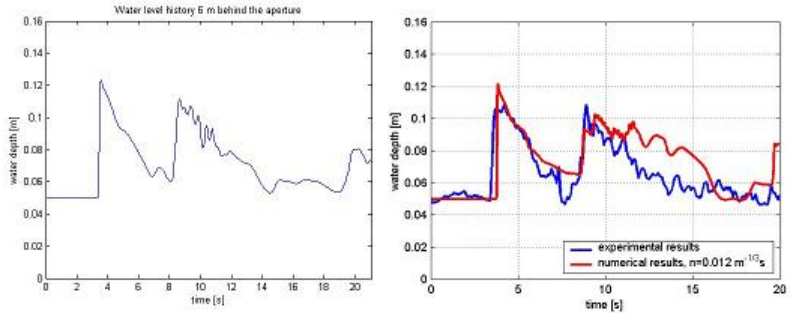

Figure 3.2.8.3 Time history of the water level 6 m behind the aperture, for the initially wet bed simulation. Delft3D-FLOW simulation results are shown in the left plot and the Stelling and Duinmeijer measurements and Delft-FLS results are shown in the right plot.

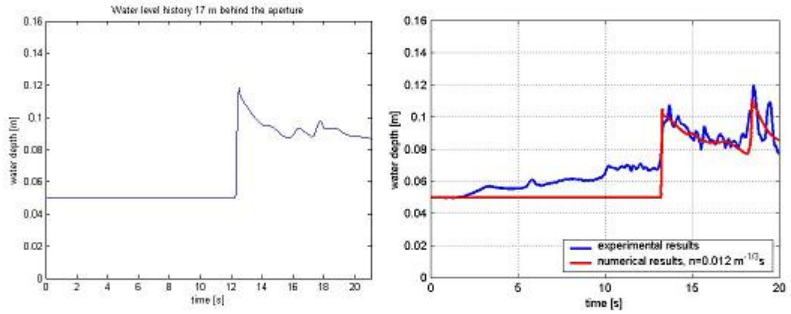

Figure 3.2.8.4 Time history of the water level 17 m behind the aperture, for the initially wet bed simulation. Delft3D-FLOW simulation results are shown in the left plot and the Stelling and Duinmeijer measurements and Delft-FLS results are shown in the right plot.

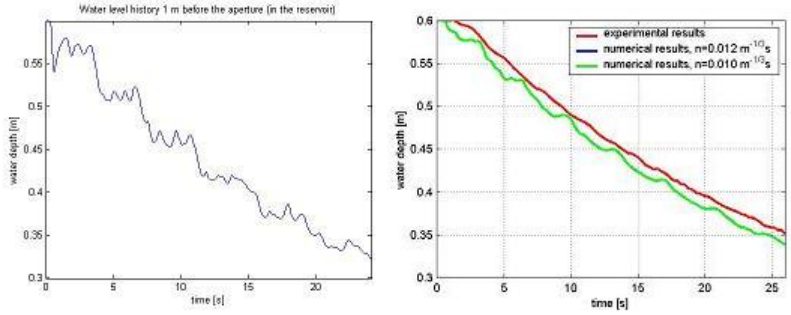

Figure 3.2.8.5 Time history of the water level in the reservoir, for the initially dry bed simulation. Delft3D-FLOW simulation results are shown in the left plot and the Stelling and Duinmeijer measurements and Delft-FLS results are shown in the right plot.

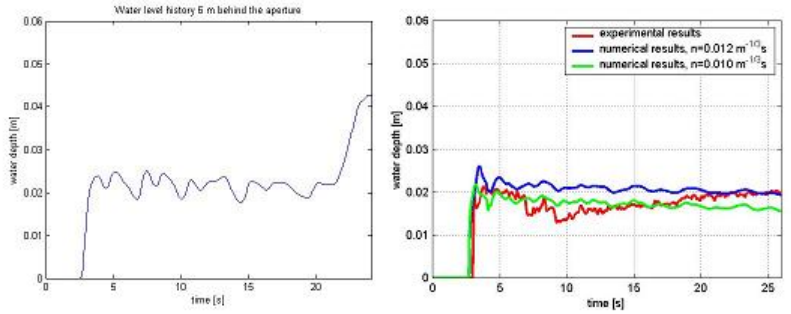

Figure 3.2.8.6 Time history of the water level 6 m behind the aperture, for the initially dry bed simulation. Delft3D-FLOW simulation results are shown in the left plot and the Stelling and Duinmeijer measurements and Delft-FLS results are shown in the right plot.

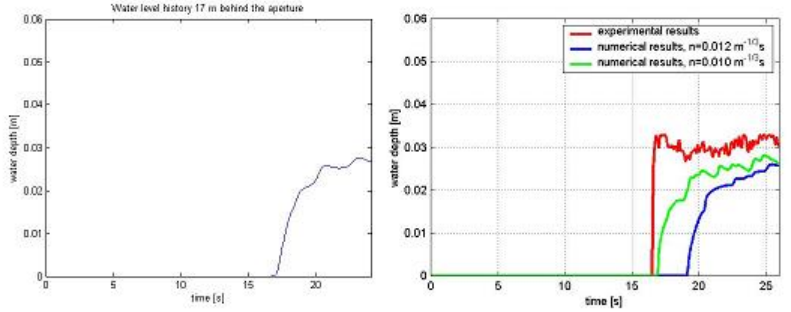

Figure 3.2.8.7 Time history of the water level 17 m behind the aperture, for the initially dry bed simulation. Delft3D-FLOW simulation results are shown in the left plot and the Stelling and Duinmeijer measurements and Delft-FLS results are shown in the right plot.

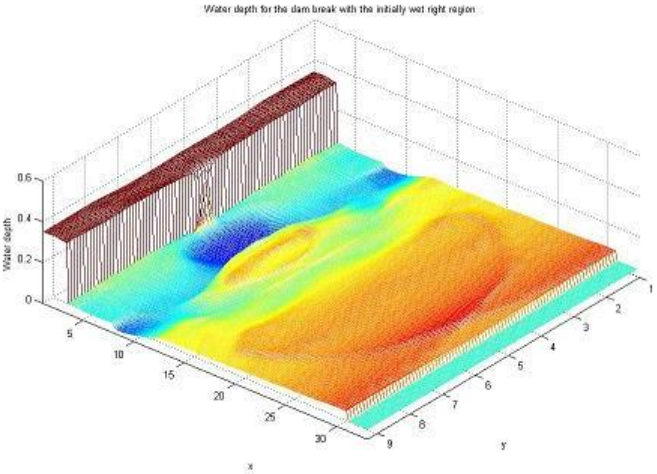

Figure 3.2.8.8 Three-dimensional surface level plot at the end of the wet bed simulation.

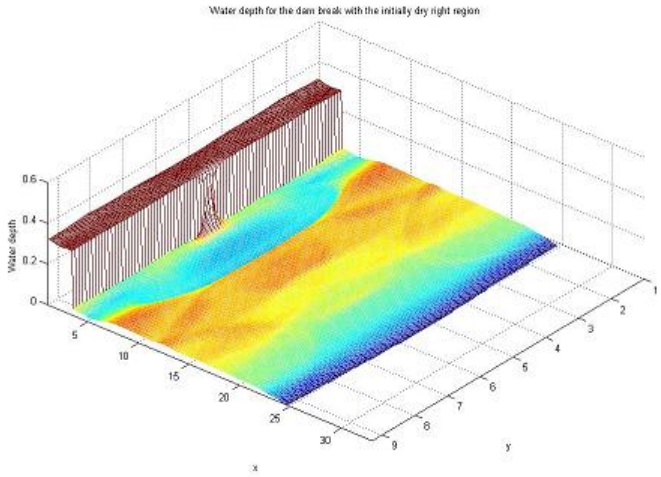

Figure 3.2.8.9 Three-dimensional surface level plot at the end of the dry bed simulation.

Conclusions

It can be concluded that Delft3D-FLOW can accurately simulate dam breaks and the interaction of reflected bores, provided that the *Flooding* scheme of Delft3D-FLOW is applied. The scheme is well-suited for this application and does not produce spurious oscillations around the bores. The numerical results obtained closely resemble those obtained in the scale experiments.

3.3 Schematic test cases

This page last changed on 02-07-2008 by platzek.

The following schematic test cases are available at present:

3.3.1 Curved back channel

This page last changed on 19-08-2008 by platzek.

Purpose

The aim of this validation study is to compare discretisation errors for rectangular and curvilinear grids in a channel bend. Furthermore, the use of the cut-cells functionality is tested. We remark that cut-cells are an approach to suppress inaccuracies near staircase boundaries.

Linked claims

Claim 2.4.2: In Delft3D-FLOW the user can choose a type of grid that is suitable for the application involved.

Approach

For this validation study a channel bend with a U-shape is investigated. The flow through such a bend is characterised by the centrifugal force in the bend, which causes a recirculation pattern in the bend. Three different model grids are examined in this study, a curvilinear grid, a rectangular grid and a rectangular grid adapted using the cut-cells functionality. Due to (mis)alignment of the grid with respect to the flow, the solutions on the three grids will be different. The discretisation errors will be the smallest on the curvilinear grid, since the grid is fully flow aligned with the closed boundaries. The solution on the curvilinear grid is therefore used as the reference solution.

Model description

The three grids are shown in Figure 3.3.1.1. At the south-west (left) end of the channel, a constant inflow velocity u = 0.5 m/s is specified. At the south-east (right) end of the channel, a water level of 10 m is prescribed. The initial water level is set at 10 m as well. The bed level is zero in the whole channel. The different model parameters for the three grids (three simulations) are given in Table 3.3.1.1.

	Curvilinear grid	**Rectangular grid**	**Cut-cells grid**
Parameter			
Chézy coefficient ($m^{1/2}/s$)	60	60	60
Δx (m)	10 (average)	5	5 (average)
Δy (m)	5	5	5 (average)
Δt (minutes)	0.1	0.1	0.02
Simulation time T (minutes)	200	200	200

Table 3.3.1.1: Model parameters for the three different grids.

No background horizontal or vertical viscosity is applied. Both 2D models (for comparing water levels) and 3D models (with ten equidistant layers for comparing current profiles) have been applied. For all simulations with the 3D model the $k-\epsilon$-model is used to simulate the turbulence quantities.

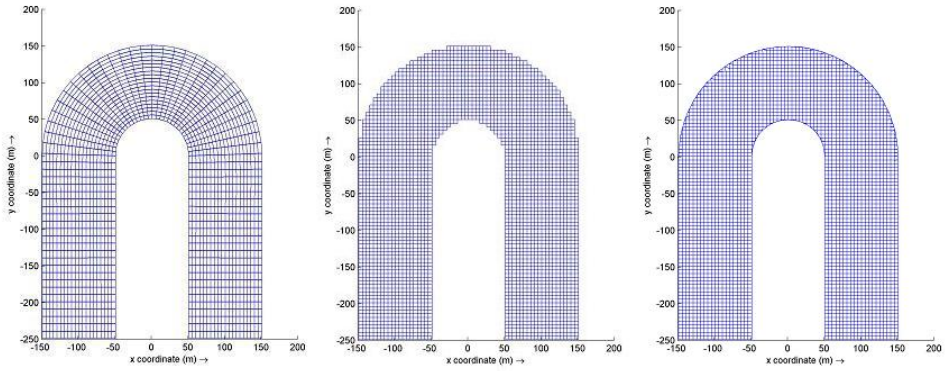

Figure 3.3.1.1: The three investigated grids: curvilinear, rectangular and rectangular with cut-cells.

Results

In Figure 3.3.1.2, the water level in the channel bend is shown at the end of the simulations for all three grids. The left panel shows the water level on the curvilinear grid, which is used as the reference solution. The mid panel shows the water level on the rectangular grid. One clearly sees the influence of the staircase boundary on the water levels. The are significant differences in water levels compared to the curvilinear grid solution. The right panel shows the water levels on the rectangular grid with the cut-cells approach switched on. Application of cut-cells significantly suppresses the stair-case problems.

In this validation study the applied grid is relatively fine. As a result, the stair-problems are relatively small as well. In the mid panel of Figure 3.3.1.2 a water level difference of 1-2 cm is observed at the inflow boundary, while for the right panel with the cut-cells correction it is in the order of a few mm. In (Vatvani, 2004) a similar test case was conducted, which shows much larger discretisation errors for a curved bend model.

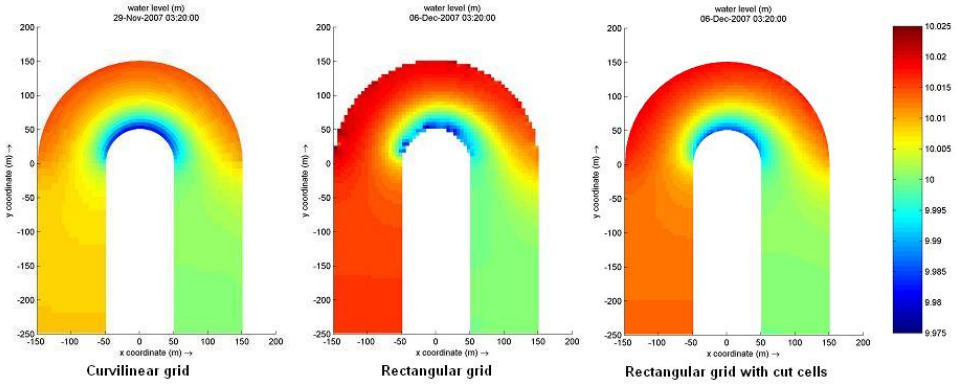

Figure 3.3.1.2: Water level in the channel bend on the curvilinear, rectangular and the cut-cells grid.

In Figure 3.3.1.3, the velocity profile in the bend is shown, for the three grids. In this figure one can observe a circulation pattern that results from the centrifugal force in the bend. The water is 'pushed' to the outer bend near the surface level and returns to the inner bend near the bed. Except for local disturbances in the inner bend, the circulation pattern for both the rectangular grid and the cut-cells grid agree well with the currents on the curvilinear grid.

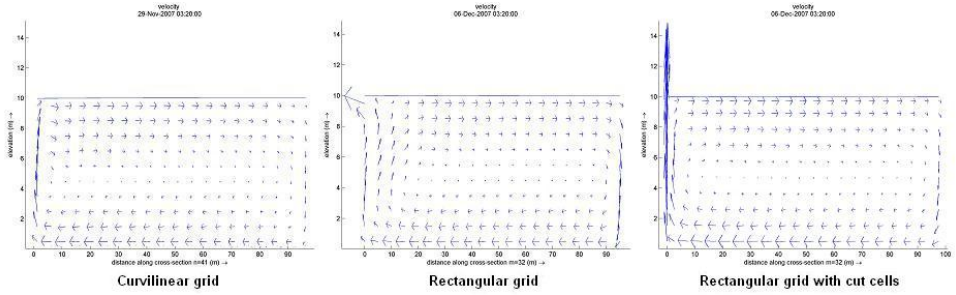

Figure 3.3.1.3: Velocity profile in the channel bend on the curvilinear, rectangular and the cut-cells grid.

It should also be noted that the simulation with the curvilinear grid converges in approximately 1 hour and 40 minutes, while the simulations on the rectangular grid - with and without cut-cells - takes more than three hours. This also confirms the introduction of disturbances in the flow due to the flow misalignment and the staircase boundaries, leading to more iterations for the underlying numerical solution methods. For consistency all simulations are performed using the same simulation period. For the grid with the cut-cells, the time step is reduced by a factor five, to ensure convergence of the solution. This time step reduction is to be expected, since the spatial resolution has become much finer at some locations along the cut-cell boundary. The smallest grid cells in general determine the maximum applicable time step.

Conclusions

This validation study shows that the flow through a bend can be simulated accurately using a grid that is aligned with the closed boundaries. Both the difference in water level between inner and outer bend and the resulting recirculation pattern are reproduced by Delft3D-FLOW. When using other grids, e.g.

rectangular grids, the cut-cells functionality is able to suppress the occurrence of disturbances in the flow due to the staircase boundaries.

3.3.2 Drying and flooding

This page last changed on 19-08-2008 by platzek.

Purpose

Test for robustness of drying and flooding algorithms in a square basin with varying depth. A 3D model is tested, using both a σ- and a Z-model.

Linked claims

Claim 2.2.2.8: Delft3D-FLOW can accurately simulate drying and flooding of tidal areas.
Claim 2.4.1: General (robustness, accuracy, efficiency).
Claim 2.4.6: Moving boundaries - representation of drying and flooding.

Approach

This validation study is conducted to examine the accuracy and the robustness of the drying and flooding algorithm in Delft3D-FLOW. This validation study consists of a square domain of 900 x 900 m^2 with an irregular bathymetry (see Figure 3.3.2.1). In southwest to northeast direction the bottom values are constant. The bathymetry varies from 5 m on the southwest to northeast diagonal to -5 m at the northwest and southeast corner.

Drying and flooding is simulated by withdrawing water at the northwest and southeast corner points, at which the bottom is deepest. Initially the water level is 4.5 m. The discharges are distributed uniformly over all layers. The simulation period is 720 minutes. In the beginning of the simulation, water is discharged into the test basin, yielding in increase in water levels. After about four minutes the discharge start to withdraw water from the basin and the water level drops. At the end of the simulation the whole model is set dry. A tracer is added to check conservation of mass in combination with drying.

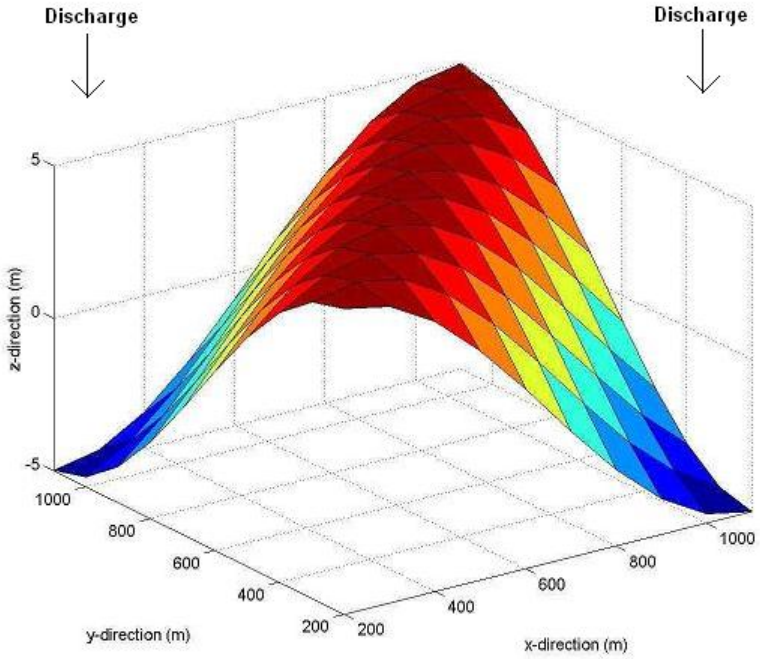

Figure 3.3.2.1: Bathymetry of the test case for drying and flooding.

Model description

Some characteristics of this model are:

- 3D Model.
- 2 Subdomains, almost of equal size (subdivision in x-direction).
- σ-model and Z-model.

- Closed basin.
- In the horizontal 9 x 9 grid cells of 100 x 100 m^2 each.
- In the vertical direction 10 uniformly distributed layers for both for the σ- and the Z-model (with Z_{bot} = -5.21 and Z_{top} = 5.5).
- Time step of 1 minute.
- Initial tracer concentration of 10 ppm.

Results

In Figures 3.3.2.2 and 3.3.2.3, the time history of water elevation at two (arbitrary) locations are shown for both the σ- and the Z-model, respectively. From the water levels one clearly sees that flooding (from T = 0.5 min to about T = 5 min) and drying (roughly from T = 8 min) occurs. Moreover, this occurs in a smooth way, because there are hardly any oscillations. In addition, these figures illustrate that also in case of local grid refinement the implementation of drying and flooding in Delft3D-FLOW is simulated in an accurate and robust way. In case of the σ-model only some small oscillations occur when the area becomes flooded. Near drying no non-physical oscillations are visible. We remark that drying and flooding yields a discontinuous movement of the closed boundaries and may therefore generate small oscillations in water levels and velocities. The oscillations introduced by the drying and flooding algorithm are in general small.

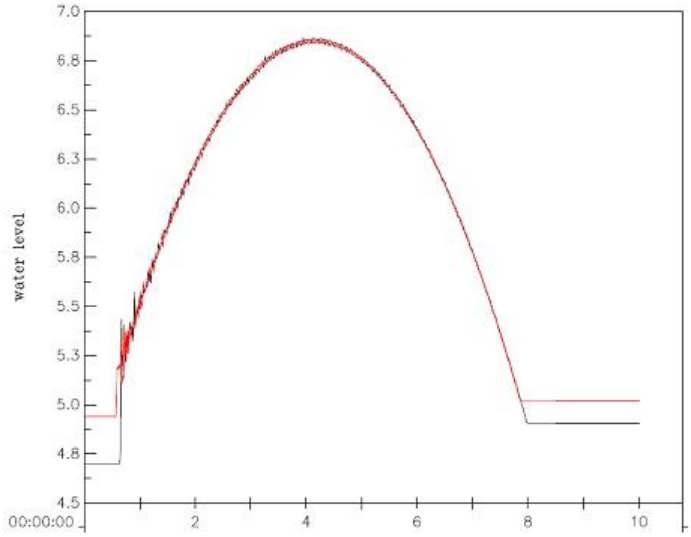

Figure 3.3.2.2: Time history of water levels (in m) for σ-model at two locations; on x-axis the time in minutes.

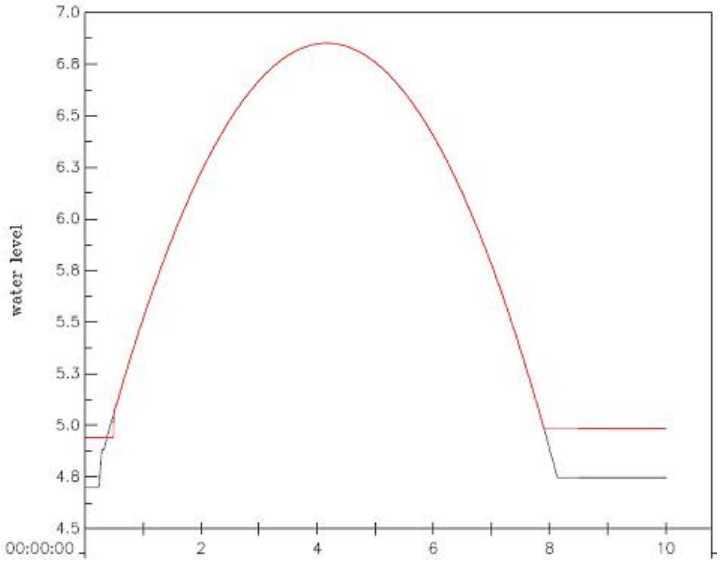

Figure 3.3.2.3: Time history of water levels (in m) for Z-model at two locations; on x-axis the time in minutes.

Conclusions

Delft3D-FLOW can be used to accurately predict drying and flooding phenomena. Simulations with both σ- and Z-models yield accurate results. In flooding situations, the σ-model gives small (numerical) oscillations near the flooding boundary due to discontinuous effects.

3.3.3 Schematised Lake Veere model

This page last changed on 19-08-2008 by platzek.

Purpose

This validation study is used to investigate the vertical mixing behaviour of Delft3D-FLOW. The Lake Veere model is a weakly dynamic system with salinity stratification. A simplified 2DV model of Lake Veere is applied and tested for both a σ- and Z-model. [Bijvelds & Nolte, 2000].

Linked claims

Claim 2.2.1.10: Thermal stratification in seas, lakes and reservoirs.
Claim 2.4.5: Suppression of artificial mixing due to σ- co-ordinates.

Approach

This validation study is a two-dimensional vertical (2DV) schematic model for Lake Veere in the Netherlands. It was developed for further investigation by WL | Delft Hydraulics of the effects on the water quality of Lake Veere after completion of the Delta works. In this simplified test case, effects of wind and temperature are neglected. The main goal is to compare the mixing behaviour of the σ- and Z-model.

Model description

The length of the model is 7000 m. Its bathymetry (see Figure 3.3.3.1) is a composition of two parabolic shaped pits (depth 20 m) with bottom slopes and depths similar to those in the actual bathymetry of Lake Veere. A third (non-physical) deep pit (depth 500 m) is added in order to prevent reflections of the salt wedge at the left boundary (Figure 3.3.3.1).

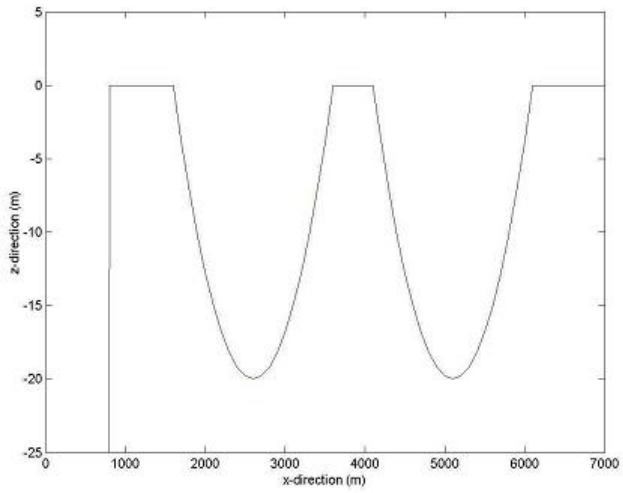

Figure 3.3.3.1: Bathymetry for the two-dimensional model for Lake Veere.

Initially, the water level of the lake is set to 5 m and there is no salinity in the lake. At the start of the numerical simulation, from 10-02-1998 00^h:00^m:00^s up to 13-02-1998 11^h:20^m:00^s, salt water is discharged (a discharge of 7.5 m^3/s with a salinity of 12.5 ppt) at the other boundary (right boundary in Figure 3.3.3.1). The discharge is only during a part of the simulation in order to test the σ- and Z-model under both forced and unforced conditions.

In the horizontal directions we discretise the domain with 70 x 1 grid cells of 100 x 150 m^2 each. For the σ-model we use 20 uniformly distributed layers in the vertical direction. For the Z-model the number of layers is 30 (with Z_{bot} = -500 m and Z_{top} = 10 m). Because of the deep non-physical pit we distribute these layers in the vertical direction as is depicted in Table 3.3.3.1:

Layer	Thickness
1 (bottom)	94.20 %
2	0.30 %
3 - 10	0.25 %
11 - 15	0.20 %
19 - 20	0.15 %
21 - 29	0.10 %
30 (top)	0.85 %

Table 3.3.3.1: Vertical layer distribution

The salt discharge is implemented at the two right grid cells in the lower layers (for the σ-model a discharge of 0.375 m^3/s per grid cell at layers 11 - 20, for the Z-model 0.75 m^3/s per grid cell at layers 19 - 23).
The total simulation period starts at 10-02-1998 00^h:00^m:00^s. The time step reads 15 seconds. For both models the $k-\epsilon$ turbulence closure model is used.

Results

We focus on the development of a stratified flow during the simulation. For that purpose, Figure 3.3.3.2 shows the change in salinity profile in pit 1 at six stages in time for both Z- and σ-model. From the figure it can be seen that for the Z-model strong stratification occurs. For the σ-model this is not the case.
To explain this, we plotted in Figure 3.3.3.3 the horizontal velocity in pit 1 at a stage in the beginning (left plot) and at the end (right plot) for both models (similar to [Bijvelds, 2001]). From this figure it can be observed that at the end of the simulation the horizontal velocity for the Z-model is almost zero, which is in line with the strong stratification. For the σ-model the horizontal velocity oscillates strongly, causing extra vertical mixing, which prevents the built-up of stratification. This mixing is illustrated by Figure 3.3.3.4, which shows the vertical velocity profile at the same state in the beginning (left plot) and at the end (right plot) of the numerical simulation. Note that the horizontal scales of these plots are much smaller than those of the plots in Figure 3.3.3.3. From the right plot in Figure 3.3.3.4 we see that, compared to the σ-model there is almost no mixing in the Z-model at the end of the simulation.

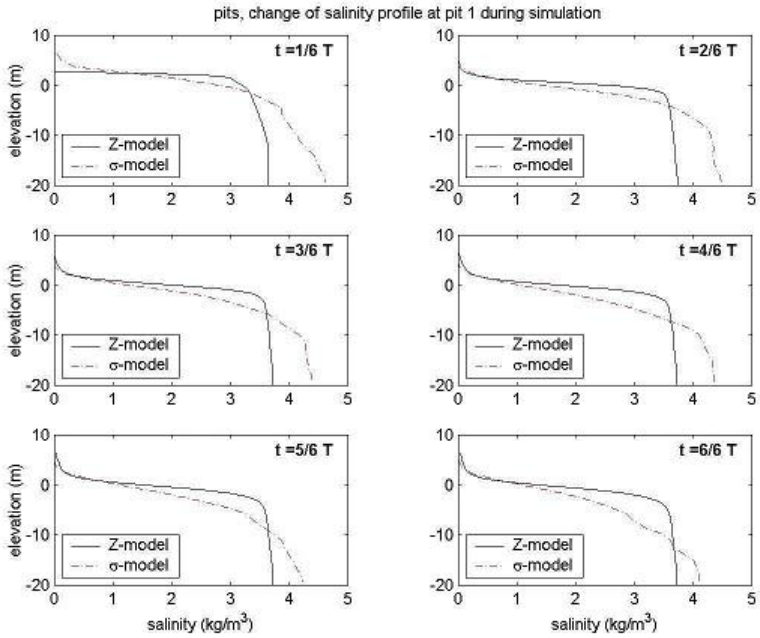

Figure 3.3.3.2: Time evolution of salinity profile at pit 1 during the numerical simulation with the Z-model (solid line) and the σ-model (dash-dotted line).

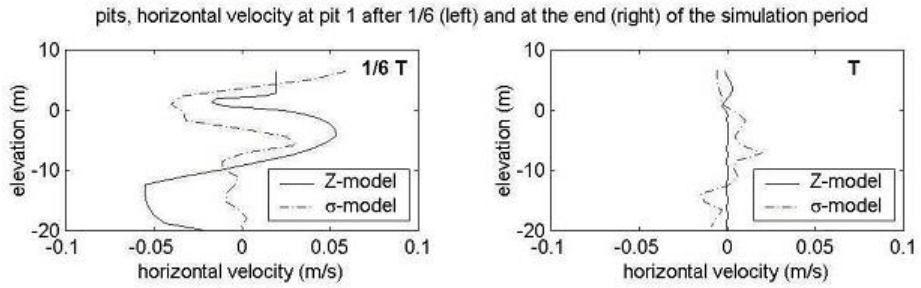

Figure 3.3.3.3 Horizontal velocity at pit 1 after 1/6 (left plot) and at the end of the numerical simulation with the Z- (solid line) and the σ-model (dash-dotted line).

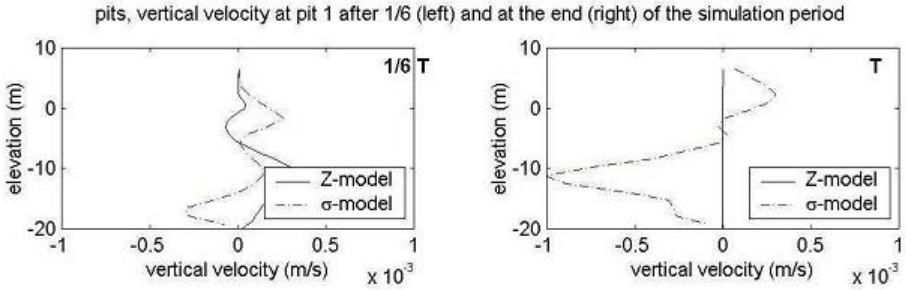

Figure 3.3.3.4 Vertical velocity at pit 1 after 1/6 (left plot) and at the end of the numerical simulation with the Z- (solid line) and the σ-model (dash-dotted line).

Conclusions

From this validation study it can be concluded that for simulating lakes or seas with deep pits and stratification, the Delft3D-FLOW Z-model shows better results than the σ-model. When the σ-model is used, artificial mixing occurs and no stratification. This is due to the oscillation of horizontal and vertical velocities near deep pits. We remark that in Delft3D-FLOW the artificial vertical mixing in σ-models can be significantly suppressed by switching on the so-called anti-creep option.

3.3.4 Buoyant jet

Purpose

This validation study is a test for near-field modelling of a buoyant jet. The performance of the hydrostatic and non-hydrostatic module of Delft3D-FLOW is investigated, see also [Bijvelds, 2003]. We remark that the non-hydrostatic module can only be used in combination with the Z-model.

Linked claims

Claim 2.2.1.4: Hydrostatic and non-hydrostatic flow.
Claim 2.2.2.2: Baroclinic flow - salinity and temperature driven flow.
Claim 2.3.3.4b: Abruptly changing bathymetry, orbital movements in short wave motions, or intensive vertical circulations such as buoyant jet plumes: non-hydrostatic Navier-Stokes equations.

Approach

The mixing behaviour of discharges is determined by the conditions in the receiving water body and by the discharge characteristics. In the near-field region of a discharge the hydrostatic pressure assumption is invalid and a accurate prediction of the jet trajectory requires a non-hydrostatic module. In this validation study, a buoyant effluent is discharged in a stagnant water body.

Model description

In order to study the behaviour of such a buoyant jet, a 2DV model is set-up. The computational domain has a length L of 60 m and a depth H of 10 m and consists of 120 by 20 grid cells (i.e. Δx = 0.5 m and Δz = 0.5 m). The validation study is performed using either the standard hydrostatic simulation or the non-hydrostatic module. For consistency, both simulations have been done using the Z-model.

The discharge is schematised by means of a 3D boundary condition in the Z-model. This means that the jet is modelled by an inflow velocity near the bottom. At all open boundary layers the velocity is set equal to zero, except at the second layer above the bed (k=2), where a velocity of 1.0 m/s is imposed. The discharge that enters the water body has a temperature which differs from the receiving water body by T_{dis} - $T_{ambient}$ = 20-15 ºC = 5 ºC. At x=L a water level boundary is imposed, keeping the average free surface level constant in time. The time step in the simulations is equal to 0.6 s. The eddy viscosity and diffusivity are computed by means of the $k-\epsilon$ turbulence model. No additional background viscosity or diffusivity have been imposed in the current model.

No measurements or analytical solutions are available for this validation study. However, in Figure 3.3.4.1 the expected trajectory of the buoyant plume is shown. From a qualitative point of view, we will compare this trajectory with the computed results.

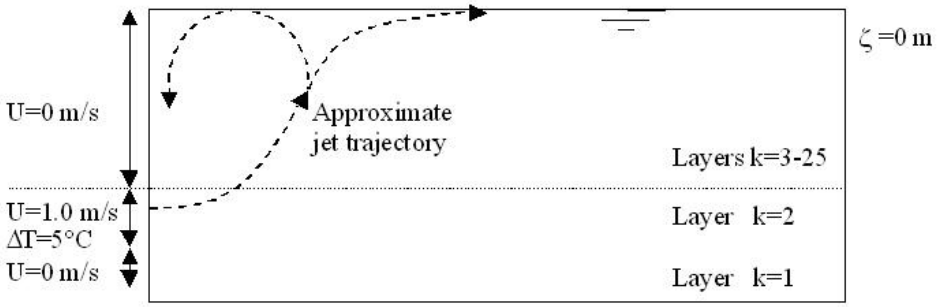

Figure 3.3.4.1: Illustration of trajectory of a buoyant plume.

Results

Two simulations have been carried out. One with the standard hydrostatic option and one with the non-hydrostatic option of Delft3D-FLOW. In Figures 3.3.4.2 (hydrostatic) and 3.3.4.3 (non-hydrostatic) the temperature evolution in time is shown for both cases. The figures clearly show that for the non-hydrostatic simulation, the trajectory of the plume is much more in line with the expected trajectory, as presented in Figure 3.3.4.1. In case of hydrostatic modelling, the hydrostatic pressure distribution yields that the plume rises much too quickly to the surface. For such applications, a non-hydrostatic module is therefore compulsory.

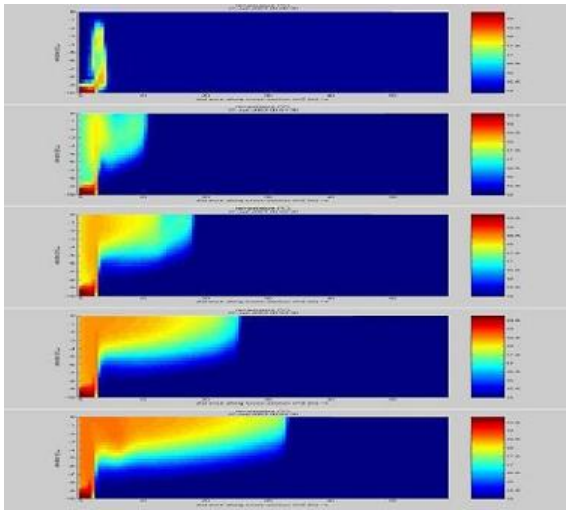

Figure 3.3.4.2: Temperature of the jet after 30 minutes, 1.5 hours, 2.5 hours, 3.5 hours and 4.5 hours, for the hydrostatic simulation.

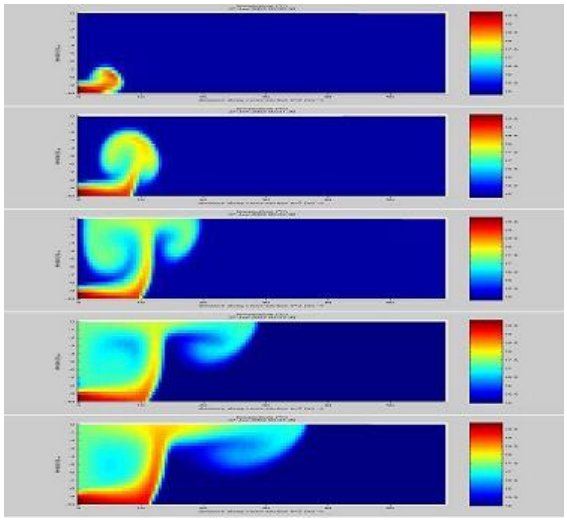

Figure 3.3.4.3: Temperature of the jet after 30 minutes, 1.5 hours, 2.5 hours, 3.5 hours and 4.5 hours, for the non-hydrostatic simulation.

Conclusions

For the simulation of dynamics of a rising buoyant plume in the near vicinity of its discharge, a hydrostatic model fails to represent physics in an accurate way. In these situations, the dynamic pressure is non-negligible compared to the hydrostatic pressure and a non-hydrostatic module should be used.

3.3.5 Migrating trench in a 1D channel

This page last changed on 19-08-2008 by platzek.

Purpose

Test for coupling of hydrodynamic and morphology processes.

Linked claims

Claim 2.2.2.4: Transport of sediments, including erosion, sedimentation and bed load transport.
Claim 2.4.8: Robust and accurate implementation of the coupling of hydrodynamic and morphology processes.

Approach

In this validation study, water flows across a steep-sided trench cut in the sand bed of a flume. The water reaches the upstream edge of the trench with an equilibrium suspended sediment concentration profile. As the flow decelerates over the deeper trench some sediment is deposited. Sediment is then picked back up by the accelerating flow at the downstream edge of the trench. Due to the spatial difference between the areas of deposition and erosion the trench appears to migrate downstream. Figure 3.3.5.1 shows the initial situation, before the trench has started to deform. Both the results of measurements carried out by Van Rijn (1984) and the computed results of Delft3D-FLOW are presented.

Model description

Initially the model has a constant depth with a trench with vertical walls in the mid of the model area. Due to the flow field (velocity ~ 0.5 m/s), the trench starts to move and changes its shape. The goal is to verify whether the trench development due to morphological impact is in agreement with the measurements.

Some model characteristics:

- Dimension of model: length of 30 m and a width = 0.5 m.
- Δx = 0.3 m and Δy = 0.1 m.
- 10 Non-equidistant layers.
- Time step of 0.24 seconds.
- Simulation period of 10 minutes; morphological changes start after T = 5 min.
- Morphological scale factor of 180, which means that at the end of the simulation the position of the trench after 15 hours is computed (5 min. of morphological changes multiplied by 180).
- Algebraic turbulence model.
- Horizontal viscosity coefficient of 5e-4 m^2/s.
- White-Colebrook bottom friction coefficient of 0.025 m.

Results

Despite significant variation in both velocity and sediment concentration profiles over the width of the trench, the Delft3D-FLOW solution generally accurately reproduces the measured results, which can be seen in Figures 3.3.5.1 and 3.3.5.2. In Figure 3.3.5.1 it is shown that the computed and measured velocity and the computed and measured sediment concentrations are in good agreement with each other at the start of the morphological changes (at T = 7.5 hours). Next, the trench starts to move. Figure 3.3.5.2 shows the measured and computed position of the trench after 15 hours. It can be verified that the trench has been reduced to approximately one half of its initial depth, and has migrated about 3 m downstream. The computed results are in good agreement with the measurements.

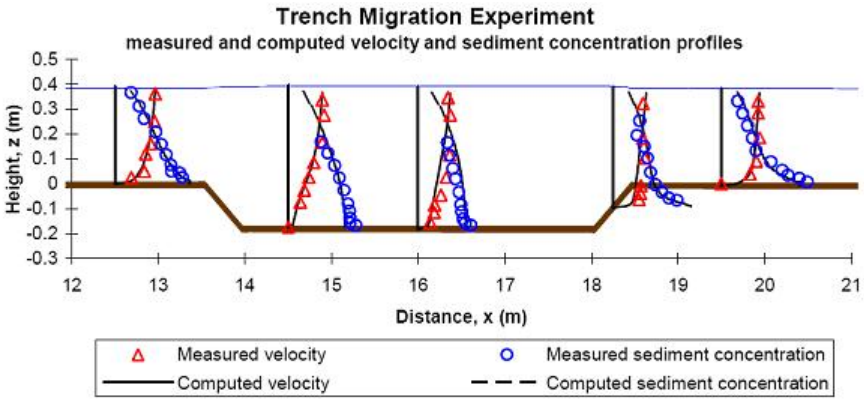

Figure 3.3.5.1: Measured and computed velocity and sediment concentration at the beginning of the morphological changes (T = 7.5 hours).

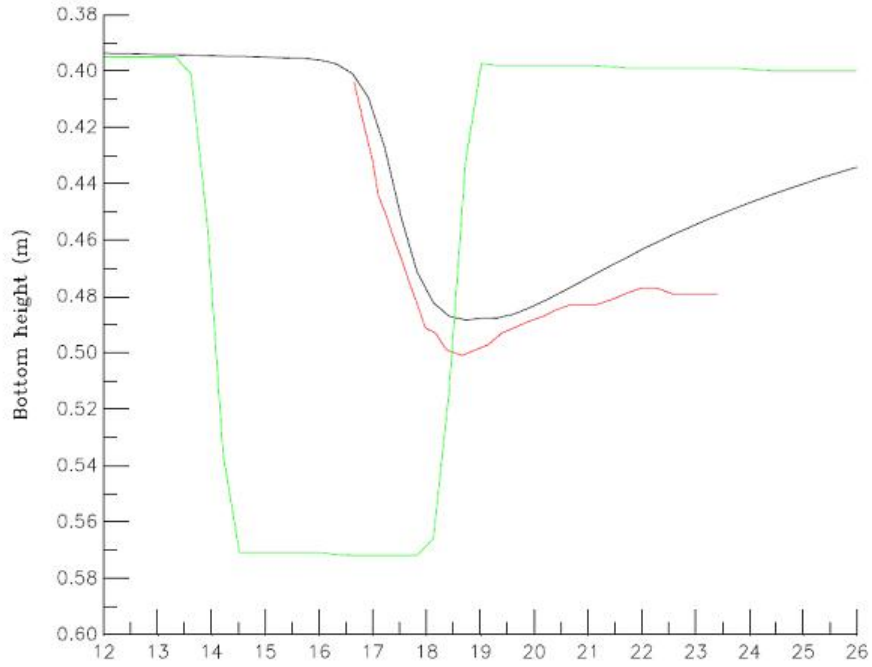

Figure 3.3.5.2: Measured and computed trench after 15 hours; initial trench (in green), computed trench after 15 hours (in black) and measured trench after 15 hours (in red).

Conclusions

This validation study shows that Delft3D-FLOW can be used for accurately predicting morphological processes in one-dimensional channels. The morphological changes that result from hydrodynamic processes in the channel agree very well with measurements.

3.3.6 Wind over a schematised lake

This page last changed on 19-08-2008 by platzek.

Purpose

Test for wind forcing. Additionally, domain decomposition is tested in this validation case.

Linked claims

Claim 2.2.1.3: Wind driven flow and storm surges.

Approach

The goal is to compute a velocity field that is consistent with the wind forcing. In the shallow parts of the model area the velocity field should be in the direction of the wind. Furthermore, this is a test case for domain decomposition, which means that artificial flow may not occur near coupling boundaries.

Model description

This validation study represents a schematised lake. It is a closed basin in which a (constant) north-western wind forcing is applied (under an angle of 45° with the grid orientation). Thus, the wind direction is not aligned along the grid lines. The left part of the schematised lake has a constant grid size of 2000 m and the right part of 1000 m, yielding a grid refinement of a factor of two. A space varying depth is applied. The schematised lake is deepest in the centre of the basin, see Figure 3.3.6.1. Due to the constant wind forcing a steady state solution is reached.

Results

Figure 3.3.6.2 contains the horizontal velocities at the steady state. The green velocity arrows correspond to the left (coarse) domain and the red arrows belong to the right (fine) domain. In the shallow areas (i.e. all areas except the mid of the basin) the flow direction is in line with the wind direction (towards the southeast corner). Consequently, in the deeper part (i.e. the mid of the lake) a return flow occurs. Furthermore, the figure shows that there is a smooth horizontal velocity field near the subdomain interface. Thus, Delft3D-FLOW computes velocity patterns that are consistent with the wind direction, also over subdomain boundaries. It is noted that the right domain has twice as many grid points as the left domain (1-to-2 refinement). However, to obtain a clear figure the velocity arrows have not been plotted at all grid points in the refined domain.

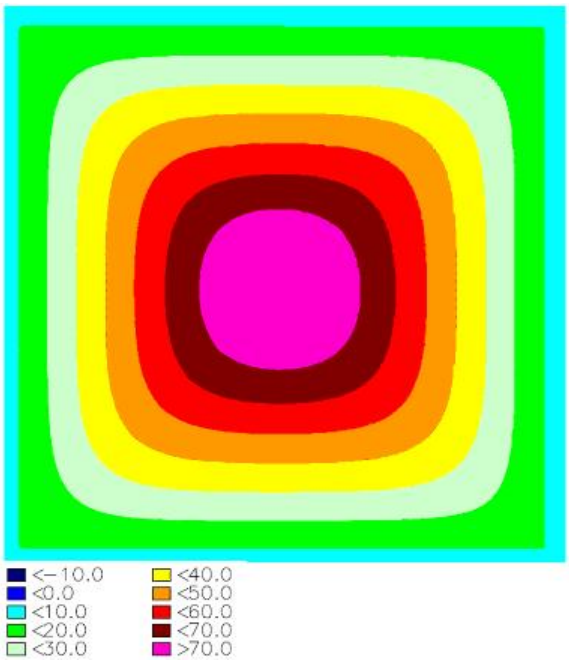

Figure 3.3.6.1: Bathymetry of schematised lake (depth in m).

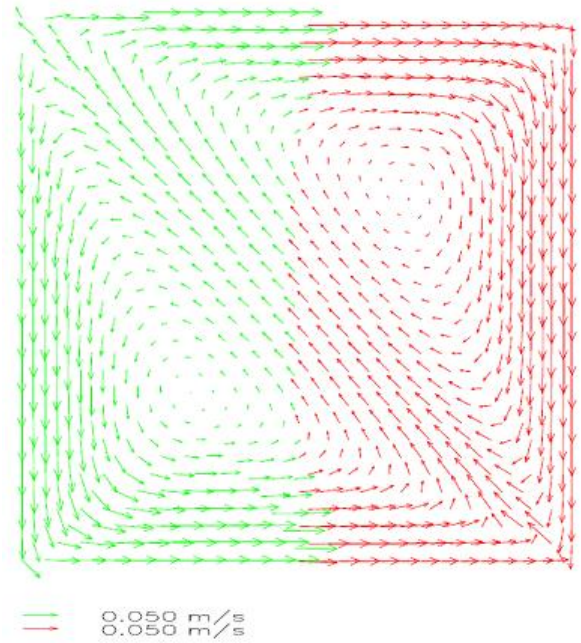

Figure 3.3.6.2: Velocity field at steady state.

Conclusions

This validation study shows that Delft3D-FLOW can reproduce the flow pattern in a lake that is known to occur when the flow is driven by wind only. In shallow parts of the lake, the flow velocity is in the direction of the wind and consequently, in the deeper parts, the return flow is directed opposite to the wind direction.

3.3.7 Tsunami

This page last changed on 19-08-2008 by platzek.

Purpose

The aim of this validation study is to examine the different advection schemes in Delft3D-FLOW (i.e. the standard Cyclic scheme and the Flooding scheme) for the simulation of a Tsunami wave height and run-up.

Linked claims

Claim 2.2.2.1: Propagation of long waves.
Claim 2.2.2.5: Propagation of short waves.
Claim 2.2.2.8: Drying and flooding of intertidal flats.
Claim 2.4.6: Moving boundaries - representation of drying and flooding.

Approach

The 1993 Okushiri tsunami caused many unexpected phenomena. One of them was the extreme run-up height of 32 m that was measured near the village of Monai in Okushiri Island (see Figure 3.3.7.1). This tsunami run-up mark was discovered at the tip of a very narrow gulley within a small cove. This benchmark problem is a 1/400 scale laboratory experiment of the Monai run-up, using a large-scale tank (205 m long, 6 m deep and 3.4 m wide) at Central Research Institute for Electric Power Industry (CRIEPI) in Abiko, Japan. It is emphasized that the focus is not to simulate the run-up of the real event, but to reproduce the laboratory measurements.

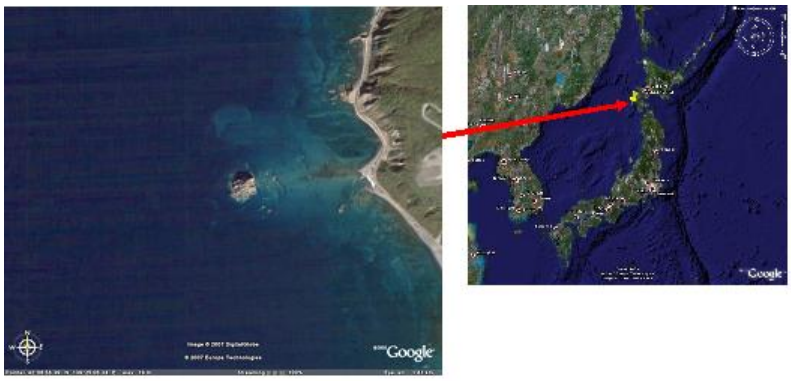

Figure 3.3.7.1: Approximate coverage of the model area in Okushiri Island (Japan).

The definition of tsunami wave height (or water level), inundation and run-up that is applied is conform the definitions in Figure 3.3.7.2:

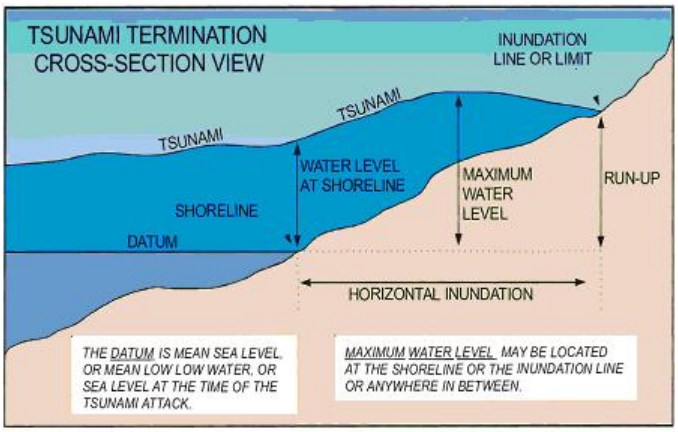

Figure 3.3.7.2: Definitions of tsunami wave height (water level), inundation and run-up (adapted from "Tsunami Glossary" - IOC/UNESCO - International Tsunami Information Centre, 2006 leaflet).

Model description

The bathymetry data file is provided on a 14 cm rectangular grid. Based on this data the Delft3D-FLOW model bathymetry is constructed (see Figure 3.3.7.3). The incident wave from offshore, at the water depth d = 13.5 cm, is specified. Note that there are reflective vertical side walls at Northern and Southern boundary of the model. The primary goal of this validation study is the temporal and spatial variations of the shoreline location, as well as the temporal variations of the water-surface variations at three specified near-shore locations.

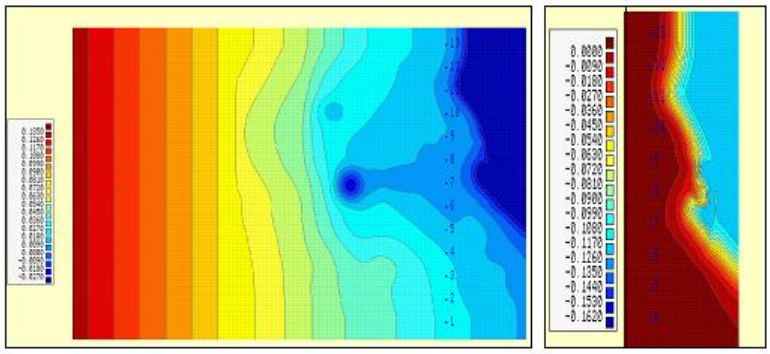

Figure 3.3.7.3: Overall (left) and detailed (right) bathymetry of the model.

The Delft3D-FLOW rectangular model for this test contains 199 by 125 points with a resolution of 28 cm. Originally, a finer resolution model with grid size of 14 cm was constructed. After some experiments it was found that the solutions of the fine model can be fully replicated by a coarser model. Therefore, it was decided to carry out the final runs with the coarse model with a mesh size of 28 m.

The simulation runs for 24 seconds as the boundary condition that was downloaded only contains data for 22.5 seconds. During the last 1.5 seconds the boundary condition is gradually decreased from 1 mm to zero. The integration time step applied is 0.025 seconds. The maximum Courant number corresponding to this time step at the start of the simulation equals 2.9. The time step has been determined after some experiments to ensure that the simulated results have converged.

A Manning (bed stress) coefficient equal to 6.5×10^{-4} has been applied to simulate a smooth concrete bed, which is assumed to be the case. An eddy viscosity value equal to 1×10^{-4} m^2/s has been applied and at the start of the simulation a zero water level initial condition is prescribed.

Results

The table below shows the benchmark parameter values for the two simulations using different solvers is presented below followed by figures showing the computed and measured wave height at stations 5, 7 and 9. Data are only available for these three stations.

Quantity: Water level [m]

Station name	mean err.	stand. dev.	RMS err.	max. err.	min. err.	obs. range	simulat. range	RMS/Obs. range
Run Q09								
5	0.0010	0.0042	0.0043	0.0093	0.0158	0.0459	0.0452	0.0947
7	0.0015	0.0033	0.0036	0.0077	0.0125	0.0462	0.0437	0.0790
9	0.0009	0.0049	0.0050	0.0112	0.0093	0.0479	0.0515	0.1038
Average	0.0011	0.0042	0.0043	0.0094	0.0125	0.0467	0.0468	0.0925
Run Q9C								
5	0.0014	0.0051	0.0052	0.0098	0.0200	0.0459	0.0467	0.1139
7	0.0017	0.0046	0.0049	0.0080	0.0191	0.0462	0.0408	0.1051
9	0.0001	0.0056	0.0056	0.0110	0.0161	0.0479	0.0478	0.1167
Average	0.0010	0.0051	0.0052	0.0096	0.0184	0.0467	0.0451	0.1119

Table 3.3.7.1: "Okushiri" benchmark results of the Delft3D model for 3 stations using the flood solver (top, run q09) and standard solver (bottom; run q9c).

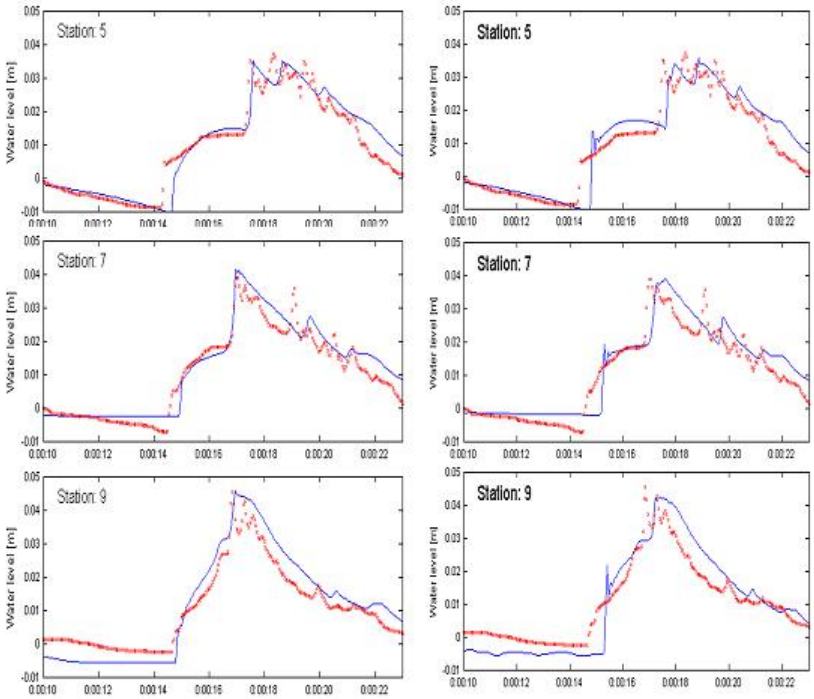

Figure 3.3.7.4: Simulated tsunami wave heights (blue line) compared to measured data (red crosses) at selected stations using the Flooding scheme (left; run q09) and Cyclic method scheme (right; run q9c).

In general, the model is able to reproduce the main characteristics of the tsunami wave quite correctly, especially the results from the Flooding method. Table 3.3.7.1 and Figure 3.3.7.4 show that the performance of the Flooding scheme is 20 to 25% better than the performance of the standard advection scheme in Delft3D-FLOW (i.e. the Cyclic method). The RMS error is for the results obtained with the Flooding scheme equals 8 to 10% of the observed wave range. The mean error is approximately 1 mm. The wave heights computed by the Cyclic method are slightly higher. Especially the first wave peak overshoots the actual wave height. For this application, it is evident that the Flooding scheme has an advantage compared to the standard advection scheme in Delft3D-FLOW.

From the figures we also observe that there is a slight mismatch between the bathymetry and initial condition that was applied in the model and the measured data. The reason for this mismatch is yet unclear. When the bathymetry is adjusted downwards uniformly with an amount of 5 mm, the location of the wave peaks (e.g. at t = approximately 20 seconds) can be shifted to arrive at earlier moment as shown in Figure 3.3.7.5. Consequently, further improvements on the performance are expected to be possible when this bathymetry discrepancy can be corrected.

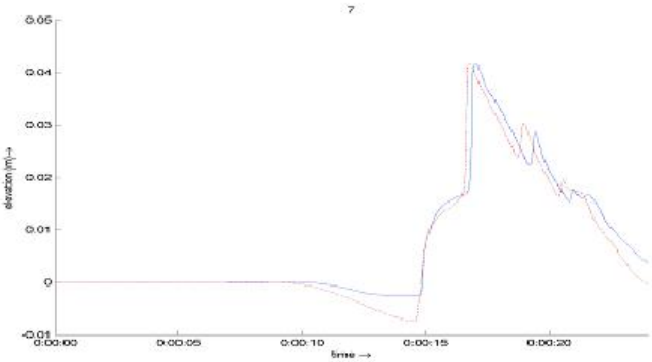

Figure 3.3.7.5: Sensitivity of the computed tsunami wave at station 7 on bathymetry; original bathymetry (straight line) and depth lowered uniformly by 5 mm (dashed line).

Conclusions

For this Tsunami validation study it can be concluded that the Flooding advection scheme is more suitable than the Cyclic method advection scheme, which is the default option in Delft3D-FLOW. The Flooding scheme computes tsunami wave heights and wave speeds that are in good agreement with the measurements.

3.4 Real-world applications

This page last changed on 02-07-2008 by platzek.

The following real-world applications are available at present:

3.4.1 3D North Sea model

This page last changed on 25-08-2008 by platzek.

Purpose

This validation study involves the onset, duration and areal extent of thermal stratification for the Southern North Sea. This study illustrates the ability of Delft3D-FLOW to accurately model the horizontal and vertical temperature distribution, including the depth of a thermocline.

Linked claims

Claim 2.2.1.3: Wind driven flow and storm surges.
Claim 2.2.1.10: Thermal stratification in seas, lakes and reservoirs.
Claim 2.4.2: Delft3D-FLOW has a flexible computational grid specification.
Claim 2.5.4: Delft3D-FLOW is a computationally efficient program.

Approach

A one-year simulation is conducted for a model representing the Southern North Sea. The period of 1 November 1988 till 1 November 1989 is chosen because of the availability of extensive observations. In-situ data for the North Sea for 1989 was measured by the NERC in the North Sea project (NSP) (Lowry et al. 1992). The NSP data set of 1989 is a very comprehensive one, having six locations on the North Sea with a series of continuous three-dimensional temperature measurements. Figure 3.4.1.1 shows the trajectory of the ship cruise and the locations of these six stations (A-F) on the North Sea.

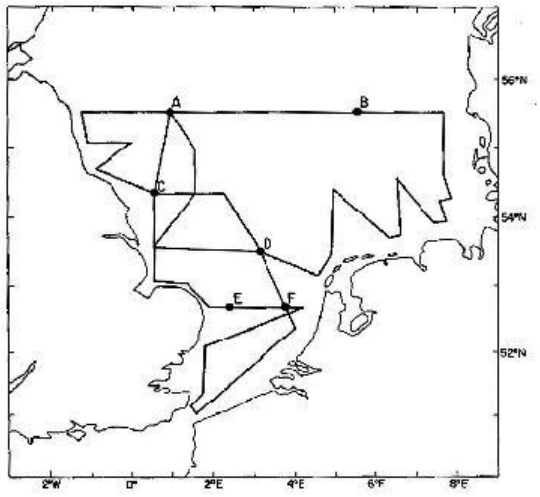

Figure 3.4.1.1 North Sea Survey cruise track (NSP project).

For the 1-year simulation we have selected stations A-D, in which a comparison is made with model results. In Table 3.4.1.1 the locations and depths of these four stations are given.

Measurement station	Geographical location	Depth (m)
A	55°0'N; 0°54'E	73.5
B	55°30'N; 5°31'E	49.5
C	54°20'N; 0°24'E	55.5
D	53°30'N; 3°0'E	29.5

Table 3.4.1.1: Overview of locations and depths of measuring stations in the NSP project.

Model description

- 134 by 65 horizontal grid points.
- 10 non-equidistant σ-layers.
- Curvilinear grid with mesh sizes varying from 1 km to 30 km.

- Water level boundaries driven with astronomical components.
- Time varying (and space constant) wind forcing.
- Time varying (and space constant) meteorological forcing (for relative humidity, air temperature and cloudiness).
- $k-\epsilon$ turbulence model.
- Time step of 300 sec.

Results

For five periods the ship track measurements have been gathered, namely for:

- 24 June to 18 July 1989 (see Figures 3.4.1.2-3).
- 24 July to 9 August 1989 (see Figures 3.4.1.4-5).
- 23 August to 3 September 1989 (see Figures 3.4.1.6-7).
- 7 September to 3 October 1989 (see Figures 3.4.1.8-9).
- 7 October to 2 November 1989 (see Figures 3.4.1.10-11).

The measurements for each period are now compared with model results at a time that is roughly in the mid of the period. Moreover, for each period both surface and bottom temperatures are shown. In the figures the measurements are in open circles.

Figures 3.4.1.12-15 contain the computed vertical profiles of temperature and the NSP measurements (in open circles) of the four stations, respectively. Day 0 corresponds to 1 November 1988 and day 365 to 1 November 1989. The figures show that the measurements from the NSP project are not available for the whole simulation period. For these four stations the vertical temperature profiles in the measurements are as follows:

- For station A data is available till 29 September '89 with a thermocline at approximately 55 m depth from 8 to 15 degrees at 29 September '89.
- For station B data is available till 28 September '89 with a thermocline at approximately 35 m depth from 11 to 15 degrees at 28 September '89.
- For station C data is available till 30 September '89 with weak stratification at 30 September '89.
- For station D data is available till 24 September '89 without any thermal stratification during the whole period (Dogger Bank location; well mixed).

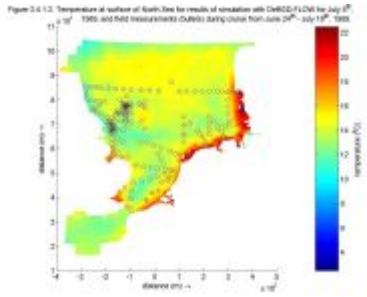

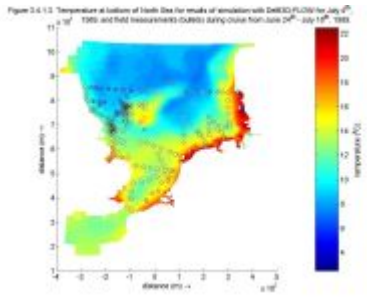

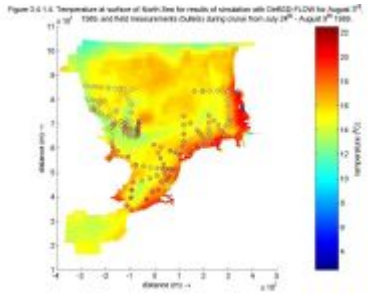

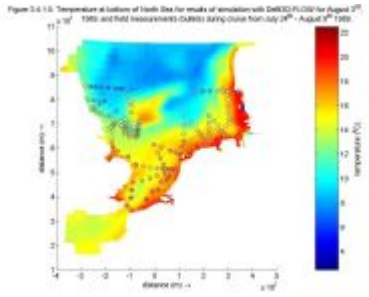

Figures 3.4.1.2-3.4.1.5

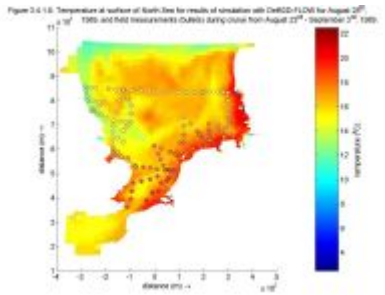

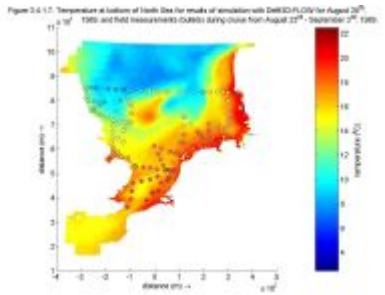

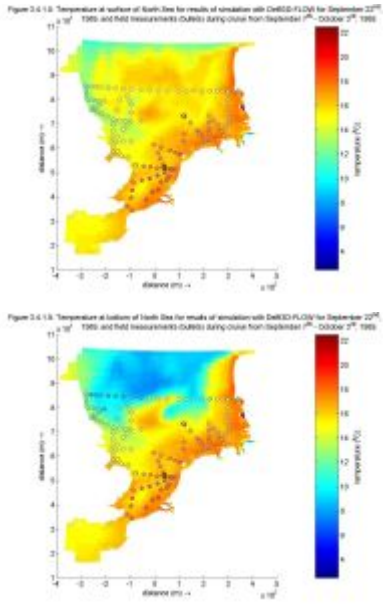

Figures 3.4.1.6-3.4.1.9

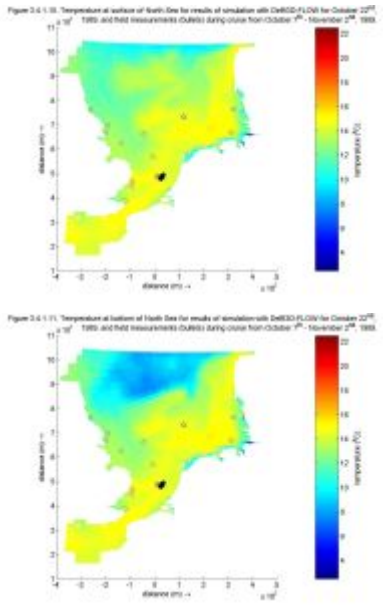

Figures 3.4.1.10-3.4.1.11

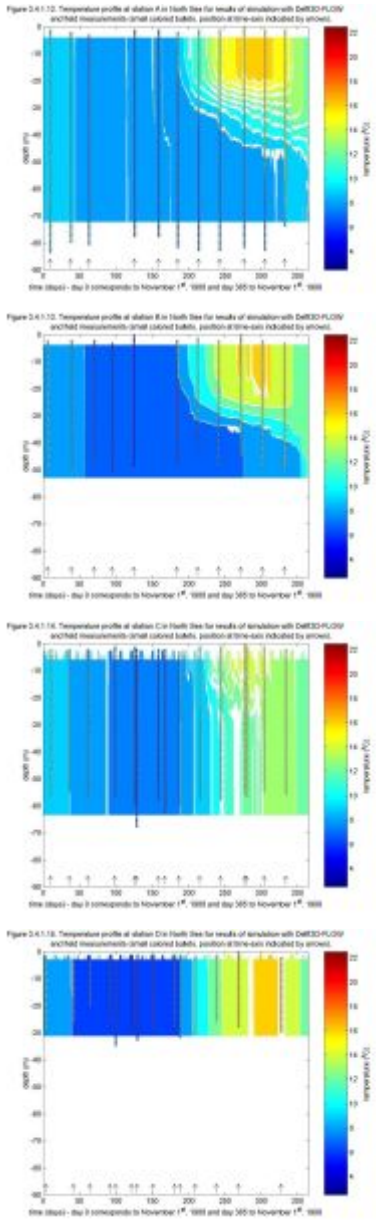

Figures 3.4.1.12-3.4.1.15

Conclusions

From the model results in Figures 3.4.1.2-15 it can be concluded that horizontal and vertical temperature distribution throughout the whole year in good agreement with the measurements. With respect to the vertical profiles, at the deepest stations (namely A and B) the onset of the thermocline is in accordance with measurements (around day 200). The model shows a more diffuse thermocline in comparison to the measurements (around day 200). The model shows a more diffuse thermocline in comparison to the measurements. Note that only ten vertical layers are applied in the vertical. At station C the measurements show a weak stratification from day 200 to day 275, which to some extent is reproduced by the model. For station D the model does not compute any stratification, which is in agreement with the measurements.

This validation study clearly demonstrates the potential of Delft3D-FLOW to accurately model thermal stratification in seas. It is noted that to accomplish this, accurate model forcing is required, in particular the meteorological forcing.

3.4.2 Zegerplas

Purpose

Test for temperature stratification using a 3D model. Both the σ- and Z-model have been tested. The simulation deals with a one-year simulation. For the simulated period measurements are available. Detailed documentation can be found in [Genseberger et al., 2003].

Linked claims

Claim 2.2.1.10: Thermal stratification in seas, lakes and reservoirs.
Claim 2.4.2: Computational grid.
Claim 2.5.4: Computationally efficient.

Approach

The present validation study originates from a project in which water quality in deep pits was studied. For training purposes a relatively coarse model was set-up for lake Zegerplas in The Netherlands. The Zegerplas is located at the east of Alphen aan de Rijn and has been used for producing salt. For this lake field measurements are available. Deep pits have their own special physical, chemical and biological properties. They are characterised by the presence of a steep gradient during part of the year. In warmer periods stratification is very strong. Due to the steep gradient of the bottom of deep pits, numerical simulations with the σ-model approach seems to be less suitable.

Model description

Two physical processes are involved, namely temperature and wind. For the wind forcing we use field measurements from 1996-1997. Initially the water level is 0 m and the temperature is 5° C. In the horizontal direction a grid with 10 x 14 grid cells of 1000 m each is applied. A schematic view of the Zegerplas and the model grid are shown in Figure 3.4.2.1.

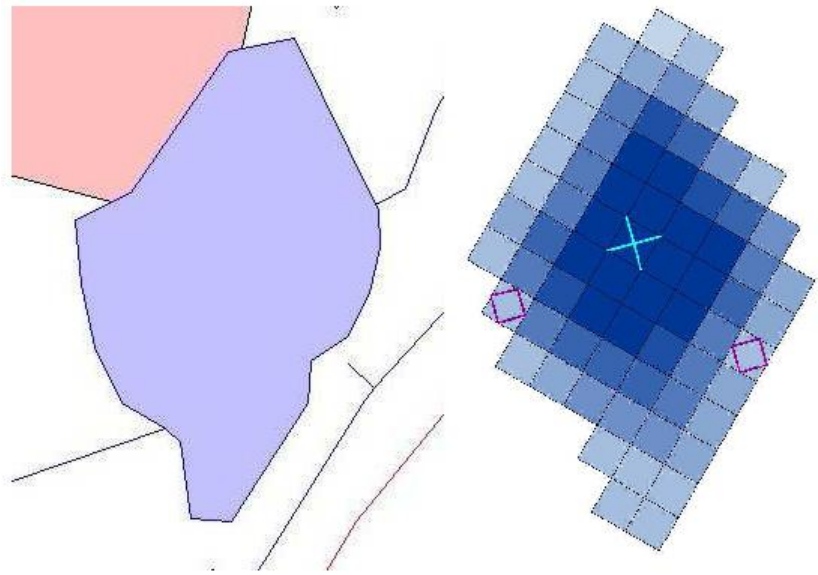

Figure 3.4.2.1 Schematic picture of the Zegerplas (left) and grid that was used (right).

For the discretisation in the vertical direction both for the σ- and Z-model (with Z_{bot} = -32.2 m and Z_{top} = 0.0 m) the non-uniform distribution of layers is as is listed in Table 3.4.2.1. The simulation period is from 01-01-1996 00^h:00^m:00^s to 31-12-1996 00^h:00^m:00^s with a computational time step of 1 minute. The $k-\epsilon$ is used for turbulence modelling.

Layer	Thickness

1	9.34 %
2	6.85 %
3	6.23 %
4	5.45 %
5	5.14 %
6	4.36 %
7	3.42 %
8	2.80 %
9	2.49 %
10	2.18 %
11	1.86 %
12	1.55 %
13-50	1.24 %
51	0.93 %

Table 3.4.2.1: Vertical layer distribution.

Results

For this validation study, the bathymetry is non-uniform and has a steep bottom gradient. At first, we examine at the temperature distribution in the vertical for both models during the simulation of one year. Figure 3.4.2.2 shows the temperature results for the σ-model, while Figure 3.4.2.3 contains the model results for the Z-model. From these two figures we observe that the Z-model reproduces the stratification in the warmer period in an realistic way, while the σ-model does not. Additional simulations with a uniform bathymetry did not show such differences between the two models. We therefore conclude that the difference between the results with the σ- and the Z-model are due to the non-uniform bathymetry with the steep gradients.

To verify that the results computed with the Z-model yield a good representation of the real life stratification, we compare the results of this simulation with field measurements. Figure 3.4.2.4 shows the temperature profile measured at August 14 1998 at the deep pit RO37 (see "+" signs), the measured profile at August 11 1999 (see crosses), and the computed results for August 12 1996 (solid line). The computed and measured results are in good agreement with each other, although some differences can be observed. Over a distance of 10 m in the vertical there is a salinity difference of roughly 15°C. The thermocline depth is computed accurately by the Z-model. Only near the surface differences with the measurements are observed, which is probably due to the heat flux input. We remark that for other periods in August 2008 we have a similar agreement between measurements and computed results.

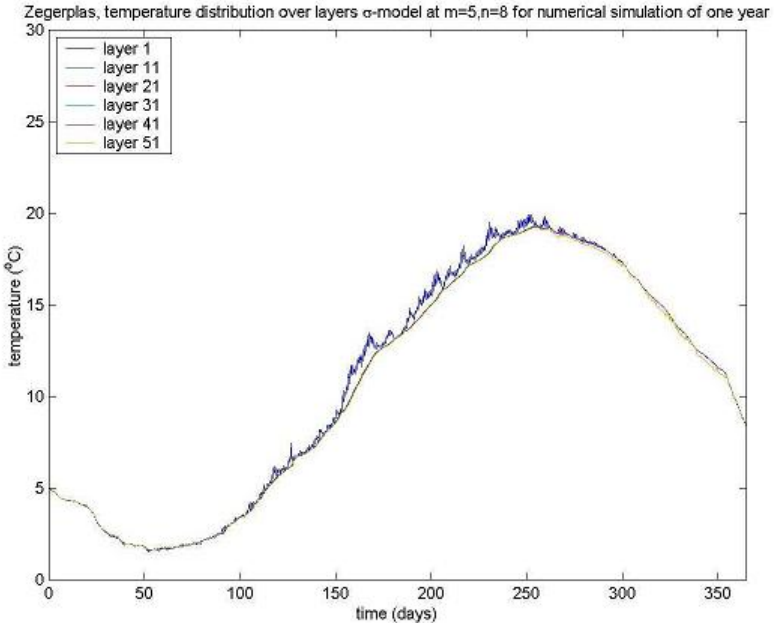

Figure 3.4.2.2: Zegerplas temperature distribution over layers of the σ-model for numerical simulation of one year.

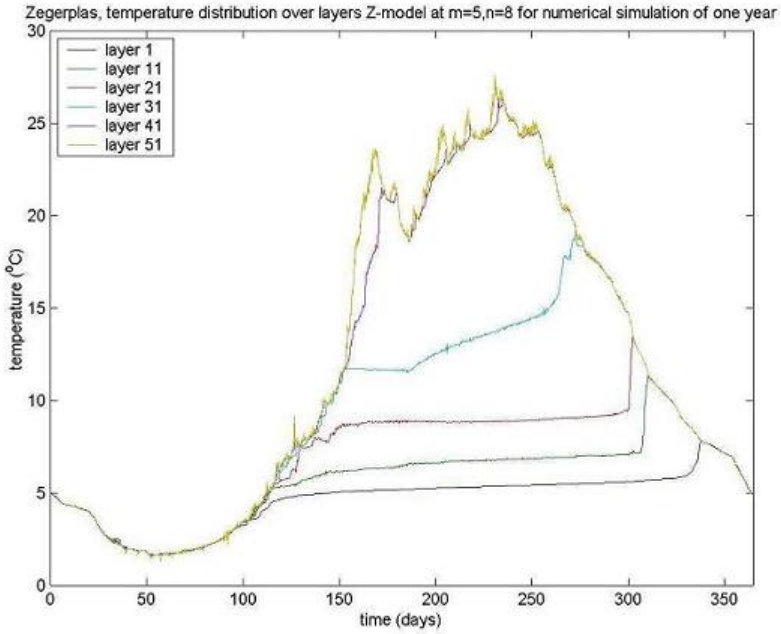

Figure 3.4.2.3: Zegerplas temperature distribution over layers of the Z-model for numerical simulation of one year.

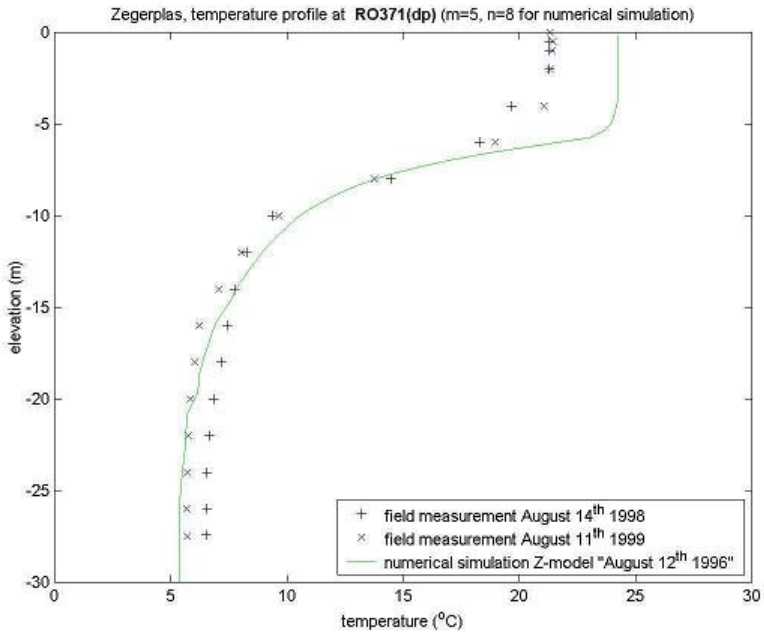

Figure 3.4.2.3: Zegerplas temperature profile at RO371; measured at August 14 1998 (the "+"-signs), measured at August 11 1999 (the crosses), and computed for August 12 1996 with the Z-model (solid line).

Conclusions

From this validation study we conclude that deep pits with relatively steep bottom gradients should be modelled with the Z-model instead of with the σ-model. Then, salinity stratification can be computed in an accurate way.

3.4.3 Lake Grevelingen

This page last changed on 25-08-2008 by platzek.

Purpose

The purpose of this validation study is to show that Delft3D-FLOW is able to reproduce both thermal and salinity stratification in terms of its duration as well as the depth of the pycnocline. The stratification is caused in this case by heat exchange through the surface as well as by baroclinic pressure gradients. Since Lake Grevelingen can be characterised as a weakly dynamic water system with steep bottom gradients, a Z-model schematisation of Delft3D-FLOW has been applied.

Linked claims

Claim 2.2.1.2: Density driven flow and salinity intrusion.
Claim 2.2.1.10: Thermal stratification in seas, lakes and reservoirs.
Claim 2.2.2.2: Baroclinic flow - salinity and temperature driven flow.
Claim 2.2.2.15: Heat exchange through the free surface, evaporation and precipitation.
Claim 2.4.2: Computational grid.
Claim 2.5.4: Computationally efficient.

Approach

This validation study involves a horizontal and vertical spatial temperature and salinity distribution as well as the variation of salinity and temperature over the year. Stratification in Lake Grevelingen is caused by heat exchange through the surface and by the inflow of water with a different salinity or temperature. This process is influenced by wind and wind induced currents. In Lake Grevelingen, the balance between these processes is very important from a physical point of view. The 3D Lake Grevelingen model has been validated against data for the year 2000, using 1999 as spin-up year. Extensive salinity and temperature profile measurements (GTSO) at 20 different locations at intervals of about 2-3 weeks have been used. The measurement locations are presented in Figure 3.4.3.1.

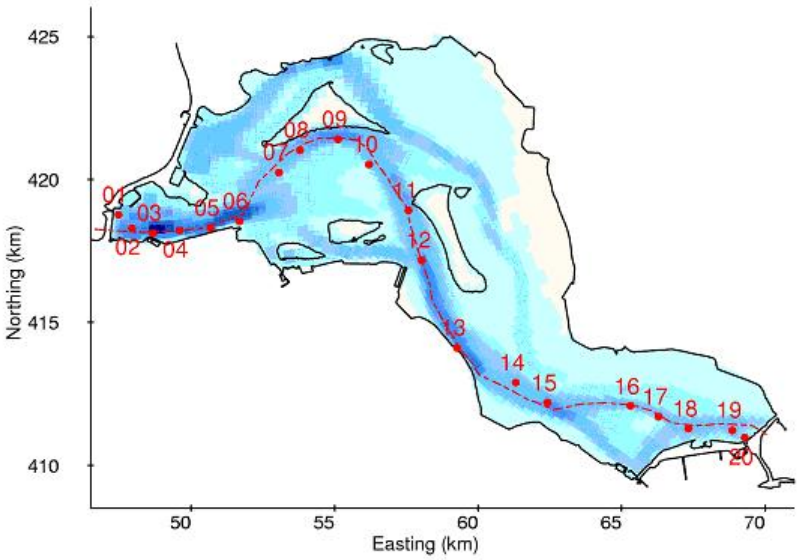

Figure 3.4.3.1: Overview of the Lake Grevelingen measurement locations (red dots); cross-sections will be plotted along the red, dashed line.

Model description

Lake Grevelingen is a closed water system. This implies that the water level is determined by the differences between the incoming and outgoing discharges. The main discharges included in the model are caused by flow through the Brouwerssluis, by precipitation, by evaporation and by river run-off. The computational grid has about 4200 active cells in the horizontal plane, with cell sizes varying between 250 m and 400 m. In the vertical, the Z-model schematisation is used with a maximum of 28 layers at

the deepest locations. The layer thickness varies from 2.5 m at the surface to 5.0 m near the bottom at the deepest locations. The bathymetry of Lake Grevelingen can be described as a system of gullies with a few deep pits (up to about 45 m), surrounded by a shallow area.

Uniform wind forcing with daily varying magnitudes and directions are applied at the surface. For computing the heat flux through the surface, the so-called Ocean Heat Flux model is applied, using daily uniform values for air temperature, relative humidity and cloud cover. A Secchi depth of 2.0 m is used, whereas the Stanton and Dalton number for the convective and evaporative heat flux are set at 3.0×10^{-3} and 1.8×10^{-3}, respectively. In the vertical the $k-\epsilon$ turbulence closure model is used with a background value for both the eddy viscosity and diffusivity of 5.0×10^{-6} m^2/s. For the horizontal a constant eddy viscosity and diffusivity of 0.5 m^2/s is applied. The computation is started with a uniform salinity of 27 ppt and a uniform temperature of 5 °C. The year 1999 is used for spin-up. Given the basin averaged residence time of about 2 months this is certainly long enough. With the applied time step of 2 minutes computing one year takes about 28 hours on a 3.6 MHz single CPU.

Results

The computational results are compared with the measurements in various ways. In Figure 3.4.3.2 and 3.4.3.3 time series of salinity and temperature are compared to measured values at both 1 m and 15 m. In Figure 3.4.3.4 the salinity and temperature results are presented in z,t-diagrams, whereas in Figure 3.4.3.6 contour plots at both 1 m and 15 m depth are shown. In Figure 3.4.3.7 cross sectional contour plots along Lake Grevelingen are compared with measurements.

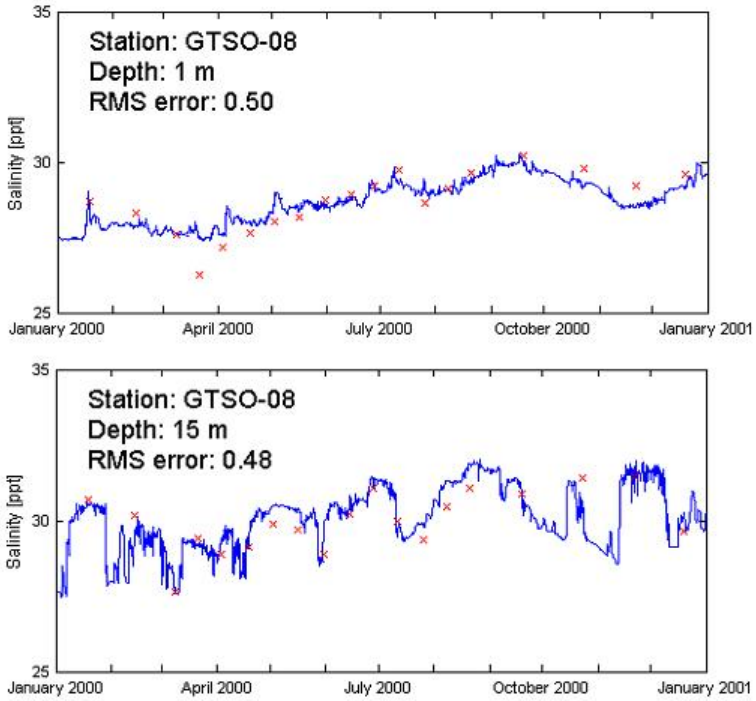

Figure 3.4.3.2: Time series of salinity (blue line) at 1 m (upper plot) and 15 m depth (lower plot) compared to measurements (red dots) at Station GTSO-08.

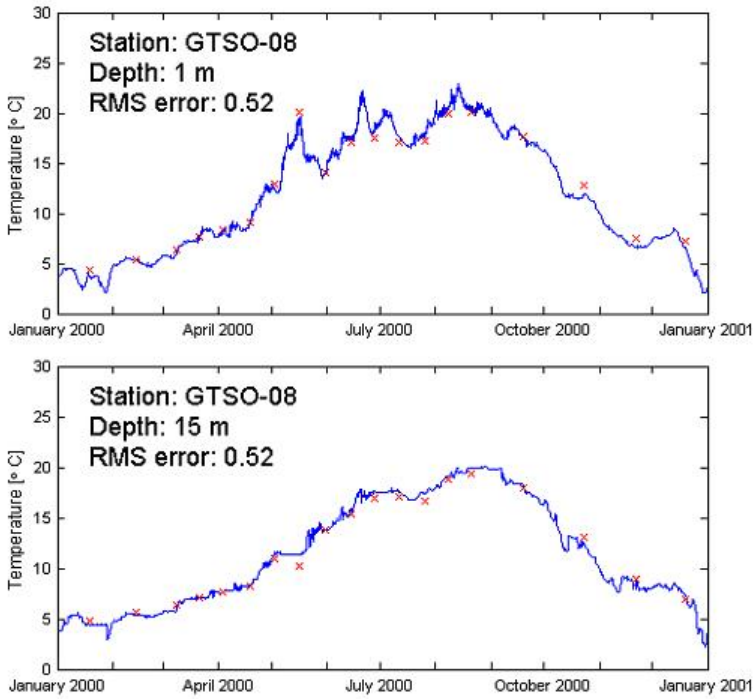

Figure 3.4.3.3: Time series of temperature (blue line) at 1 m (upper plot) and 15 m depth (lower plot) compared to measurements (red dots) at Station GTSO-08.

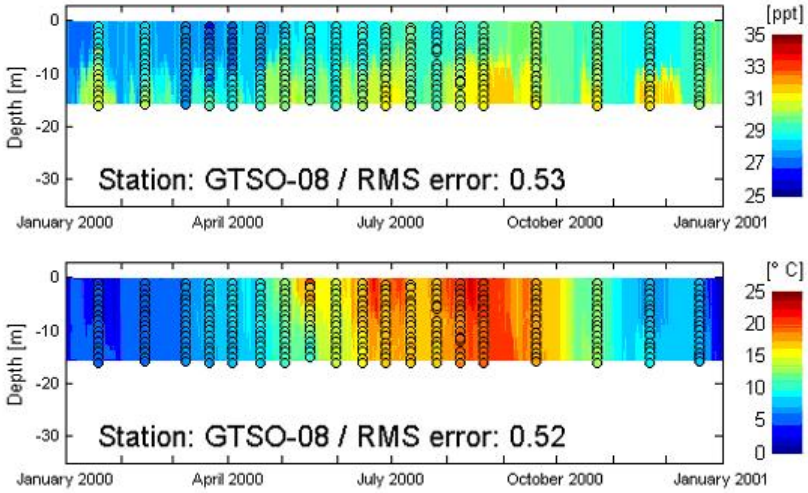

Figure 3.4.3.4: Z,t-diagrams of salinity (upper plot) and temperature (lower plot) for Station GTSO-08. The coloured dots represent measured values.

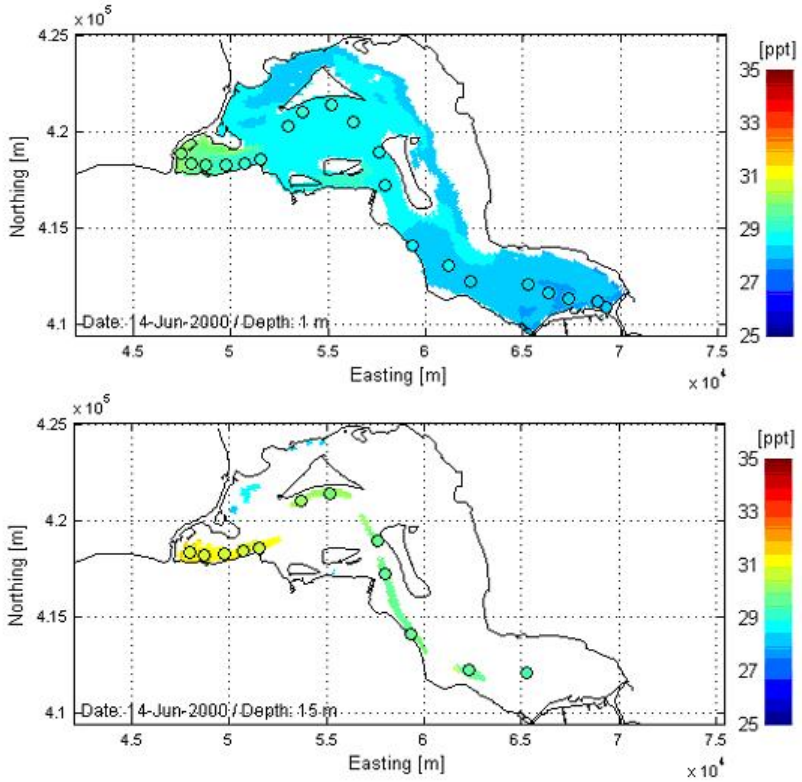

Figure 3.4.3.5: Salinity contour plots at 1 m (upper plot) and 15 m depth (lower plot) compared to measurements (coloured dots) at 14 June.

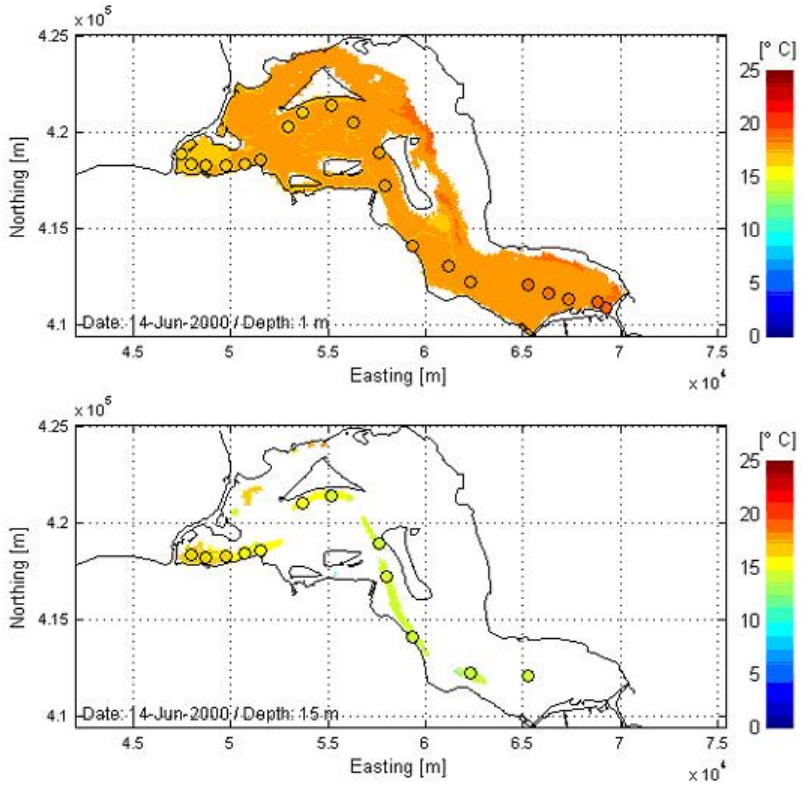

Figure 3.4.3.6: Temperature contour plots at 1 m (upper plot) and 15 m depth (lower plot) compared to measurements (coloured dots) at 14 June.

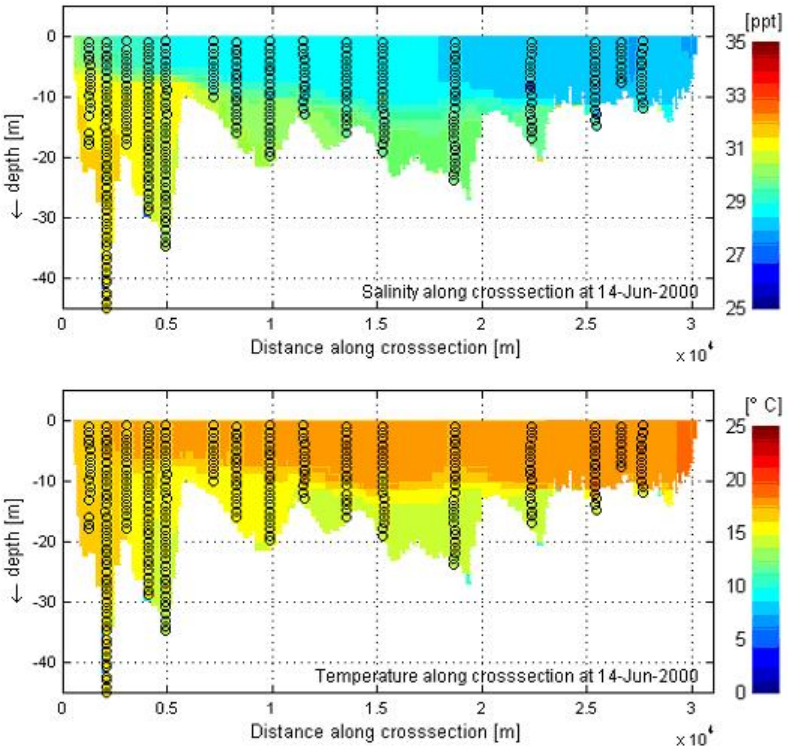

Figure 3.4.3.7: Salinity (upper plot) and temperature (lower plot) along a cross-section through Lake Grevelingen. The coloured dots represent measurements.

Conclusions

Figure 3.4.3 shows that there is a very good agreement between the computed temperature time series and the corresponding measurements. This holds both for the surface and the bottom layer, which implies that the temperature stratification in Lake Grevelingen, and especially the seasonal variation thereof, is modelled accurately. As the time series shown here represent only one location, the station averaged RMS temperature errors are computed at 1 m and 15 m. These average RMS errors are 0.61 °C and 0.53 °C, respectively. Compared to a seasonal variation in temperature of about 20 °C at the water surface, this is a very good result. Therefore, it can be concluded that Delft3D-FLOW can be used to accurately predict thermal stratification in lakes (Claim 2.2.1.10). Furthermore, it can be concluded that the heat exchange through the surface can be computed using Delft3D-FLOW, yielding very good results with respect to seasonal variations in thermal stratification (Claim 2.2.2.15). For salinity the agreement of computed time series with measurements is also good (cf. Figure 3.4.3.2). The station averaged RMS errors are 0.55 ppt and 0.60 ppt at 1 m and 15 m respectively, which means a good agreement with measurements is obtained. This, together with the very good results in terms of temperature, shows that Delft3D-FLOW is capable of accurately simulating baroclinic (density driven) flows (Claim 2.2.2.2 and Claim 2.2.1.2).

The same claims also hold when looking at the results in the z,t-diagrams (cf. Figure 3.4). In particular, this is the for the accurate reproduction of the measured pycnocline depths and the variations therein. The station averaged RMS errors for the results in the z,t-diagrams are 0.61 ppt and 0.74 °C for salinity and temperature, respectively. Compared to the variations both in time and in the vertical, these are very good results. The contour plots at 1 m and 15 m depth (cf. Figure 3.4.3.5 and 3.4.3.6) show a good agreement with measured salinity and temperature data in a spatial way. Both in the upper and the lower layer the horizontal distribution of temperature and salinity is reproduced well. This supports Claims 2.2.1.2 and 2.2.2.2. The accurate prediction of thermal stratification using Delft3D-FLOW (Claim 2.2.1.10) is shown in Figure 3.4.3.7, in which computed results are presented in terms of cross-sectional contour plots.

3.4.4 Sea of Marmara

This page last changed on 25-08-2008 by platzek.

Purpose

The purpose of validation study is to show that Delft3D-FLOW is able to reproduce both thermal and salinity stratification in terms of its duration as well as the depth of the pycnocline. The stratification is caused by heat exchange through the surface as well as by baroclinic pressure gradients caused by a permanent density difference between the Black Sea and the Aegean Sea.

Linked claims

Claim 2.2.1.2: Density driven flow and salinity intrusion.
Claim 2.2.1.3: Wind driven flow and storm surges.
Claim 2.2.1.10: Thermal stratification in seas, lakes and reservoirs.
Claim 2.2.2.2: Baroclinic flow - salinity and temperature driven flow.
Claim 2.2.2.12: Impact of space and time varying wind shear stress at the water surface.
Claim 2.2.2.14: Impact of space and time varying atmospheric pressure on the water surface.
Claim 2.2.2.15: Heat exchange through the free surface, evaporation and precipitation.
Claim 2.4.2: Computational grid.
Claim 2.5.4: Computationally efficient.

Approach

The Sea of Marmara is a permanently stratified water body. Differences in salinity in the two large adjacent basins, with the lower salinity in the Black Sea and higher salinity in the Northern Aegean, result in an overall upper layer of lower salinity flowing from Black Sea through the Sea of Marmara to the Northern Aegean, and a lower layer return flow of higher salinity. This basic density driven circulation varies under the influence of seasonally varying fresh water river discharges of major rivers on the Black Sea, precipitation and evaporation. The waters are also thermally stratified. The variation in temperature stratification is mainly determined by the seasonal variation in the surface heat flux. Varying winds and pressure variations further affect the hydrodynamic situation.

The 3D Sea of Marmara Model is validated against data for the year 2003, using 2002 as a spin-up year. We use extensive salinity and temperature profile measurements from the regular monthly ISKI monitoring campaign. These data are available at 19 different stations in the Bosporus and its Black Sea and Sea of Marmara approaches. The validation involves horizontal and vertical spatial temperature and salinity distribution as well as the variation of salinity and temperature over the year. Furthermore, hourly water level series for 2003 are available for stations representative of the northern and southern approaches of the Bosporus. The water level response due to wind and pressure forcing is validated against these data. Apart from comparison with measurements, validation will be based on the representation of observed characteristic features and natural phenomena such as the existence in the Sea of Marmara of a Cold Intermediate Layer (CIL) during summer, the occurrence of inverse stratification (where the upper layer is colder than the lower layer) and a seasonally changing pycnocline depth.

Model description

The area of interest for the model is the Sea of Marmara and the two straits (Bosporus and Dardanelles) connecting it to adjacent water bodies (Black Sea and Aegean Sea). For reasons of consistency (of forcing), flexibility and simplicity, both the Black Sea and the northern Aegean Sea are included in the model as well. A 3D Z-model is applied with about 10,000 grid cells in the horizontal and a maximum of 30 layers in the vertical direction. Horizontal grid sizes vary from about 250 m in the Bosporus to about 25 km in the northern and eastern part of the Black Sea to match local spatial scales, whereas the vertical resolution varies between 2.5 m at the surface to about 450 m in the deepest part of the Black Sea. The model consists of three domains (grids) and are online coupled by means of domain decomposition.

The model has one open boundary, running across the Aegean Sea. A relatively weak tidal water level elevation is imposed here. More important is the wind and pressure surface forcing, provided on a 0.5° by 0.5° data grid in a space and time varying (6 hourly) manner. The same holds for the input parameters of the heat flux model (Ocean Heat Flux Model). This model uses relative humidity, cloud cover, air

temperature, wind and pressure as well as the latitude of each grid cell to compute the net heat flux through the water surface.

For vertical turbulence closure the $k-\epsilon$ turbulence model is used without background eddy viscosity and diffusivity. The horizontal viscosity and diffusivity is constant and varies spatially between 10 m^2/s and 50 m^2/s. With an applied time step of 2.5 minutes, a simulation of one year takes about two weeks on a single CPU (3.6 GHz).

Results

The computational results of the 3D Sea of Marmara model are compared with the available measurements. water levels, fluxes through cross sections, salinity and temperature (both in horizontal and vertical direction) are considered. In Figures 3.4.4.1 and 3.4.4.2, time series of measured water level elevation are compared to the model results. In Figures 3.4.4.3 and 3.4.4.4, the computed fluxes through the upper and lower layer of the Bosporus are presented for different seasons, whereas in Figure 3.4.4.5 time series of temperature are compared to measured values at both 1 m and 40 m (representing the upper and lower layer). In Figures 3.4.4.6 and 3.4.4.7, salinity and temperature results are presented in z,t-diagrams for two different locations. The last type of presentation is in the form of cross sectional contour plots. In Figures 3.4.4.8 and 3.4.4.9 this is done for two different times, showing a cross section along the Dardanelles, the Sea of Marmara, the Bosporus and a small part of the Black Sea, whereas Figure 3.4.4.10 has been zoomed in on the Bosporus only in order to make comparison with measured values easier.

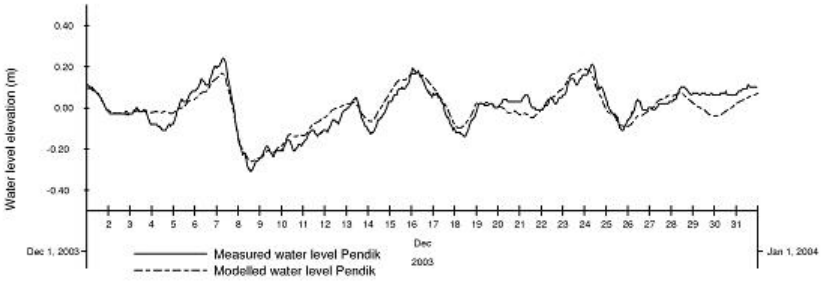

Figure 3.4.4.1: Computed (dashed line) and measured (solid line) water level elevation in Pendik (near southern Bosporus entrance) for December 2003.

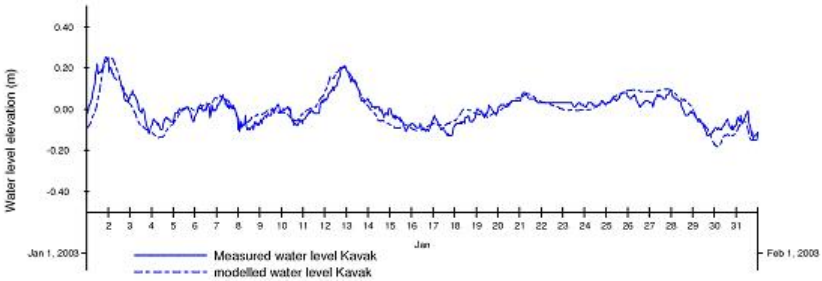

Figure 3.4.4.2: Computed (dashed line) and measured (solid line) water level elevation in Kavak (near northern Bosporus entrance) for January 2003.

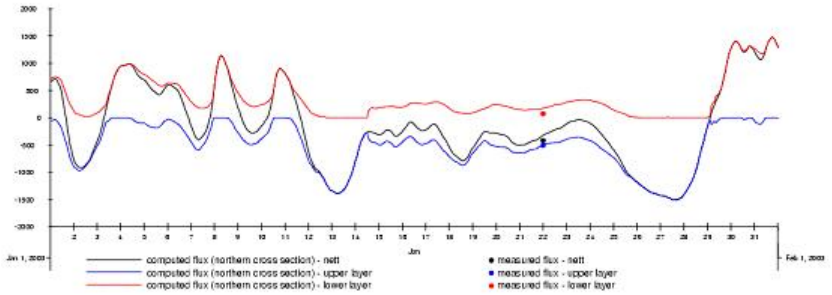

Figure 3.4.4.3: Modelled upper (blue), lower (red) and net (black) flux variation through northern cross-section in the Bosporus for January 2003. The coloured dots represent fluxes derived from ADCP measurements (units are in km^3/yr).

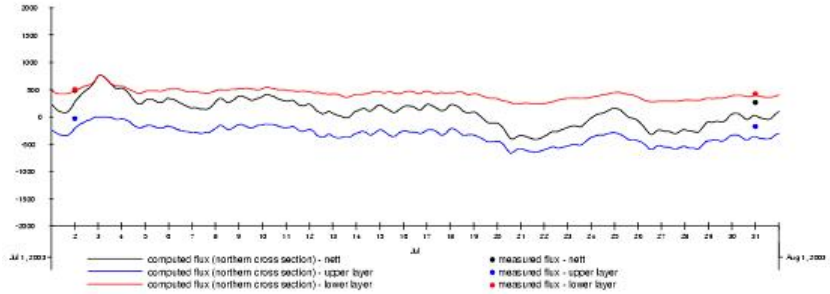

Figure 3.4.4.4: Modelled upper (blue), lower (red) and net (black) flux variation through northern cross-section in the Bosporus for July 2003. The coloured dots represent fluxes derived from ADCP measurements (units are in km^3/yr).

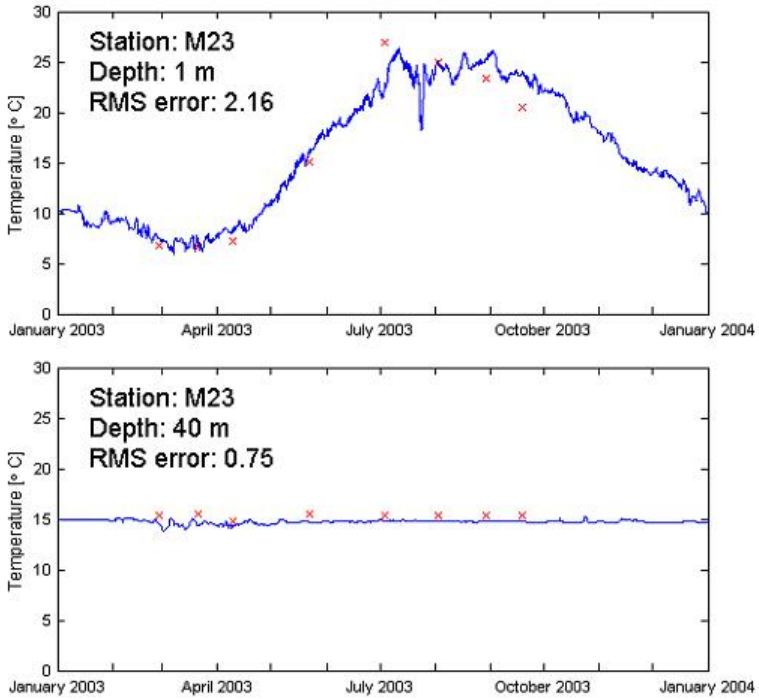

Figure 3.4.4.5: Time series of temperature (blue line) at 1 m (upper plot) and 40 m depth (lower plot) compared to measurements (red dots) at Station M23 in the north east of the Sea of Marmara.

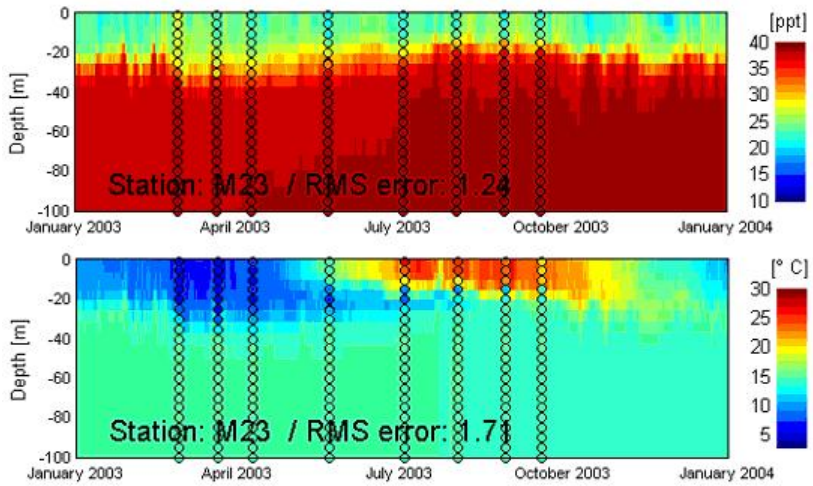

Figure 3.4.4.6: Z,t-diagrams of salinity (upper plot) and temperature (lower plot) for Station M23 in the north east of the Sea of Marmara. The coloured dots represent measured values.

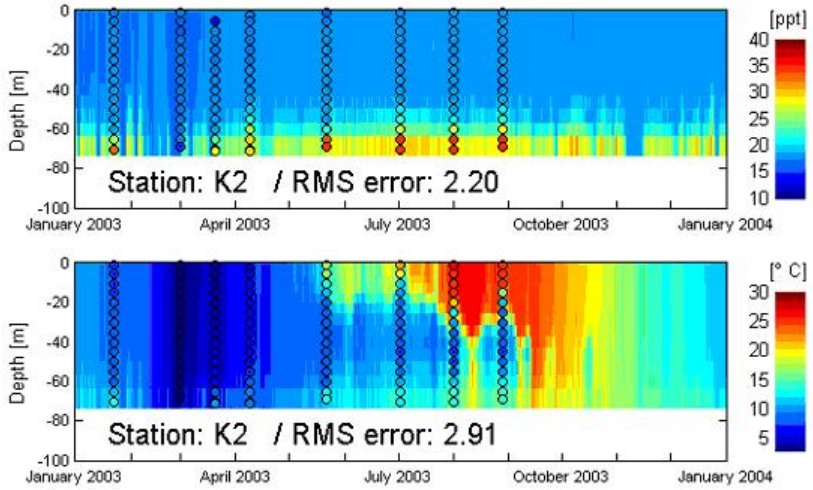

Figure 3.4.4.7: Z,t-diagrams of salinity (upper plot) and temperature (lower plot) for Station K2 in the south west of the Black Sea. The coloured dots represent measured values.

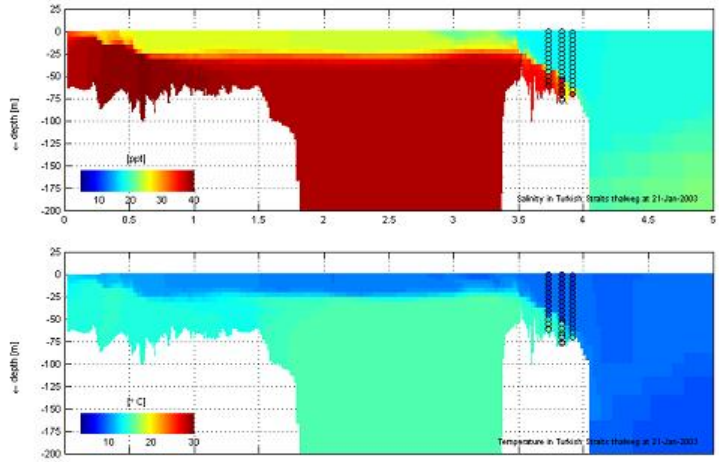

Figure 3.4.4.8: Salinity (upper plot) and temperature (lower plot) along a cross section through the Dardanelles, the Sea of Marmara, the Bosporus and the south east of the Black Sea for January 21, 2003. The coloured dots represent measurements.

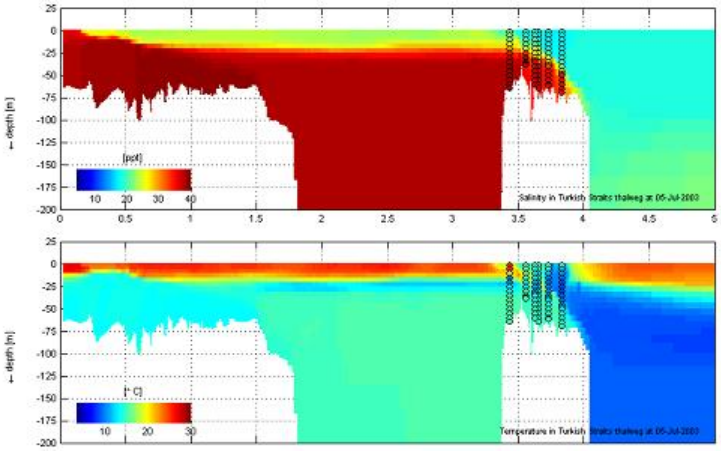

Figure 3.4.4.9: Salinity (upper plot) and temperature (lower plot) along a cross section through the Dardanelles, the Sea of Marmara, the Bosporus and the south east of the Black Sea for July 5, 2003. The coloured dots represent measurements.

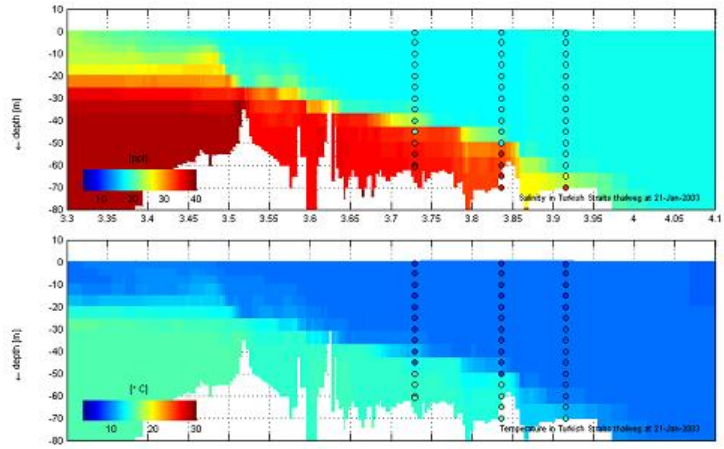

Figure 3.4.4.10: Salinity (upper plot) and temperature (lower plot) along a cross section through the Bosporus for January 21, 2003. The coloured dots represent measurements.

Conclusions

A first indicator of the model representation is the verification of the barotropic response to space- and time-varying wind. The water level variation in station Kavak in the northern part of the Bosporus, which is mainly determined by wind in the Black Sea, is well represented in Figure 3.4.2. The modelled water levels at Pendik, near the southern entrance of the Bosporus, depend much more on the representation of the exchange flows through the Bosporus and the water level variation at the open boundary due to inverse barometer effects. The results presented in Figure 3.4.1, show a good reproduction of these water level variations. These results show that Delft3D-FLOW is clearly capable of modelling the impact of space and time varying wind shear stress and atmospheric pressure at the water surface (Claims 2.2.2.12 and 2.2.2.14).

The variation in time of the modelled upper and lower layer fluxes through the Bosporus are presented in Figures 3.4.3 and 3.4.4 for January 2003 and July 2003, respectively. These fluxes and variations thereof are induced by variations in water level at both entrances of the Bosporus (barotropic effects) as well as by a permanent density difference between the two adjacent water bodies for which it forms a connection (baroclinic effects). The results show that both the upper layer and lower layer fluxes show a larger variability in January compared to July. This was to be expected given the fact that wind speeds are generally higher during winter as this is the storm season. From measurements it is known that blocking events occur in the Bosporus, where one of the layers ceases to exist. These blocking events are represented in the model. This can be seen in the plots when one of the coloured lines coincides with the black line representing the net flux, with the other line being at zero level. For January, the model simulates seven blocking events (five events of blocking of the upper layer and two events of the lower layer). In July one blocking event (of the upper layer) occurs. Again, the seasonally varying frequency of blocking shown by the model is to be expected, due to seasonal variations in wind climate. Furthermore,

the results show good agreement with the ADCP derived upper and lower fluxes of the January and July measurements, indicated by dots. From all this, it can be concluded that Delft3D-FLOW is capable of reproducing wind and density driven (baroclinic) flow (Claims 2.2.1.3, 2.2.1.2 and 2.2.2.2).

Figure 3.4.5 presents the simulated temperature annual cycle against measurement data in Station 23 at a depth of 1 m (upper layer) and 40 m (lower layer). The winter results are very good, as is the surface temperature increase in spring and early summer. Only, the modelled cooling of the surface layer lags behind the measured cooling. As in the measurements, the lower layer has a more or less constant temperature over the year. Comparing the modelled temperatures in the upper and lower layer shows that in winter, the upper layer is colder than the lower layer (inverse temperature stratification). Only due to strong salinity stratification does this yields a stable temperature profile. This inverse stratification is a known natural phenomenon in the Sea of Marmara. These results confirm that Delft3D-FLOW is capable of correctly modelling heat exchange through the free surface as well as the resulting thermal stratification (Claims 2.2.1.10 and 2.2.2.15).

In Figure 3.4.6, results in station M23, located in the Sea of Marmara near the southern entrance of the Bosporus, are presented as z,t-plots. The modelled results presented in this figure show very good agreement with observations, in terms of both the values of upper and lower layer salinities and temperatures. Apart from a good agreement with measurements, known natural phenomena like the forming of the Cold Intermediate Layer during summer, the inverse temperature stratification during spring and the seasonal vertical variation of the halocline are also represented correctly in the model. To give an idea of the extent of the spatial variation in vertical temperature and salinity distributions, the z,t-plot of measurement location K2, located in the Black Sea, near the northern entrance of the Bosporus, is shown in Figure 3.4.7. The model results at K2 accurately capture the blocking event which occurs around February/March 2003. In general, the lower layer salinity near the bed in Stations K2 is somewhat too low, however. Also here, a Cold Intermediate Layer exists in both the model results and the measurements. These results further corroborate the Claim that Delft3D-FLOW is capable of reproducing thermal stratification and density driven flow (Claims 2.2.1.10 and 2.2.1.2), as well as the heat exchange through the free surface (Claim 2.2.2.15).

The vertical cross section in Figure 3.4.8 shows again the inverse temperature stratification in January, whereas in Figure 3.4.9 the modelled Cold Intermediate Layer is clearly visible in July. Figure 3.4.10 is a zoom-in at the Bosporus in January. In this figure the good agreement between modelled and measured temperature and salinity profiles along the Bosporus is clearly shown. This holds for both the agreement with measurements and for the reproduction of the inverse temperature stratification representing the Cold Intermediate Layer (Claims 2.2.1.10 and 2.2.1.2).

3.4.5 South China Sea

This page last changed on 25-08-2008 by platzek.

Purpose

This validation study involves the modelling of the seasonal, basin-scale temperature cycle of the South China Sea, including large-scale baroclinic flow, heat exchange through the free surface, lateral exchange with external systems and thermal stratification. This is examined by using a non-tidal model.

Linked claims

Claim 2.2.1.10: Thermal stratification in seas, lakes and reservoirs.
Claim 2.2.2.2: Delft3D-FLOW can accurately simulate density driven (or baroclinic) flows.
Claim 2.2.2.15: Heat exchange through the free surface, evaporation and precipitation.
Claim 2.2.2.18: External lateral forcing.
Claim 2.4.2: Computational grid.
Claim 2.5.4: Computationally efficient.

Approach

Model simulations for a climatological year are performed using a non-tidal three-dimensional baroclinic model representing the South China Sea and Indonesian Archipelago. Focus is on the large-scale, seasonal temperature cycle due to the availability of synoptic forcing and validation data at this scale. The model applies a reduced depth approach, in which the depth is truncated at 300 meters depth, which is below the maximum annual thermocline depth. This reduced depth approach is justified because the energy exchange to deeper levels is assumed to be negligible, see [Qu, 2001].

The model has 20 equidistant σ layers in the vertical and includes both temperature and salinity as transport parameters. Heat exchange at the free surface is determined by the Ocean heat flux model based on space and time varying atmospheric state input. Exchange with external systems like the Pacific Ocean is achieved by lateral temperature and salinity forcing and by water level forcing at the open model boundaries [Twigt et al., 2006].

Model description

- 124 by 133 horizontal grid points, equidistant with a spacing of 1/4° [Gerritsen et al. 2003].
- Reduced depth, truncated at 300 meters with 20 equidistant σ layers.
- Water level boundaries driven by altimetric sea surface anomalies [Gerritsen et al. 2004].
- Space and time varying lateral temperature and salinity open boundary forcing.
- Space and time varying wind and atmospheric pressure forcing.
- Space and time varying heat flux forcing (relative humidity, air temperature, cloudiness).
- $k-\epsilon$ turbulence model.
- Time step of 2 hours.

Results

The heat flux model coefficients and model forcing applied are optimized based on a series of sensitivity analysis as described in [Twigt et al. 2006]. Figure 3.4.5.1 shows the models surface layer temperature during the Northeast (NE, January) and Southwest (SW, August) monsoon highs. Model results are compared with climatological, monthly-mean sea surface temperature data obtained from AVHRR remote sensing satellites [Vazquez 2004]. Figure 3.4.5.2 shows model temperature profiles compared with profile data from the World Ocean Atlas 2001 [Levitus 1982] at two stations.

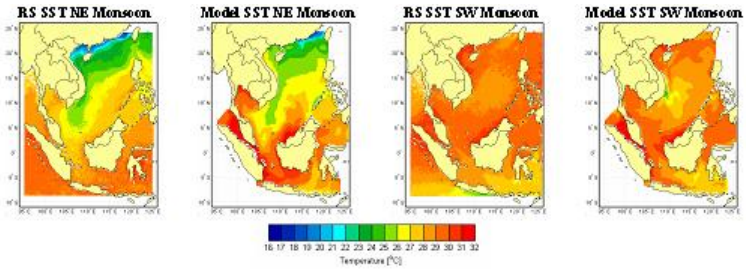

Figure 3.4.5.1: Surface layer temperature during the Northeast (NE, January) and Southwest (SW, August) monsoon highs. Model results compared with monthly-mean, climatological Remotely Sensed Sea Surface Temperature (RS SST) data obtained from [Vazquez 2004].

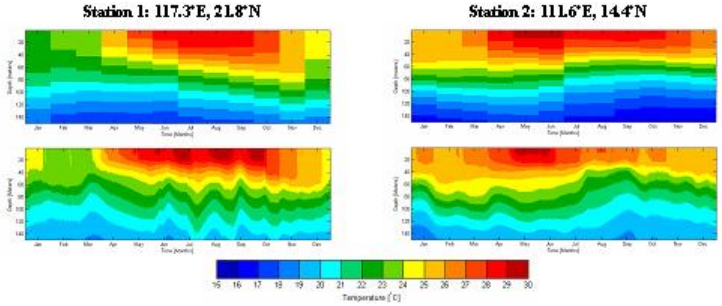

Figure 3.4.5.2: Profile data at selected model stations. Model results (lower panel) compared with monthly-mean, climatological profile data from the World Ocean Atlas 2001 (upper panel) [Levitus 1982].

Conclusions

From the model results in Figure 3.4.5.1, we conclude that the characteristic large-scale surface layer temperature features as observed from the remotely sensed validation data are resolved by the model to a reasonable degree. These features include large-scale cold water intrusions through the open model boundaries, wind driven mixing and baroclinic transport during the NE monsoon. During the SW monsoon a strong increase in net surface heat flux amounts to higher and more uniform surface layer temperatures. The results imply that the model resolves the large-scale baroclinic flow, external lateral forcing and heat exchange through the free surface to a good degree. Model discrepancies, like higher surface layer temperatures in the Southern South China Sea during the NE monsoon period, are attributed mainly to the quality of the model forcing data [Twigt et al., 2006].

From model results in Figure 3.4.5.2 it is concluded that the model captures the characteristic cycle of seasonal stratification to a good degree. This cycle varies for the different regions of the South China Sea as a result of different forcing processes involved. Station 1 shows results for a station situated in the Northern South China Sea, near Luzon Strait and Taiwan Strait. The sudden breakdown of the thermocline around November as observed at this station is explained by cold water influx through the open model boundaries and large-scale (horizontal) transport of this colder water by baroclinic flow. The model resolves this to a good degree, implying that both lateral exchange through the open boundaries and baroclinic transport are resolved. Station 2 shows model results in the central South China Sea, where the surface heat flux is the main driver in the seasonal stratification cycle. The model captures this cycle to a good degree, implying that the heat exchange at the free surface is resolved. Results at Stations 1 and 2 indicate that the model resolves the seasonal thermal stratification to a good degree.

This validation study clearly demonstrates the ability of Delft3D-FLOW to model baroclinic circulation and thermal stratification in a deep-water region like the South China Sea. To achieve this, free surface heat flux forcing and external lateral forcing play an essential role. Both features are resolved to a good degree by the model.

4 References

Abbott, M.B., 1997: Range of tidal flow modelling. Special Issue of J. Hydr. Eng., April 1997, ASCE.

Balzano, A., 1998: Evaluation of methods for numerical simulation of wetting and drying in shallow water models. Coastal Engineering, Vol. 34, 83-107.

Batchelor, G., 1967: An Introduction to Fluid Dynamics. Cambridge University Press, London.

Beji, S. and Battjes, J.A., 1994: Numerical Simulation of Nonlinear Waves Propagation Over a Bank. Coastal Engineering, 23:1-16. 3.2.1.

Bendat, J.S. and A.G. Piersol, 1971: Random data: analysis and measurement procedures. John Wiley-& Sons, Inc. New York.

Bijvelds, M.D.J.P., 2003: A non-hydrostatic module for Delft3D-FLOW; technical documentation, verification and practical aspects. Internal documentation for CDW project.

Bijvelds, M.D.J.P. and A.J. Nolte, 2000: 3D modelling of Lake Veere. Delft Hydraulics report Z2800 (for RIKZ, in Dutch)

Bijlsma, A.C., 1988: Generation and dissipation of storm surges in the North Sea, with application to the major storm surges of 1953 and 1983. Delft Hydraulics Report Z96-01.

Bijlsma, A.C., S.A.H. van Schijndel and H.R.A. Jagers, 2003: Computations with Delft3D, in combination with HLES. Shallow Flows Symposium 2003, Vol III, 213-219.

Bijlsma, A.C., R.E. Uittenbogaard and T. Blokland, 2003: Horizontal large eddy simulation applied to stratified flows. Proc. Shallow Flows. Delft, 16-18 June, Balkema, Rotterdam.

Bijlsma, A.C., 2007. Numeriek modelonderzoek naar de reductie van de neer in de monding van de voorhaven van IJmuiden. Delft Hydraulics Report H4926.Bundesanstalt für Wasserbau, 2002: Mathematical Model UnTRIM. Validation Document Version 0.3, 61 pp. (see http://www.hamburg.baw.de/hnm/untrim/hnm_untrim-en.htm).

Dee, D., 1993: A framework for the validation of generic computational models. Delft Hydraulics Report X109.

De Goede, E.D., J.N. Roozekrans, J.M. de Kok and R.J. Vos, 2000: REST3D – Remote Sensing sea surface temperature for 3D North Sea modelling, Netherlands Remote Sensing Board Report NRSP-2-00-16, BCRS, Delft.

De Goede, E.D. and B. van Maren, 2005: Impacts of Maasvlakte 2 on the Wadden Sea and North Sea coastal zone. Track 1: Detailed modelling research. Part I: Hydrodynamic modelling. WL | Delft Hydraulics report Z3945.20. Royal Haskoning report 9R2847.A0.

De Kok, J. M., C. de Valk, J.A.Th.M. van Kester, E.D. de Goede and R.E. Uitenbogaard, 2001: Salinity and temperature stratification in the Rhine plume. Estuarine, Coastal and Shelf Science, Vol. 53, 467-475.

Eckart, C., 1958: Properties of water, Part II. The equation of state of water and sea water at low temperatures and pressures. American Journal of Science, Vol. 256, pp. 225-240.

EDF-DER, 2000: TELEMAC-2D Validation document version 5.0., Electicité de France, 124 pp.

Forester, C.K., 1979: Higher Order Monotonic Convective Difference Schemes. Journal of Computational Physics, Vol. 23, pp. 1-22.

Genseberger, M. and J.A.Th.M. van Kester, 2002: Delft3D-FLOW test cases for Z model. WL | Delft Hydraulics Research Report M3421,.

Gerritsen, H. and A.C. Bijlsma, 1988: Modelling of tidal and wind-driven flow; the Dutch Continental Shelf Model. In: B.A. Schrefler, ed. Proc. Int. Conf. on Computer Modelling in Ocean Engineering, pp. 331-338, A.A. Balkema, Rotterdam.

Gerritsen, H. and G.K. Verboom, 1994: The Coastal Modelling System. pp. 118-128 in: M.B. Abbott, ed. J. of Hydraulic Research, 1994, Vol. 32.

Gerritsen, H., J.W. de Vries and M.E. Philippart, 1995: The Dutch Continental Shelf Model, in: D.R.Lynch and A.M.Davies, eds. AGU Coastal and Estuarine Studies, Volume 47, pp. 425-467.

Gerritsen, H., R.J. Vos, Th. van der Kaaij, A. Lane and J.G. Boon, 2000: Suspended sediment modelling in a shelf sea (North Sea), Coastal Engineering Vol. 41,1-3, 317-352.

Gerritsen, H., E.J.O. Schrama and H.F.P. van den Boogaard, 2003: Tidal model validation of the seas of South East Asia using altimeter data and adjoint modelling. Proc. XXX IAHR Congress, Thessaloniki, 24-28 August 2003, Vol. D, 239-246.

Gresho, P.M. and R.L. Lee, 1979: Don't suppress the wiggles, they're telling you something. Finite Element Methods in Convection Dominated Flows (Ed. T.J.R. Hughes), ASME Winter Annual Meeting.

Hesselink, A. W., G.S. Stelling, J.C.J. Kwadijk and H. Middelkoop, 2003: Inundation of a Dutch river polder, sensitivity analysis of a physically based inundation model using historic data. Water Resources Research, Vol. 39, No. 9.

Holthuisen, L.H., R.C. Ris and N. Booij, 1998. A verification of the third-generation wave model SWAN, 5th International Conference on Wave Hindcasting and Forecasting, Melbourne, Florida, 223-230.

Hulsen, L.J.M., 1989: Region Model: TRISULA-2DH hydrodynamic model WL | Delft Hydraulics report Z358.

IAHR, 1994: Guidelines for Documenting the Validity of Computational Modelling Software. International Association for Hydraulic Research, P.O. Box 177, 2600 MH Delft, The Netherlands.

Karelse, M., 1996: Validation of Delft3D-FLOW with tidal flume measurements. WL | Delft Hydraulics report Z810.

Karelse, M. and L.J.M. Hulsen, 1995: Pembroke Power station, marine discharge study, Milford Haven-phase 11, 3D hydrodynamic and water quality model. WL | Delft Hydraulics report Z755.

Kernkamp, H.W.J. and R.E. Uittenbogaard, 2001: 2D-LES of a free-surface mixing layer. In B.J. Geurts, R. Friedrich & O. Metais (ed.) Direct and Large-Eddy simulation Workshop, Kluwer Academic Publishers, pp. 409-418.

Kernkamp, H.W.J., H. Gerritsen and L.J.M. Hulsen, 2004: A spherical curvilinear approach in coastal ocean modeling – typhoon driven storm surges in the South China Sea. Proceedings 6th International Conference on Hydrodynamics, Singapore 2004, Vol.1, pp. 586-593.

Kernkamp, H.W.J., H.A.H. Petit, H. Gerritsen and E.D. de Goede, 2005: A unified formulation for the three-dimensional shallow water equations using orthogonal co-ordinates: theory and application. Ocean Dynamics. Vol. 55. pp. 351-369.

Kolmogorov, A.N., 1942: Equations of turbulent motion in incompressible fluid, Izv. Akad. Nauk. SSR, Seria fizicheska Vi., No.1-2, pp. 56-58 (English translation: 1968 Imperial College, Mech. Eng. Dept. Rept. ON/6).

Leendertse, J.J., 1990: Turbulence modelling of surface water flow and transport: part IVa. J. Hydr. Eng., Vol. 114, No. 4, 603-606.

Leer, van, B., 1974: Towards the ultimate conservative difference scheme II. Monotonicity and conservation combined in a second-order scheme. J. Comput. Phys., Vol. 32, 101-136.

Lesser, G., J. van Kester and J.A. Roelvink, 2000. On-line sediment transport within Delft3D-FLOW, Report Z2899, WL | Delft Hydraulics.

Lesser, G., J.A. Roelvink, J. van Kester and G.S. Stelling, 2004. Development and validation of a three-dimensional morphological model. Coastal Engineering, Vol. 51, 883–915.

Malvern, L.E. 1969: Introduction to the Mechanics of a Continuous Medium. Prentice-Hall, Englewood Cliffs, N. J.

Mellor, G.L. and A.F. Blumberg, 1985: Modelling vertical and horizontal diffusities and the sigma coordinate system, Monthly Weather Review, Vol. 113, 1379-1383.

Murphy, A.H. and E.S. Epstein, 1989: Skill scores and correlation coefficients in model verification. Monthly Weather Review, Vol. 117, pp. 572–581.

Pedlosky, J., 1979: Geophysical Fluid Dynamics. Springer Verlag, New York.

Phillips, N.A., 1957: A coordinate system having some special advantages for numerical forecasting, J. of Meteorology, vol. 14.

Postma, L., G.S. Stelling and J. Boon, 1999: Three-dimensional water quality and hydrodynamic modelling in Hong Kong. Stratification and water quality. Proceedings of the 2nd Int. Symp. on Environmental Hydraulics, Hong Kong, Balkema, Rotterdam. December 1998, 43-49.

Prandtl, L., 1945: Über ein neues Formelsystem für die ausgebildete Turbulenz, Nachr. Akad. Wiss., Göttingen, Math.-Phys. Klasse, p. 6.

Ruessink, G. and J.A. Roelvink, 2000. Validation of On-line Mud Transport within Delft3D-FLOW. Report, WL | Delft Hydraulics.

Richardson, J.F. and W.N. Zaki, 1954: Sedimentation and fluidization: part I. Transactions of the Institute of Civil Engineers, Vol. 32, pp. 35-53.

Ris, R.C., 1997. Spectral Modelling of Wind Waves in Coastal Areas. Ph.D. Dissertation Delft University of Technology), also Communications on Hydraulic and Geotechnical Engineering, report No. 97-4, Delft, the Netherlands

Roelvink, J.A., R.E. Uittenbogaard and G.A. Liek, 1999: Morphological modelling of the impact of coastal structures. Proceedings Coastal Structures '99, Vol.2, pp. 865-871.

Roelvink, J.A., T. van der Kaaij and B.G. Ruessink, 2001: Calibration and verification of large-scale 2D/3D flow models. Phase 1, Parcel 2, Subproduct 2, ONL Flyland project.

Rodi, W., 1984: Turbulence models and their application in Hydraulics, State-of-the-art paper article sur l'etat de connaissance. Paper presented by the IAHR-Section on Fundamentals of Division II: Experimental and Mathematical Fluid Dynamics, The Netherlands.

Schrama, E.J.O., 2002: Availability and quality of global tide models, Delft Hydraulics, report Z3341.

Smits, J., 2000: Modelling framework for water quality management in Lake Victoria (LVMF), rapid assessment for phase 2 of the development of LVMF, Delft Hydraulics, report Q2652.

Stelling, G.S., 1984: On the construction of computational methods for shallow water flow problems. Rijkswaterstaat communications, No. 35, The Hague, Rijkswaterstaat.

Stelling, G.S., A.K. Wiersma, J.B.T.M. Willemse, 1986: Practical aspects of accurate tidal computations, J. of ASCE Hydraulics Engineering, Vol. 9, pp. 802-812.

Stelling, G.S. and J.J. Leendertse, 1991: Approximation of Convective Processes by Cyclic AOI methods, Proceeding 2nd ASCE Conference on Estuarine and Coastal Modelling, Tampa, pp. 771-782.

Stelling, G.S. and J.A.Th.M. van Kester, 1994: On the approximation of horizontal gradients in sigma co-ordinates for bathymetry with steep bottom slopes, Int. J. Num. Meth. Fluids, Vol. 18, 915-955.

Stelling, G.S., Duinmeijer, S.P.A., 2003: A numerical method for every Froude number in shallow water flows, including large scale inundations, Int. J. Num. Meth. in Fluids. Vol. 43, 1329-1354.

Tartinville, B., E. Deleersnijder, P. Lazure, R. Proctor, K.G. Ruddick and R.E. Uittenbogaard, 1998. A coastal ocean model intercomparison study for a three-dimensional idealised test case. Appl. Math. Modelling vol. 22, pp. 165-182.

Twigt, D.J., E.D. de Goede, H. Gerritsen and E.J.O. Schrama, 2007: Analysis and modeling of the seasonal South China Sea temperature cycle using remote sensing, Int. Journal for Ocean Dynamics, Vol. 57, 467-484.

Uijttewaal, W.S.J. and R. Booij, 2000: Effects of shallowness on the development of free-surface mixing layers. Physics of Fluids, Vol. 12, No. 2, pp. 392-402.

Uittenbogaard, R.E., 1988: Measurement of turbulence fluxes in a stably stratified mixing layer. Proceedings 3rd Int. Symp. Refined Flow Modelling and Turbulence Measurements, Tokyo, 26-28 July, paper T11-3.

Uittenbogaard, R.E., 1998: Model for eddy diffusivity and viscosity related to sub-grid velocity and bed topography. Note, WL | Delft Hydraulics.

Uittenbogaard, R.E., J.A.Th.M. van Kester and G.S. Stelling, 1992: Implementation of three turbulence models in 3D-TRISULA for rectangular grids. Delft Hydraulics, report Z81.

Uittenbogaard, R.E. and J. Imberger, 1993: The importance of internal waves for mixing in a stratified estuarine tidal flow. Delft Hydraulics, report Z694.

Uittenbogaard, R.E. and B. van Vossen, 2003: Subgrid-scale model for quasi-2D turbulence in shallow water. *Proc. Shallow Flows. Delft, 16-18 June,* Balkema, Rotterdam.

Van Banning, G.K.F.M., 1995: Stroomonderzoek sluizen IJmuiden, verslag numeriek modelonderzoek. Delft Hydraulics Report H2251.

Van der Kaaij, T., 2007: Near- and far-field modelling of bouyant discharges. Delft Hydraulics Report Z4147.

Van Kester, J.A.Th.M., 1994: Validatie Delft3D voor menglaagproef. Fase 1: Verbeterde implementatie k-ε model. Delft Hydraulics Report Z810 (in Dutch).

Van Kester, J.A.Th.M. and G.S. Stelling, 1992: Versnellen van TRISULA-3D. Delft Hydraulics Report Z81.

Van Kester, J.A.Th.M., R.E. Uittenbogaard and G.S. Stelling, 1993: Some verifications of TRISULA-3D with three turbulence models. Delft Hydraulics report Z81.

Van Rijn, 1993: Principles of sediment transport in rivers, estuaries and coastal seas. Aqua publications, Amsterdam.

Van Schijndel, S.A.H. and H.R.A. Jagers, 2003: Complex flow around groynes. *Proc. Shallow Flows. Delft, 16-18 June,* Balkema, Rotterdam.

Vatvani, D.K., 2004: Delft3D-FLOW met CDW functionaliteit; eindrapportage. Delft Hydraulics Report M3521.

Vatvani, D.K., H. Gerritsen, G.S. Stelling and A.V.R. Krishna Rao, 2002. Cyclone-induced storm surge and flood forecasting system for India. In: Proc. Int. Conf. Solutions to coastal disasters, San Diego, February 2002, pp. 473-487. Reston, VA: ASCE.

Verboom, G.K., J.G. de Ronde and R.P. van Dijk, 1992: A fine grid tidal flow and storm surge model of the North Sea. Continental Shelf Research, Vol. 12, No. 2/3, pp. 213-233.

Vreugdenhil, C.B., 1994: Numerical methods for shallow-water flow. Water Science and technology library. Kluwer Academic Publishers.

Wallingford, 200X: HYDRALAB-III JRA1; Validation of numerical models. Technical Note CBS0327/01.

Walstra, D.J.R., J.A. Roelvink and J. Groeneweg, 2000: Calculation of wave-driven currents in a 3D mean flow model. Proc. of 27th Int. Conf on Coastal Engng., Sydney, pp. 1050-1063.

Wang, Z.B., C. Jeuken, H. Gerritsen, H.J. de Vriend and B.A. Kornman, 2002: Morphology and asymmetry of the vertical tide in the Westerschelde estuary, Continental Shelf Research, Vol/Issue 22/17, p2599-2609.

Willemse, J.B.T.M., G.S. Stelling and G.K. Verboom, 1986: Solving the shallow water equations with an orthogonal coordinate transformation. DELFT HYDRAULICS Communication No. 356.

WL | Delft Hydraulics, 1994: Test document Delft3D-MOR. WL | Delft Hydraulics report Z630.

WL | Delft Hydraulics and Rijkswaterstaat, 2001: Standard FORTRAN90 programming rules. OMS report number 2001-01.

WL | Delft Hydraulics, 2007: Delft3D-FLOW. Simulation of multi-dimensional hydrodynamic flows and transport phenomena, including sediments, Version 3.13. User Manual. Delft Hydraulics. (November 2007).

5 Glossary

***Algorithmic implementation**:* the conversion of the conceptual model into a finite set of rules suitable for computation. This may involve spatial discretisation schemes, time integration methods, solution procedures for algebraic equations, decision algorithms, etc.

***Conceptual model**:* a mathematical/logical/verbal representation of a physical system or process. This representation may involve differential equations, discrete algebraic equations, decision graphs, or other types of conceptual descriptions.

***Computational model**:* software whose primary function is to model a certain class of physical systems. The computational model may include pre- and post-processing features, a user interface, and other ancillary programmes necessary in order to use the model in applications. However, this validation document primarily concerns the core of the computational model, consisting of the underlying conceptual model, its algorithmic implementation and software implementation.

***Software implementation**:* the conversion of the algorithmic implementation into a computer code. This includes coding of algorithms, use of standard mathematical software, design and implementation of data structures, etc. The term software implementation, for the purposes of this document, is limited to the computational core of the model. It does not include pre- and post-processing software, user interfaces, or other ancillary programmes associated with the computational model.